Alternate and Random Copolymers of Bay substituted Rylenebisimides for Energy Applications

Thesis Submitted to AcSIR for the Award of
the Degree of

DOCTOR OF PHILOSOPHY
In Chemical Sciences

By

Sandeep Kumar Sharma

Registration Number: 10CC13A26015

Under the Guidance of

Dr. S. K. ASHA

Polymer Science and Engineering Division

CSIR-NATIONAL CHEMICAL LABORATORY

PUNE – 411008, INDIA

June 2018

Dedicated to

My Family and Friends

DECLARATION

I hereby declare that the research work embodied in the thesis entitled "**Alternate and Random Copolymers of Bay substituted Rylenebisimides for Energy Applications."** has been carried out by me. This work was carried out at the Polymer Science and Engineering Division of CSIR-National Chemical Laboratory, Pune under the supervision of Dr. S. K. Asha. I also affirm that this work is original and has not been submitted in part or full, for any other degree or diploma to this or any other University or Institution.

.

Sandeep Kumar Sharma **June 2018**
Polymer Science and Engineering Division
CSIR-National Chemical Laboratory
Pune- 411 008

राष्ट्रीय रासायनिक प्रयोगशाला
(वैज्ञानिक तथा औद्योगिक अनुसंधान परिषद)
डॉ. होमी भाभा रोड, पुणे - 411 008. भारत
NATIONAL CHEMICAL LABORATORY
(Council of Scientific & Industrial Research)
Dr. Homi Bhabha Road, Pune - 411008. India

Certificate

This is to certify that the work incorporated in this Ph.D. thesis entitled **"Alternate and Random Copolymers of Bay substituted Rylenebisimides for Energy Applications"** submitted by **Mr. Sandeep Kumar Sharma** to **Academy of Scientific and Innovative Research (AcSIR)** in fulfillment of the requirements for the award of the Degree of Doctor of Philosophy, embodies original research work under my supervision. I further certify that this work has not been submitted to any other University or Institution in part or full for the award of any degree or diploma. Research material obtained from other sources has been duly acknowledged in the thesis. Any text, illustration, table etc., used in the thesis from other sources, have been duly cited and acknowledged.

Sandeep Kumar Sharma
(Student)

Dr. S. K. Asha
(Supervisor)

Communications Channels ☎ +91 20 25902000 +91 20 25893300 +91 20 25893400 Fax +91 20 25902601 (Director) +91 20 25902660 (Admin.) +91 20 25902639 (Business Development) URL : www.ncl-india.org

ACKNOWLEDGMENT

Any human achievement is the culmination of numerous contributions and endeavors. There are many helping hands in one's success, and the present thesis is not an exception. As I completed my journey towards the most cherished dream, it gives immense pleasure and sense of satisfaction to record my heartfelt gratitude to all the persons who have made this possible for me.

First and foremost, I wish to express my heartfelt gratitude to my research supervisor, ***Dr. Asha S. K.*** *for believing in my abilities and providing me an incredible opportunity to pursue my career as a Ph. D. student. I thank her for her excellent guidance, constant encouragement, sincere advice, understanding and unstinted support during all the times of my doctoral research. She taught me everything she knows and always encourages me to think creatively and be prepared to learn new scientific methods. I am grateful to her for all the ways in which he has prepared me to move forward in my career as well as life. I consider very fortunate for my association with her, which has given a decisive turn and a significant boost in my career.*

I would like to offer my sincere thank to Dr. M. Jayakannan for his fruitful advices, support and constant encouragement. His immense knowledge about the polymer chemistry helped a lot during my Ph.D. His passion and enthusiasm to do scientific research always motivated me. My sincere gratitude to you sir for your valuable guidance, friendly and energetic approach.

I wish to express my sincere thanks to the Doctoral Advisory Committee members, Dr. C. V. Ramana, Dr. P. P. Wadgaonkar and Dr. K. Krishnmoorthy for their continued support, guidance, and suggestions. I am grateful to Prof. A. K. Nangia, Director, NCL, Dr. V. K. Pillai and Prof. S. Pal (Former Director, NCL), Dr. Ulhas Kharul, Head, PSE Division, and Dr. A. K. Lele (Former HoD, PSE Division) for giving me this opportunity and providing all necessary infrastructure and facilities.

I also acknowledge the financial support of UGC, New Delhi and CSIR-NCL for providing the best infrastructure for a fruitful research.

My sincere thank to Dr. Vinay Gupta (CSIR-NPL, New Delhi) for his active collaboration which helped me to understand my systems in better way and gave fruitful results. I would like to thank Prof. Sunder Kumar Iyer (IIT-Kanpur), for giving me a opportunity to learn device fabrication technique. I am also grateful to Dr. K. Sreekumar and Roby for their active collaboration within the NCL to understand a new aspect of research in the field of energy storage.

I would like to thank all the instrumental in charges of NCL and J-wing who helped me to carry out analysis of my samples. I extend my thanks to Mr. Shamal K. Menon for helping me in GPC. I would also like to thank Mrs. B. Shantakumari, Mr. Venkatesh Thogiti, and Mr. Pankaj for helping me in various characterization. I would like to thank all the members of NMR division for analysis of my samples.

My sincere thanks to Dr. Nagesh B. Kolhe, my senior lab mate who taught me the basic of instruments for this work and the field. I extend my sincere thanks to all my seniors Dr. Kaushlendra Kumar, Dr. Rekha Narayan, Dr. T. Senthil Kumar, Dr. Nisha, Dr. Shekhar Shinde, Dr. Saibal Bhaumik, Dr. Swapnil, and Dr. Prajitha for providing a good platform for my research work. My special thanks to all my seniors from IISER Pune; Dr. Pramod, Dr. Smita, Dr. Ananthraj, Dr. Bapu, Dr. Rajendra Dr. Narsimha (Bhagwan) for valuable suggestions and helping me to use their instrumental facility.

I would like to express my special thanks to all my labmates and friends from CSIR-NCL and IISER Pune: Dr. Suresh, Bhagyashree, Sonashree, Nilesh, Sarabjot, Mehak, Shrikant, Moumita, Dheeraj, Navnath, Akhil, Aryan, Sharath, Dilna, Ganesh, Ruma, Mishika, Utrreshwar for their support, motivation and maintaining cheerful environment in the lab. I also want to thank past and present project traines: Alok, Vikash, Akshta, Harish, Vidhya, Priyanka, Devendra, Sherya, Durga, Sharnya, Anju, Suchitra, Agnus, Indrajith, Nithin, Anjali, Shifana, Harita for bringing cheerful environment. A special thanks to all the members of D-WING for giving such a fantastic environment which alert me to keep on working.

My special thanks to my best companion Dr.Vijay, Amit, Manoj, Dharmesh, Dr. Sandip, Dr. Pradeep, Dr. Anup (Bhau), Bhanu for their friendship and support which made my life easier here. I also want to thank Swechchha for her support and care during my up and downs. I extended my sincere thanks to all OHR friends for making hostel life memorable. I also like

to thank all my NCL friends Manik, Bhawana, Ruchi, Vinita, Ragini, Yogita, Garima, Sharad, Pravin, Praveen, Pragati, Durgaprasad, Indrapal for their care and support.

Finally, I would like to thanks my beloved parents for their support throughout my Ph.D study. A special thanks to my grandparents for showing belief in me. I would like to thank my uncle aunty for their love and support. My special thanks to all my relatives and family members for their unconditional love and support.

Sandeep Kumar Sharma

TABLE OF CONTENTS

List of Abbreviations

Abbreviations	Expansion
A	Ampere
AC	Alternating Current
ATR	Attenuated total reflectance
C	Capacitance
$CHCl_3$	Chloroform
CNTs	Carbon Nanotubes
$CDCl_3$	Deuterated chloroform
O-DCB	1,2 –Dichlorobenzene
CH_3CN	Acetonitrile
DCM	Dichloromethane
DMAc	N,N-Dimethylacetamide
DMF	N,N-Dimethylformamide
DMSO-d6	Deuterated dimethyl sulfoxide
DSC	Differential scanning calorimetry
TGA	Thermo gravimetric Analysis
DFT	Density functional theory
dL	Deciliter
F.F.	Fill factor
FT-IR	Fourier transform infrared
GPC	Gel permeation chromatography
g	Gram
HCl	Hydrochloric acid
H_2SO_4	Sulfuric acid
ITO	Indium tin oxide
KJ	Kilojoule
K_2CO_3	Potassium carbonate
KI	Potassium iodide
LC	Liquid crystal
LCPs	Liquid crystalline polymers
MALDI-TOF	Matrix-assisted laser desorption ionization-time of flight

mg	Milligram
mL	Milliliter
µL	Micro liter
mmol	Milli mole
MHz	Megahertz
Mn	Number average molecular weight
Mw	Weight average molecular weight
NMR	Nuclear magnetic resonance
N_2	Nitrogen
nm	Nanometer
OD	Optical density
PDI	Polydispersity index
ppm	Part per million
PLM	Polarized light microscope
RI	Refractive index
SEM	Scanning electron microscope
TEM	Transmission electron microscopy
AFM	Atomic force microscopy
SEC	Size exclusion chromatography
SiO_2	Silicon dioxide
THF	Tetrahydrofuran
TFA	Trifluoroacetic acid
T_m	Melting temperature
T_g	Glass transition temperature
T_c	Crystallization temperature
T_D	Decomposition temperature
UV	Ultraviolet
FL	Fluorescence
VTXRD	Variable temperature X-ray diffraction
WXRD	Wide angle X-ray diffraction
OFET	Organic field effect transistor
OLED	Organic light emitting diode
OPV	Organic photovoltaic

SAM	Surface assemble monolayer
SC	Supercapacitor
RCA	Radio corporation of America
Au	Gold
Ag	Silver
Al	Aluminum
HMDS	Hexamethylenedisilazane
SCLC	Space charge limited current
ZnO	Zinc oxide
V	Volt
eV	Electron volt
n-Bu_4PF_6	Tetrabutyl ammonium hexafluorophospahte
Eg (opt)	Optical band gap
Eg (ele)	Electronic band gap
HOMO	Highest occupied molecular orbital
LUMO	Lowest occupied molecular orbital
PCE	Power conversion efficiency
Jsc	Current density
Å	Angstrom
cm	Centimeter
s	Second
λ	Wavelength
Voc	Open circuit voltage

PREFACE

The rapid depletion of fossil fuel-based non-renewable energy resources is a major cause for concern. The energy crisis can be reduced by efficient utilization of renewable energy resources such as solar, tidal, wind, etc. Solar energy is the most significant energy resource which directly converts sunlight into electricity. Inorganic material based solar cell devices are currently available in the market. These solar devices are installed on rooftops of buildings. However, the cost of these devices is rather very high. The scientific community has given considerable attention to developing a new cost-effective material for energy generation. This is the primary motivation for the development of organic photovoltaic (OPV) materials and a device, which exhibits flexibility, are low cost, and are available in abundant quantities. Equally important to energy generation is the energy storage systems as it plays a major role in the availability of sustainable renewable energy on demand. Supercapacitors have gained much attention as energy storage devices due to their high power density, excellent cycle life, etc. Along with other materials like metal oxides, metal sulphides, carbonaceous materials, and conducting polymers, conjugated polymers are also explored as electrode materials for energy storage. Composite electrode materials developed from hybrids of carbonaceous material with conjugated polymers are known to perform by electrical energy storage by both electrostatic (Electrode Double layer effect) and redox (Pseudocapacitance) processes at the electrode surface.

Statement of Problem, Objective:

Naphthalene and perylene diimides based polymers are promising candidates for energy generation application because they exhibit good optical and semiconducting properties. These building blocks could be utilized to construct n-type materials with a unique combination of desired properties such as absorption in the visible region, high electron mobility and excellent thermal and photostabilities.

The objective of the present thesis work was to design and synthesize various copolymers of bay substituted naphthalene and perylene diimides, aimed at fine-tuning the HOMO-LUMO band gap, electrochemical properties as well as modifying their structural characteristics to suit their application in Energy generation and Energy storage. This thesis has been divided into six chapters. **Chapter 1** gives a glimpse of donor-acceptor based n-type polymers and their application in the organic solar cell as well as in Energy storage devices such as supercapacitors. It deals with detailed literature survey on organic solar cell based n-type polymers along with a detailed study of energy storage devices.

Key Findings

Chapter 2: Improved All-Polymer Solar Cell Performance of *n*-type Napthalennce diimide-bithiophene P(NDI2OD-T2) Copolymer by Incorporation of Perylene diimide as Co-acceptor.

Naphthalene diimide bithiophene P(NDI2OD-T2) polymer, also known as N2200, is a commercially available donor-acceptor polymer, which is extensively investigated for its high electron mobility (> 0.85 cm^2 V^{-1} s^{-1} in OFET), high power conversion efficiency (PCE) ~5% in all-polymer solar cells (PSC)s, good solution processability, high crystallinity and light absorption capability near-visible and infrared region. However, the inherent π-stacking tendency of the naphthalene diimide unit hampers good intermixing with donor copolymers when used in solar cell devices. We have attempted to overcome this issue by developing copolymers of P(NDI2OD-T2) incorporating varying mole ratios of the higher analogue - perylene diimide randomly. These random copolymers (NDI-Th-PDIx; xPDI, x = 15, 30, 50 mole % of PDI) were synthesized by Stille coupling copolymerization. Proton NMR spectra recorded in $CDCl_3$ showed that the π-π stacking induced aggregation among the naphthalene units could be successfully disrupted by the random incorporation of bulky PDI units.

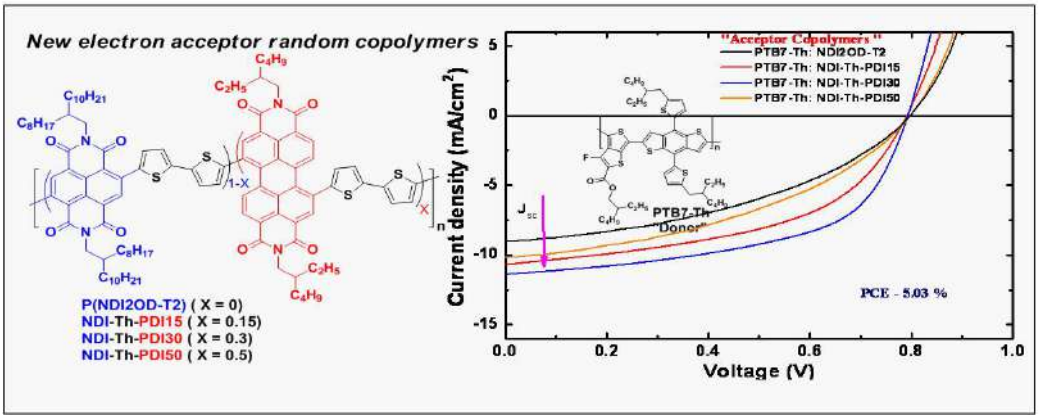

The newly synthesized random copolymers were investigated as electron acceptors in BHJ all-PSCs, and their performance was compared with P(NDI2OD-T2) as reference polymer. Compared to the 2.97 % PCE for a blend of lab-made reference acceptor polymer P(NDI2OD-T2) with Donor polymer - PTB7-Th (PCE10), the 30 mole % Perylene diimide incorporated random copolymer exhibited an enhanced PCE of 5.03 %. SCLC bulk carrier mobility measured for blend devices showed enhanced hole mobility compared to reference polymer, with PTB7-Th: NDI-Th-PDI30 blend device exhibiting the highest hole and electron mobility of 5.2×10^{-4} cm^2/Vs and 1.5×10^{-4} cm^2/Vs respectively. This work demonstrated the importance of molecular design via random copolymer strategy to control

the bulk crystallinity, compatibility, blend morphology and solar cell performance of n-type copolymers.

Chapter 3: All-Polymer Solar Cell Performance of *n*-type Naphthalene diimide-bithiophene P(NDI2OD-T2) Copolymer with PCBM as Co-acceptor.

In this molecular structure design strategy, we have attempted to improve the electron mobility of P(NDIOD-T2) by covalent incorporation of small amounts (5 – 15 %) of PCBM (Phenyl-C61-butyric acid methyl ester) on the polymer backbone. Although PCBM has several disadvantages like poor solubility and weak absorption in the visible region, it is still regarded as one of the best n-type material due to its higher electron mobility and better charge transportation. All-polymer solar cells fabricated with the PCBM modified P(NDI2OD-T2) as the acceptor polymer, and PTB7-Th as the donor polymer in the active layer demonstrated improved device performance with a (PCE) of 2.45 % for the 7.5 % PCBM incorporated polymer. The reference solar cell fabricated using unmodified P(NDI2OD-T2), and PTB7-Th exhibited only 1.5 % PCE under identical conditions.

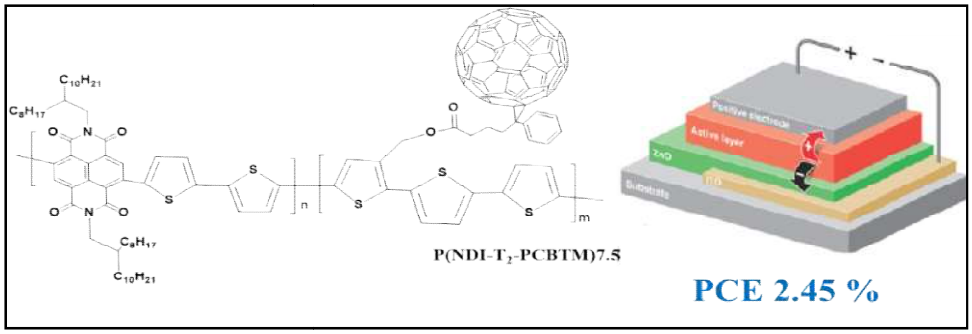

Chapter 4: Naphthalene diimide Based Copolymers by Direct Arylation Polycondensation as Highly Stable Supercapacitor Electrode Materials.

The energy storage efficiency of naphthalene diimide based π conjugated polymers was explored by utilizing their hybrid with carbon nanotube (CNT) as Type III supercapacitor electrode materials in devices and employing 0.5 M H_2SO_4 as the electrolyte. The polymers with naphthalene diimide (NDI) as acceptor and thiophene terminated oligo phenylenevinylene as donor moieties were synthesized using the direct (hetero) arylation (DHAP) polymerization route. Nitrile groups were introduced at the vinylene linkage in one copolymer (named as P_2) to fine-tune its electrochemical properties. P_2 exhibited a blue shifted intramolecular charge transfer (ICT) band in the absorption spectrum as well as a lower reduction potential in the cyclic voltammogram compared to the analogous polymer without the nitrile substitution (P_1). The two polymers were evaluated as Type III

supercapacitor materials by preparing composite electrodes with carbon nanotubes (CNTs) and employing 0.5 M H_2SO_4 as the electrolyte. Their performance was compared with that of P(NDI2OD-T2) as a reference polymer. The nitrile substituted polymer exhibited a specific capacitance of 124 F/g with excellent stability up to 5000 cycles with almost 100 % retention of the initial capacitance in the potential window of -0.7 to 0.5 V. P_1 exhibited a specific capacitance of 84 F/g, while the corresponding value for the reference Polymer P(NDI2OD-T2) was 61 F/g under identical conditions.

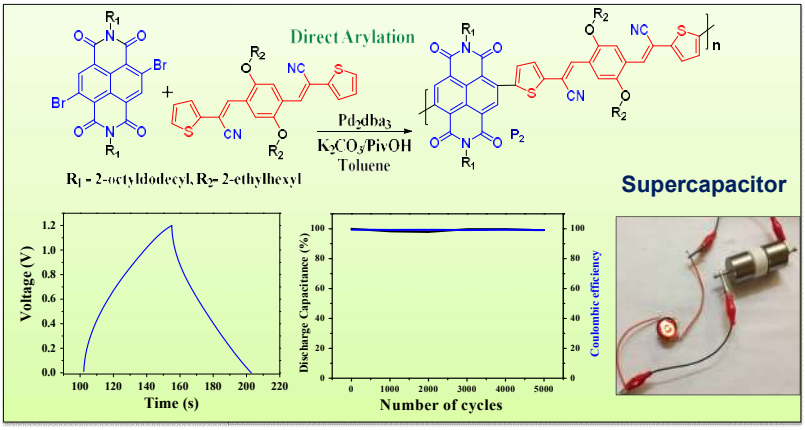

Chapter 5: Naphthalene diimide and Perylene diimide Based Alternate and Random Copolymers for Supercapacitor Electrode Materials.

Alternate and random copolymers of naphthalene diimide and perylene diimide with Benzadithiophene (BDT) were synthesized in good yield and characterized. These polymers were evaluated as supercapacitors materials. The alternate copolymer exhibited better capacitance compared to the random copolymer due to the proper ordering of the polymer chain and higher conductance in the former compared to the latter architecture.

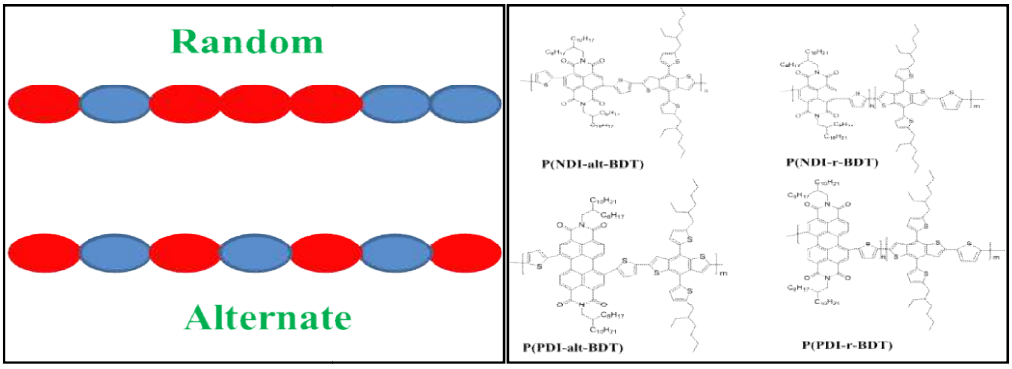

Chapter 6: Conclusions and outlook

This chapter summarizes the overall outcome of the research work carried out in the present Ph.D. thesis.

Chapter 1

Introduction

1.1 Introduction

In the present global scenario energy is a primary focus of scientific community and the major world powers. Energy requirements are mainly fulfilled by non-renewable fossil fuel-based resources. The current non-renewable energy resources are coal, oil and gas. There are more costly and environmentally harmful and is diminishing very fast. Hence, it is very important to find an efficient, cost-effective and sustainable approach to produce and store energy. Sustainable energy resources play a crucial role to fulfill the current energy needs and also for future generations. Sustainable energy is the energy which is collected from a sustainable source such as wind energy, solar energy, geothermal energy, wave power, tidal power, bioenergy, etc.[1]

The primary source of renewable energy is the sun. Solar energy can be used directly for producing electricity and for solar cooling, water heating, and a variety of industrial and commercial applications.[2]

The sun's heat also initiates the winds moving air is called wind and it is generated by uneven heating of earth's surface. Winds energy is collected through wind turbines. Then, the sun's heat and winds allows water to evaporate. When this vapors converts into rain and flows into rivers, their energy can be caught through hydroelectric power.[3]

Along with the snowfall and rain, sunlight also helps plants to grow. Agricultural and other plant waste known as biomass, can be utilized to produce chemicals and electricity. The use of biomass for these purposes is known as bioenergy.[4]

All renewable energy resources do not originate from the sunlight. For instance, geothermal energy or earth's internal heat can be utilized for different purposes, including the heating and cooling of buildings, and electric power production. Another example is the energy of the oceans tides which comes from the sun and the gravitational pull of the moon.[5]

The most essentially renewable energy resource which can meet the world's rising high energy demand is solar energy. Sun is the star of our planet. Per day, approximately 14 TW power reaches on the earth's surface and the whole world's necessity is nearly 10% of this value. Solar energy is a clean, nonpolluting and lifetime available energy source. The research on harvesting solar energy has become a hot topic not only for scientific interest but also for social demands. Photosynthesis is the natural phenomena where chlorophyll (the pigment present in green plants) absorbs energy and converts water and carbon dioxide into carbohydrate. The energy produced during this process is saved in the form of energy known as adenosine triphosphate (ATP). A mimicking phenomenon, photovoltaic effect was invented by Alexandre-Edmond Becquerel; the generation of electrical current or voltage in

the material after exposure to light is the basic principle of a photovoltaic cell or a solar cell, that is the production of electric power from sunlight.[6-7] Solar cells, which directly convert sunlight into electricity are one of the most efficient and promising technologies to produce energy. The first solar cell device was made from selenium wafers with power conversion efficiency (PCE) of approximately 1 %.[8] The solar cell devices are mainly divided into 1) inorganic 2) organic solar cell 3) dye-sensitized solar cell depending upon the semiconductor material used as active layer. Inorganic solar cells are mostly based on silicon. Today standard solar cell devices such as Monocrystalline and Multi-crystalline silicon have power conversion efficiency, 24.4 and 19.8 %, respectively.[9] The first and second generation solar cells based on the crystalline silicon, amorphous and multi-crystalline silicon and metal chalcogens such as copper indium germanium selenide (CIGS) and other thin film absorber has been developed that shows a relatively high power conversion efficiency around 15−20 % and therefore, dominate over commercially available solar technologies.[10] Dye-sensitized solar cell introduced by Gratzel is a kind of hybrid solar cell where a ruthenium based dye acts as the solar harvester.[11] Even though this concept gives a constant high performance of 12 %, the long-term stability of the device is still a challenge. However, cost of inorganic solar cells is still too high, and these are not readily processable. Therefore it becomes exciting and challenging for scientists to develop alternate energy generation devices with high power conversion efficiency.

Organic solar cells are a fast-growing research area because of the necessity of an alternative energy generation source. The very high demand for energy arises when the sun is not shining, which requires to storage of the harvested energy. The most general ways to store energy is batteries. Despite their extensive use, batteries are not the best technique to store the energy. Many research groups are searching alternative ways to store the electricity. Supercapacitors are one of the alternatives to batteries.

1.1 Energy Generation: Organic Solar Cell

Organic solar cells are a revolutionary technology which converts the sunlight into electrical energy using organic semiconductor material as active layer. This technology is very promising due to its lightweight, mechanical flexibility, large area and low fabrication cost.

The basic organic solar cell device architecture consists of a photoactive layer of organic or polymeric semiconductor material sandwiched between indium tin oxide (ITO) electrode (anode) and a metal electrode (cathode).[12] With active materials electron transporting (ETL) and hole transporting layers (HTL) are used for better charge transportation. Dependence

upon the nature of transporting layer, two device architecture can be identified; a) Conventional solar cell b) Inverted solar cell (shown in **Figure 1.1**).

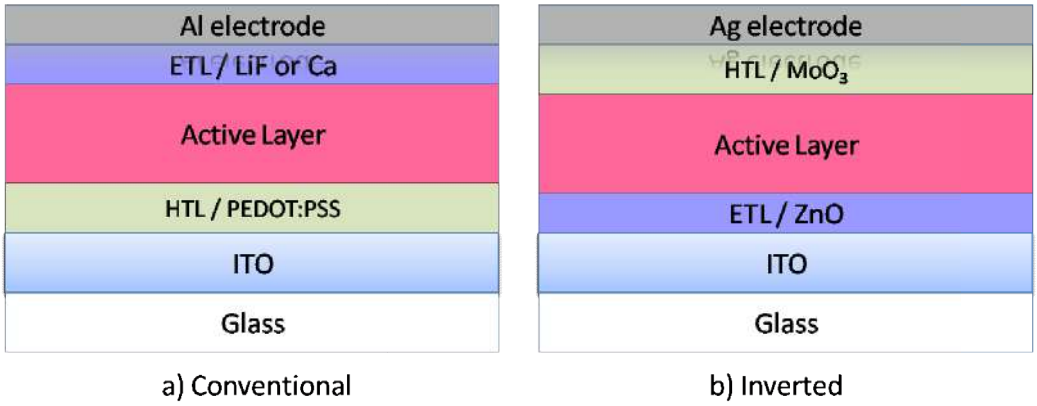

Figure 1.1. Schematic of organic solar cells a) Conventional, b) Inverted

1.1.1 Working Principles of Organic Solar Cells

The working principle of typical bilayer organic solar cell is shown in **Figure 1.2.** In the basic working principle of the organic solar cell, four steps are involved.[13-14]

a) Absorption of Light and Exciton Generation

A photon of light incident on an active organic semiconductor material, having higher energy than the semiconductor band gap, excites an electron from highest occupied molecular orbital (HOMO) state or valence band to the lowest unoccupied molecular orbital (LUMO) or conduction band, generates an electron-hole pair. Upon excitation, the excited electron is still bound to its hole (positively-charged), this electron-hole pair is known as an exciton.

b) Exciton Diffusion

After the exciton generation, the exciton will not dissociate under normal conditions. Some driving force is required to make it favorable for the exciton to convert into free charge carriers. Excitons migrate between adjacent donor moieties via a "hopping" mechanism, in which the exciton transitions between adjacent to localized energy states on different donor moieties. The rate of exciton diffusion is governed by how closely the electronic clouds of adjacent donor molecules overlap, as well as the availability of similar energy levels on different moieties for the exciton to occupy. If the donor material has strong π-π interactions with itself; it will show better diffusion of excitons. The diffusion length of an exciton varies between 5-20 nm.[15]

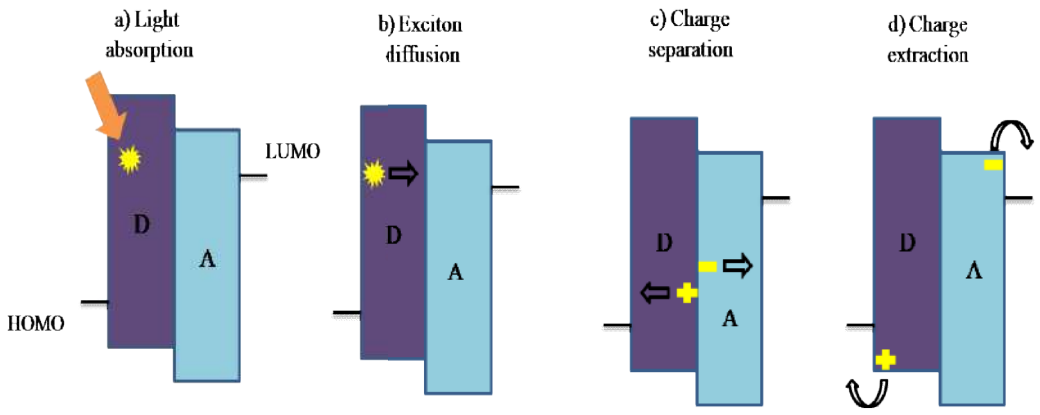

Figure 1.2: Mechanism of bilayer organic solar cell.

Due to the high exciton binding energy, exciton shows limited stability and has very less time, which allows electron-hole pair recombination. This recombination results in energy loss, which decreases PCE of the device.

c) Exciton Dissociation

Exciton dissociation is referred to the process of separating the electrostatically attached electron-hole pair (exciton) into free charge carriers. The dissociation of excitons occurs at interfaces of the donor-acceptor. The donor and acceptor materials are designed in a such way that they exhibit a difference in LUMO energy levels of the materials, which allows the dissociation of exciton. For the efficient dissociation, difference between the LUMO of donor and acceptor should be higher than the binding energy of exciton. Usually the difference is around 0.2-0.3 eV.

d) Charge Collection

After exciton dissociation, the electrons and holes travel through the acceptor and donor domains, respectively, to reach their respective electrodes. The free charge carriers (electrons and holes) are directed to their respective electrodes built into the device. This electric conductivity is created by using asymmetric electrode materials with different work functions.[16-19]

1.1.2 Parameters of Organic Solar Cell Performance Measurement

Figure 1.3 shows a typical current density-voltage (*J-V*) curve of the organic solar cell in the dark and under the light. In the dark, there is no current flow in the circuit, and *J-V* curves pass through the origin. When the photon of light is incident on the cell, the *J-V* curves are shifted in the fourth quadrant of the graph. A lot of important parameters can be extracted

from J-V curves such as short circuit current density (J_{sc}), open circuit voltage (V_{oc}), fill factor (FF) and power conversion efficiency (PCE or η).[20]

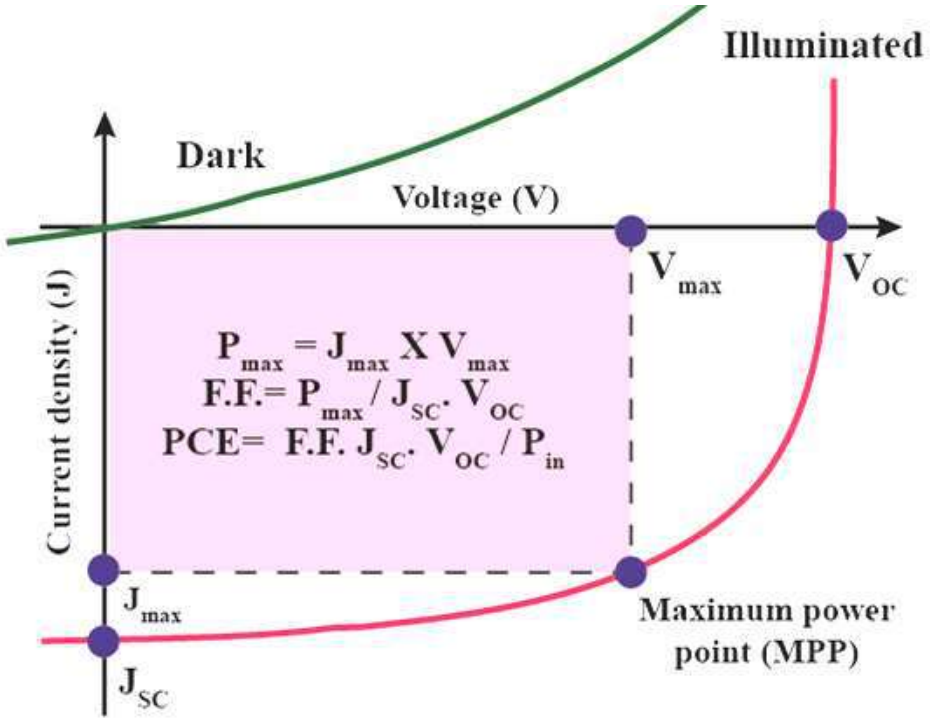

Figure 1.3. Typical current density-voltage (*J-V*) curve under dark (blue) and under Light (red) for polymer solar cell.

The p_{in} is the sum over all wavelengths fixed at intensity of 100 W/cm^2. The equation for the calculation of PCE is given in **Figure 1.3** which shows that PCE is directly proportional to the $V_{oc,}$ J_{sc}, and *FF*. The J_{sc} value depends upon the photon collecting capability of the active layer of the device, charge separation at donor-acceptor interface, charge transport and charge collection at electrodes. V_{oc} depends upon the energy gap between HOMO of the donor and LUMO of acceptor. The following factors have to be taken care of while designing new materials for organic solar cell application. 1) Broad absorption in visible and near IR region to match solar spectrum. 2) Suitable HOMO and LUMO energy level to maintain V_{oc} as well as energy offset for exciton dissociation at interface. 3) High charge carrier mobility (electron mobility for acceptor and hole mobility for donor) to improve the charge transport. 4) Optimal morphology of donor-acceptor blend within a nanoscale level of the active layer which improves $V_{oc,}$ J_{sc}, and *FF*.

1.1.3. Organic Photovoltaic Architectures

The organic solar cell can be divided into a) single layer organic solar cell b) bilayer organic solar cell c) bulk heterojunction solar cell (BHJ) according to their device fabrication. (See **Figure 1.4**)

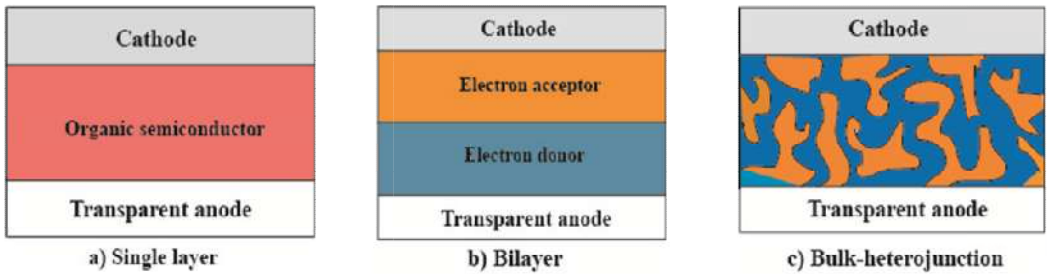

Figure 1.4. Schematic representation. a) single layer b) bilayer and c) bulk-heterojunction (BHJ) OPV device.

In single layer organic solar call one kind of active material (either donor or acceptor) is sandwiched between the two electrodes. In 1994, Marks *et al*. reported solar cell based on poly (*p*-phenylenevinylene) (PPV).[21] However, this device fabrication could not achieve high efficiency. Bilayer organic solar cell consists of both the electron donor and acceptor moieties sandwiched in between the two electrodes. The first organic solar cell with power conversion efficiency (PCE) ~ 1 % reported by Tang et al.[22-23] belongs to this category. MEH-PPV polymer as donor and PCBM ([6,6] -phenyl C60 butyric acid methyl esters) as an acceptor layer which is sandwiched between two electrodes is an example for bilayer solar cell.[24]

The bilayer configuration where the donor and acceptor layer was fabricated separately with layer thickness 80-100 nm each consecutively resulted in large macrophase separation between donor and acceptor layer. The exciton generated 10-20 nm apart from donor-acceptor interface only was able to reach interface and dissociate in to free charge carriers. All exciton generated inside the active layer is not able to reach the interface before which they will recombine. Consequently, the power conversion efficiency is low. In most of the cases the exciton recombination will happen is before reaching the respective interfaces. The hole-electron pair will recombine so that the number of charge carriers get reduced and the performance drops out. So the exciton diffusion length plays a very crucial role in the device performance.

To overcome this drawback bulk-heterojunction (BHJ) solar cell was introduced where the donor and acceptor were mixed in the proper ratio to form a blend, due to which in some region the length scale of donor-acceptor in the blend is nearly equal to exciton diffusion

length. Excitons generated in the material may reach the D-A interface efficiently, where excitons can dissociate efficiently, thus the PCE increases. Up to now, the highest efficiency in bulk-heterojunction (BHJ) solar cell obtained is 14.2 % %.[25] Furthermore, the tandem solar cells have reached up to 15%. [26]

1.1.4. Type of Organic Semiconductors

Based on the electronic properties and nature of charge transport, the organic semiconductors are further classified into three types namely p-type (Donor or electron rich), n-type (Acceptor or electron deficient) and Donor-Acceptor or ambipolar (both electron and hole).

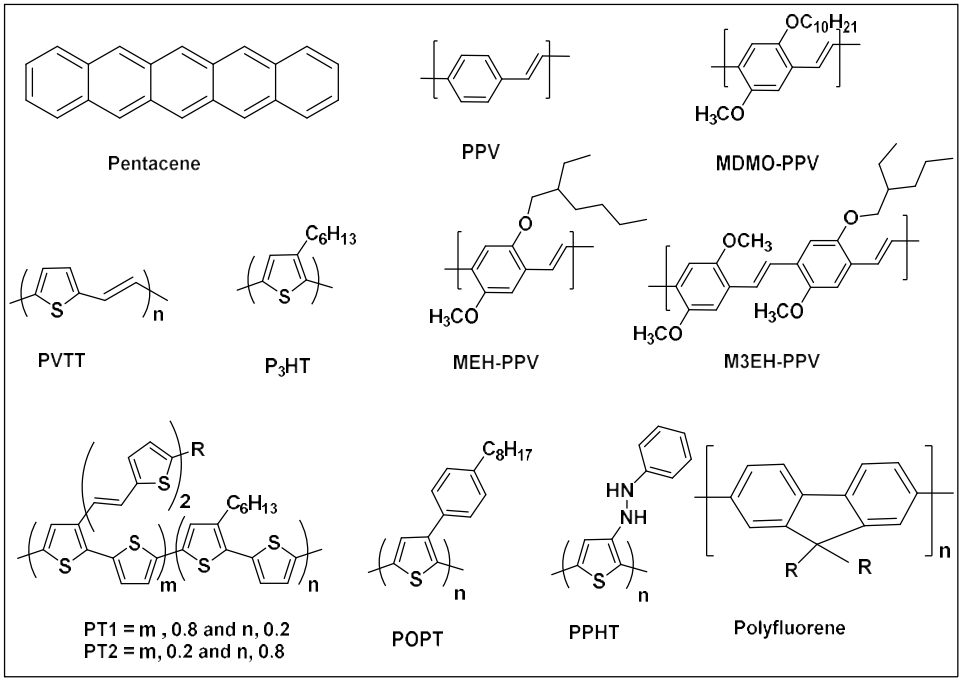

Chart 1.1 p-type semiconducting materials.

p-type organic semiconductor is also known as a donor or hole transporting material. p-type semiconductors are electron rich and has tendency to donate the electron and create a hole which is then transported through the semiconducting material in the applied electric field. The charge transport in the p-type semiconducting material occurs by extracting electron or injecting the holes from highest occupied molecular orbital (HOMO). To attain better electron extraction or hole injection, the HOMO energy level of the semiconducting material should be in the range of 4.8 to 5.2 eV. In the last few decades scientific community have done extensive research on the design and synthesis of p-type air-stable materials, and now an enormous collection of materials based on polymers and small molecules are available with high hole mobility. Chemical structures of some of the typical p-type organic

semiconductors are shown in **Chart 1.1,** which have been utilized in the Organic Solar cells. [12, 20, 27]

n-type organic semiconductors are known as acceptor or electron transporting material. These are electron deficient in nature and have tendency to accept the electrons. n-type organic semiconductors are used as counterpart of p-type semiconductors in p-n junction devices, but n-type materials development has lagged behind the p-type semiconducting materials. Reson behind this shortage of the n-type organic semiconductor is instability of their ambient charge carriers. The anions (negative charge carriers) are generally trapped by reactive species like oxygen and water that diffuses into the semiconducting layer. The air stability issue of n-type materials was conquered up to a certain extent by giving more insight into the design strategies of the organic semiconductors.[28-29] The most useful and important strategy to enhance the air stability of organic n-type semiconductor is by introducing electron withdrawing groups such as cyanide, by which redox potential of n-type semiconductors can be fine-tuned. In addition to that the lower level of LUMO also helps for better charge injection. The chemical structures of some of the typical n-type organic semiconductors shown in **Chart 1.2** have been utilized in the Organic Solar cells.

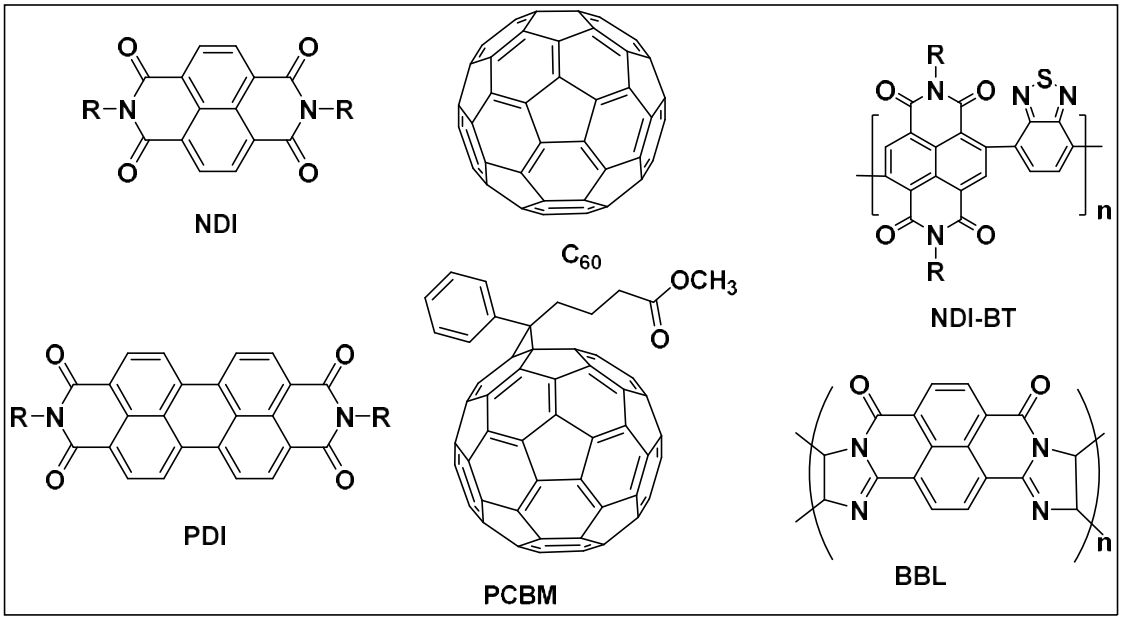

Chart 1.2 n-type semiconducting materials.

There is a new class of semiconducting materials which exhibits both donor and acceptor moieties. These are low band gap materials which exhibit better charge transport properties and often used as p-type or n-type material depending upon their HOMO and LUMO levels,

so the energy level of the polymers can be easily fine-tuned. Some of the materials are shown in **chart 1.3.**[20, 22, 27]

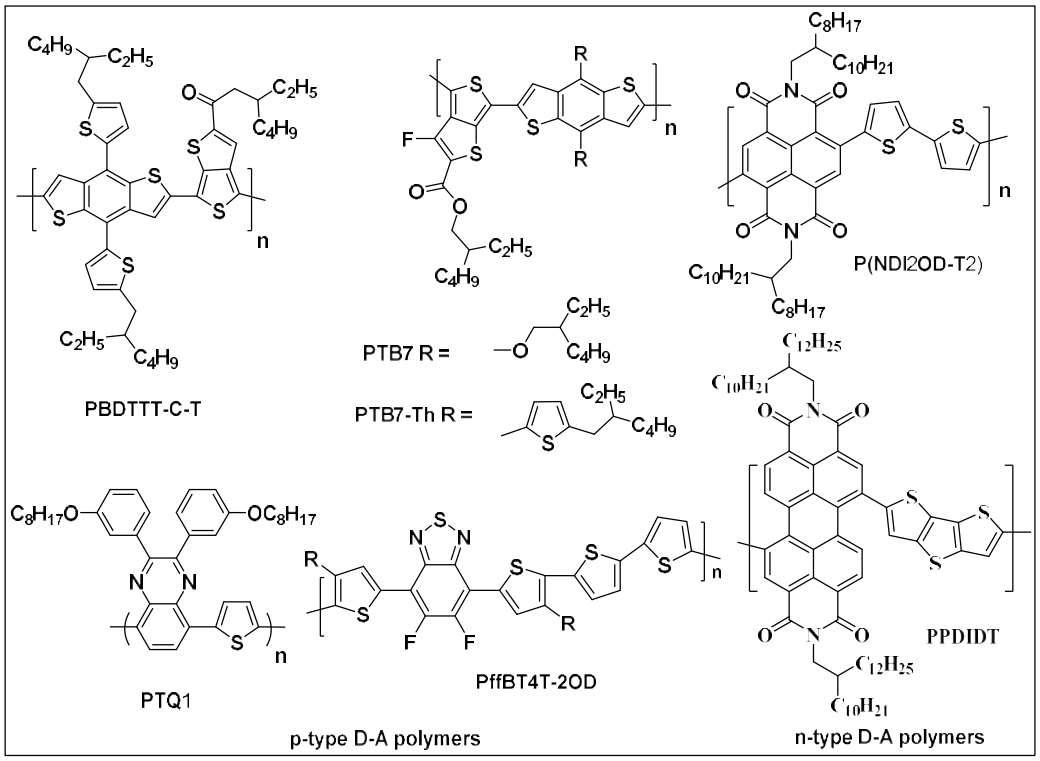

Chart 1.3. Donor-acceptor type semiconducting polymers.

1.1.5 All-Polymer Solar Cells

There is a library of thiophene-based molecules available as p-type (Donor) materials which exhibit good device performance. The most commonly used n-type (Acceptor) system is PCBM and its derivatives. However, PCBM has many drawbacks like poor solubility, phase separation, weak absorption in the solar region. So there exists an urgent requirement for alternative derivatives which can overcome these challenges. Naphthalene and perylene bisimides are polyaromatic hydrocarbons which can be easily derivatized into highly soluble materials which have good quantum yield and photo and thermal stability. Nowadays research is progressing in this direction where PCBM is replaced with naphthalene and perylene based polymers. Among the two, naphthalene exceeds perylene as a charge transporting material whereas the latter has good absorption in the visible region of solar spectrum. So a combination of both can result in better performance. Small molecule-based systems have many advantages like high crystallinity and better charge transporting. However, making thin films of small molecules is difficult. Polymers based on these systems

can have very good thin film formation so that they can be easily processed. Bay substitution of these moieties will help to tune the band gap efficiently so that it can absorb a major part of the visible light.

Bay substituted naphthalene diimide with a bithiophene alternating comonomer (P(NDI2OD-T2)) was first synthesized by the group of Fachetti and later commercialized as PolyeraActivInk N2200 (bay substituted naphthalene diimide with a bithiophene comonomer).[31] This P(NDI2OD-T2) polymer exhibited very high electron mobilities in organic field effect transistors (OFET) of ~ 0.85 cm^2/Vs. P3HT/P(NDI2OD-T2) blends have shown balanced hole and electron mobilities of 2 x 10^{-3} cm^2/Vs and 4 x 10^{-3} cm^2/Vs respectively. Later on, this moiety has been well explored by different research groups varying the donor moiety, processing parameters like solvents, temperature, etc., and donor /acceptor weight combinations.[20] Loi and Sirringhaus et al. measured the solar cell efficiency of P(NDI2OD-T2) independently in solvents like o-dichlorobenzene (o-DCB), chlorobenzene (CB), chloroform, or p-xylene for device fabrication and a maximum PCE of 0.2 % was obtained which was not a good number.[32-33] Neher and co-workers improved the PCE to 1.4 % by using P(NDI2OD-T2) as acceptor and P3HT as donor material using a 1:1 solvent mixture of chloronapthalene (CN) and p-xylene.[34] The reduction of polymer aggregation in the 1:1 solvent mixture of chloronaphthalene: p-xylene was expected to be a reason for high efficiency. Later on, Facchetti et al. reported P(NDI2OD-T2) and PTB7 as donor in different processing solvents such as xylene, chlorobenzene, and chloroform, which exhibited PCE of 2.7 %, 1.35 %, and 1.78 % respectively.[35] PCE higher than 4 % was achieved by Benten et al. using poly[2,3-bis-(3-octyloxyphenyl)quinoxaline-5,8-diyl- *alt* -thiophene-2,5-diyl] (PTQ1) as the donor and P(NDI2OD-T2) as the acceptor polymer.[36] 30:70 wt % combination of P(NDI2OD-T2): PTQ1 showed open circuit voltage of 0.84 V, short-circuit current density of 8.85 mA/cm^2 and a fill factor of 0.55 resulting in PCE more than 4 %.[37] The inverted type solar cell with PTB7-Th as the donor and P(NDI2OD-T2) acceptor polymer were fabricated by Kim et al. using chloroform as the solvent and optimized blend ratio of 1.3:1 (w/w) donor to acceptor got an efficiency of 4.6%.[38] Side chain tuning P(NDI2OD-T2) with flouro substitution in the thiophene group (P(NDI2OD-FT2)) was done by Jen et al. where the fluorine substitution on thiophene could increase the electron accepting power of the polymer, and this concept clicked for PTB7-Th/P(NDI2OD-FT2) with a maximum power conversion effciency of 6.3 %.[39] The blend of donor PTB7-Th with fluorine substituted P(NDI2OD-FT2) showed better thin-film crystallinity with a improved face-on orientation which enhances the vertical charge transport in devices to result in higher J_{sc} and FF. In

addition, this combination exhibited wide band gap and slightly higher LUMO value which improved the V_{oc} compared to P(NDI2OD-T2). Recently Facchetti et al. reported newly synthesized NDI co-polymerized with alkoxy-functionalized thienyl-vinylene (TVTOEt) (building-block P(NDI- TVTOEt) (shown in **Chart 1.4)** and their photovoltaic properties**.** The organic solar cell device were fabricated from the blend of P(NDI- TVTOEt): PTB7 showed PCE of 1.7 %. [40]

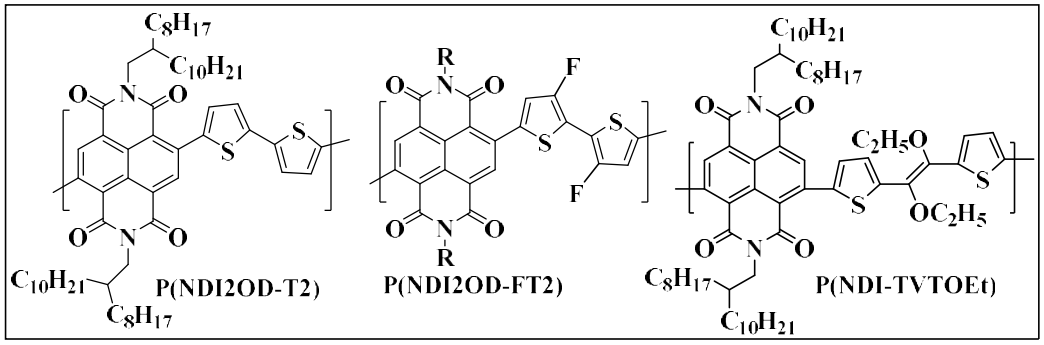

Chart 1.4 Structure of NDI based copolymers

1.2. Energy Storage: Supercapacitors

One of the major difficulties in utilizing the solar energy efficiently is the challenges in storing the harvested energy until it is needed. A very high demand of energy occurs when the sunlight is not available, which demands to store the energy. The most general way to store the energy is to use batteries.[41] There are two broad categories of batteries: primary and secondary. Primary batteries are non-rechargeable, and it is not recyclable. Primary batteries are applied for uses that require infrequent power, but they can get costlier in continuous use. There are different types of secondary batteries available in the market. The most common secondary batteries are lithium-ion batteries and lead-acid batteries. Despite their extensive use, batteries are not the best technology to store the energy. Many research groups are searching alternative ways to store the electricity. Supercapacitors are another alternative way of storing energy.

1.2.1 Lead-acid Batteries

Lead-acid batteries contain lead oxide (PbO_2) and lead (Pb) electrodes embedded deep in aqueous solution of H_2SO_4. While discharging, the lead (Pb) electrode is oxidized, and lead oxide (PbO_2) electrode is reduced by $H2SO_4$ to form lead sulfate ($PbSO_4$). While charging, electrons are extracted from $PbSO_4$ to form PbO_2 at the positive electrode and these electrons are used to reduce the $PbSO_4$ to Pb at the negative electrode.[42]

Lead-acid batteries are very attractive due to their low production cost and high power-to-weight ratio. However, despite their extensive use, these batteries having some drawbacks. Over a period of time, repeated charge-discharge cycles cause mechanical stress at the electrodes, decrease the mechanical strength, thus charge capacity can be reduced. In addition to that if the battery is not fully charged or after being discharged, sulfate deposits increase and break the electrode plates.[43] Lead is a very toxic metal; the discarding of these batteries is a very big environmental issue. Although these batteries can be recycled, a major proportion still reaches the dumping yard.

1.2.2 Lithium-ion Batteries

Lithium-ion batteries are well known for automobiles, and in consumer electronics and other applications. Lithium-ion batteries work on a somewhat different working principle compared to lead-acid batteries. Lithium-ion batteries work on the principle of intercalation/de-intercalation of Li^+ ions. Cathode (positive electrode) is made up of metal oxide, while anode (negative electrode) is generally made up of carbon and mostly it is graphitic carbon. Both electrodes are embedded deep in the electrolyte. Generally, organic carbonates having a lithium complex are used as the electrolyte. During charging, the metal oxide is oxidized and the electron diffuses to the carbon electrode where they meet the Li^+ ions. While discharging, Li^+ ions which are located in the carbon matrix leave the electrode and flow to the cathode, where the metal oxide is reduced. [44]

Lithium-ion batteries have high energy density compared to lead-acid batteries, these are getting more attention in various important electronics applications. However, lithium-ion batteries also suffer from dropping capacity upon repetitive charging-discharging cycles due to the generation of irreversible lithium oxides. In general, most of the lithium-ion batteries have less than three years lifetime.[45] Also, the abundance of lithium is available in only a few areas of the world - primarily Asia and South America.[46] It is relatively energy and time-intensive to purify the lithium from these salt deposits. Despite the high energy density of lithium-ion batteries, several issues affect their cost-effectiveness and efficiencies.

1.2.3 Supercapacitors

Supercapacitors, also known as an ultracapacitor, have electrode materials with the high surface area and thin electrolytic dielectrics to achieve very high capacitances compared to typical capacitors.[47-49] Supercapacitors, have significantly emerged over the past few decades with significant advances in energy storage.

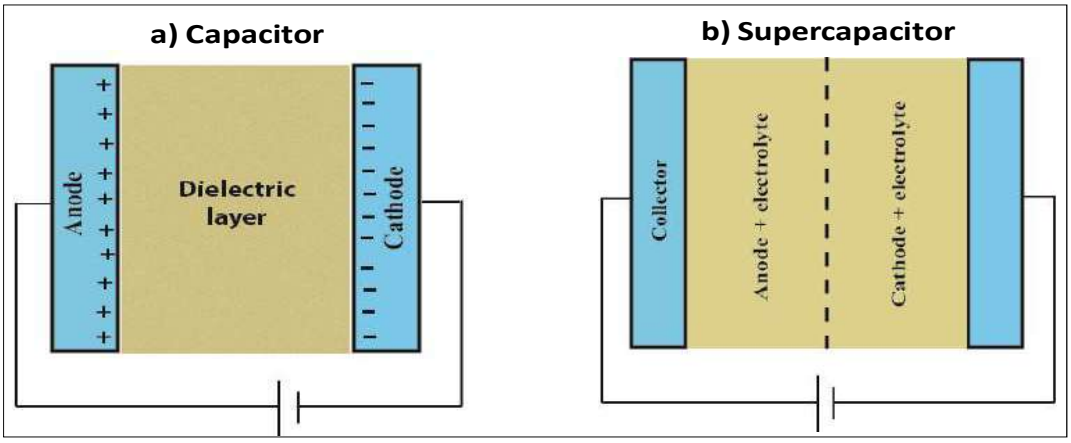

Figure 1.5 Typical structure of a) Capacitor b) Supercapacitor

Conventional capacitors having an insulating dielectric material separating two metal electrodes is shown in **Figure 1.5.a**. When a voltage is applied to the capacitor, opposite charges gather on the electrode surfaces. The dielectric separates the charges, consequently an electric field is generated that allows the capacitor to store energy.

Capacitance C is the ratio of Q and V, where Q is stored charge and V is the applied voltage.

$$C = \frac{Q}{V} \qquad (1)$$

For a conventional capacitor, capacitance C is directly proportional to the electrodes surface area A and inversely proportional to the D distance between the two electrodes.

$$C = \varepsilon_0 \varepsilon_r \frac{A}{D} \qquad (2)$$

Where C is the capacitance of the capacitor, ε_r, is permittivity of the insulating material and ε_0 is the permittivity of free space. A is the area of the electrodes and D is the distance between two electrodes. The energy stored in a supercapacitor is directly proportional to the capacitance.[50]

The two primary characteristics of a capacitor are power density and energy density. The energy density can be calculated as a quantity per unit volume or per unit mass. The energy E stored in a capacitor is directly proportional to capacitance:

$$E = \frac{1}{2} CV^2 \qquad (3)$$

In common, the power P is the energy exhausted per unit time. The components of the capacitor (e.g., electrodes, dielectric material, and current collectors) also contribute to the resistance of the capacitor, which is known as equivalent series resistance (ESR). These resistances decide the voltage during the discharge of the capacitor. P_{max} the maximum power for a capacitor[41-42] is calculated by the formula:

$$P_{max} = \frac{V^2}{4 \times ESR} \qquad (4)$$

This equation shows how the ESR can limit the maximum power of a capacitor.

Conventional capacitors have relatively low energy densities, but relatively high power densities, compared to fuel cells and batteries. Batteries can store more energy than a capacitor, but it cannot provide it very fast, which confirms its very low power density. Instead, capacitors store relatively less energy, but they can discharge quickly to produce high power, so it confirms that capacitors have high power density.

Supercapacitors also work on the same principles on which conventional capacitors work. However, they exhibit higher surface area (A) for electrodes and much thinner dielectric layer that decreases the distance (D) between the two electrodes. While charging, free charges gather on the surface of the electrodes. This initiates migration of the opposite charges in the electrolyte towards the electrode while counter ions will migrate towards the separator; for example, at the negative electrode, electrolyte cations will move towards the electrode while the anions will migrate towards the separator. These solvated ions are covered with a shell of solvent molecules, generally restricting direct contact between the electrolyte ions and the electrode surface. In the fully charged state, solvent molecules and ions of opposite charge will be filled in crevices of the porous electrode. Consequently, supercapacitors work as capacitors on a molecular level using a process called electric double layer capacitance (EDLC). In EDLC, the charged porous material used as the electrodes and ions served as the electrolyte while solvent molecules are used as the dielectric material. This allows supercapacitors to significantly store more charge compared to the same dimension capacitors. In addition, if the electrode materials can involve in oxidation-reduction (redox) reactions with the electrolyte ions (electrochemically active), the method of charge storage via redox reaction is known as pseudocapacitance (PC). Both EDLC and PC determine the overall capacitance of a supercapacitor, generally a redox-active electrode material store more charge compared to EDLC.[50]

Hence, from equations 2 and 3, supercapacitors exhibiting higher energy and capacitance. In addition, supercapacitors also can achieve relatively high power densities by maintaining the low ESR characteristic of conventional capacitors. Supercapacitors also have several

advantages over fuel cells and batteries, such as minimal charging time, higher cycle life and improved power density, and. **Figure 1.5.b** shows a typical supercapacitor device structure.

The performance of supercapacitor is shown in the "Ragone plot." (**Figure 1.6)**. This graph shows on the Y- axis, the power densities of different energy storage devices, versus their energy densities on the X-axis.[49] In **Figure 1.6**, it is observed that supercapacitors occupy a region between batteries and conventional capacitors. Even though they have higher capacitances than conventional capacitors, still they have to match their energy densities to fuel cells and batteries. Accordingly, a lot of studies are focused on developing better supercapacitor devices to improve their energy densities compared to batteries. Supercapacitors commonly avoid the use of corrosive materials and metals, therefore, supercapacitors are more environmentally friendly compared to batteries.

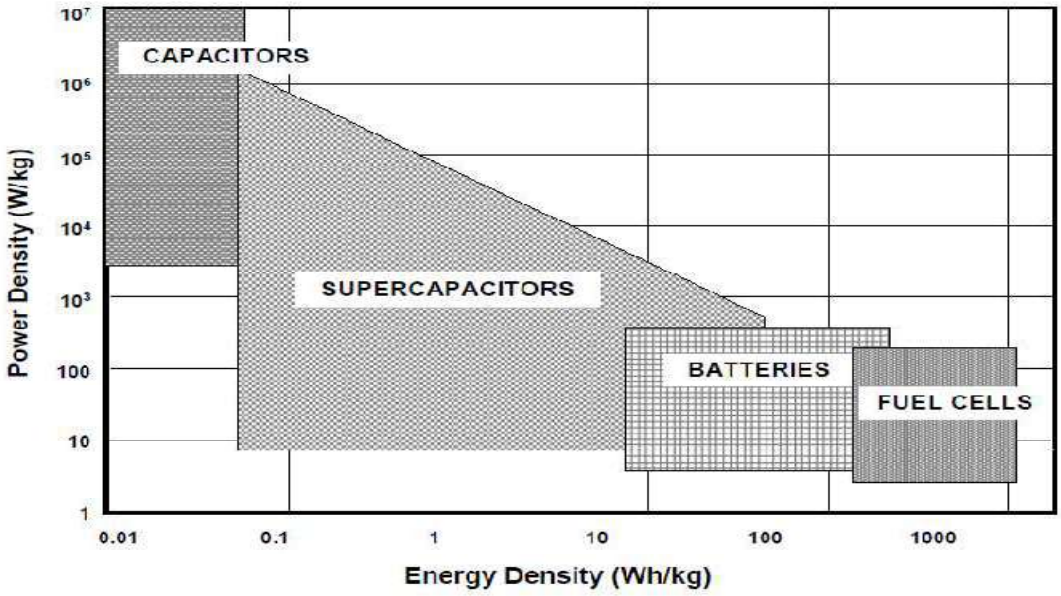

Figure 1.6. Ragone plot of energy device (Adapted from Ref. 49).

1.2.4 Type of Supercapacitors

Supercapacitors can be divided into three types based on the mechanism of storing charge.These are: electrochemical double-layer capacitors, pseudocapacitors, and hybrid supercapacitors. These are non-faradic, faradic and combination of two respectively. Faradaic processes involve the transfer of charges between electrode and electrolyte, known for oxidation-reduction reactions. A non-faradaic mechanism does not involve the transfer of charges between electrode and electrolyte. Charges are distributed by physical processes on the surfaces that do not involve the chemical transformation (oxidation-reduction).

a) Electrochemical Double Layer Capacitors (EDLC)

Electrochemical double-layer capacitors (EDLCs) are made up of two porous electrodes based on carbon, electrolyte, and separator. Figure **1.5.b** shows a typical EDLC. EDLCs store charge non-faradaically or, electrostatically, like conventional capacitors, and there is no exchange of charges between electrolyte and electrodes (Shown in **Figure 1.7.a**). When a potential is applied, charge gather on the electrode surfaces. Following the natural attraction of opposite charges, ions in the electrolyte solution diffuse through the separator into the pores of the electrode of opposite charge.[50-51] However, the electrodes are designed to prevent the recombination of the ions. Thus, a double-layer of charge is generated at each electrode. These double-layers known as electrochemical double-layer, coupled with an increase in the surface area using porous electrode and a decrease in the distance between two electrodes, allow EDLCs to attain higher energy densities than conventional capacitors.[52]

As there is no charge transfer associated with electrode and electrolyte solution, there is no chemical reaction involved in non-faradaic processes. Because of this, charge storage is very much reversible in EDLCs, which enhance their cycle life. EDLCs usually works with very high-performance for many charge-discharge cycles, sometimes up to 10^6 cycles. In contrast, electrochemical batteries are stable for a maximum up to 10^3 cycles. Due to their higher cycling stability, EDLCs are suitable for wide range of applications.

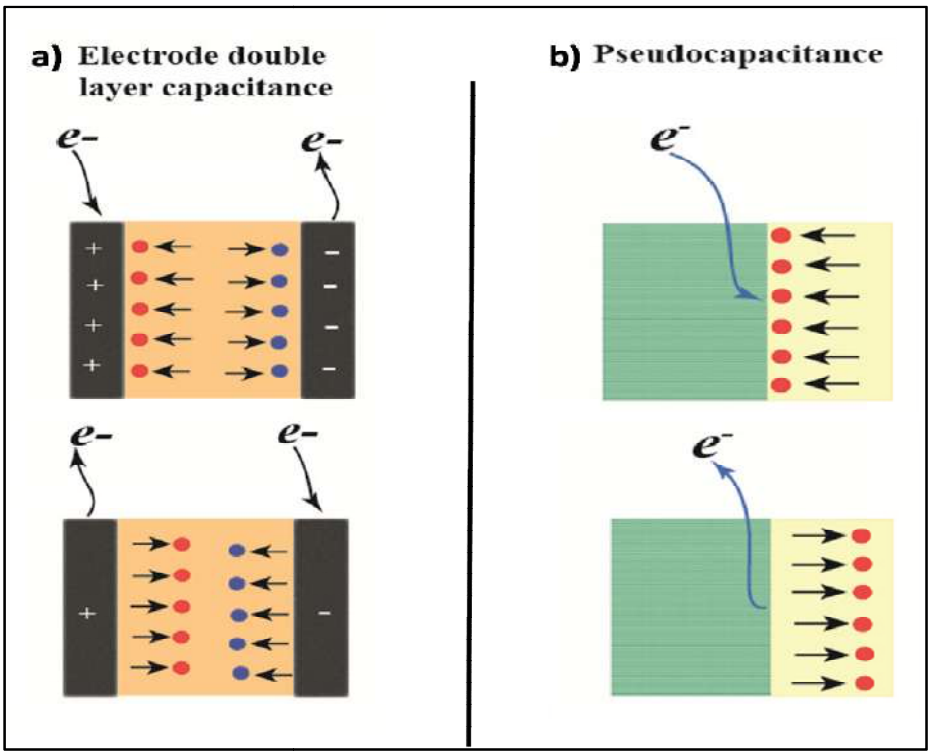

Figure 1.7. Mechanism of supercapacitors a) Electrode bouble layer. b) Pseudocapacitors.

The performance of an EDLC can be tuned by changing the nature of the electrolyte. For EDLC either an aqueous or organic electrolyte can be utilized. Aqueous electrolytes, such as H_2SO_4 and KOH, generally have lower equivalent series resistance (ESR) and lower minimum pore size requirements compared to organic electrolytes, such as acetonitrile. However, aqueous electrolytes also have lower breakdown voltages. Therefore, in choosing between an aqueous or organic electrolyte, one must consider the tradeoffs between capacitance, ESR, and voltage. The choice of electrolyte normally depends on the intended application of the supercapacitor. The nature of the electrolyte is very important in supercapacitor design; the subclasses of EDLCs are distinguished primarily by the form of carbon they use as an electrode material. Carbon electrode materials generally have higher surface area, more established fabrication techniques, and lower cost than other materials, for example, conducting polymers and metal oxides. Different forms of carbon materials can be used for storing charge in EDLC electrodes such as activated carbons,[53] carbon aerogels,[54-58] and carbon nanotubes.[59-64]

b) Pseudocapacitors

Pseudocapacitors can store charge through electrochemical processes (Shown in **Figure 1.7.b**). This is accomplished through intercalation processes, electrosorption, and reduction-oxidation reactions (Redox reaction). These electrochemical processes can allow pseudocapacitors to achieve higher energy densities and capacitances compared to EDLCs. Basically two types of electrode materials are used to store charge as pseudocapacitors - metal oxides and conducting polymers.

I) Metal Oxides

Because of their high conductivity metal oxides have been explored as an electrode material for pseudocapacitors. The majority of research is based on ruthenium oxide as it has high capacitances compared to other metal oxides. The capacitance is achieved through the intercalation or insertion and removal of protons into its amorphous structure. Higher capacitance compared to carbon-based and conducting polymer materials is achieved in ruthenium oxide hydrous form.[65-66] Metal oxides have shown excellent supercapacitive properties, but these materials are more expensive than carbon-based electrode materials and require extensive processing to fabricate the SCs devices. Therefore, metal oxide supercapacitors are not commercially viable so far.

II) Conducting Polymers

Conducting polymers exhibits comparatively high conductivity and capacitance, and relatively low equivalent series resistance (ESR) and lower cost compared to carbon-based SC electrode materials. Particularly, the n/p-type polymer composition, where one positively charged (p-doped) and one negatively charged (n-doped) conducting polymer electrode, exhibit excellent potential energy and power densities. But, shortage of efficient, n-doped conducting polymer materials has prevented these pseudocapacitors from reaching their goal. Furthermore, the mechanical stress of conducting polymers during redox reactions and chemical reaction limits the stability of pseudocapacitor materials. This lower cycling stability has hindered the development of pseudocapacitors based on conducting polymer. The more detailed discussion is provided in **section 1.2.5.**

c) Hybrid Capacitors

Hybrid capacitors utilize the advantages and moderate the disadvantages of EDLCs and pseudocapacitors to achieve better performance. Employing both processes non-faradaic and faradaic to store the charge, hybrid capacitors have accomplished higher power and energy densities compared to EDLCs without sacrificing its affordability and cycling stability that have limited the success of pseudocapacitors. More detailed discussion on hybrid capacitors were included in coming sections.

1.2.5. Semiconducting Polymers as Supercapacitor Electrode Materials

There is a requirement to find an inexpensive electrode material that can still achieve very high capacitance by pseudocapacitance. Semiconducting polymers are a very promising material for electrode fabrication because they are inexpensive to fabricate and process, and they involve in redox reactions. Their physical and electrochemical properties can be tuned by synthetic chemistry. Porosity and pore size can be tuned for conducting polymers. In addition, the electronic performance of conducting polymers can be tuned to change their charge carrier majority and to improve their electrochemical stability and conductivity.

Conjugated polymers are very promising because they exhibit very high charge density and low production cost. The electrochemical properties of conjugated polymers can be improved by composite formation. Composites can form between the conjugated polymer and other materials such as carbon-based materials, metal oxides, and other metal compounds. This section will focus on the conjugated polymers which are generally used for supercapacitor

devices. Examples of such type of polymers are polyaniline, polypyrrole, polythiophene and its derivatives, and donor-acceptor polymers.

a) Polyaniline (PANi)

Polyaniline was extensively studied as a supercapacitor electrode material. The structure of polyaniline is shown in **Chart 1.4**. Polyaniline has various attractive properties for use as electrode material for supercapacitor devices; it has a high doping level, high electroactivity, a high specific capacitance (400–500 F g^{-1} in acidic medium) and excellent stability.[67] Also, it has very good electrical conductivity, better environmental stability, and easy processability. Polyaniline has an ample range of capacity from 44 to 270 mAh g^{-1}.[68] This variation in capacity depends on various factors such as synthetic method, type and amount of binders and additives, polymer morphology, and electrode thickness. Polyaniline shows variable specific capacitance compared to other conducting polymers; electrodeposited polyanilines showed higher specific capacitance compared to chemically synthesize one.

Interfacial polymerization is comparatively easy and cheap. PANi synthesized via interfacial polymerization method by Sivakkumar et al. was evaluated for electrochemical performance in two-electrode cell setup, and the supercapacitor device showed good specific capacitance of 554 F/g at 1.0 A/g current, but it had very less cycling stability.[69] Experimental and theoretical specific capacitance of PANi in sulfuric acid was studied by Li et al. The maximum theoretical specific capacitance of PANi is 2000 F/g, while the experimental values are much lower than this.[70]

Different types of PANi-carbon nanocomposites were studied, such as carbon nanotubes , PANi/(CNTs),[71-73] PANi/carbon nanofibers,[74] PANi/carbon spheres,[75] PANi/carbon particles,[76] PANi/Graphene,[77-78] and PANi/ Graphene oxide (GO) or reduced GO (rGO).[79-81] PANi/Graphene composites reported by Zhang et al. via an in-situ polymerization method, exhibited a very high specific capacitance of 480 F/g at a current density of 0.1 A/g.[82]

b) Polypyrrole (PPy)

Polypyrrole is a very important polymer for supercapacitors, having advantages such as simple synthesis process, relatively high cycling stability and high capacitance. PPy films via interfacial polymerization were reported by Yang et al. The polymer exhibited exceptional electrochemical properties, with the specific capacitance of 261 F/g at 25 mV/s and cycling stability up to 1000 cycles with 75% retention of initial specific capacitance values at the same scan rate.[83] Li et al. reported PPy based flexible film via a chemical oxidation method

with a reactive degradable template methyl orange-$FeCl_3$.[84] The PPy film has very good electrochemical properties with specific capacitance of 576 F/g at current density of 0.2 A/g and the cycle stability up to 1000 cycles (82% retention) in the electrolyte of 1 M KCl aqueous solution at a current density of 3 A/g. Xu et al. reported PPy nanorods coated with conductive cotton fabrics via an in-situ polymerization method where $FeCl_3$-methyl orange (MO) complex was used as the template.[85] These films exhibited a higher specific capacitance of 325 F/g and energy density of 24.7 W h/kg, the current density of 0.6 mA/cm^2, but its cycling life was poor. The electrochemical properties of PPy based SC electrodes are affected by some factors such as preparing method, dopant, template and substrate, etc. Electrochemical properties of PPy can be improved by fine-tuning these factors. However, PPy based electrodes can not fulfill all the requirements of the practical application. Hence, researchers have focused on Carbon/ PPy composites, and other PPy-based composites are also very important.

Researchers have designed various types of PPy/Carbon nanotube (CNTs) composites in the last decade. An et al. reported PPy composite electrode with single-walled carbon nanotubes (SWCNTs) and showed a specific capacitance of 265 F/g, which was higher than pristine PPy and SWCNTs.[86] Multi-walled carbon nanotubes (MWCNT) and PPy composites prepared by Song et al. with homogeneous and in core/shell structures via an in-situ interfacial polymerization method showed improved chain packing and better molecular conformation, resulting in better electrical conductivity.[87]

c) Thiophene Based Conducting Polymers

Polythiophene (PTh) and its derivatives are very promising supercapacitor electrode materials. These have attracted considerable attention due to their high environmental stability, high electrical conductivity, and broad absorption.[88-90] Many research groups have studied extensively PTh based supercapacitor electrode and their electrochemical performance and various synthetic methods have been applied to improve their performance. Laforgue and coworker's synthesized polythiophene via the chemical method and it showed a high specific capacitance of 40 mAh/g and it exhibited excellent cycle stability up to 500 cycles.[91] Gnanakan et al. synthesized pure PTh nanoparticles and PTh-tartaric acid nanoparticles, where tartaric acid was used as dopant.[92,93] The specific capacitance of these nanoparticles was 134 and 156 F/g for polythiophene and PTh-tartaric acid nano-particles respectively. Patil et al. synthesized polythiophene based amorphous thin films via

consecutive ionic layer adsorption at room temperature, oxidation agent $FeCl_3$ was used and the specific capacitance of 252 F/g in 0.1 M LiClO4 solution was observed.[94]

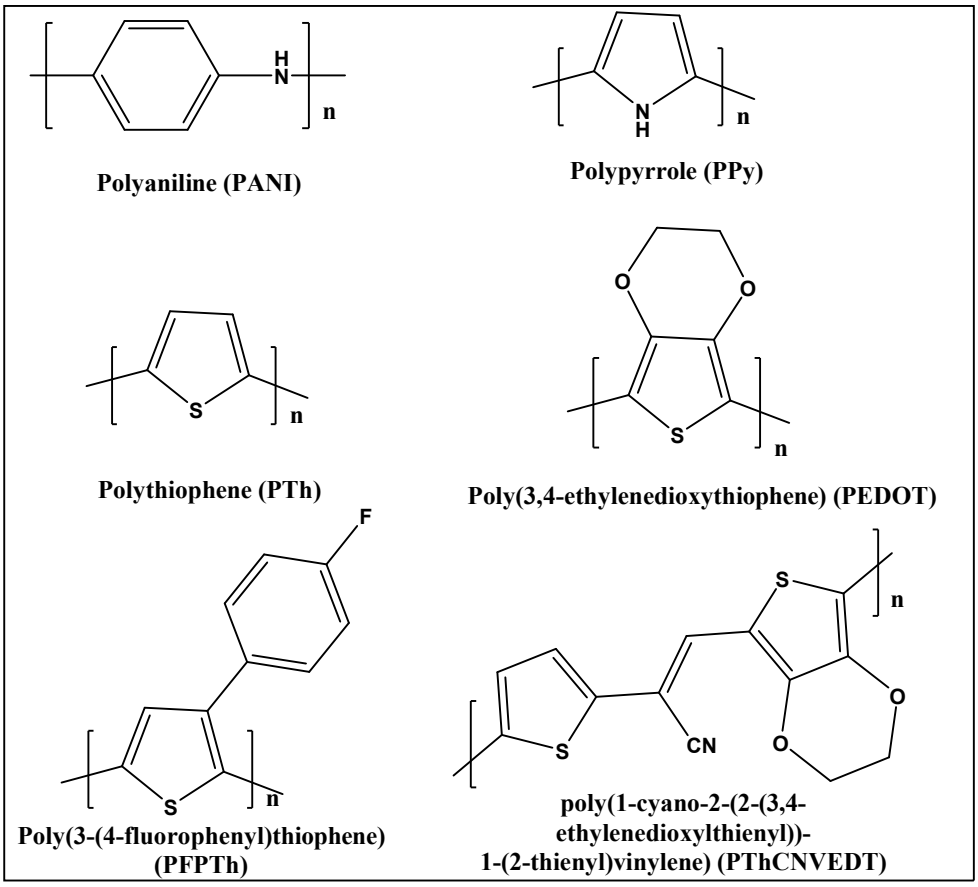

Chart 1.4 Various conducting polymer structures.

Low band-gap polythiophene derivatives can be synthesized by substitution at the thiophene rings 3- position with ethyl, alkoxy, and phenyl groups. It can improve the stability to oxygen and water. Another strategy was to introduce electron withdrawing groups to thiophene ring. Some of the examples are poly(3,4-ethylene dioxythiophene) (PEDOT)., poly(3-(3,4-difluorophenyl)thiophene) (MPFT), poly(1-cyano-2-(2-(3,4- ethylenedioxylthienyl))-1-(2-thienyl)vinylene) (PThCNVEDT) and poly(3-(4-fluorophenyl)thiophene) (PFPT). Because of intrinsic difficulties in the n-doping process there are very less reports of n-doped thiophene derivatives. To overcome the problem of the n-doped material a very successful approach is to use carbon based negative electrode in an asymmetric SC device, with the p-doped polymer based as the positive electrode. Poly(3,4-ethylene dioxythiophene) (PEDOT) is a thiophene derivative and its structure is given in **Chart 1.4.** PEDOT has a higher voltage range of 1.4 V, but exhibits lower specific capacitance due to the high molecular weight of

the monomer and the low doping level.[95] The extensive literature on PEDOT has grown rapidly in recent years due to its extremely desirable properties.[96-98]

d) Donor-acceptor Polymers

Donor-acceptor polymers are very promising for organic photovoltaics, these are ideally suitable for symmetric supercapacitor devices with high operating potential **(Chart 1.5)**. Reynolds at el. synthesized a novel donor-acceptor polymer, P((BEDOT-iI), in SCs.[99] The isoindigo functionality allows the material to accept a negative charge and the EDOT moieties allow the material to accept the positive charge. This polymer was used in symmetric SCs device with a 2.25 V operating voltage but cycle stability was poor. Seferos et al. demonstrated donor-acceptor polymers P(DEQ) and P(DDDBT) in SCs with large voltage windows of 2.5 V and better specific capacitance of 91 F g^{-1} at 50 mV s^{-1} and 201 F g^{-1} at 100 mV s^{-1} for P(DDDBT) and P(DEQ) respectively.[100] The poor cycling stability gives more insight into performance improvement for donor-acceptor polymers by increasing the amount of acceptors in the polymer lead to improve charge stabilization. Further increasing the amount of acceptor in donor-acceptor polymers can improve the stability and enhance the conductivity.

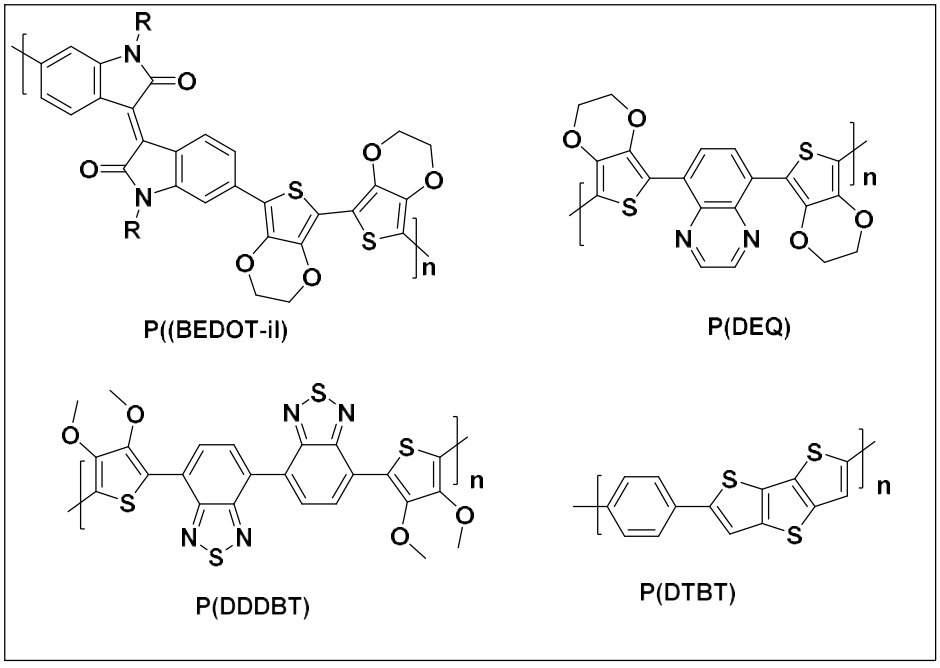

Chart 1.5 Donor-Acceptor polymers for supercapacitor devices**.**

The donor-acceptor polymer P(DTBT) was studied by Unalan et al. for its electrochromic and electrochemical properties. It shows different colors in each charged state, P(DTBT) is an

ideal material for smart electronic application as an energy storage device.[101] P(DTBT) has a moderate specific capacitance of 112.4 F g^{-1} at 1.0 A g^{-1}, and 59.8 F g^{-1}at 16.0 A g^{-1}, but it showed exceptional cycling stability (12,500 cycles at 1.0 A g^{-1} with 82% capacity retention) and 100% columbic efficiency. The electrodes could reach a high maximum specific energy of 49.8 W h Kg^{-1} and 16.6 kW Kg^{-1}at maximum power density. These polymers showed excellent cycling stability only in the positive charge-accepting regime.

To develop supercapacitor devices with high cycle stability and good capacitance is still a challenging task. Donor-acceptor or n-type copolymer based hybrid supercapacitor devices have potential to be developed as very highly stable (cyclic stability) devices with good capacitance.

1.3 Aim of the Thesis

The detailed introduction emphasized the potential application of semiconducting materials for energy generation as well as for energy storage. The objective of the thesis is to explore the application of n-type polymers based on perylene and naphthalene diimide (NDI) for the energy generation as well as energy storage. Chapter 2 and 3 explores the field of energy generation using naphthalene diimide based random copolymers for organic solar cell. While chapter 4 and 5 explores NDI and PDI based alternate and random copolymers for energy storage devices (supercapacitors).

Naphthalene diimide (NDI) based copolymers are very promising materials for organic solar cells because NDI exhibits broad absorption, high electron mobility, easy structural modification as well as good thermal stability. NDI exhibits π-π stacking which governs self-aggregation of polymers. This self-aggregation will govern the phase separation in the active layer, which in turn diminishes the performance. To improve the optoelectronic performance we can tune their aggregation behavior via multiple processes such as different solvent system, different substitution on the backbone and via introducing new moieties.

Polymer P(NDI2OD-T2) is a very promising material for energy generation due to its better photo-physical and semiconducting properties. It exhibits high electron mobility > 0.85 $cm^2V^{-1}s^{-1}$ in OFET, high PCE ~5% in all-polymer solar cells, high crystalline nature, light absorption capability near-visible and infrared region and solution processability. However, it exhibits strong tendency to form self-aggregates in specific organic solvents that leads to macro-phase separation instead of the proper donor-acceptor micro-phase separation. Random incorporation of Perylene diimide in P(NDI2OD-T2) will help to reduce the self-aggregation and form desirable microphase separation.

Naphthalene diimide based polymers specially P(NDI2OD-T2) is very promising material, but still, their electron mobility is lower than PCBM. The electron mobility of the polymer can be improved by the incorporation of PCBM into the polymer via covalent attachment. Small incorporation of PCBM can be done by random polymerization, and it will not affect the solubility of the polymer. Improved electron mobility will help to enhance the power conversion efficiency of the polymers. Small incorporation of PCBM also prevents the large-scale phase separation of the PCBM.

NDI based polymers also show promising properties in the field of energy generation. These polymers also can be utilized for supercapacitors devices. The last two working chapters of this thesis work explore the electrochemical properties of the polymers in different electrolytes. Aqueous electrolyte is a very good system for the environment, but it has a small potential window which limits its application. Organic electrolyte will cover large potential window which will be very useful for devices. It also explores the effect of electron withdrawing group in the polymer backbone which will enhance the electrochemical properties.

Random and alternate copolymer strategy was explored in the last working chapter, in which new copolymers were designed, and utilized in flexible supercapacitor device. Chapter 6 gives an overall summary and conclusion of this thesis work.

1.4 References

(1) Mohtasham, J. *Energy Procedia.* **2015,** *74*, 1289-1297.

(2) Morton, O. *Nature* **2006**, *443*, 19-22.

(3) Panwar, N. L.; Kaushik, S. C.; Kothari, S. *Renew. Sust. Energ. Rev.* **2011**, *15*, 1513-1524

(4) Long, H. L.; Li, X. B.; Wang, H.; Jia, J. D. *Renew. Sust. Energ. Rev.* **2013**, *26*, 344-352.

(5) Shortall, R.; Davidsdottir, B.; Axelsson G. *Renew. Sust. Energ. Rev.* **2015**, *44*, 391-406.

(6) Becquerel, A. E. *C. R. Acad. Sci.* **1839**, *9*, 145-149.

(7) Becquerel, A. E. *C. R. Acad. Sci.* **1839**, *9*, 561-567.

(8) Fritts, C. E. *Am. J. Sci.* **1883**, *26*, 465-472.

(9) Zhao, J.; Wang, A.; Green, M. A.; Ferrazza, F. *Appl. Phys. Lett*, **1998**, *73*, 1991-1993.

(10) Badawy, W.A. *J. Adv. Res*. **2015**, n*6*, 23-132.

(11) O'Regan, B.; Grätzel, M. *Nature*, **1991**, *353*, 737-739.

(12) Günes, S.; Neugebauer, H.; Sariciftci, N. S. *Chem. Rev.* **2007**, *107*, 1324-1338.

(13) Hoppe, H.; Sariciftci, N. S. *J. Mater. Res.* **2004**, *19*, 1924-1945.

(14) Forrest, S. R. *MRS bulletin* **2005**, *30*, 28-32

(15) Heremans, P.; Arkhipov, V. I.; Bassler, H. *Appl. Phys. Lett.* **2003**, *82*, 4605-4607.

(16) Chiechi, R. C.; Havenith, R. W. A.; Hummelen, J. C.; Koster, L. J. A.; Loi, M. A. *Materials Today* **2013**, *16*. 281-289.

(17) Bässler, H.; Köhler, A. *Top. Curr. Chem.* **2012**, *312*, 1-65.

(18) Zhu, X. Y.; Yang, Q.; Muntwiler, M. *Acc. Chem. Res*. **2009**, *42*, 1779-1787.

(19) Wetzelaer, G.-J. A. H.; Blom, P. W. M. *NPG Asia Mater.* **2014**, *6*, e110.

(20) Kolhe, N. B.; Shinde, S.; Saibal, B.; Asha, S. K. *Org. Photonics Photovolt*. **2015**, *3*, 71-100.

(21) Marks, R N.; Halls, J. J. M.; Bradley, D. D. C.; Friend, R. H.; Holmes, A, B, *J. Phys.: Condens. Matter.* **1994**, *6*, 1379-1394.

(22) Lin, Y.; Li, Y. Zhan, X. *Chem. Soc. Rev.* **2012**, *41*, 4245-4272.

(23) Tang, C. W. *Appl. Phys. Lett.* **1986**, *48*, 183-185.

(24) Yu, G.; Gao, J.; Hummelen, J. C.; Wudl, F.; Heeger, A. J. *Science* **1995**, *270*, 1789-1791.

(25) Li, S.; Ye, L.; Zhao, W.; Yan, H.; Yang, B.; Liu, D.; Li, W.; Ade, H.; Hou, J. *J. Am. Chem. Soc***. 2018,** (in press). DOI**:** 10.1021/jacs.8b02695.

(26) Che, X.; Li, Y.; Qu, Y.; Forrest, S. R. *Nature Energy* **2018**, *3*, 422–427.

(27) Benten, H.; Mori, D.; Ohkita, H.; Ito,S. *J. Mater. Chem. A*, **2016**, *4*, 5340-5365.

(28) Zaumseil, J.; Sirringhaus, H. *Chem. Rev.* **2007**, *107*, 1296-1323.

(29) Wen, Y.; Liu, Y. *Adv. Mater.* **2010**, *22*, 1331-1345.

(30) Zhang, X.-H.; Domercq, B.; Kippelen, B. *Appl. Physc. Lett.* **2007**, *91*, 092114.

(31) Yan, H.; Chen, Z.; Zheng, Y.; Newman, C.; Quinn, J. R.; Dötz, F.; Kastler, M.; Facchetti, A. *Nature* **2009**, *457*, 679-686.

(32) Fabiano, S.; Chen, Z.; Vahedi, S.; Facchetti, A.; Pignataro, B.; Loi, M. A. *J. Mater. Chem.* **2011**, *21*, 5891-5896.

(33) Moore, J. R.; Seifried, S. A.; Rao, A.; Massip, S.; Watts, B.; Morgan, D. J.; Friend, R. H.; Mcneill, C. R.; Sirringhaus, H. *Adv. Energy Mater.* **2011**, *1*, 230-240.

(34) Schubert, M.; Dolfen, D.; Frisch, J.; Roland, S.; Steyrleuthner, R.; Stiller, B.; Chen, Z.; Scherf, U.; Koch, N.; Facchetti, A.; Neher, D. *Adv. Energy Mater.* **2012**, *2*, 369-380.

(35) Zhou, N.; Lin, H.; Lou, S. J.; Yu, X.; Guo, P.; Manley, E. F.; Loser, S.; Hartnett, P.; Huang, H.; Wasielewski, M. R.; Chen, L. X.; Chang, R. P. H.; Facchetti, A.; Marks, T. J. *Adv. Energy Mater.* **2014**, *4*, 1300785.

(36) Mori, D.; Benten, H.; Okada, I.; Ohkita, H.; Ito, S. *Adv. Energy Mater*. **2014**, *4*, 1301006.

(37) Zhou, E.; Nakano, M.; Izawa, S.; Cong, J.; Osaka, I.; Takimiya, K.; Tajima, K. *ACS Macro Lett.* **2014**, *3*, 872-875.

(38) Kang, H.; Kim, K. H.; Choi, J.; Lee, C.; Kim, B. J. *ACS Macro Lett.* **2014**, *3*, 1009-1014.

(39) Jung, J. W.; Jo, J. W.; Chueh, C. C.; Liu, F.; Jo, W. H.; Rusell, T. P.; Jen, A. K. Y. *Adv. Mater.* **2015**, *27*, 3310-3317.

(40) Huang, H.; Zhou, N.; Ortiz, R. P.; Chen, Z.; Loser, S.; Zhang, S.; Guo, X.; Casado, J.; Navarrete, J. T. L.; Yu, X.; Facchetti, A.; Marks, T. J. Adv. Funct. Mater. **2014**, *24*, 2782-2793.

(41) Poullikkas, A. *Renew. Sust. Energ. Rev.* **2013**, *27*, 778-788

(42) Linden, David; Reddy, Thomas B. *Handbook of Batteries,* **2002,** New York: McGraw-Hill. p. 23

(43) Ruetschi, P. *J. Power Sources* **2004**, *127*, 33-44

(44) Goodenough, J. B.; Park, K. S. *J. Am. Chem. Soc.* **2013**, *135*, 1167-1176

(45) Kanewskii, L. S.; Dubasova, V. S. *Russ. J. Electrochem.* **2005**, *41*, 1-16

(46) Tahil, W. "The Trouble with Lithium: Implications of Future PHEV Production for Lithium Demand", **2006**, http://www.evworld.com/library/lithium_shortage.pdf

(47) Conway, B. E. *Electrochemical Supercapacitors: Scientific Fundamentals and Technological Applications.* **1999**, New York, Kluwer-Plenum.

(48) Burke, A. *J. Power Sources.* **2000**, *91*, 37-50.

(49) Kotz, R.; Carlen, M.; *Electrochim. Acta* **2000**, *45*, 2483-2498.

(50) Halper, M. S.; Ellenbogen, J. C. "Supercapacitors: A Brief Overview", **2006**, MITRE Nanosystems Group, http://www.mitre.org/tech/nanotech.

(51) Arico, A. S.; Bruce, P.; Scrosati, B.; Tarascon, J. M.; Schalkwijk, W. V. *Nature Mater.* **2005**, *4*, 366-377.

(52) Frackowiak, E; Beguin, F. *Carbon* **2001**, *39*, 937-950.

(53) Candelaria, S. L.; Shao, Y.; Zhou, W.; Li, X.; Xiao, J.; Zhang, J. G.; Wang, Y.; Liu, J.; Li, J.; Cao, G. *Nano Energy* **2012**, *1*, 195-220

(54) Gomez, A. G.; Miles, P.; Centeno, T. A.; Rojo, J. M. *Electrochim. Acta* **2010**, *55*, 8539

(55) Wang, J.; Zhang, S. Q. *J. Electrochem. Soc.* **2001**, *148*, 75-77

(56) Kim, S. J.; Hwang, S. W.; Hyun, S. H. *J. Mater. Sci.* **2005**, *40*, 725-731

(57). Calvo, E. G.; Ania, C. O.; Zubizarreta, L.; Menendez, J. A.; Arenillas, A. *Energ. Fuels* **2010**, *24*, 3334

(58) Fang, B.; Binder, L. *J. Power Sources* **2006**, *163*, 616-622.

(59) An, K. H.; Kim, W. S.; Park, Y. S.; Choi, Y. C.; Lee, S. M.; Chung, D. C.; Bae, D. J.; Lim, S. C.; Lee, Y. H. *Adv. Mater.* **2001**, *13*, 497-500

(60) Bordjiba, T.; Mohamedia, M.; Dao, L. H. *Adv. Mater.* **2008**, *20*, 815-819.

(61) Pico, F.; Rojo, J. M. *J. Electrochem. Soc.* **2004**, *151*, 831-837.

(62) Niu, C.; Sichel, E. K.; Hoch, R.; Moy, D.; Tennet, H. *Appl. Phys. Lett.* **1997**, *70*, 1480-1482.

(63) Du. C. S.; Yeh, J. Pan, N. *Nanotech.* **2005**, *16*, 350-353.

(64) Frackowiak, E.; Metenier, K.; Bertagna, V.; Beguin, F. *Appl. Phys. Lett.* **2000**, *77*, 2421-2423.

(65) Zheng, J. P.; Jow, T. R. *J. Electrochem. Soc.* **1995**, *142*, L6-L8.

(66) Zheng, J. P.; Cygan, P. J.; Jow, T. R. *J. Electrochem. Soc*. **1995**, *142*, 2699-2703.

(67) Talbi, H.; Just, P. E.; Dao, L. H. *J. Appl. Electrochem.* 2003, *33*, 465-473.

(68) Sivakkumar, S. R.; Saraswathi, R. *J. Power Sources* **2004**, *137,* 322-328.

(69) Sivakkumar, S. R.; Kim, W. J.; Choi, J. A.; Macfarlane, D. R.; Forsyth, M.; Kim, D. W. *J. Power Sources* **2007**, *171*, 1062-1068.

(70) Li, H. L.; Wang, J. X.; Chu, Q. X.; Wang, Z.; Zhang, F. B.; Wang, S. C. *J. Power Sources* **2009**, *190*, 578-586.

(71) Imani, A.; Farzi, G. *J. Mater. Sci. Mater. Electron.* **2015**, *26*, 7438-7444.

(72) Niu, Z. Q.; Luan, P. S.; Shao, Q.; Dong, H. B.; Li, J. Z.; Chen, J.; Zhao, D.; Cai, L.; Zhou, W. Y.; Chen, X. D.; Xie, S. *Energy Environ. Sci.* **2012**, *5*, 8726-8733.

(73) Mi, H. Y.; Zhang, X. G.; An, S. Y.; Ye, X. G.; Yang, S. D. *Electrochem. Commun.* **2007**, *9*, 2859-2862.

(74) Chau, T.; Singhal, R.; Lawrence, D.; Kalra, V. *J. Power Sources* **2015**, *293*, 373-379.

(75) Shen, K. W.; Ran, F.; Zhang, X. X.; Liu, C.; Wang, N. J.; Niu, X. Q.; Liu, Y.; Zhang, D. J.; Kong, L. B.; Kang, L.; Chen, S. W. *Synth. Met.* **2015**, *209*, 369-376.

(76) Khosrozadeh, A.; Xing, M.; Wang, Q. *Appl. Energy* **2015**, *153*, 87-93.

(77) Sun, H.; She, P.; Xu, K. L.; Shang, Y. X.; Yin, S. Y.; Liu, Z. N. *Synth. Met.* **2015**, *209*, 68-73.

(78) Wang, H. L.; Hao, Q. L.; Yang, X. J.; Lu, L. D.; Wang, X. *Electrochem. Commun.* **2009**, 11, 1158-1161.

(79) Gomez, H.; Ram, M. K.; Alvi, F.; Villalba, P.; Stefanakos, E.; Kumar, A. *J. Power Sources* **2011**, *196*, 4102-4128.

(80) Wang, S. Y.; Ma, L.; Gan, M. Y.; Fu, S. N.; Dai, W. Q.; Zhou, T.; Sun, X. W.; Wang, H. H.; Wang, H. N. *J. Power Sources* **2015**, *299*, 347-355.

(81) Cong, H. P.; Ren, X. C.; Wang, P.; Yu, S. H. *Energy Environ. Sci.* **2013**, *6*, 1185-1191.

(82) Zhang, K.; Zhang, L. L.; Zhao, X. S.; Wu, J. S. *J. Mater. Chem. A* **2010**, *22*, 1392-1401.

(83) Yang, Q. H.; Hou, Z. Z.; Huang, T. Z. *J. Appl. Polym. Sci.* **2015**, *132*, 41615 (1-5).

(84) Li, M.; Yang, L. L. *J. Mater. Sci. Mater. Electron.* **2015**, *26*, 4875-4879.

(85) Xu, J.; Wang, D. X.; Fan, L. L.; Yuan, Y.; Wei, W.; Liu, R. N.; Gu, S. J.; Xu, W. L. *Org. Electron.* **2015**, *26*, 292–299.

(86) An, K. H.; Jeon, K. K.; Heo, J. K.; Lim, S. C.; Bae, D. J.; Lee, Y. H. *J. Electrochem. Soc.* **2002**, *149*, A1058-A1062.

(87) Song, H. J.; Cai, K. F.; Wang, J.; Shen, S. *Synth. Met.* **2016**, *211*, 58-65.

(88) Simon, P.; Gogotsi, Y. *Nat. Mater.* **2008**, *7*, 845-854.

(89) Snook, G. A.; Kao, P.; Best, A. S. *J. Power Sources* **2011**, *196*, 1-12.

(90) Nyholm, L.; Nystrom, G.; Mihranyan, A.; Stromme, M. *Adv. Mater.* **2011**, *23*, 3751-3769.

(91) Laforgue, A.; Simon, P.; Sarrazin, C.; Fauvarque, J. F. *J. Power Sources* **1999**, *80*, 142-148.

(92) Gnanakan, S. R. P.; Rajasekhar, M.; Subramania, A. *Int. J. Electrochem. Sci.* **2009**, *4*, 1289-1301.

(93) Gnanakan, S. R. P.; Muruganantham, N.; Subramania, A. *Polym. Adv. Technol.* **2011**, *22*, 788-793.

(94) Patil, B. H.; Jagadale, A. D.; Lokhande, C. D. *Synth. Met.* **2012**, *62*, 1400-1405.

(95) Wang, Y.; Guo, J.; Wang, T. F.; Shao, J. F.; Wang, D.; Yang, Y. W. *Nanomaterials* **2015**, *5*, 1667-1689.

(96) Das, T. K.; Prusty, S. *Polym. Plast. Technol.* **2012**, *51*, 1487-1500.

(97) Yang, L. F.; Shi, Z.; Yang, W. H. *Electrochim. Acta* **2015**, *153*, 76-82.

(98) Wang, G. P.; Zhang, L.; Zhang, J. J. *Chem. Soc. Rev.* **2012**, *41*, 797-828.

(99) Estrada, L. A.; Liu, D. Y.; Salazar, D. H.; Dyer, A. L.; Reynolds, J. R. *Macromolecules* **2012**, *45*, 8211-8220.

(100) DiCarmine, P. M.; Schon, T. B.; McCormick, T. M.; Klein, P. P.; Seferos, D. S. *J. Phys. Chem. C* **2014**, *118*, 8295-8307.

(101) Yuksel, R.; Cevher, S. C.; Cirpan, A.; Toppare, L.; Unalan, H. E. *J. Electrochem. Soc.* **2015**, *162*, A2805-A2810.

Chapter 2

Improved All-Polymer Solar Cell Performance of n-type Naphthalene Diimide-bithiophene P(NDI2OD-T2) Copolymer by Incorporation of Perylene Diimide as Co-acceptor

This chapter has been adapted from the following publication.

Sandeep Sharma, Nagesh B. Kolhe, Vinay Gupta,* Vishal Bharti, Abhishek Sharma, Ram Datt, Suresh Chand, S. K. Asha*. *Macromolecules 2016, 49, 8113−8125*.

2.1. **Introduction**

Extensive research has been done on the naphthalene diimide (NDI) based polymers as active layer materials for energy harvesting. They have high electron affinity, good absorption, thermal and photochemical stability, and π-stacking behavior which facilitates favorable solid-state packing.[1-3] Particularly, the low band gap core-substituted NDI donor-acceptor polymers comprising of bithiophene and selenophene donors have attracted much attention due to their high electron mobility in OFET and high PCE efficiency in solar cells.[4-17] As was discussed in the previous chapter, P(NDI2OD-T2) polymer is extensively utilized in all-PSCs and OFET applications due to its desirable photo-physical and semiconducting properties. [4, 16] It exhibited properties like high electron mobility > 0.85 $cm^2V^{-1}s^{-1}$ in OFET, high PCE efficiency > 5% in all-PSCs, solution processability, high crystalline nature and light absorption capability near-visible and infrared region.[4, 5, 9] However, it exhibited strong tendency to form aggregates in specific organic solvents that resulted in large-scale phase separation instead of the desirable pure donor / acceptor micro-phase separation.[17] Consequently, the earlier reports on the all-PSC measurements of P3HT/P(NDI2OD-T2) blend showed very low device efficiency value (PCE, 0.2%).[18-19] Later studies showed that the aggregation in P(NDI2OD-T2) could be suppressed significantly in the early stage of film formation by using more polar aromatic solvents.[20] Indeed, the solar cell devices prepared from such non-aggregated solution showed improved PCE due to good intermixing of donor and acceptor components, thereby efficiently harvesting photogenerated excitons at donor-acceptor interface. Beyond the solvent induced morphological control, the structural variations also plays a vital role in improving the blend morphology, bulk crystallinity, molecular orientation, highest occupied and lowest unoccupied molecular orbital (HOMO-LUMO) energy level and charge transport properties of polymer. Random copolymerization is another promising design strategy utilized for synthesis of NDI containing acceptor polymers which showed significant improvement in the PCE in all-PSCs. NDI based random copolymers were synthesized either by varying two different donor monomers with NDI [21-23] or by varying the acceptor comonomer (such as PDI) with NDI along with a common donor co component. [7, 24, 25] Recent reports on the synthesis of NDI based random copolymers involved the use of donor monomers such as bithiophene (BT) and thiophene (T), [21] thiophene (T) and selenophene (Se), [22] thieno[3,2-b]thiophene (TT) and thienylene-vinylene-thienylene (TVT). [23] Li et al. demonstrated great improvement in the PCE of P(NDI2OD-T2) polymer by modulating its crystallinity by replacing a certain amount of bithiophene (BT) units with single thiophene (T) (shown in **Figure 2.1**). [21] One of the composition containing

10 mole % (PNDI-T10) showed optimal bulk crystallinity and miscibility with donor PTB7-Th, which lead to PCE as high as 7.6% after solvent annealing.

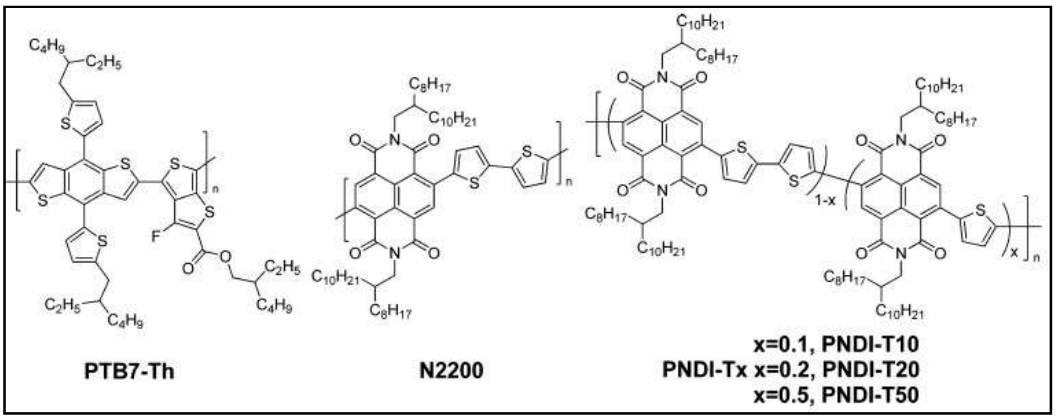

Figure 2.1.Chemical structure of donor-acceptor polymer (Adapted from ref. 21)

The use of two mixed acceptors NDI and PDI in random copolymer along with common donor also showed promising enhancement in the PCE. Particularly Jenekhe *et al*. demonstrated enhancement of PCE up to 6.3 % in NDI-selenophene copolymer by synthesizing NDI-selenophene/PDI-selenophene random copolymers with different incorporation of PDI into copolymer backbone (shown in **Figure 2.2**).[7] These NDI-selenophene/PDI-selenophene random copolymers are one of the best reported n-type copolymers which showed optimum bulk crystallinity and compatible blend morphology with donor polymer that has resulted in improved PCE in the solar cell.

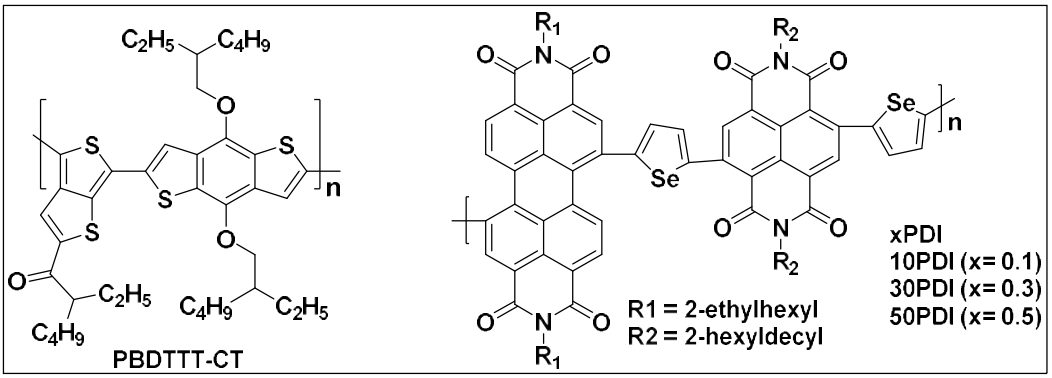

Figure 2.2 Chemical structure of donor-acceptor polymer (Adapted from ref. 7).

Most of the aforementioned reports demonstrated the importance of systematic tuning of polymer bulk crystallinity via optimizing the different comonomer compositions in random copolymers. Bulk crystallinity is one of the key factors that are responsible for the bulk morphology of donor: acceptor blend in all-PSCs.[21-23] The optimum crystallinity of acceptor

polymer is highly desirable to ensure proper intermixing with donor polymer in the blend to achieve good D/A microphase separation.

Inspired by these strategies, we have synthesized a series of new *n*-type NDI-bithiophene/PDI-bithiophene random copolymers (NDI-Th-PDI*x*) by incorporating varying amounts of perylene diimide (PDI) as co-acceptor along with NDI. The effect of random copolymer compositions on their energy level, optical properties, bulk crystallinity, blend morphology, charge transport and all-PSC performance was investigated.

The all-PSCs performance of the newly synthesized random copolymers was investigated in combination with PTB7 or PTB7-Th as the donor polymer. The device efficiency was compared with that of P(NDI2OD-T2) polymer as reference (Shown in **Scheme 2.1**). The bulk charge transport properties were measured by space charge limited current (SCLC) method, the surface morphology of blends was investigated by atomic force microscopy (AFM) and thin film organization using X-ray diffraction (XRD) and photoluminescence (PL) measurements.

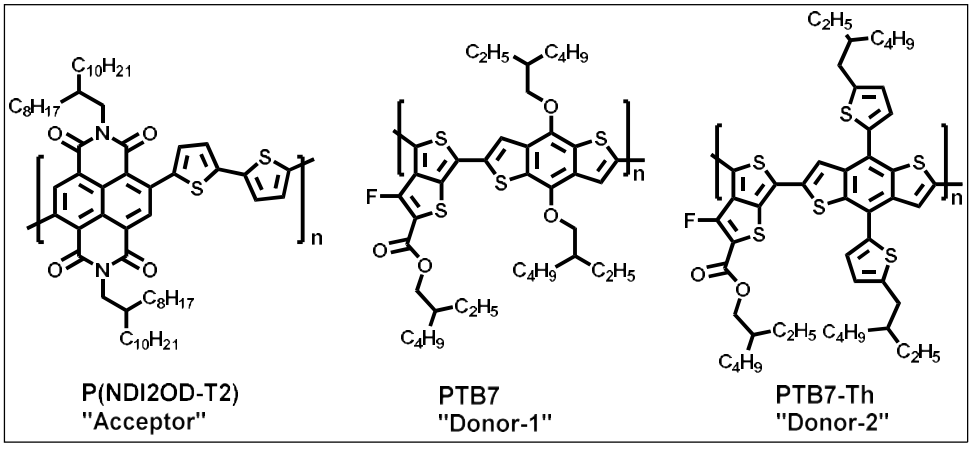

Scheme 2.1 Chemical structure of P(NDI2OD-T2) acceptor and PTB7 / PTB7-Th donor polymers.

2.2. Experimental Section

2.2.1. Material

1,4,5,8-Naphthalenetetracarboxylicdianhydride (NTCDA), 3,4,9,10- perylene tetracarboxylicdianhydride (PTCDA), 5,5'-bis (trimethylstannyl)-2,2'-bithiophene 97%, 2-octyldodecanol, 2-ethylhexylamine, bis(triphenylphosphine) palladium (II) dichloride ($Pd(Ph_3)_2Cl_2$) were purchased from Sigma Aldrich and used without further purification. The donor polymers PTB7 and PTB7-Th and electron transport layer PFN (poly [(9,9-bis(3′-

(N,N-dimethylamino)propyl)-2,7-fluorene)-alt-2,7-(9,9–dioctylfluorene)] used in all-polymer solar cell study were purchased from 1-Materials, Canada.

2.2.2. Measurements

^{1}H NMR and ^{13}C NMR spectra were recorded using 200 and 400 MHz Brucker NMR spectrophotometer in $CDCl_3$ containing small amounts of TMS as internal standard. Mass spectra were recorded on Voyager-De-STR MALDI-TOF (Applied Biosystems, Framingham, MA, USA) equipped with 337 nm pulsed nitrogen laser used for desorption and ionization. The molecular weights of polymers were determined using gel permeation chromatography (GPC). GPC measurements were carried on a Thermo Quest (TQ) GPC at 25 ^{o}C using chloroform as the mobile phase. The analysis were carried out at a flow rate of 1 mL/min using a set of five μ-Styragel HT columns (HT-2 to HT-6) and a refractive index (RI) detector. Columns were calibrated with polystyrene standards and the molecular weights are reported with respect to polystyrene. FT-IR spectra were recorded with ATR mode using Brucker α-T spectrophotometer in the range of 4000 to 400 cm^{-1}. Absorption spectra were recorded using Perkin Elmer Lambda -35 UV-Vis spectrophotometer. Thermogravimetric analysis (TGA) was performed using a TGA Q 5000 thermogravimetric analyser. Samples were run from 40 to 900 °C with a heating rate of 10 °C/min under nitrogen. DSC (differential scanning calorimetry) measurements were performed on TA Q10 differential scanning calorimeter at a heating rate of 10 °C/min under nitrogen atmosphere. The thin film X-ray diffraction data were recorded using a Rigaku model Dmax-2500 diffractometer using Cu Kα (1.54 Å) emission, and the spectra were recorded in the range of (2θ) 2–50°. Electrochemical behavior of NDI polymers were analyzed by cyclic voltammetry by using BAS-Epsilon potentiostat. The surface morphology of active layers of actual bulk-heterojunction (BHJ) solar cells were characterized by AFM imaging technique using the Agilent 5500 AM scanning probe microscopy in tapping mode using Si probe. PL Measurements were carried out on PTi quanta Master-400 fluorescence spectrometer. Solar cell device fabrication work was carried out at CSIR-NPL, New Delhi.

2.2.3. Sample Preparation

For the UV-Vis absorption studies, thin films were prepared by dissolving polymer in chloroform (10 mg/ml) and spin coating (600 rpm/60sec) on quartz plates. For the XRD analysis, films were prepared by drop-casting the highly concentrated (20 mg/ml) polymer solution in chloroform on glass slide followed by thermal annealing at 160 ^{o}C for 10 minutes.

Thin film samples of the blend donor:acceptor polymers for PL and XRD measurements were prepared by mixing the donor PTB7-Th and acceptors P(NDI2OD-T2) / NDI-Th-PDI*x* in 1.3:1 (w/w) ratio in chloroform under similar conditions as that for the photovoltaic device fabrication.

2.2.4. Fabrication and Characterization of the Photovoltaic Cells

PTB7 or PTB7-Th as donor and P(NDI2OD-T2) and NDI-Th-PDI*x* (*x* = 15, 20, 30 mole % of PDI) acceptors were used. PTB7 or PTB7-Th was blended with each of the four acceptors separately in chloroform, and stirred at 40 °C for more than 24 h in a glovebox. The optimized donor:acceptor (D:A) ratio was 1.3:1 (w/w) and total concentrations of (D+A) in chloroform solution was ~12 mg/ml. The optimized volume fraction of 1,8-diiodooctane (DIO) additives to (D+A) in chloroform solution was 1.25 vol%. PFN (2 mg/ml) was prepared in methanol in the presence of a small amount of acetic acid (2 µl ml^{-1}). Preparation of ZnO sol-gel was done as follows. Zinc acetate dihydrate [$Zn(CH_3COO).2H_2O$] (Aldrich, 99.9%) with 0.1 M concentration was first dissolved in anhydrous ethanol [CH_3CH_2OH] (99.5 + % Aldrich) and vigorously stirred for 2–3 h at 80 °C. Subsequently, ethanolamine was added to the solution as sol stabilizer followed by thorough mixing process with magnetic stirrer for 12-15 h at 60 °C. Inverted type all polymer solar cells were fabricated using an indium tin oxide (ITO)/ZnO/PFN/active layer/MoO_3/Al structure. ITO-coated glass substrates were subjected to ultrasonication in soap, deionized water, acetone and in isopropyl alcohol. The substrates were then dried for several hours in an oven at 120 °C. The ITO substrates were treated with UV-ozone before ZnO sol-gel was spin-coated on the ITO-coated glass substrate with 3000 rpm for 60 sec. The ZnO films were annealed at 200 °C for 1 h in the air. The thickness of ZnO film was approximately 30 nm, as determined by a profilometer. PFN was spin-coated on ITO at 2,000 rpm for 60 sec and baking for 15 min at 80 °C in N_2 glove box. Then, each active blending solution was spin-casted onto an ITO/ZnO/PFN substrate at 2000 rpm for 120 s. The final thickness of each films was 100~110 nm. Then, MoO_3 (~ 10 nm) was thermally deposited in high vacuum (~8 x 10^{-7} torr). Finally Al (~100 nm) was deposited in same high vacuum (~8 x 10^{-7} torr), over the MoO_3 through shadow mask. The active area of the devices was 10 mm^2 in all the cases.

The photovoltaic performance of the devices was characterized using a solar simulator (SCIENCTECH SS150 Solar Simulators) with an air-mass (AM) 1.5 G filter. The intensity of the solar simulator was carefully calibrated using an AIST-certified silicon photodiode. The current-voltage behavior was measured using a Keithley 2400 SMU. EQE spectra of

fabricated devices were measured using a Keithley 2600 source meter and a CEP-25ML Spectral Response Measurement System which shines light with AM 1.5 G spectral distribution and calibrated using an AIST-certified silicon photodiode to an intensity of 1000 W/m^2.

2.2.5. SCLC Measurement

The hole and electron mobilities of all-polymer blends and polymer neat films were measured by the space-charge-limited current (SCLC) method using hole only configuration ITO/MoO_3 (10 nm)/active layer (~100 nm)/Au (200 nm) structure and electron only configuration ITO/ZnO (30 nm)/active layer (~100 nm)//Al (100 nm). In both the cases, active layer was spin-casted exactly the same way as it was done in the case of photovoltaic cells discussed above. Current-voltage measurements in the range of 0-10 V were taken, and the results were fitted to a space-charge-limited function with active area of the devices as 10 mm^2. The carrier mobility was extracted by fitting the J−V curves in the near quadratic region according to the modified Mott−Gurney equation: [26]

$$J(V) := \frac{9}{8}\varepsilon \cdot \mu \cdot \left(\frac{V^2}{L^3}\right) \cdot e^{\left(0.89 \cdot \beta \cdot \sqrt{\frac{V}{L}}\right)}$$

Where J is the current density, ε_0 (8.85×10^{14} F/cm) is the permittivity of free space, ε is the dielectric constant of the organic semiconductor (assumed to be 3.2), μ is the zero-field mobility, V is the applied voltage, L is the thickness of active layer, and β is the field activation factor.

2.2.6. Synthesis of NDI and PDI Monomers

I) N, N'-Bis (2-octyldodecyl)-2,6-dibromo-1,4,5,8-naphthalenediimide (NDI-2OD-Br_2)

2,6-Dibromo-1,4,5,8-naphthalenetetracarboxylic acid dianhydride (5 g, 11.73 mmole) was suspended in 25 mL of glacial acetic acid and stirred for a short period of time to get a homogeneous dispersion which was followed by addition of 2-octyldodecyl amine (13.96 g, 46.94 mmol). The reaction mixture was stirred and refluxed (at 120 °C) to complete dissolution for 3h and cooled to room temperature. The reaction mixture was concentrated under reduced pressure to about $1/10^{th}$ of original volume and then precipitated into methanol to yield reddish brown powder that was filtered and dried under vacuum. The crude product was column purified by using pet ether/ethyl acetate solvent system and again recrystallized from 1:1 mixture of hexane and acetone to get yellow powder of pure compound. Yield = 1.8

g (15 %, by considering 2, 6 isomer). Melting point (85-86 °C); ^{1}H NMR (200 MHz, $CDCl_3$) δ ppm: 8.98 (s, 2H, aromatic), 4.15 (d, 4H), 1.97 (m, 2H), 1.22, (m, 64 H), 0.86 (m, 12H). ^{13}C NMR, $CDCl_3$, δ ppm: 161.16, 161.00, 139.14, 128.36, 127.73, 125.27, 124.06, 45.43, 36.44, 31.90, 31.87, 31.53, 30.01, 29.62, 29.58, 29.52, 29.33, 26.32 29.28, 22.67, 14.11. FTIR (ATR, cm^{-1}): 3050, 2920, 2851,1707, 1652, 1557, 1432, 1363, 1308, 1230, 1199, 990; MALDI-TOF MS (Calcd m/z 985.06); Found m/z = 985.345. Anal. Calcd. for $C_{54}H_{84}N_2O_4Br_2$: C, 65.84; H, 8.60; N, 2.84. Found C, 66.09; H, 8.67; N, 2.27.

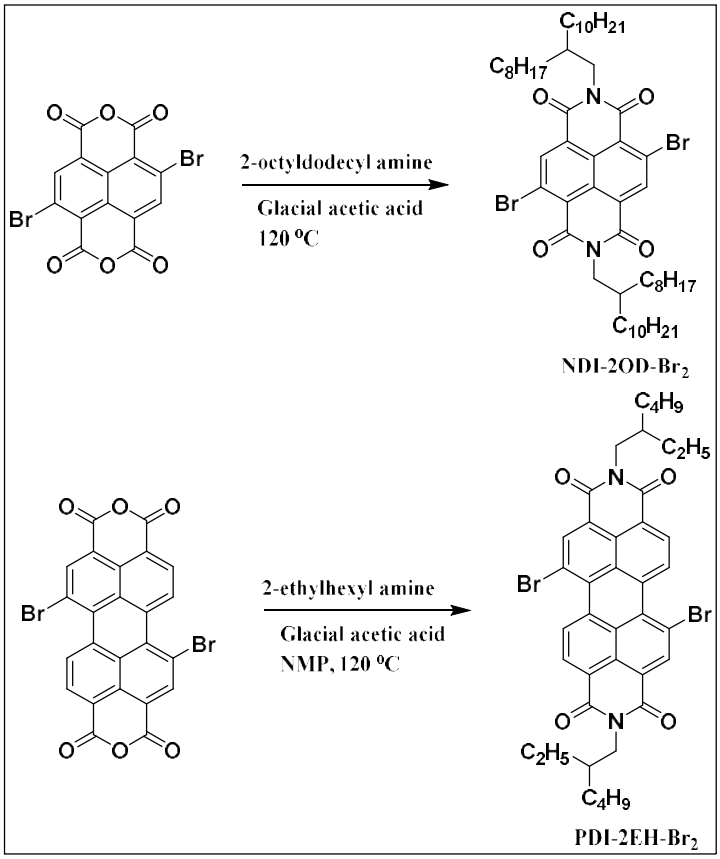

Scheme 2.2. Synthesis of monomers.

II) N, N'-Bis (2-ethylhexyl)-1,7-dibromo -3,4,9,10-perylene tetracarboxylicdianhydride(PDI-2EH-Br_2)

1,7-Dibromo-3,4,9,10-peryleneetetracarboxylic acid dianhydride (3 g, 5.61 mmole) was suspended in the mixture of 20 mL glacial acetic acid and 60 mL N-methyl pyrrolidine and purged with argon. The mixture was stirred and heated to 60 °C for 20 minute to get a homogeneous dispersion which was followed by addition of 2-ethylhexyl amine (2.11 g, 16.36 mmol). The reaction temperature was raised to 120 °C. After 12 hours, the reaction mixture was cooled to room temperature and poured in to 500 mL water. The water

suspension was stirred for 2 hours and filtered on Buchner funnel under vacuum. The residue was washed with large amount of water and dried under vacuum. The crude product was column purified by using pet ether/ethyl acetate (1:6) and pet ether/DCM (50:50) solvent system to get red powder of pure compound. Yield = 3.0 g (29 %), Melting point (225-227°C). ^{1}H NMR (400 MHz, $CDCl_3$) δ ppm: 9.35 (d, 2H,), 8.80 (s, 2H), 8.57 (d, 2H), 1.92 (m, 2H), 1.35, (m, 16 H), 0.95 (m, 12H). ^{13}C NMR, $CDCl_3$, δ ppm: 163.09, 162.60, 137.96, 132.56, 129.91, 129.01, 128.32, 126.80, 123.04, 122.60, 120.76, 44.42, 37.91, 30.74, 28.66, 24.00, 23.05,14.11, 10.60. FTIR (ATR, cm^{-1}): 2954, 2923, 2857, 1699, 1658, 1586, 1501, 1432, 1386, 1325, 1232, 1181, 1146, 1094, 857, 808, 739, 678; MALDI-TOF MS (Calcd m/z 772.56); Found m/z = 773.98, 795.96 (M+ Na^{+}). Anal. Calcd. for $C_{40}H_{40}N_2O_4Br_2$: C, 62.19; H, 5.22; N, 3.63. Found C, 62.28; H, 5.05; N, 3.34.

2.2.7. Synthesis of Homo and Random Copolymers

I) Poly{[N,N′-bis(2-octyl-dodecyl)-1,4,5,8-naphthalenedicarboximide-2,6-diyl]-alt-5,5′-(2,2′-bithiophene)}, P(NDI2OD-T2)

NDI-2OD-Br_2 (0.4 g, 0.406 mmole) and 5,5'-bis (trimethylstannyl)-2,2'-bithiophene (0.199 g, 0.406 mmole) were taken in Schlenk tube under N_2 atmosphere. Dry toluene 18 mL was added in the tube followed by purging with nitrogen for half-hour. Bis(triphenylphosphine) palladium (II) dichloride ($Pd(Ph_3)_2Cl_2$) (15 mg, 0.0211 mmol) was added to the tube quickly by opening rubber septa and the whole mixture was degassed by four freeze-vacuum-thaw cycles. The reaction mixture was stirred at 90-95 °C for 3 days. Bromobenzene (0.2 mL) was then added and reaction mixture was further stirred at 90-95 °C for 12 hours. Upon cooling to room temperature, a solution of potassium fluoride (1 g) in 2 mL water was added and stirred for 2 hours. The reaction mixture was extracted with chloroform (250 mL x 3). The organic layer was washed with water, dried over anhydrous sodium sulfate and concentrated on a rotary evaporator. The obtained residue was dried in vacuum oven and subjected to a Soxhlet extraction with acetone (48 hours) and chloroform (12 hours). Half of the chloroform was evaporated on rota and concentrated polymer solution was precipitated in 500 mL methanol, stirred for 2 hours, filtered on Buchner funnel, washed with plenty of methanol and dried in vacuum. The polymer was obtained as a deep blue solid, Yield: 0.380 g (95 %) ^{1}H NMR (400 MHz, $CDCl_3$) δ ppm: 8.82-8.5 (br , 2H),7.33 (br, 4H), 4.11 (br, 4H), 1.98 (br, 2H), 1.24 (br, 64H), 0.84 (br, 12 H). (FTIR ATR, cm^{-1}): 2919, 2923, 2857, 1699, 1658, 1586, 1501, 1432, 1386, 1325, 1232, 1181, 1146, 1094, 857, 808, 739, 678; GPC: M*n*, 26.4 kDa; M*w*, 152 kDa; *Đ*, 5.7

II) Poly {([N N' -bis(2-octyldodecyl)-naphthalene-1,4,5,8- bis-(dicarboximide)-2,6-diyl]-alt-5,5 ′-2,2′-bithiophene)-ran-([N,N′-bis(2-ethylhexyl)-1,7-dibromo-3,4,9,10-perylenediimide]-alt-5,5 ′-2,2′-bithiophene)

All the random copolymers i,e NDI-Th-PDI15, NDI-Th-PDI30 and NDI-Th-PDI50 were synthesized using same procedure as that given for P(NDI2OD-T2), but with different mole ratios of NDI-2OD-Br_2 to PDI-2OD-Br_2.

III) NDI-Th-PDI15

NDI-Th-PDI15 was synthesized using (0.199 g,0.406 mmole) of 5,5'-bis (trimethylstannyl)-2,2'-bithiophene, (0.340 g, 0.345 mmole) of NDI-2OD-Br_2, (47 mg, 0.0609 mmole) of PDI-2EH-Br_2 and (15 mg, 0.0211 mmole) of $Pd(Ph_3)_2Cl_2$. Yield: 0.360 g (86 %) ^{1}H NMR (400 MHz, $CDCl_3$) δ ppm: 8.81, 8.5 (br, 2H naphthalene aromatic), 8.73 (br, 2H perylene aromatic), 8.37 (br, 4H perylene aromatic), 7.33 (br, 4H bithiophene), 4.10 (br, 8H), 1.97 (br, 4H), 1.24 (br, 80H), 0.84 (br, 24 H). (FTIR (ATR, cm^{-1}): 2919, 2851, 1703, 1662, 1571, 1574, 1433, 1377, 1305, 1243, 1188, 1053, 965, 928, 787, 717; GPC: M*n*, 16.4 kDa; M*w*, 60.7 kDa; *Đ*, 3.7.

IV) NDI-Th-PDI30

NDI-Th-PDI30 was synthesized using (0.250 g,0.508 mmole) of 5,5'-bis (trimethylstannyl)-2,2'-bithiophene, (0.350 g, 0.355 mmole) of NDI-2OD-Br_2, (117 mg, 0.152 mmole) of PDI-2EH-Br_2 and (18 mg, 0.0264 mmole) of $Pd(Ph_3)_2Cl_2$. Yield: 0.450 g (88 %) ^{1}H NMR (400 MHz, $CDCl_3$) δ ppm: 8.81 (br, 2H naphthalene aromatic), 8.71, 8.5 (br, 2H perylene aromatic), 8.36 (br, 4H perylene aromatic), 7.31 (br, 4H bithiophene), 4.11 (br, 8H), 1.97 (br, 4H), 1.23 (br, 80H), 0.84 (br, 24 H). (FTIR (ATR, cm^{-1}): 2919, 2852, 1702, 1660, 1572, 1513, 1433, 1401, 1306, 1243, 1186, 1174, 1043, 963, 927, 881, 853, 768, 713, 670; GPC: M*n*, 16.8 kDa; M*w*, 49.8 kDa; *Đ*, 2.9.

V) NDI-Th-PDI50

NDI-Th-PDI50 was synthesized using (0.250 g, 0.508 mmole) of 5,5'-bis (trimethylstannyl)-2,2'-bithiophene, (0.250 g, 0.254 mmole) of NDI-2OD-Br_2, (0.197 g, 0.254 mmole) of PDI-2EH-Br_2 and (18 mg, 0.0264 mmole) of $Pd(Ph_3)_2Cl_2$ Yield: 420 g (86 %) ^{1}H NMR (400 MHz, $CDCl_3$) δ ppm: 8.79 (br, 2H naphthalene aromatic), 8.69 (br, 2H perylene aromatic), 8.35 (br, 4H perylene aromatic), 7.33 (br, 4H bithiophene), 4.11 (br, 8H), 1.96 (br, 4H), 1.21 (br, 80H), 0.81 (br, 24 H). (FTIR (ATR, cm^{-1}): 2921, 2852, 1700, 1660, 1587, 1433, 1401,

1374, 1313, 1244, 1188, 1036, 860, 712, 755, 715, 761; GPC: M*n*, 12.6 kDa; M*w*, 32.4 kDa; *Đ*, 2.5.

2.3. Results and Discussion

2.3.1. Synthesis and Characterization

The poly{[N,N′-bis(2-octyl-dodecyl)-1,4,5,8-naphthalenedicarboximide-2,6-diyl]-alt-5,5′-(2,2′ bithiophene)} P(NDI2OD-T2) and its random copolymers NDI bithiophene / PDI bithiophene incorporating various mole percentage of perylenediimide (PDI) were synthesized by Stille coupling polymerization. The molecular structure of P(NDI2OD-T2) is depicted in **Scheme 2.1** and the synthesis of their monomers and random copolymers are outlined in **Scheme 2.2** and **Scheme 2.3** respectively**.** The synthesis of monomers *N,N*'-bis(2-octyldodecyl)-2,6-dibromonaphthalene-1,4:5,8 tetracarboxylicdiimide (NDI-2OD-Br_2) and *N*, *N*'-bis (2-ethylhexyl)-1,7-dibromo -3,4,9,10-perylene tetracarboxylicdiimide (PDI-2EH-Br_2) were carried out according to previously reported procedures.[27-29]

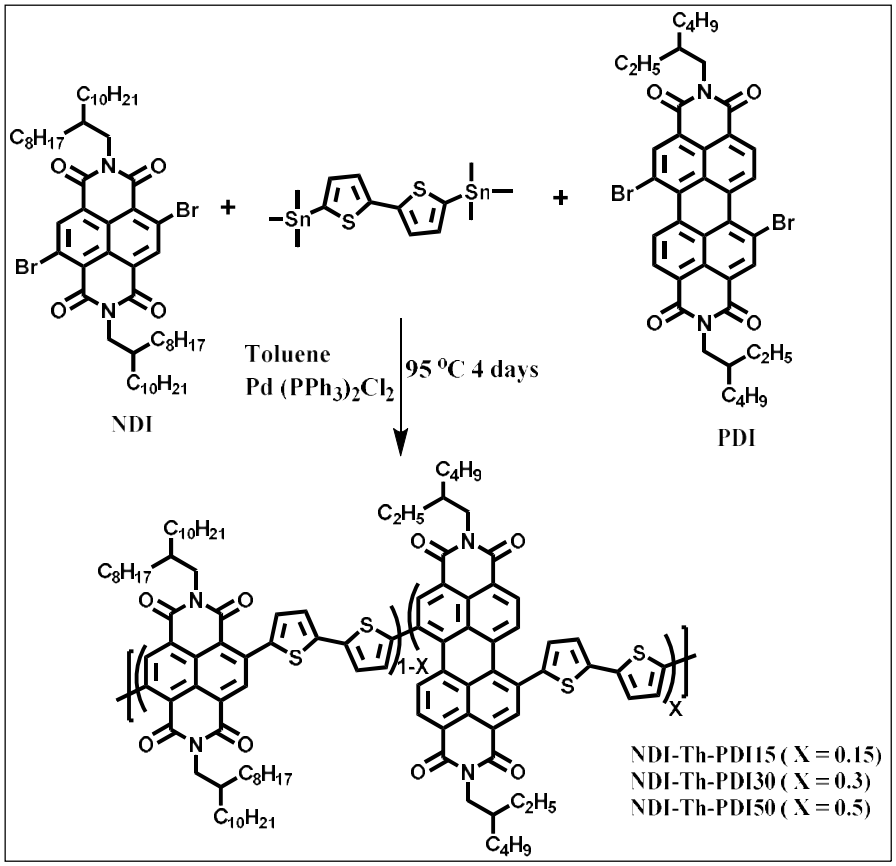

Scheme 2.3 Synthesis of n-type NDI-bithiophene /PDI-bithiophene random copolymers.

Elemental analysis of the monomers was carried out to confirm the purity and the observed CHN values were matching with the calculated values. The monomers were subsequently subjected to MALDI-TOF analysis recorded using 2,5-dihydroxybenzoic acid as the matrix and molecular ion peaks were obtained for cationic species such as [M+1], [M+Na^+]. The MALDI spectra of the monomers are given in **Figure 2.3**.

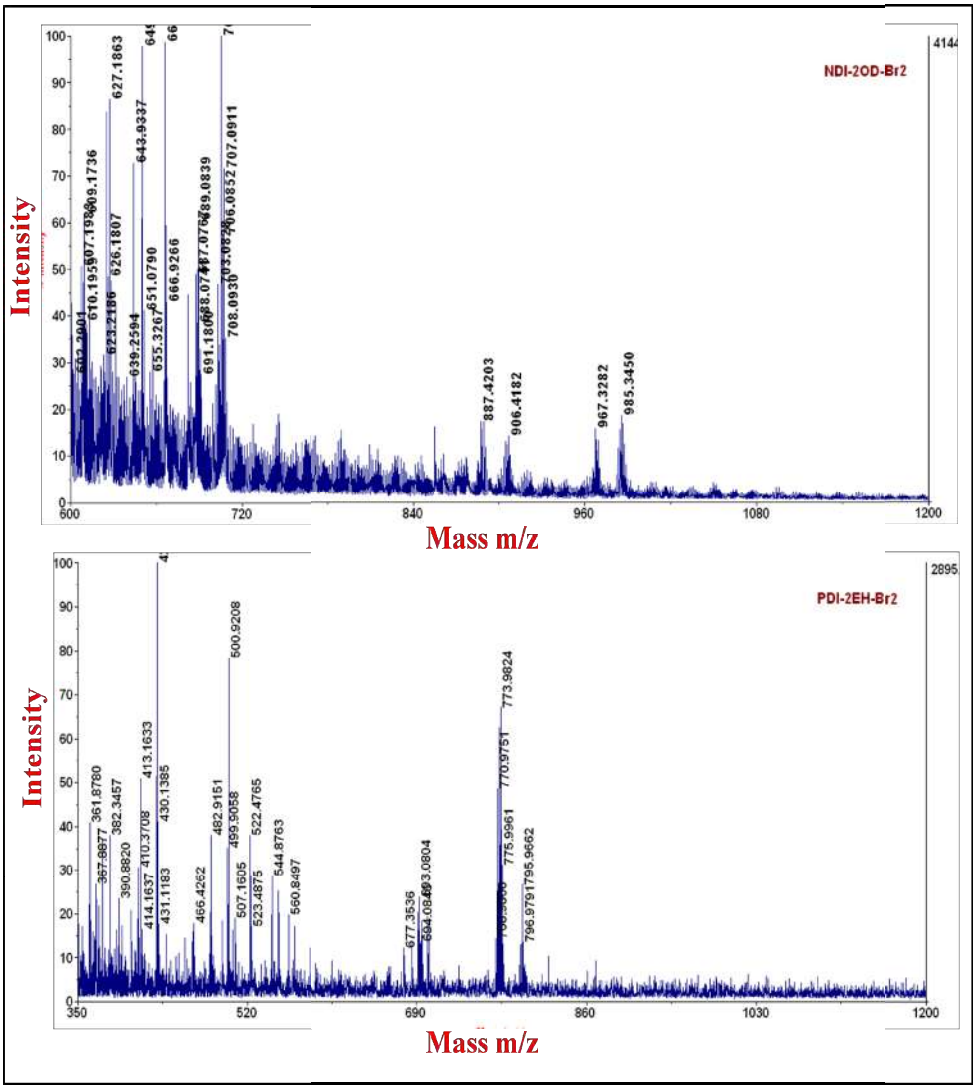

Figure 2.3 MALDI-TOF mass spectra for NDI-2OD-Br_2 and PDI-2EH-Br_2

Three random copolymers i.e. NDI-Th-PDI15, NDI-Th-PDI30 and NDI-Th-PDI50 were synthesized by varying the feed ratio of the two monomers NDI-2OD-Br_2 and PDI-2EH-Br_2 (15, 30, 50 mole % of PDI) while maintaining the concentration of the donor bithiophene comonomer constant (1 mole) in feed. The higher incorporation of PDI-2EH-Br_2 monomer having short alkyl side chain (2-ethylhexyl) produced random copolymers which had limited

solubility in common organic solvents. The maximum incorporation of 50 mole percentage of PDI in random copolymer (NDI-Th-PDI50) was found to retain good solubility in common organic solvents like chloroform, chlorobenzene and dichlorobenzene etc. The alternate copolymer NDI-bithiophene (P(NDI2OD-T2) was also synthesized as a reference benchmark. The structure of monomers and polymers were characterized by NMR, FTIR spectra. The NMR, MALDI-TOF spectra and elemental analysis of the molecules confirmed the structure and high purity of the monomers. The labeled ^{1}H NMR spectra of monomer (NDI-2OD-Br_2 and PDI-2EH-Br_2) and copolymers are given in **Figures 2.4-2.9.** The actual incorporation of the PDI in the random copolymers could be determined from the proton NMR spectra.

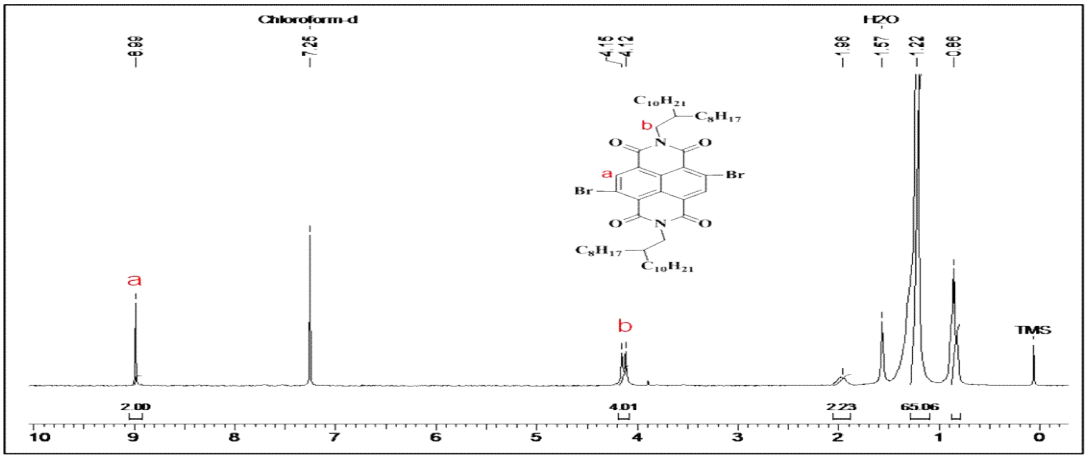

Figure 2.4 ^{1}H NMR spectrum of monomer (NDI-2OD-Br_2) recorded in $CDCl_3$.

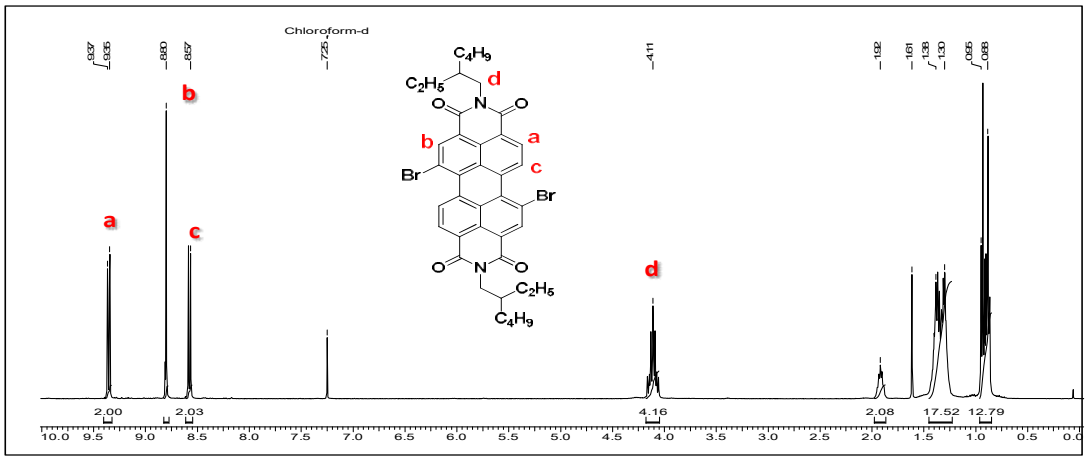

Figure 2.5 ^{1}H NMR spectrum of monomer (PDI-2EH-Br_2) recorded in $CDCl_3$.

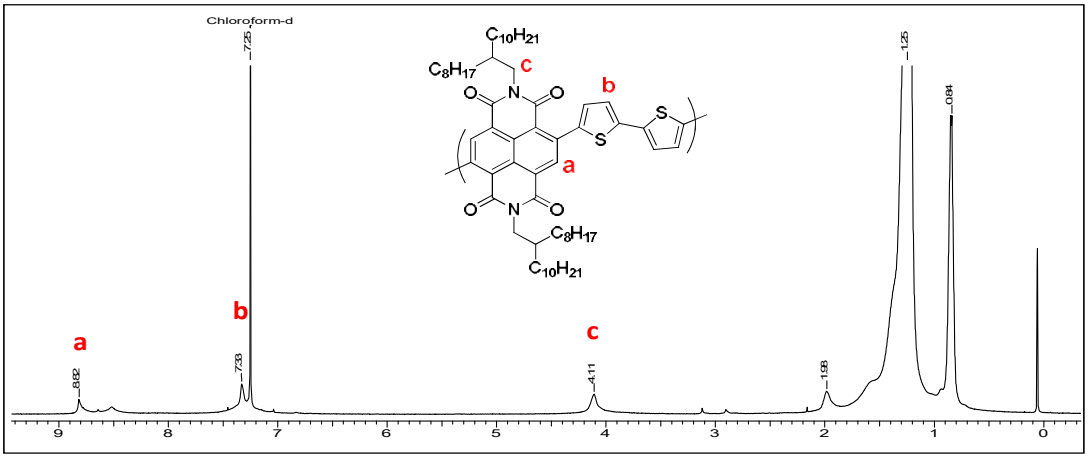

Figure 2.6 ^{1}H NMR spectrum of P(NDI2OD-T2) recorded in $CDCl_3$.

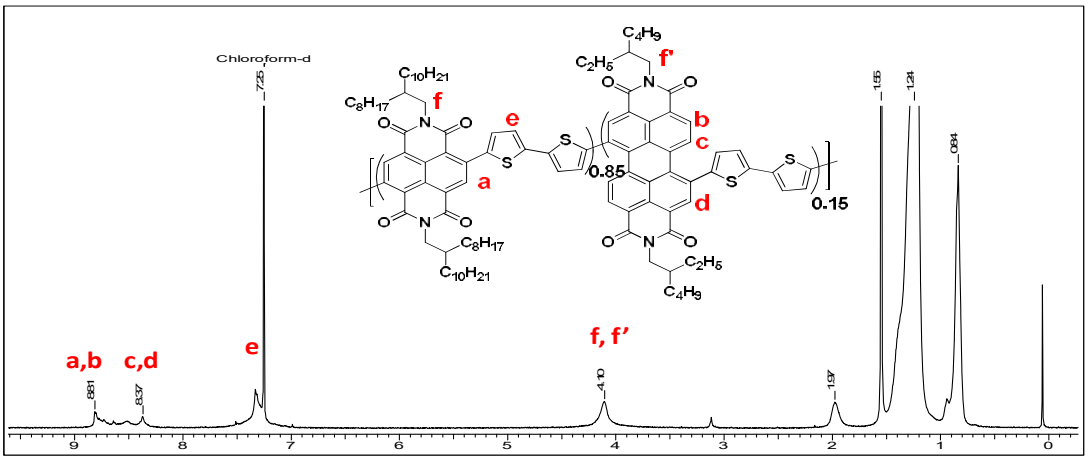

Figure 2.7 ^{1}H NMR spectrum of NDI-Th-PDI15 recorded in $CDCl_3$.

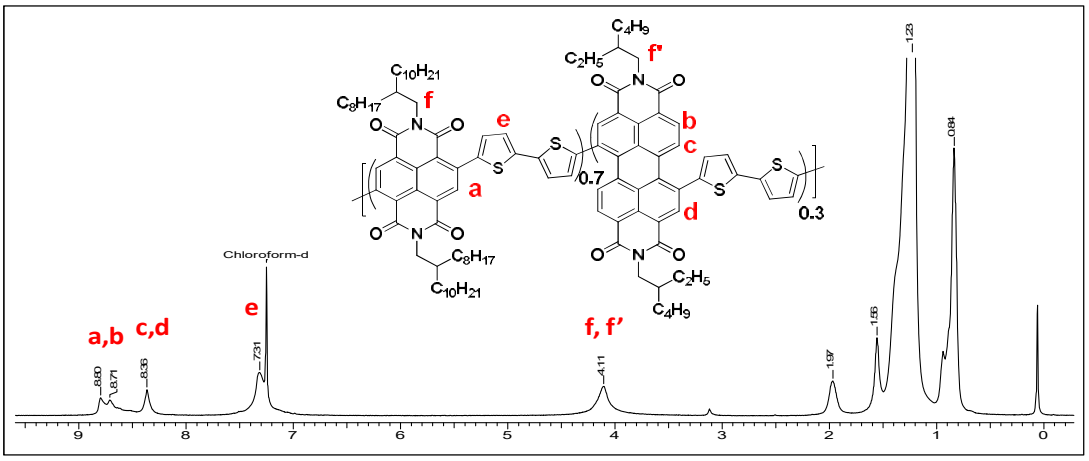

Figure 2.8 ^{1}H NMR spectrum of NDI-Th-PDI30 recorded in $CDCl_3$.

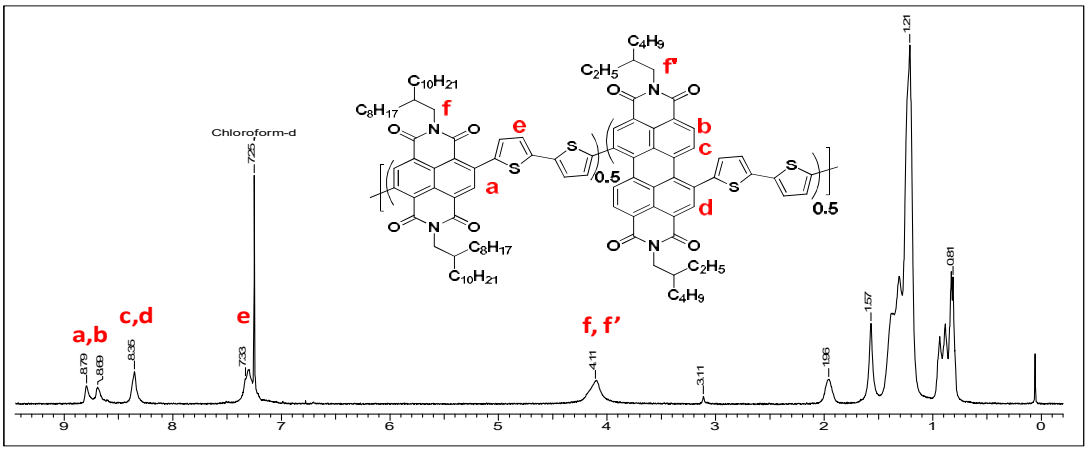

Figure 2.9 ^{1}H NMR spectrum of NDI-Th-PDI50 recorded in $CDCl_3$.

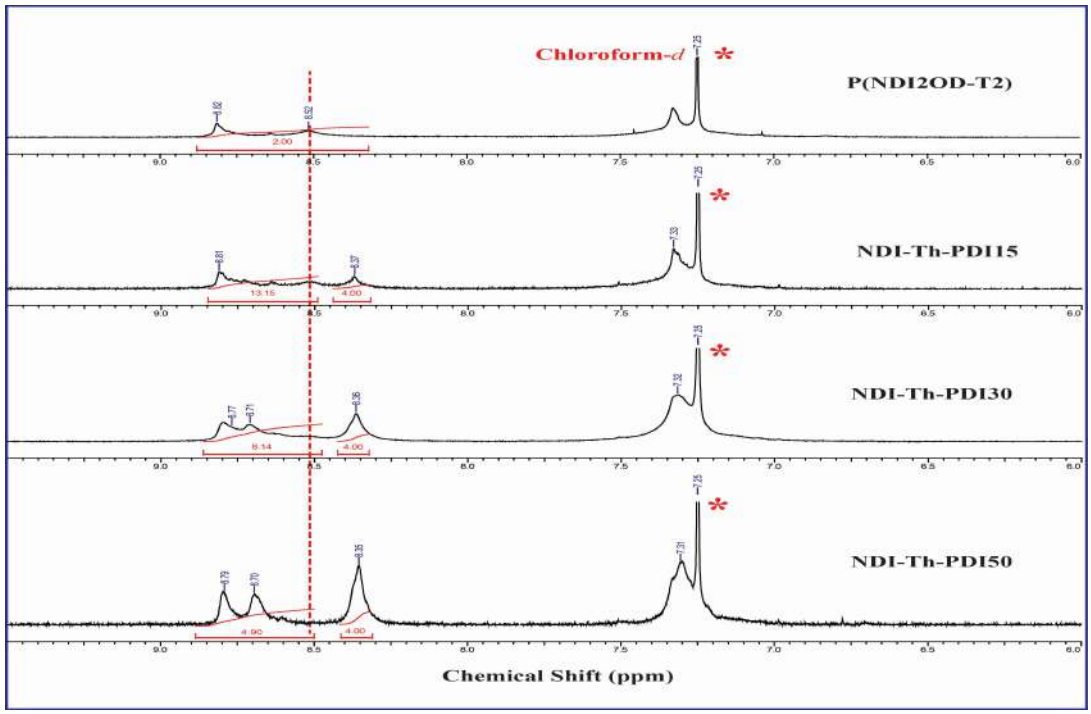

Figure 2.10 ^{1}H NMR spectra of copolymers (expanded aromatic region) recorded in $CDCl_3$

Figure 2.10 shows the expanded aromatic region (6.0 to 9.5 ppm) in the proton NMR spectra of the reference and random copolymers. The ^{1}H NMR spectra of reference polymer P(NDI2OD-T2) exhibited one extra broad peak at ~8.5 ppm which has been attributed to strong inter-chain aggregation of P(NDI2OD-T2) in chloroform.[17, 18, 30] The peaks at 8.5 and 8.82 ppm together accounted for the two aromatic protons of naphthalene core, while the peak at 7.33 ppm corresponded to the four protons of the bithiophene unit. From the figure it could be seen that in the random copolymers the extra peak for aggregation diminished progressively with the incorporation of PDI units and two new peaks at ~8.35 ppm (4

protons) and ~8.70 (2 protons) ppm appeared for PDI aromatic protons, whose intensity increased progressively. The dotted line in **Figure 2.10** indicates the position of the aggregated naphthyl aromatic protons. The peak at 8.70 ppm for two aromatic protons of PDI overlapped with the aromatic protons of NDI. However, knowing the contribution of single PDI proton from the PDI proton integration at 8.35 ppm, the value could be subtracted from the integration in the 8.5 to 8.8 ppm region. Thus, the PDI incorporation was calculated as 15 %, 29 % and 43 % respectively for the three copolymers having 15 %, 30 % and 50 % mole of PDI in the feed. For the sake of simplicity, the polymers were labeled as NDI-Th-PDI15, NDI-Th-PDI30 and NDI-Th-PDI50 even though the actual incorporation was slightly different. The reference as well as newly synthesized random copolymers showed good solubility in common organic solvents like chloroform, chlorobenzene and dichlorobenzene etc and their molecular weights were determined by gel permeation chromatography (GPC), using polystyrene standards for the calibration with chloroform as solvent. The GPC traces are shown in **Figure 2.11**.

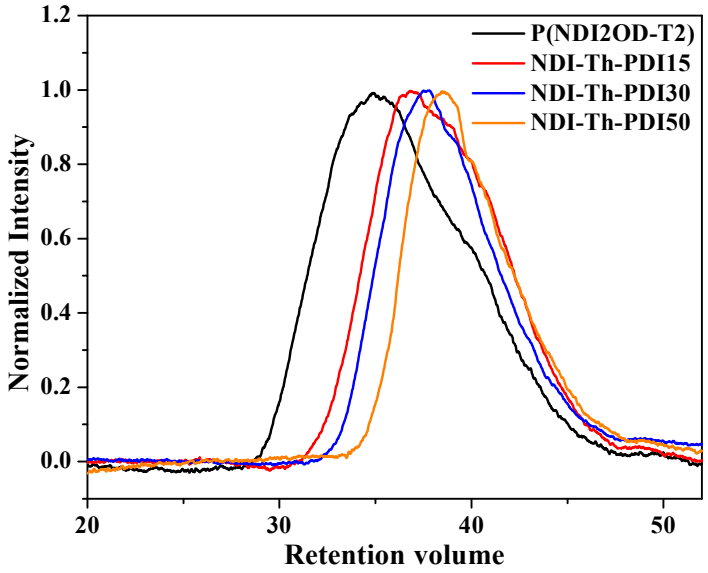

Figure 2.11 GPC chromatograms of copolymers recorded using chloroform as eluent.

The benchmark copolymer P(NDI2OD-T2) showed weight average molecular weight (Mw) of 152 kDa with (Đ) of 5.7. These values are comparable with literature reports.[27-28] Random copolymers showed lower weight average molecular weight (Mw) and (Đ) with Mw in the range of 32.4-60.7 kDa and PDI (Đ) in range of 2.5-3.1 (**Table 2.1**). Furthermore, the Mw and (Đ) were found to decrease as the content of PDI unit increased in the random copolymer. The lower value of Mw and (Đ) in random copolymers indicated their less interchain aggregation in chloroform compared to the reference polymer P(NDI2ODT2). The

reduced solubility of the PDI comonomer having short alkyl side chain (2-ethylhexyl) could also be a reason for the decrease in molecular weights in copolymers with higher PDI incorporation.

Table 2.1 GPC molecular weight, and thermal characteristics of P(NDI2OD-T2) and NDI-Th-PDI*x* random copolymers.

Polymer	Mw[a] (kDa)	Đ[b]	T_d[c] (°C)	T_m[d] (°C)	ΔH_m[d] (J/g)	$\Delta H_{m,\ blend}$[e] (J/g)
P(NDI2OD-T2)	152	5.7	422	287	6.65	2.57
NDI-Th-PDI15	60.7	3.7	437	289	12.57	1.77
NDI-Th-PDI30	49.8	2.9	435	284	6.55	1.49
NDI-Th-PDI50	32.4	2.5	436	269	4.41	

[a] Weight-average molecular weight (M*w*). [b] Polydispersity index (Đ). [c] The decomposition temperature (5% weight loss) estimated using TGA under N_2. [d] Measured using DSC under N_2. [e] Enthalpy for blend PTb7-Th: P(NDI2OD-T2) and PTB7-Th:NDI-Th-PDIx (1.3:1, w/w).

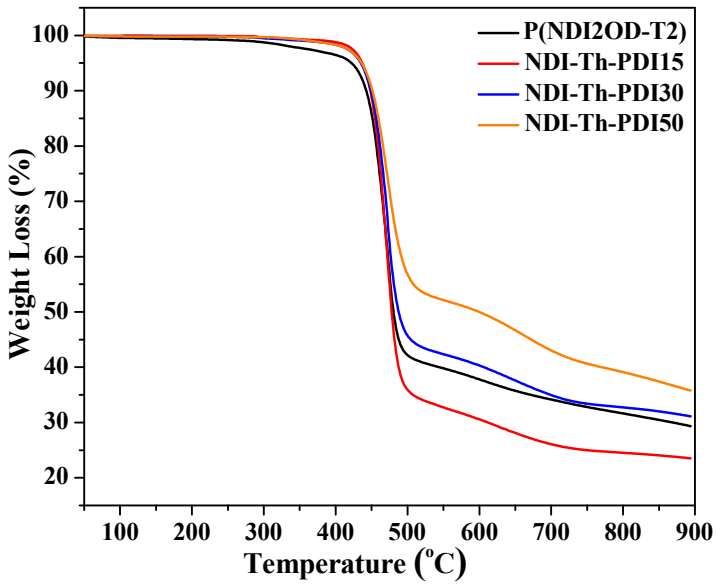

Figure 2.12 TGA thermograms of copolymers at 10 °C /min under N_2 atmosphere.

The thermal properties of the copolymers were determined by thermo gravimetric analysis (TGA) as well as differential scanning calorimetry (DSC) measured under nitrogen atmosphere. TGA curves given in **Figure 2.12** showed good thermal stability for all random copolymers with onset decomposition temperature (T_d) of over > 400 °C. Literature cites

melting transition for P(NDI2OD-T2) with onset around 280 °C (heating scan), indicating the crystalline nature of the polymer.[4, 31] DSC curves were recorded for all polymers by heating from -50 °C till 330 °C at 10 °C /min under N_2 atmosphere. P(NDI2OD-T2) showed a broad thermal transition with endothermic peak (T_m) at 287 °C and exothermic peak at (T_c) 244 °C with melting and cooling enthalpy values (ΔH_m) 6.65 J/g and (ΔH_c)7.37 J/g respectively. NDI-Th-PDI15 and NDI-Th-PDI30 also showed the melting and crystallization transitions in their second heating and cooling cycles. However, NDI-Th-PDI50 did not exhibit a reversible thermal transition in the cooling cycle, but a transition was observed in the first and second heating cycles. In order to compare the relative crystallinity of the polymers based on the enthalpies of transition, a quench-cooling experiment was carried out to obtain perfectly reproducible thermograms. Essentially, this experiment involved heating carefully weighed samples (5-6 mg) of the polymer in a crimped DSC pan from room temperature (25 °C) to 330 °C to melt them and then immediately quenching the DSC sample pan using liquid nitrogen. The sample pan was then later heated from -50 °C to 330 °C and then again cooled back to -50 °C. This procedure enables to cool and equilibrate quickly in order to detect the complete crystallization during the next heating cycle. **Figure 2.13** gives the heating and cooling scans collected for all the four polymers after the quenching experiment. **Table 2.1** lists the melting temperature (T_m) and corresponding enthalpies (ΔH_m) obtained for the four polymers. NDI-Th-PDI15 showed much sharper melting and crystallization transitions with almost double the value for enthalpy compared to P(NDI2OD-T2). Its transition temperatures were also slightly higher compared to the reference polymer. NDI-Th-PDI30 had almost similar transition temperature and enthalpy values compared to the reference polymer. For the reference as well as NDI-Th-PDI15 and NDI-Th-PDI30 polymers very good reversibility was observed for the endo as well as exothermic transitions. However, NDI-Th-PDI50 showed a broad endothermic transition at 269 °C, which was much low compared to the reference polymer (286.9 °C) and no exothermic transition was observed during the cooling cycle. The enthalpy of melting (ΔH_m) obtained from the area of melting transition could be correlated to the crystallinity. [21, 32] The comparison of ΔH_m showed that NDI-Th-PDI15 exhibited relatively higher crystallinity (ΔH_m, 12.57 J/g) compared to the reference polymer P(NDI2OD-T2) (ΔH_m, 6.65 J/g), while NDI-Th-PDI30 (ΔH_m, 6.45 J/g) had slightly lower and NDI-Th-PDI50 (ΔH_m, 4.41 J/g) had the lowest crystallinity. The observation from DSC suggested that low incorporation of PDI (< 15 mole %) did not disrupt the packing of the polymer chain backbone, whereas > 30 mole % of PDI in the backbone disrupted the chain

packing leading to sluggishness in crystallization. Furthermore, the reduction in crystallinity of NDI-Th-PDI30 and NDI-Th-PDI50 with high PDI incorporation supported the observation from the proton NMR spectra of reduced NDI stacking with increased PDI content.

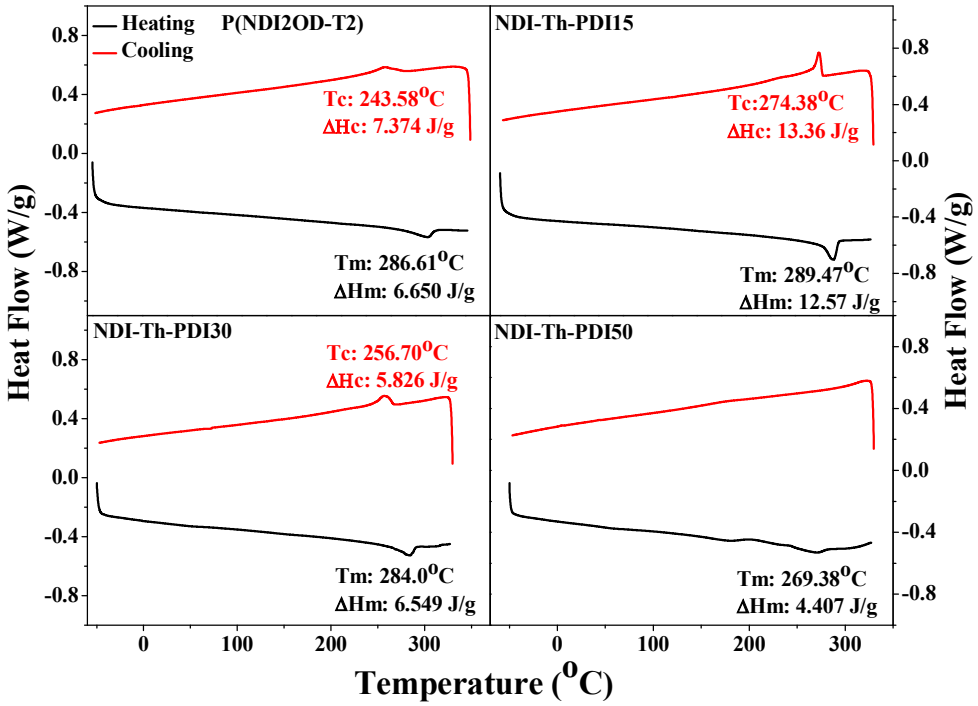

Figure 2.13 Second heating/cooling curves of quench-cooled samples of the copolymers in the DSC scans conducted at 10 °C /min under N_2 atmosphere.

2.3.2. Optical and Electrochemical Properties

UV-Vis absorption spectra of random copolymers (NDI-Th-PDI*x*) and reference P(NDI2OD-T2) were recorded in both dilute chloroform solution as well as in thin-film spin coated on glass substrate and are shown in **Figure 2.14**. In solution (top) all copolymers showed two distinct absorption bands; the first high energy absorption band at ~300-425 nm was accounted for by π-π* transition and another low energy band at ~460- 800 nm was assigned to intra-molecular charge transfer (ICT) from bithiophene unit to NDI/PDI.[17] The reference polymer P(NDI2OD-T2) showed typical absorption spectrum with π-π* absorption peak at ~400 nm and ICT peak at 645 nm. In the random copolymers the position of the π-π* absorption peak remained unchanged, while the ICT absorption band was found to be blue shifted (hypsochromic shift). It was observed at 630 nm in NDI-Th-PDI15, 618 nm in NDI-Th-PDI30, and 605 nm in NDI-Th-PDI50. The progressive hypsochromic shift observed in

ICT absorption band of random copolymers could be accounted for by the reduced planarity of the polymer backbone when compared to P(NDI2OD-T2).

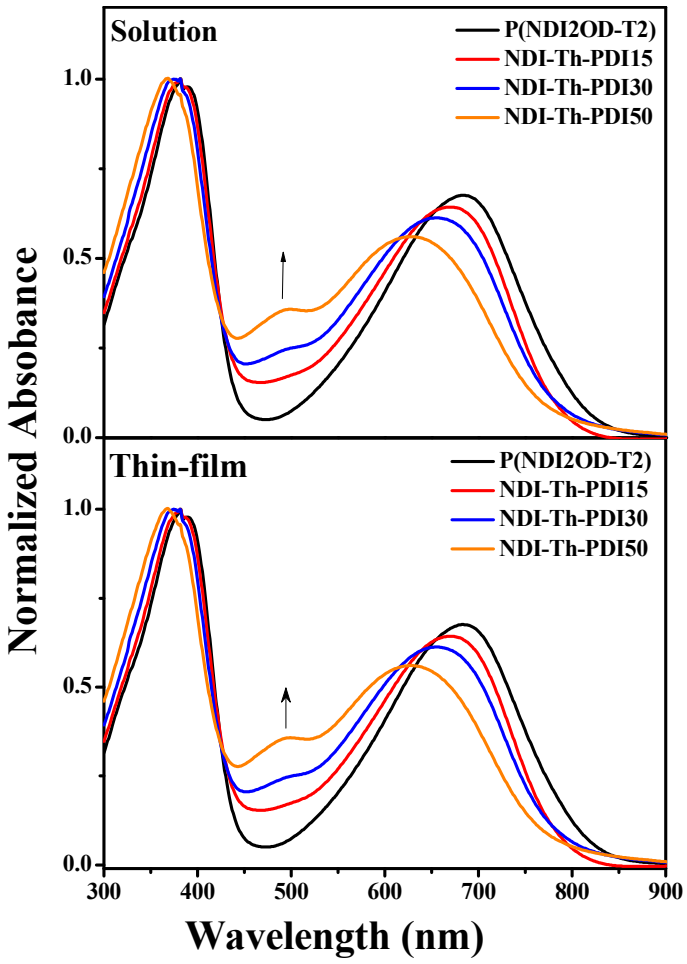

Figure 2.14. UV-Vis absorption spectra of dilute solutions of reference P(NDI2OD-T2) and random copolymers in chloroform (top) and thin film (bottom) on glass substrate.

The reference polymer P(NDI2OD-T2) is well known to form self-aggregates in chloroform due to strong inter-chain stacking of more planar polymer backbone, which leads to a red shifted ICT band.[17] Incorporation of the large PDI units in the random copolymers reduced the planarity of the polymer backbone as well as inter-chain aggregation.[24] Consequently, the ICT band was shifted to lower wavelength. Furthermore, an additional broad peak at ~500 nm was obtained for all random copolymers which was absent in P(NDI2OD-T2) and the intensity of this peak at ~500 nm was found to increase with the increase in the content of PDI unit. This additional peak was assigned for the typical absorption of the PDI component in the random copolymer. The spin coated thin-films of all copolymers showed similar absorption spectra as that in solution (**Figure 2.14**, bottom), except for the large red-shifting

of the ICT band in the solid state compared to that in solution due to the inter-chain aggregation and chain planarization.[24] The reference copolymer P(NDI2OD-T2) showed ICT band at 685 nm. On the other hand, random copolymers NDI-Th-PDI15, NDI-Th-PDI30 and NDI-Th-PDI50 exhibited blue shifted ICT band along with decreased absorption coefficient at 670 nm, 655 nm and 630 nm respectively. The large blue shifting of ICT band in random copolymer indicated less inter-chain stacking and aggregation in solid state compared to P(NDI2OD-T2). The reduced self-aggregation of random copolymer could be beneficial to improve the intermixing of n-type random copolymer with donor polymer to form compatible blend which is discussed later on in the all-PSCs device section. The optical band gaps (E_g^{opt}) of random copolymers were calculated from lower energy absorption band edge of thin-film and is listed in **Table 2.2**. An optical band gap of 1.52 eV was obtained for reference copolymer P(NDI2OD-T2) which was slightly increased to 1.55 eV, 1.57 eV and 1.60 eV in NDI-Th-PDI15, NDI-Th-PDI30 and NDI-Th-PDI50 respectively. Electrochemical redox behavior and electronic energy levels of new n-type random copolymers were analyzed by cyclic voltammetry. Thin-films of polymer were deposited on the platinum working electrode. The measurement was carried out in acetonitrile solvent with ferrocene/ferrocenium as an internal standard and tetrabutylammonium hexafluorophosphate (*n*-Bu4NPF$_6$ 0.1M/ acetonitrile) as supporting electrolyte.[33]

Cyclic voltammograms for all copolymers are shown in **Figure 2.15** and the calculated HOMO and LUMO energy levels are given in **Table 2.2.** Thin-film of reference polymer P(NDI2OD-T2) exhibited two reversible reduction peaks, which were attributed to the formation of radical anion and dianions of NDI in the polymer backbone.[16] All random copolymers showed quasi-reversible reduction peaks with almost similar values of electrochemical reduction like P(NDI2OD-T2). None of the copolymer showed oxidation peak during anodic scan up to 2V. The lowest occupied molecular orbital (LUMO) energy levels were estimated based on the onset value of first reduction peak and reference energy level of ferrocene (4.8 eV below the vacuum level) according to E_{LUMO} (eV) = -e × (E^{red} onset + 4.8) below the vacuum level.[33] The highest occupied molecular orbital (HOMO) levels were calculated based on the optical band gap obtained from the solid-state absorption onset measurements. The LUMO and HOMO energy levels of P(NDI2OD-T2) was found to be -3.90 eV and -5.42 eV respectively which resembles the previously reported values.[16, 33] Newly synthesized random copolymers exhibited almost similar values for energy level (LUMO and HOMO) (**Table 2.2**) like reference polymer P(NDI2OD-T2). This suggested that there was negligible effect of incorporation of PDI unit on the energy level of random

copolymers and both the components - NDI and PDI exhibited almost similar electron accepting strength.

Table 2.2 UV-visible absorption, optical band gap, electronic energy levels and Thin-film XRD data of thermally annealed random copolymers of P(NDI2OD-T2) and NDI-Th-PDI*x* random copolymers.

Polymer	λ_{max} (nm) Solution	λ_{max} (nm) Thin-film	E_g^{opt} (eV)	LUMO (eV)	HOMO (eV)	2θ°		*d*-spacing (Å)	
						(100)	(010)	d_{100}	d_{010}
P(NDI2OD-T2)	367, 645	381, 685	1.52	3.90	5.42	4.06	23.10	21.72	3.84
NDI-Th-PDI15	367, 630	381, 670	1.55	3.94	5.49	4.21	23.03	20.96	3.85
NDI-Th-PDI30	367, 618	374, 655	1.57	3.94	5.51	4.58	22.59	19.27	3.93
NDI-Th-PDI50	367, 605	368, 630	1.60	4.00	5.60	4.80	21.92	18.38	4.00

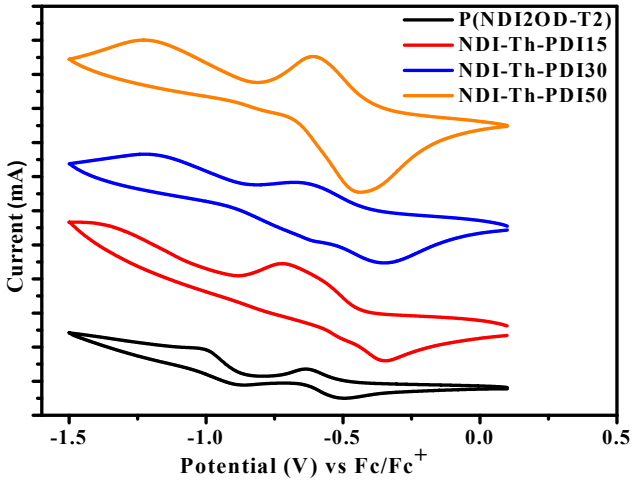

Figure 2.15 Cyclic voltammograms of reference P(NDI2OD-T2) and random copolymers as thin film on platinum working electrode in 0.1 M*n*-Bu_4NPF_6 acetonitrile at a scan rate of 100 mV/s.

2.3.3. Thin-film Crystallinity

The molecular packing and bulk crystalline nature of reference P(NDI2OD-T2) and new n-type random copolymers were analyzed using wide-angle X-ray diffraction (XRD) measurement. **Figure 2.16** shows the X-ray diffraction patterns of thermally annealed (at 160 °C, 10 min) thin-films of copolymer on glass substrate and relevant data is given in **Table 2.2**. XRD pattern of reference polymer P(NDI2OD-T2) showed lamellar peak (100) at 2θ =

4.06° and π-π stacking peak (010) at 2θ = 23.10° which corresponded to lamellar packing distance of 21.72 Å and π-π stacking distance of 3.84 Å. The lamellar peak (100) for random copolymers were observed at 2θ = 4.21°, 4.58° and 4.80° with *d*-spacing 20.96 Å, 19.27 Å, and 18.38 Å for NDI-Th-PDI15, NDI-Th-PDI30 and NDI-Th-PDI50 respectively. The lamellar packing distance was found to decrease progressively with increasing incorporation of PDI moiety in the random copolymer chain.

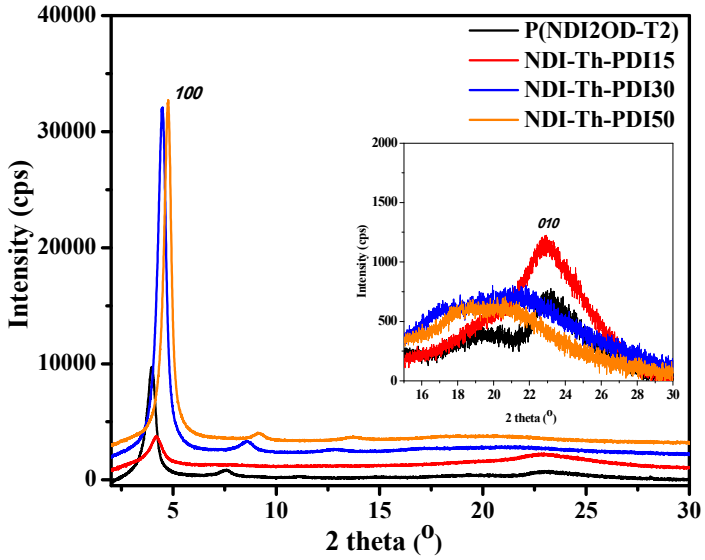

Figure 2.16. Thin-film XRD diffraction patterns of reference P(NDI2OD-T2) and random copolymers.

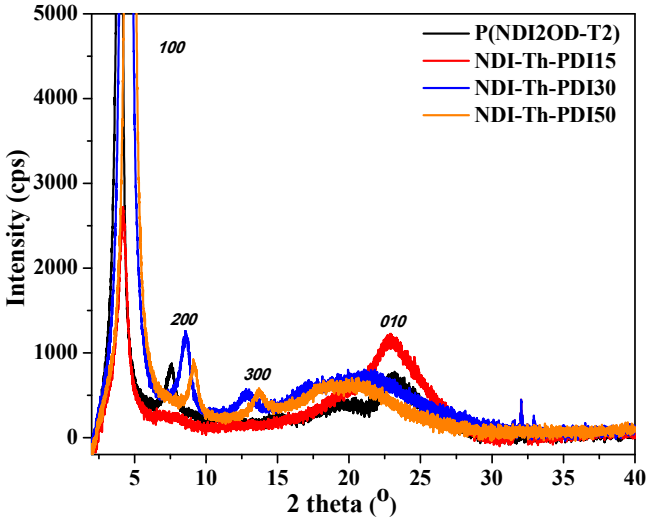

Figure 2.17. Thin-film XRD diffraction patterns of P(NDI2OD-T2) and random copolymers.

This observation is very similar to the previous results by Jenekhe *et al.* and could be attributed to the shorter 2-ethylhexyl side chains on PDI moiety.[18] In contrast, the π-π

stacking distance increased linearly with increasing incorporation of PDI moiety into the copolymer chain (**Figure 2.16** inset). It increased from 3.84 Å in reference P(NDI2OD-T2) to 3.85 Å, 3.93 Å, and 4.00 Å in NDI-Th-PDI15, NDI-Th-PDI30 and NDI-Th-PDI50 respectively. Overall, all the random copolymers (NDI-Th-PDI*x*) exhibited sharp and intense peaks with the lamellar ordering observed up to third order in XRD (**Figure 2.17**), indicating their high crystalline nature.

2.3.4. D:A Blend Property Analysis

It is important to study the behavior of the donor: acceptor copolymer blend in order to understand their photovoltaic device performance. Therefore, blend samples were prepared by mixing donor: acceptor (D:A) in the ratio 1.3:1 (w/w) choosing PTB7-Th as the standard donor polymer which produced relatively higher PCE. This D:A blend ratio (1.3:1) was found to be optimum for all-PSCs which is described later on. The thermal analysis of the blend samples were performed using DSC under identical quench-cool conditions as was employed for the pristine samples. The thermograms of the blends of the reference as well as PDI copolymers are given in the **Figure 2.18** and the values of the melting transition enthalpies (ΔH_m) are listed in **Table 2.1**.

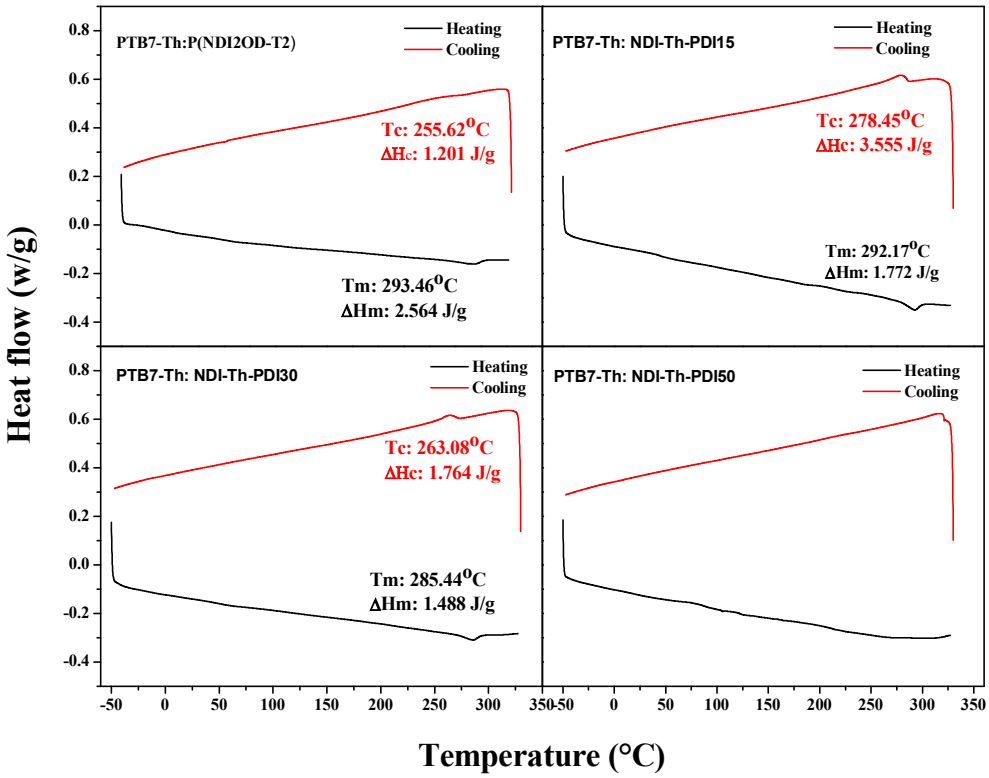

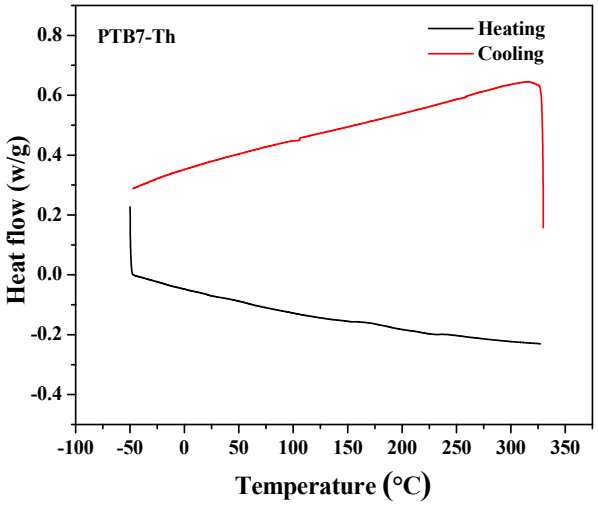

Figure 2.18 Second heating/cooling curves of quench-cooled samples of the Blend and PTB7-Th in the DSC scans conducted at 10 ^{o}C /min under N_2 atmosphere.

The donor PTB7-Th did not exhibit a melting transition under similar conditions. All blend samples exhibited reduction in the enthalpy of melting (2.56 J/g, 1.77 J/g and 1.49 J/g for P(NDI2OD-T2), NDI-Th-PDI15 and NDI-Th-PDI30 respectively) compared to the pristine samples (6.65 J/g, 12.57 J/g and 6.55 J/g respectively). The NDI-Th-PDI50 copolymer blend did not exhibit any transition even after being subjected to quench cooling procedure. The reduced crystallinity indicated better donor:acceptor miscibility in the blend. The thin films of the blends were next analyzed using wide angle X-ray diffraction studies and corresponding diffraction patterns are shown in **Figure 2.19**. It was observed that the sharp and intense peaks for the lamellar ordering observed in the pristine samples (**Figure 2.16**) were mostly retained in the blends of PTB7-Th with P(NDI2OD-T2) and NDI-Th-PDI15 (indicated by arrow in the **Figure 2.19**). It could be seen that the reference blend PTB7-Th:P(NDI2OD-T2) exhibited relatively more number of peaks compared to the random copolymers, which suggested that it did not form good compatible blends. The higher ordered lamellar peaks were mostly not observed in the blends of NDI-Th-PDI30 and NDI-Th-PDI50. The (100) and the π-π stacking peak were the only prominent peaks in these blends. The absence of higher ordered lamellar peaks indicated that the copolymers with higher PDI content like the NDI-Th-PDI30 and NDI-Th-PDI50 formed more compatible donor-acceptor blends. The PTB7-Th: acceptor blend films were further analyzed by photoluminescence (PL) quenching experiments to investigate the exciton diffusion and dissociation.

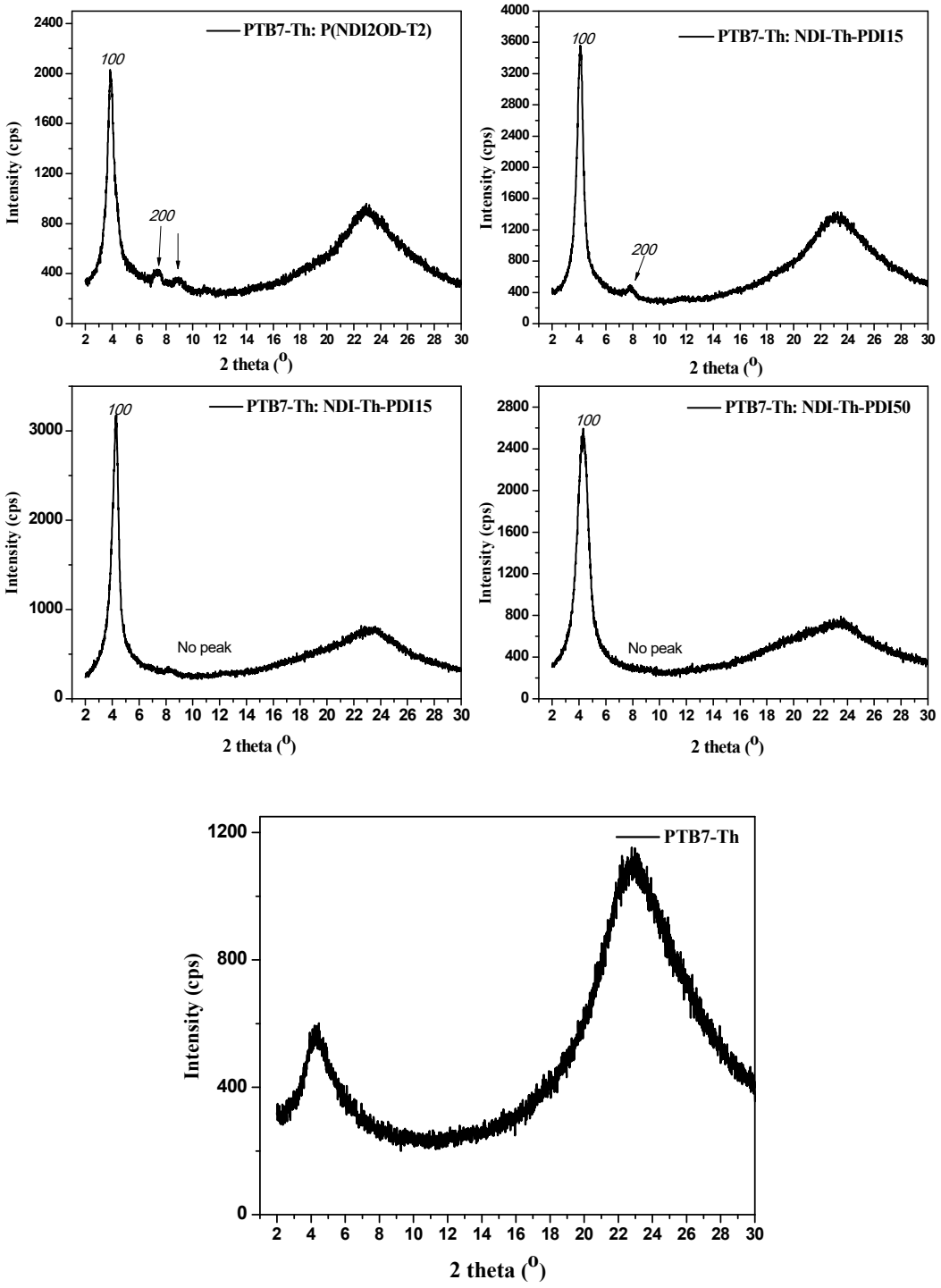

Figure 2.19 Thin-film XRD diffraction patterns of blend and PTB7-Th.

Figure 2.20 shows the steady-state PL spectra of the neat PTB7-Th, P(NDI2OD-T2), NDI-Th-PDI15, NDI-Th-PDI30 and NDI-Th-PDI50 along with their blend films with PTB7-Th. The PL spectra (at excitation wavelength 645 nm)[21] of neat PTB7-Th showed peak maxima at ~755 nm, while acceptor polymers exhibited broad peaks in the range of ~800-830 nm. All

D/A blend films showed significant PL quenching compared to neat PTB7-Th. The relative PL quenching efficiency (ΔPL) was estimated by measuring the intensity of various D/A blend with respect to neat PTB7-Th (**Figure 2.21**).[21] PTB7-Th:P(NDI2OD-T2) reference blend showed ΔPL ~76 %, while PTB7-Th:NDI-Th-PDI15, PTB7-Th:NDI-Th-PDI30 and PTB7-Th:NDI-Th-PDI50 exhibited ΔPL of ~86 %, ~87 % and ~91 % respectively. Higher ΔPL in the random copolymer blends indicated efficient exciton dissociation at D/A interface as a result of good intermixing of acceptor polymer with PTB7-Th. Overall, the thermal property, crystallinity as well as PL quenching efficiency of the blends pointed towards the copolymers ability to perform better in photovoltaic devices compared to the reference polymer, specially for the copolymers with higher PDI content i.e PTB7-Th:NDI-Th-PDI30 and PTB7-Th:NDI-Th-PDI50.

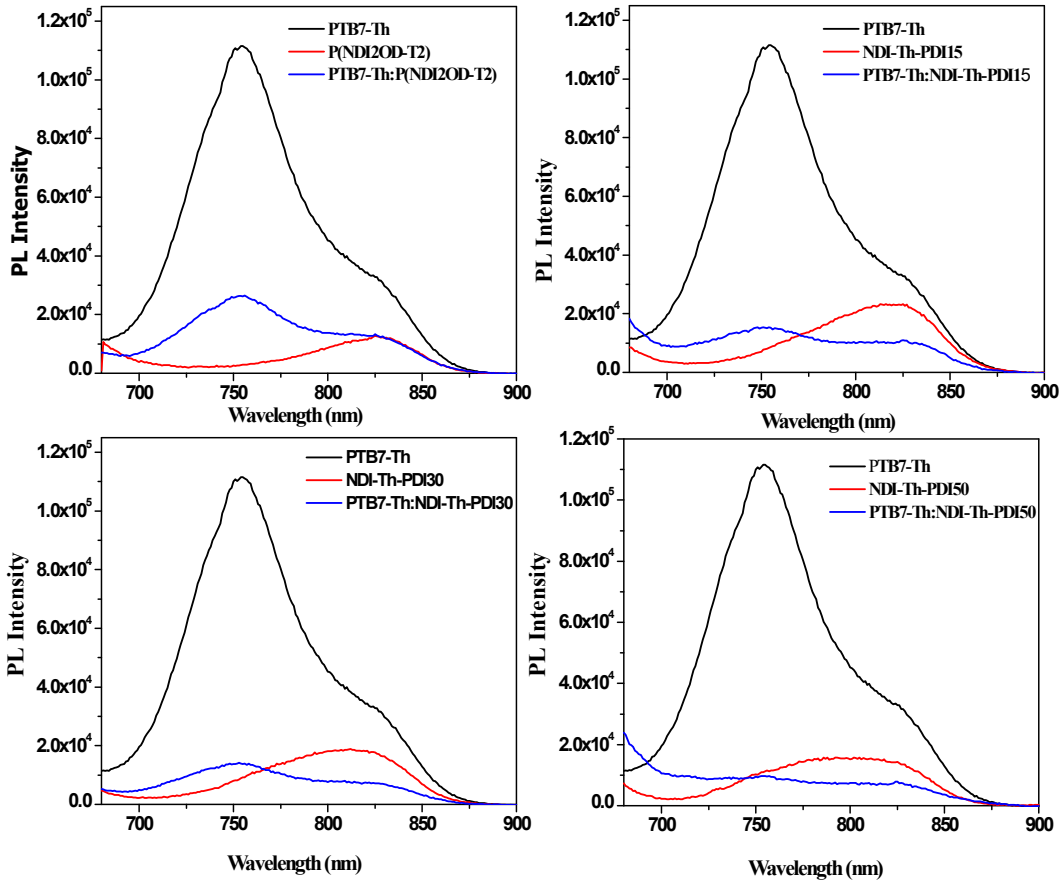

Figure 2.20 PL spectra recorded for the blend film of (a) PTB7-Th:P(NDI2OD-T2) (b) PTB7-Th:NDI-Th-PDI15 (c) PTB7-Th:NDI-Th-PDI30 (d) PTB7-Th:NDI-Th-PDI50 blends.

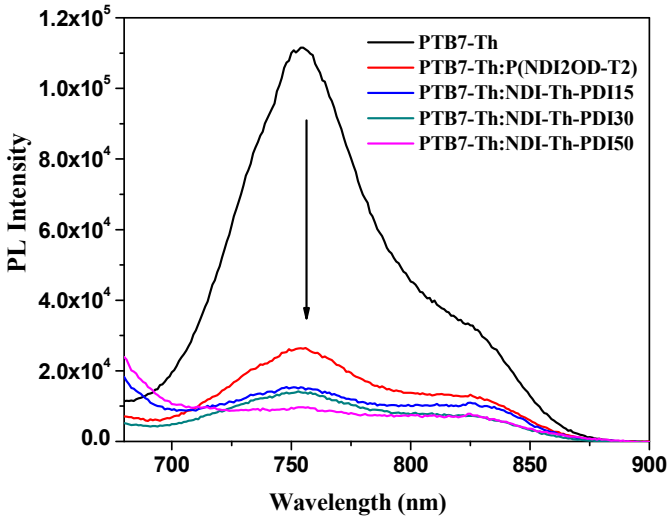

Figure 2.21 The combined PL spectra of donor: acceptor blends film and neat PTB7-Th donor.

2.3.5. All-Polymer BHJ Solar Cells

The potential application of random copolymers (NDI-Th-PDI*x*) as acceptor (n-type) materials in all-polymer solar cells was explored by fabricating BHJ all-PSCs using PTB7 or PTB7-Th polymers as electron donor materials. The inverted devices with configuration of ITO/ZnO/PFN/polymer blend/Al were fabricated. The detailed procedure for device structure and fabrication is given in experimental section. The all- PSCs device using n-type reference polymer P(NDI2OD-T2) was also fabricated for comparison. The blend active layers of donor: acceptor polymers were deposited by spin coating from chloroform solution (12 mg/ml) containing 1.25 % volume fraction of 1,8-diiodooctane (DIO) additives. The optimum donor:acceptor (D:A) blend ratio and thickness of BHJ active layer films were found to be 1.3:1 (w/w) and 100~ 110 nm, respectively. **Figure 2.22** shows the current density-voltage (*J-V*) curves for both donor: acceptor polymer blend all-PSCs. The optimized solar cell parameters including short-circuit current density (Jsc), the open-circuit voltage (Voc), fill factor (FF), and PCE, are summarized in **Table 2.3**.The reference polymer P(NDI2OD-T2) is a well-studied acceptor material used with various low bandgap polymer and small molecule donors in all-polymer solar cells. In our study, using PTB7 as the donor material, P(NDI2OD-T2) exhibited maximum PCE of 2.06% (Jsc of 6.26 mA/cm^2, Voc of 0.81 V, and FF of 40.5 %) in device based on PTB7: P(NDI2OD-T2) blend, and a maximum PCE of 2.97 % was obtained (Jsc of 9.05 mA/cm^2, Voc of 0.797 V, and FF of 41.3 %) using PTB7 as the donor material; this optimized PCE is comparable with the previously reported values.[5, 10, 19, 34- 36]

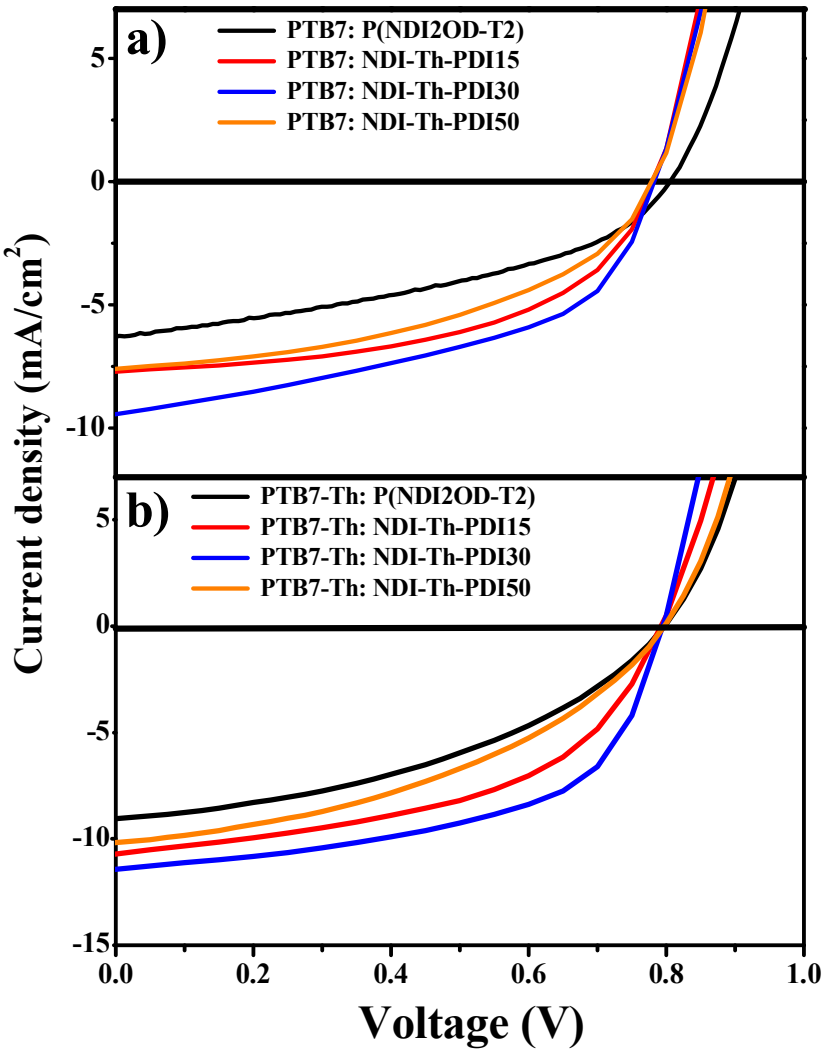

Figure 2.22. Current density- Voltage (*J – V*) characteristics for all polymers using (a) PTB7 as the donor and (b) PTB7-Th as the donor.

The device performance of the various PTB7: NDI-Th-PDI*x* blend devices showed that all the newly synthesized random copolymers (NDI-Th-PDI15, NDI-Th-PDI30, NDI-Th-PDI50) exhibited significant improvement in the PCE as compared to reference polymer P(NDI2OD-T2) with the two donor polymers. For instance, PTB7: NDI-Th-PDI15 blend device showed PCE of 3.15 % (Jsc of 7.71 mA/cm^2, Voc of 0.78, and FF of 52.3 %). Further enhancement in the photovoltaic performance was observed in PTB7: NDI-Th-PDI30 blend device which exhibited PCE of 3.56 % (Jsc of 9.45 mA/cm^2,Voc of 0.78, and FF of 48.0 %). However, PTB7: NDI-Th-PDI50 blend with highest incorporation of PDI (50 %) showed lower PCE of 2.72 % (Jsc of 7.60 mA/cm^2, Voc of 0.77, and FF of 45.9 %), which was still higher compared to the reference polymer P(NDI2OD-T2). A similar trend of enhanced photovoltaic

performance was observed for blend devices of the random copolymers with PTB7-Th as the donor. The PCE values obtained were 4.22 %, 5.03% and 3.33 % respectively for PTB7-Th: NDI-Th-PDI15, PTB7-Th: NDI-Th-PDI30 and PTB7-Th: NDI-Th-PDI50 blend devices respectively. The dependence of the PCE on the varying incorporation of PDI unit in the copolymer is shown in **Figure 2.23**. From **Figure 2.23** it could be observed that NDI-Th-PDI30 reflected the best optimized composition with both donor polymers and further increase in PDI incorporation into (NDI-Th-PDI*x*) random copolymer did not result in improvement of the photovoltaic performance. The improved device performance upon using PTB7-Th as donor instead of PTB7 in the blend devices with the random copolymers was expected since PTB7-Th had shown face-on molecular orientation and superior photovoltaic properties with various electron acceptor materials.[30]

The enhancement in the PCE values of random copolymers NDI-Th-PDI*x* based all-PSCs devices were mainly due to the increase in the Jsc value. Additionally, the observed variations in the Jsc values with different copolymer compositions were well reflected in the changes of their spectral response in EQE spectrum which is shown in **Figure 2.24**. All random copolymer blend PTB7: NDI-Th-PDI*x* devices exhibited broad photoresponse in the region of 300-800 nm with higher photocurrent generation compared to reference polymer P(NDI2OD-T2). Particularly, NDI-Th-PDI30 showed highest EQE of 48 % at ~605 nm for blend device with PTB7 and 55 % ~ 615 nm for blend device with PTB7-Th, that was consistent with the observed Jsc value [within 2 %].

Table 2.3 Photovoltaic properties of PTB7: NDI-Th-PDI*x* and PTB7: P(NDI2OD-T2) blend all-polymer solar cells.

Active layer	Voc (V)	Jsc (mA/cm^2)	FF (%)	PCE (%)
PTB7 Donor				
PTB7: P(NDI2OD-T2)	0.807±0.05	6.19±0.07	40.1±0.04	2.00±0.06
PTB7: NDI-Th-PDI15	0.777±0.03	7.66±0.05	52.1±0.02	3.10±0.05
PTB7: NDI-Th-PDI30	0.780±0.02	9.41±0.04	47.8±0.02	3.50±0.06
PTB7: NDI-Th-PDI50	0.774±0.05	7.55±0.05	45.5±0.04	2.65±0.07
PTB7-Th Donor				
PTB7-Th: P(NDI2OD-T2)	0.793±0.04	8.96±0.09	41.0±0.03	2.91±0.06
PTB7-Th: NDI-Th-PDI15	0.787±0.05	10.65±0.06	49.3±0.04	4.13±0.09
PTB7-Th: NDI-Th-PDI30	0.792±0.03	11.39±0.04	55.2±0.02	4.98±0.05
PTB7-Th: NDI-Th-PDI50	0.793±0.04	10.10±0.06	40.7±0.05	3.26±0.07

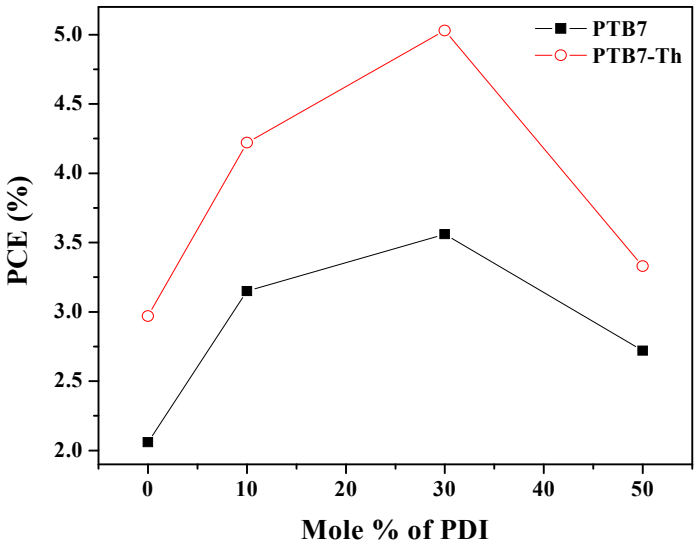

Figure 2.23. Dependence of PCE on random copolymer composition.

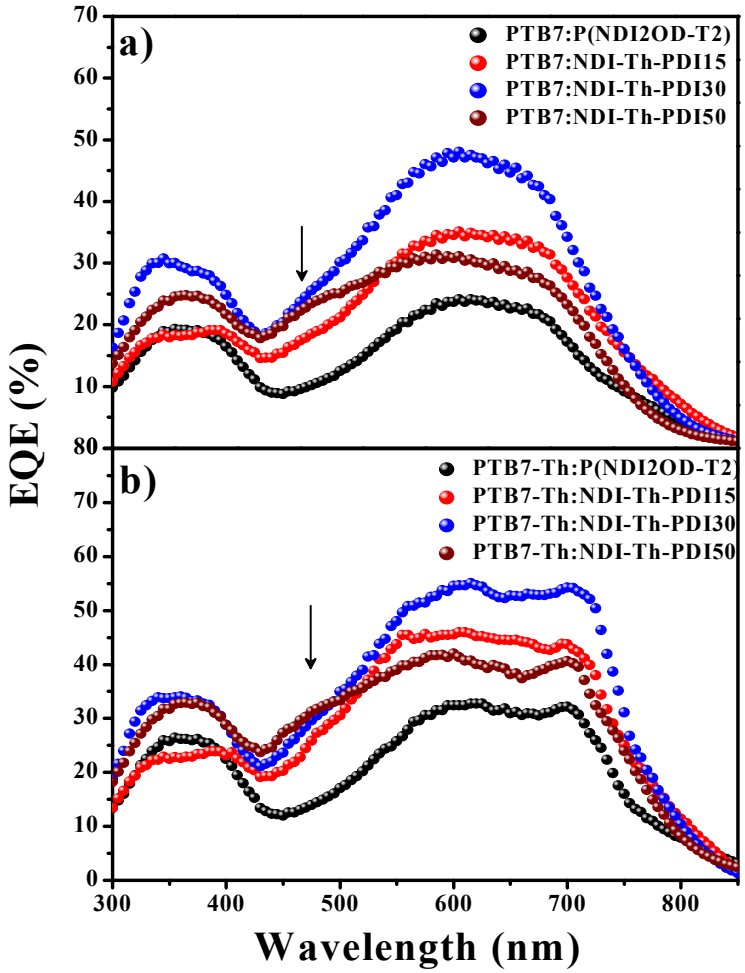

Figure 2.24. EQE spectra of all-PSCs using (a) PTB7 as the donor and (b) PTB7-Th as the donor in the blend polymer devices (under AM1.5G 100mW/cm^2 illumination).

A careful observation of EQE spectra revealed the presence of an additional broad peak at ~480 nm for all random copolymers (shown by arrow in **Figure 2.24**) that was also observed in their absorption spectra, which was attributed to PDI unit. Thus the observed EQE spectra showed that the acceptor polymer in blend also contributed to light harvesting and in photocurrent generation.

2.3.6. Bulk Carrier Charge Transport in BHJ Blend Film

The effect of charge carrier transport properties on the photovoltaic performance was investigated by measuring the bulk electron and hole mobility of polymer/polymer blend films using space charge limited current (SCLC) technique. Mobility measured by SCLC method is more relevant to the bulk process e.g. organic photovoltaic device and OLED (organic light emitting device) devices.[37, 38] All donor: acceptor polymer blend film devices were made similarly as the all-PSCs devices. The electron-only device was fabricated using ITO/ZnO/active layer/Al structure and hole-only device was fabricated using ITO/MoO_3/active layer/Au structure (the detailed procedure of device fabrication is given in experimental section).

Table 2.4 SCLC electron and hole mobilities of donor:acceptor copolymer blend. (In one series PTB-7 was the donor while in the second series PTB7-Th was used as donor.)

Active layer	μ_h (cm^2/Vs)	μ_e (cm^2/Vs)	μ_h/μ_e
PTB7 Donor			
PTB7: P(NDI2OD-T2)	$6.7(\pm0.4)\times10^{-5}$	$7.5(\pm0.5)\times10^{-5}$	0.89
PTB7: NDI-Th-PDI15	$0.8(\pm0.3)\times10^{-4}$	$8.6(\pm0.4)\times10^{-5}$	0.93
PTB7: NDI-Th-PDI30	$3.8(\pm0.2)\times10^{-4}$	$0.8(\pm0.2)\times10^{-4}$	4.75
PTB7: NDI-Th-PDI50	$3.5(\pm0.3)\times10^{-4}$	$7.6(\pm0.4)\times10^{-5}$	4.60
PTB7-Th Donor			
PTB7-Th: P(NDI2OD-T2)	$0.9(\pm0.3)\times10^{-4}$	$0.7(\pm0.4)\times10^{-4}$	1.28
PTB7-Th: NDI-Th-PDI15	$2.6(\pm0.4)\times10^{-4}$	$0.9(\pm0.3)\times10^{-4}$	2.88
PTB7-Th: NDI-Th-PDI30	$4.7(\pm0.5)\times10^{-4}$	$1.1(\pm0.4)\times10^{-4}$	4.27
PTB7-Th: NDI-Th-PDI50	$4.0(\pm0.4)\times10^{-4}$	$1.1(\pm0.3)\times10^{-4}$	3.63

a)

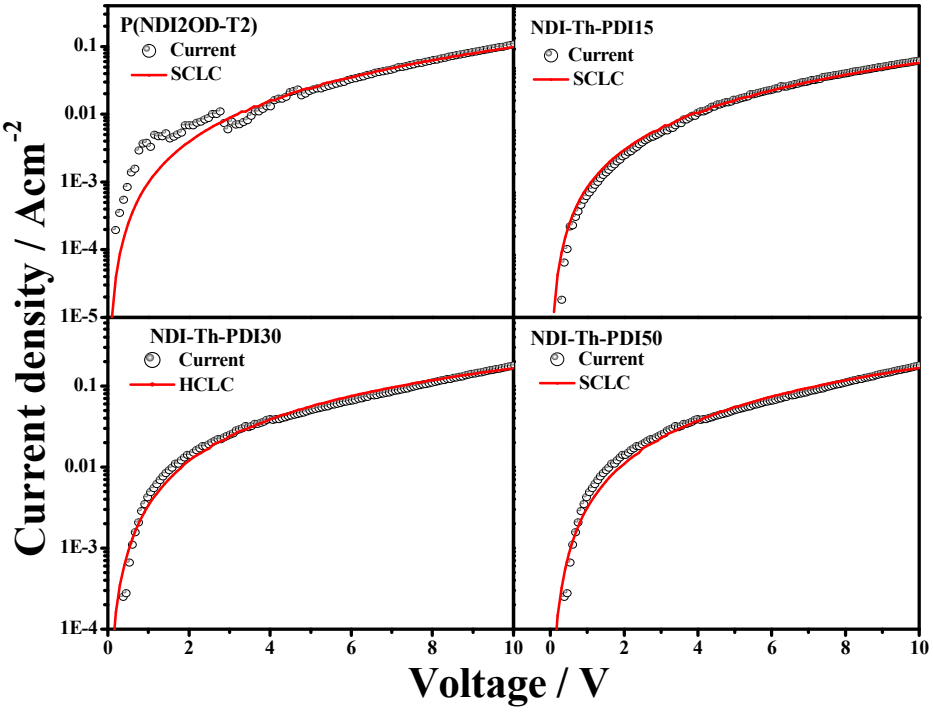
P(NDI2OD-T2)
Current
SCLC
NDI-Th-PDI15
Current
SCLC
NDI-Th-PDI30
Current
HCLC
NDI-Th-PDI50
Current
SCLC
Current density / Acm-2
Voltage / V

b)

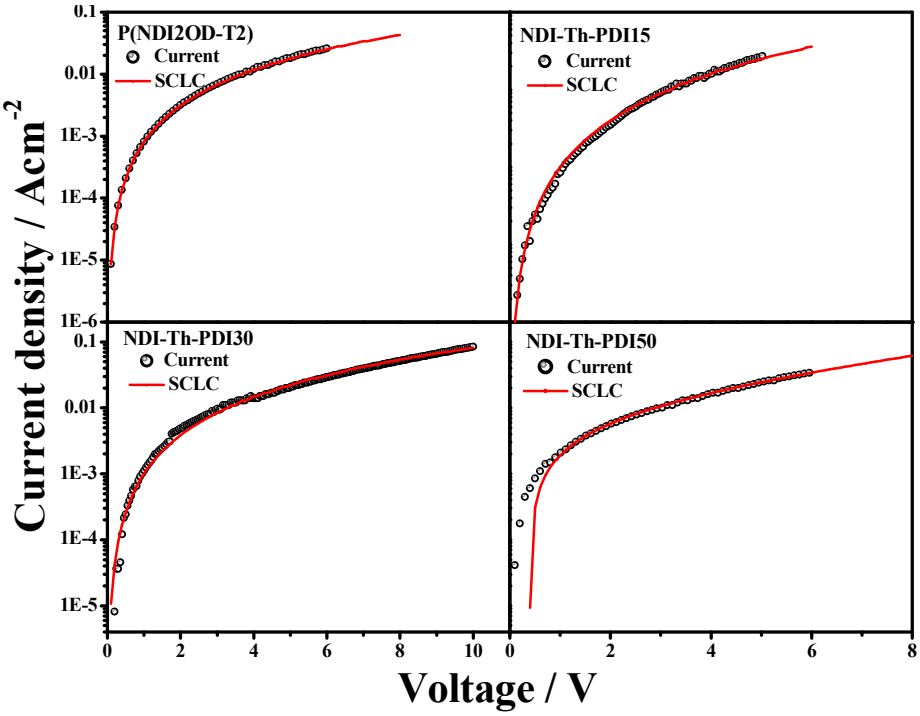
P(NDI2OD-T2)
Current
SCLC
NDI-Th-PDI15
Current
SCLC
NDI-Th-PDI30
Current
SCLC
NDI-Th-PDI50
Current
SCLC
Current density / Acm-2
Voltage / V

c)

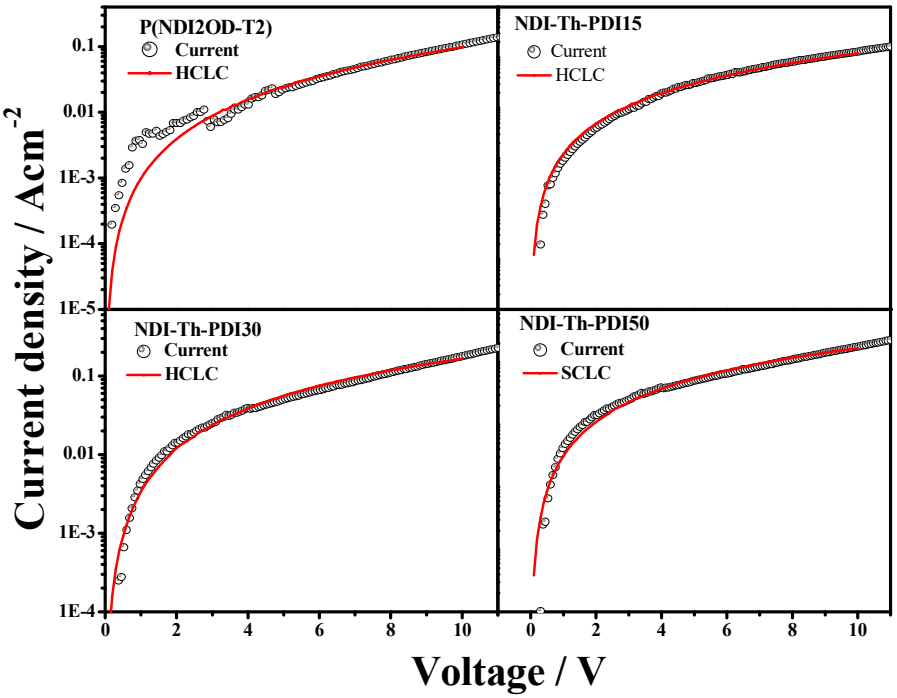

d)

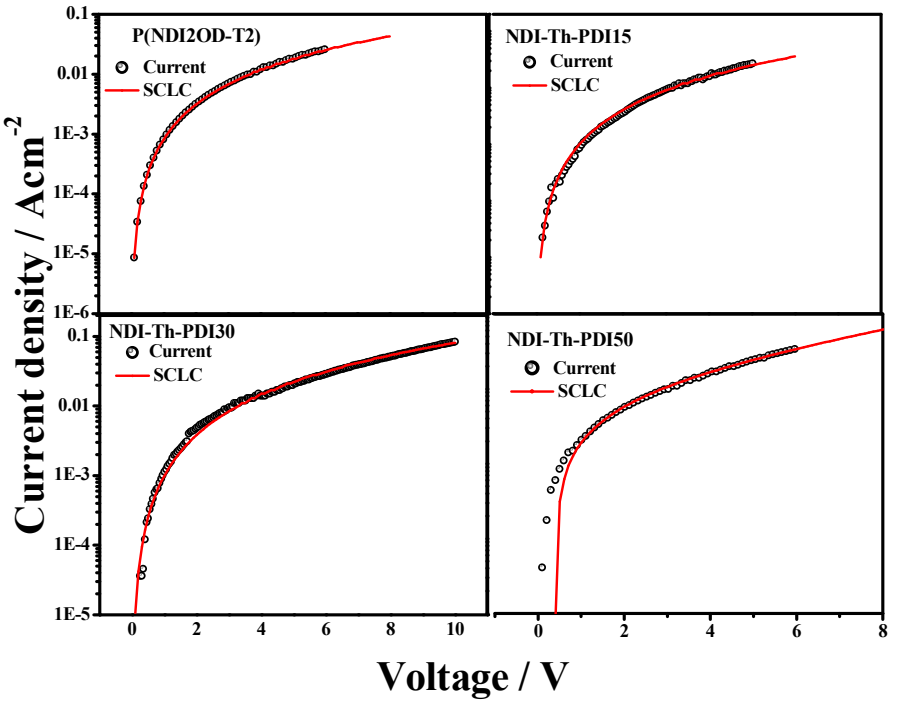

Figure 2.25. Current (*J*) - Voltage (*V*) characteristics and SCLC fittings of PTB7:reference /copolymer blend films (a) Hole-only device and (b) electron-only device and for PTB7-Th: reference / copolymer blend films (c) Hole-only device and (d) electron-only device.

2.3.7. BHJ Solar Cell Morphology

Among various other parameters, the BHJ morphology of active layer (D/A) is one of the important factor that influences the photovoltaic performance.[35] AFM images of donor: acceptor polymer blends were captured, to investigate the surface morphology all-PSCs BHJ devices. The donor: acceptor polymer (1.3:1 w/w) blend films were prepared in identical ways as that for all-PSCs devices. **Figure 2.26** and **Figure 2.27** shows AFM height images (3 μm x 3μm) of PTB7/PTB7-Th: P(NDI2OD-T2) and PTB7/PTB7-Th: NDI-Th-PDI*x* blend solar cell. The reference PTB7: P(NDI2OD-T2) or PTB7-Th: P(NDI2OD-T2) blend film showed rather coarsened morphology with average root mean square (RMS) surface roughness of 2.06 nm and 1.87 nm respectively due to the formation of large polymer aggregate domains. The large phase-separated granular morphology observed in PTB7/PTB7-Th: P(NDI2OD-T2) blend film indicated insufficient donor/acceptor intermixing at nanometer scale.[18-42]

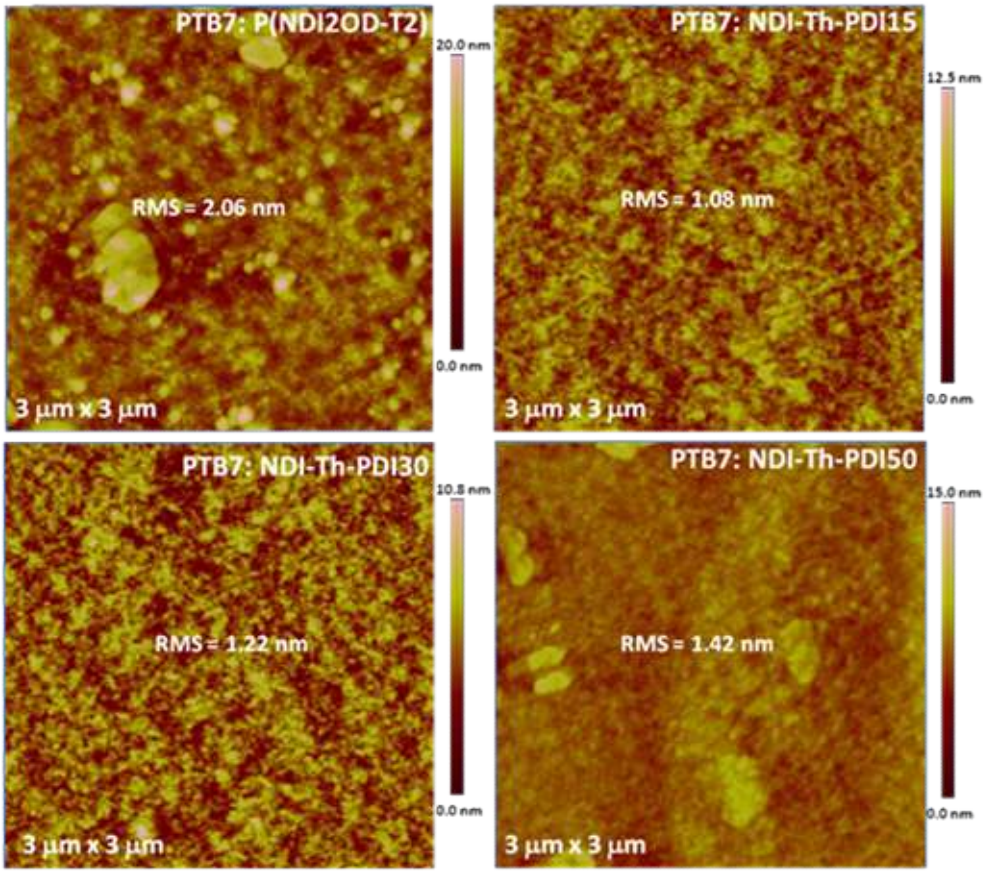

Figure 2.26. AFM height images (3 μm x 3μm) of PTB7: P(NDI2OD-T2) (1.3:1 w/w) and PTB7: NDI-Th-PDI*x* (1.3:1 w/w) blend solar cell.

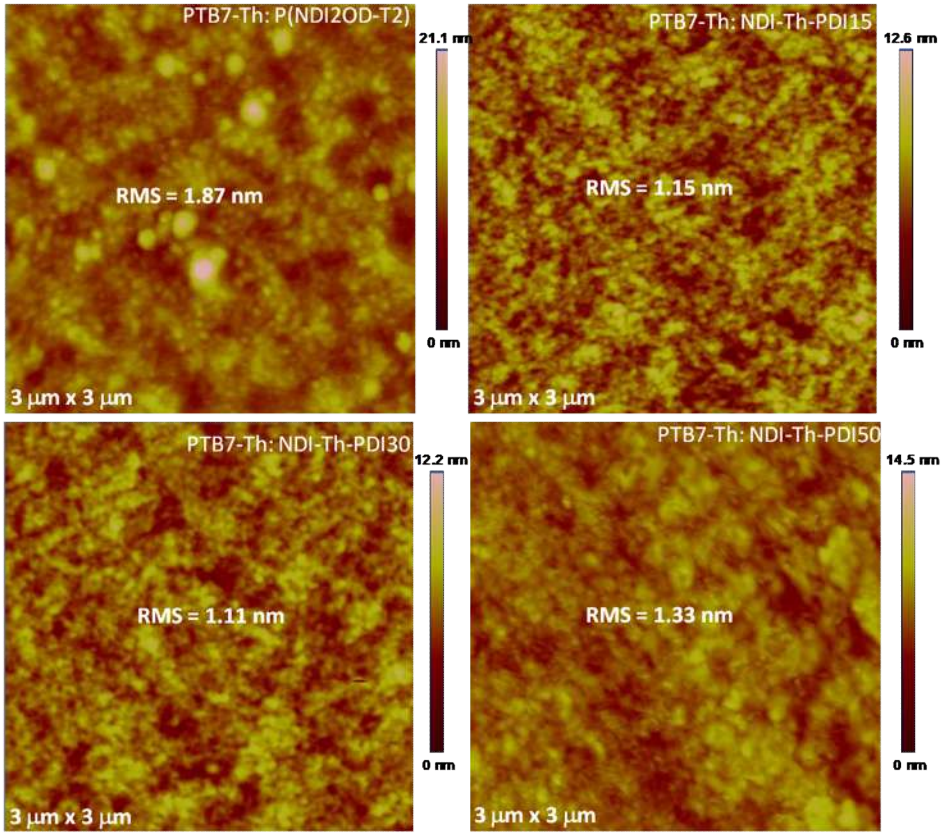

Figure 2.27. AFM height images (3 μm x 3μm) of PTB7-Th: P(NDI2OD-T2) (1.3:1 w/w) and PTB7-Th: NDI-Th-PDI*x* (1.3:1 w/w) blend solar cell.

The incorporation of large PDI unit in the random copolymer showed dramatic change in the surface morphology of PTB7/PTB7-Th: NDI-Th-PDI*x* blend films compared to reference blend. The PTB7: NDI-Th-PDI15 and PTB7: NDI-Th-PDI30 blend films showed proper uniform micro-phase separation with smaller phase-separated domain size. Furthermore, the RMS surface roughness decreased to 1.08 nm in PTB7: NDI-Th-PDI15 blend and 1.22 nm in PTB7: NDI-Th-PDI30 blend which suggested the formation of less aggregated domain leading to better donor/acceptor intermixing at nanometer scale. The well-developed nano-scale interpenetrating network observed in PTB7: NDI-Th-PDI15 and PTB7: NDI-Th-PDI30 blend films is beneficial for exciton dissociation and charge carrier transport.[39] Compared to the other two random copolymer blend, the PTB7: NDI-Th-PDI50 blend film showed high RMS surface roughness of 1.42 nm with coarsened morphology, which was still more uniform with smaller phase-separated domain size compared to the reference PTB7: P(NDI2OD-T2) blend. A similar trend was observed in the blend films with PTB7-Th as the donor (**Figure 2.27**). PTB7-Th: NDI-Th-PDI15 blend and PTB7-Th: NDI-Th-PDI30 blend

films showed more uniform microphase separation (as indicated by the reduced RMS surface roughness) compared to the reference polymer blend. The reduced roughness can play an important role in the charge collection process as it decreases surface recombination and increases the current density as observed from the J-V curves.

2.4. Conclusions

In this study, we synthesized a series of new n-type semiconducting random copolymers NDI-bithiophene/PDI-bithiophene (NDI-Th-PDIx) by incorporating various amount of perylene diimide (PDI) (xPDI = 15, 30, 50 mole % of PDI) co-acceptor unit into P(NDI2OD-T2) polymer. The properties of these acceptor copolymers were investigated in depth in the pristine form as well as their donor-acceptor (D:A) blends with PTB7-Th as donor in order to understand the structural features that influence the all-PSCs performance. Proton NMR, XRD and DSC studies of pristine copolymers showed that increasing PDI content in the random copolymers resulted in progressive reduction of self-aggregation tendency, increased π-π stacking distance and lowering of crystallinity. Although the copolymer with lowest PDI content composition (NDI-Th-PDI 15) exhibited higher ΔHm compared to P(NDI2OD-T2), its D:A blend with PTB7-Th showed reduced crystallinity compared to PTB7-Th:P(NDI2OD-T2) blend. Analysis of blend properties of these acceptor copolymers with PTB7-Th gave important findings such as 1) overall reduction of crystallinity in blends was observed as evidenced by their much lower ΔHm values compared to the pristine samples. 2) All random copolymers exhibited lower extent of crystallinity compared to P(NDI2OD-T2) and the crystallinity was found to decrease as PDI content increased. 3) XRD of the blend films showed disappearance of the higher ordered lamellar peaks in the random copolymers; the reference polymer seemed to retain them in the blend as well. 4) Higher PL quenching was observed in random copolymer blends as compared to P(NDI2OD-T2). Overall, the random copolymers showed reduced inter-chain interaction promoting better compatibility with the donor polymer compared to P(NDI2OD-T2). This was reflected in their bulk photovoltaic properties as well with the random copolymers exhibiting higher PCE compared to P(NDI2OD-T2). A maximum PCE of ~**5 %** was observed in the case of PTB7-Th:NDI-Th-PDI30 blend devices. A precise correlation of the structural variation in the random copolymers with their device performance was not very straightforward. For instance, although least self-aggregation was observed in NDI-Th-PDI50, it did not exhibit the highest PCE value among the random copolymers. AFM imaging analysis indicated large surface roughness for this blend combination. A probable reason for this discrepancy could be the

comparatively low molecular weight of the NDI-Th-PDI50, which was the lowest due to the reduced solubility of the short ethyl hexyl side chain on the PDI unit. Our studies showed that presumably NDI-Th-PDI30 exhibited optimal crystallinity and miscibility with donor polymer which lead to the best D/A compatibility, nano-scale phase separation and bulk carrier charge transport in blend. Thus, it is evident from the structure-property analysis that the incorporation n-type PDI building block into P(NDI2OD-T2) polymer is a very effective strategy to tune its photovoltaic parameters and improved PCE observed in new n-type random copolymers proves its potential application in future all-PSCs.

2.5. References

(1) Zhan, X.; Facchetti, A.; Barlow, S.; Marks, T. J.; Ratner, M. A. *Adv. Mater.* **2011**, *23*, 268-284.

(2) Würthner, F.; Stolte, M. *Chem. Commun.* **2011**, *47*, 5109.

(3) Guo, X.; Facchetti, A.; Marks, T. J. *Chem. Rev.* **2014**, *114*, 8943-9021.

(4) Yan, H.; Chen, Z.; Zheng, Y.; Newman, C.; Quinn, J. R.; Dötz, F.; Kastler, M.; Facchetti, A. *Nature* **2009**, *457*, 679-686.

(5) Kang, H.; Kim, K.-H.; Choi, J.; Lee, C.; Kim, B. J. *ACS Macro Lett.* **2014**, *3*, 1009-1014.

(6) Jung, J. W.; Jo, J. W.; Chueh, C. C.; Liu, F.; Jo, W. H.; Russell, T. P.; Jen, A. K. Y. *Adv. Mater.* **2015**, *27*, 3310-3317.

(7) Hwang, Y. J.; Earmme, T.; Courtright, B. A. E.; Eberle, F. N.; Jenekhe, S. A. *J. Am. Chem. Soc.* **2015**, *137*, 4424-4434.

(8) Kim, Y.; Long, D. X.; Lee, J.; Kim, G.; Shin, T. J.; Nam, K.-W.; Noh, Y.-Y.; Yang, C. *Macromolecules* **2015**, *48*, 5179-5187.

(9) Kang, H.; Uddin, M. A.; Lee, C.; Kim, K.-H.; Nguyen, T. L.; Lee, W.; Li, Y.; Wang, C.; Woo, H. Y.; Kim, B. J. *J. Am. Chem. Soc.* **2015**, *137*, 2359-2365.

(10) Mori, D.; Benten, H.; Okada, I.; Ohkita, H.; Ito, S. *Adv. Energy Mater.* **2014**, *4*, 1301006.

(11) Hwang, Y.-J.; Courtright, B. A. E.; Ferreira, A. S.; Tolbert, S. H.; Jenekhe, S. A. *Adv. Mater.* **2015**, *27*, 4578-4584.

(12) Earmme, T.; Hwang, Y. J.; Murari, N. M.; Subramaniyan, S.; Jenekhe, S. A. *J. Am. Chem. Soc.* **2013**, *135*, 14960-14963.

(13) Kim, R.; Amegadze, P. S. K.; Kang, I.; Yun, H. J.; Noh, Y. Y.; Kwon, S. K.; Kim, Y. H. *Adv. Funct. Mater.* **2013**, *23*, 5719-5727.

(14) Hwang, Y. J.; Murari, N. M.; Jenekhe, S. A. *Polym. Chem.* **2013**, *4*, 3187.

(15) Hwang, Y. J.; Earmme, T.; Subramaniyan, S.; Jenekhe, S. A. *Chem. Commun.* **2014**, *50*, 10801.

(16) Chen, Z.; Zheng, Y.; Yan, H.; Facchetti, A. *J. Am. Chem. Soc.* **2009**, *131*, 8-9.

(17) Steyrleuthner, R.; Schubert, M.; Howard, I.; Klaumünzer, B.; Schilling, K.; Chen, Z.; Saalfrank, P.; Laquai, F.; Facchetti, A.; Neher, D. *J. Am. Chem. Soc.* **2012**, *134*, 18303-18317.

(18) Fabiano, S.; Chen, Z.; Vahedi, S.; Facchetti, A.; Pignataro, B.; Loi, M. A. *J. Mater. Chem.* **2011**, *21*, 5891.

(19) Moore, J. R.; Seifried, S. A.; Rao, A.; Massip, S.; Watts, B.; Morgan, D. J.; Friend, R. H.; McNeill, C. R.; Sirringhaus, H. *Adv. Energy Mater.* **2011**, *1*, 230-240.

(20) Schubert, M.; Dolfen, D.; Frisch, J.; Roland, S.; Steyrleuthner, R.; Stiller, B.; Chen, Z.; Scherf, U.; Koch, N.; Facchetti, A. *Adv. Energy Mater.* **2012**, *2*, 369-380.

(21) Li, Z.; Xu, X.; Zhang, W.; Meng, X.; Ma, W.; Yartsev, A.; Inganäs, O.; Andersson, M. R.; Janssen, R. A. J.; Wang, E. *J. Am. Chem. Soc.*, **2016**, *138,* 10935-10944.

(22) Kim, Y.; Cho, H. H.; Kim, T.; Liao, K.; Kim, B. *Polymer Journal* **2016**, *48*, 517-524.

(23) Li, X.; Sun, P.; Wang, Y.; Shan, H.; Xu, J.; You, C.; Xu.; Z.-X .; Chen, Z-K. *Polym. Chem.* **2016**, *7*, 2230-2238.

(24) Dai, S.; Cheng, P.; Lin, Y.; Wang, Y.; Ma, L.; Ling, Q.; Zhan, X. *Polym Chem* **2015**, *6*, 5254-5263.

(25) Kozycz, L. M.; Gao, D.; Tilley, A. J.; Seferos, D. S. *J. Polym. Sci. Part A: Polym. Chem.* **2014**, *52*, 3337-3345.

(26) Mott, N. F.; Gurney, R. W. Electronic Processes in Ionic Crystals; Oxford University Press: London, 1940.

(27) Jones, B. A.; Ahrens, M. J.; Yoon, M. H.; Facchetti, A.; Marks, T. J.; Wasielewski, M. R. *Angew. Chem. Int. Ed.* **2004**, *43*, 6363-6366.

(28) Popere, B. C.; Della Pelle, A. M.; Thayumanavan, S. *Macromolecules* **2011**, *44*, 4767-4776.

(29) Kolhe, N. B.; Ashar, A. Z.; Narayan, K. S.; Asha, S. K. *Macromolecules* **2014**, *47*, 2296-2305.

(30) Jung, J.; Lee, W.; Lee, C.; Ahn, H.; Kim, B. J *Adv. Energy Mater.***2016**, *16,* 1614-6832.

(31) Schuettfort, T.; Huettner, S.; Lilliu, S.; Macdonald, J. E.; Thomsen, L.; McNeill, C. R., *Macromolecules* **2011***, 44,* 1530-1539.

(32) Lee, W.; Lee, C.; Yu, H.; Kim, D. J.; Wang, C.; Woo, H. Y.; Oh, J. H.; Kim, B. J. *Adv. Funct. Mater.* **2016**, *26*, 1543-553.

(33) Durban, M. M.; Kazarinoff, P. D.; Luscombe, C. K. *Macromolecules* **2010**, *43*, 6348-6352.

(34) Jung, J. W.; Russell, T. P.; Jo, W. H. *Chem. Mater.* **2015**, *27*, 4865-4870.

(35) Zhou, N.; Lin, H.; Lou, S. J.; Xinge, Y.; Guo, P.; Manley, E. F.; Loser, S.; Hartnett, P.; Huang, H.; Wasielewski, M. R.; Chen, L. X.; Chang, R. P. H.; Facchetti, A.; Marks, T. J. *Adv. Energy Mater.* **2014**, *4*, 1300785.

(36) Mori, D.; Benten, H.; Okada, I.; Ohkita, H.; Ito, S. *Energy Environ. Sci.* **2014**, *7*, 2939-2943.

(37) Steyrleuthner, R.; Schubert, M.; Jaiser, F.; Blakesley, J. C.; Chen Z.; Facchetti, A.; Neher, D. *Adv. Mater.* **2010**, *22*, 2799-2803.

(38) Rivnay, J.; Steyrleuthner, R.; Jimison, L. H.; Casadei, A.; Chen, Z.; Toney, M. F.; Facchetti, A.; Neher, D.; Salleo, A. *Macromolecules*, **2011**, *44*, 5246-5255.

(39) Huang, Y.; Kramer, E. J.; Heeger, A. J.; Bazan, G. C. *Chem. Rev.* **2014**, *114*, 7006-7043.

Chapter 3

All-Polymer Solar Cell Performance of n-type Naphthalene diimide-bithiophene P(NDI2OD-T2) Copolymer with PCBM as Co-acceptor

3.1. Introduction

As discussed in the previous chapter, random incorporation of n-type PDI building block into P(NDI2OD-T2) polymer is a very effective strategy to fine-tune its photovoltaic properties and improve PCE. Incorporation of PDI unit in the polymer reduced the self-aggregation of the polymer which improved the PCE. Random copolymerization is a promising designed strategy to develop new NDI based acceptor copolymers which exhibit significant improvement in the power conversion efficiency.

As discussed in **chapter 1** the most commonly used n-type system is PCBM (phenyl-C61-butyric acid methyl ester) and its derivatives. PCBM is used in bulk heterojunction blend as acceptor material with various donor polymers for high efficiency.[1] Heeger et al. reported for the first time PCBM as an acceptor blended in BHJ solar cells with MEH-PPV polymer as a donor. Since then, PCBM has been extensively used in the BHJ solar cells fabrication.[2] PCBM has some drawbacks such as phase separation and weak absorption, but still, PCBM is one of the best acceptor materials so far.[3] PCBM exhibits outstanding characteristics such as high charge carrier mobility,[4-6] small reorganization energy,[7-9] very high electron affinity[10] and compatible energy levels. For P3HT/PCBM blend system nearly 4% PCE has been achieved. There are several reports in the literature for covalent incorporation of PCBM, mostly as side chain substitution of π-conjugated block copolymers.[11-18] The covalent approach is expected to reduce phase segregation issues and improve the device performance.

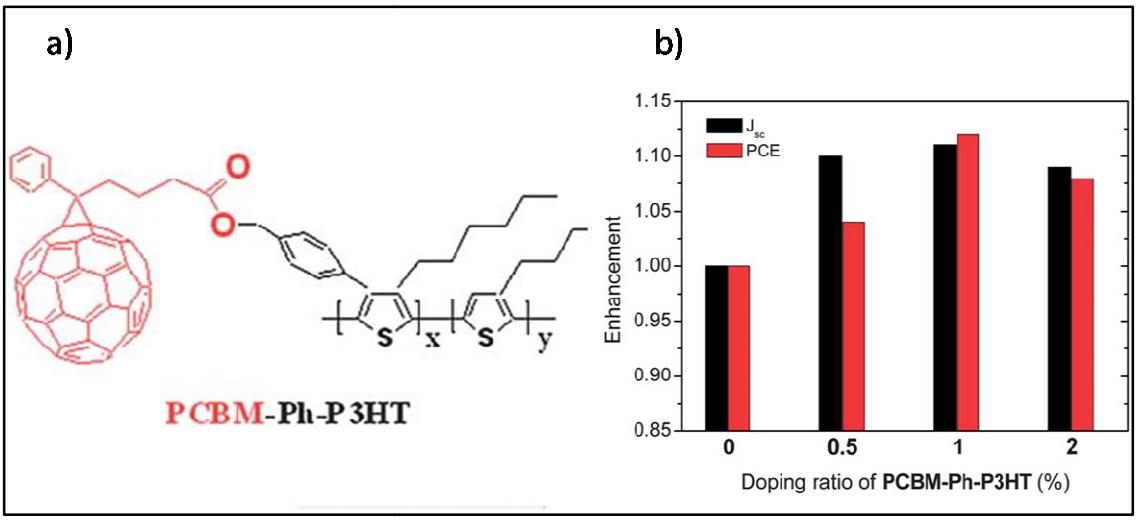

Figure 3.1. a) Structure of the polymer PCBM-Ph-P3HT. b) Dependence of the enhancement of Jsc and PCE of PCBM-Ph-P3HT:P3HT: PCBM BHJ-PSC devices on the doping ratio of PCBM-Ph-P3HT (Adapted from ref. 19).

Yang et al. reported side chain substitution of P3HT via PCBM. Polymer PCBM-Ph-P3HT was doped in the blend formation with P3HT: PCBM in different weight ratios.[19] PCBM-Ph-P3HT improved the interpenetrating networks of the P3HT:PCBM due to its amphiphilicity toward PCBM and P3HT components like a "surfactant." P3HT:PCBM devices doped by PCBM-Ph-P3HT showed enhanced PCE, with the maximum PCE being 3.40 % at the optimum PCBM-Ph-P3HT doping ratio of 1 wt %, which was 12 % enhancement compared to that of the reference P3HT: PCBM device. The enhancement of PCE is attributed to the increase of Jsc, and the improvement emphasizes that the improvement in bicontinuous interpenetrating networks lead to enhancement of charge carrier mobility in the blend (shown in **Figure 3.1**).

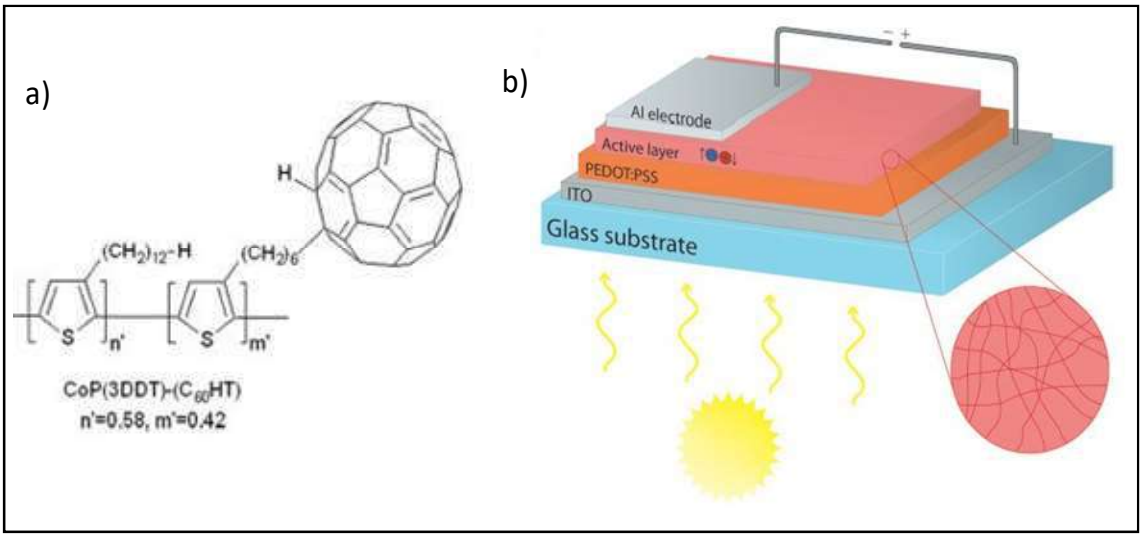

Figure 3.2. Copolymer structure (a) and device architecture (b) (Adapted From ref. 20).

Pierini et al. reported fullerene grafted polythiophenes for single material organic solar cells (SMOCs), shown in **Figure 3.2**.[20] The polymer showed high power conversion efficiency of 5.58 %. The efficiency enhancement confirmed that the design of novel macromolecules were supported by the development of a well defined architecture which confirmed the active layer nanostructure formation and polymer supramolecular arrangement in order to obtain high performance.

Polymer P(NDI2OD-T2) has good photovoltaic properties,[21-22] but it is still not high enough to be considered as an alternative of PCBM. So to improve the charge carrier mobility and efficiency of the polymer, we have synthesized a series of new *n*-type NDI-bithiophene/PCBM-bithiophene random copolymers (PNDI-Th-PCBM*x*) by incorporating varying amounts of thiophene substituted PCBM as co-acceptor along with NDI. The effect

of random copolymer compositions on their energy level, optical properties, crystallinity, blend morphology, and all-PSC performance was scrutinized. The all-PSCs performance of the newly synthesized random copolymers was investigated with PTB7-Th as the donor polymer. The device efficiency was compared with that of P(NDI2OD-T2) polymer as a reference.

3.2. Experimental Section

3.2.1 Materials

1,4,5,8-Naphthalenetetracarboxylicdianhydride (NTCDA), 2-octyldodecanol, 2-ethylhexylamine, 3-thiophenemethanol 98%, [6,6]-phenyl C61 butyric acid methyl ester >99.5% , N′-ethylcarbodiimide hydrochloride (EDC), 4-(dimethylamino)pyridine ≥99 %, bis(triphenylphosphine) palladium (II) dichloride ($Pd(Ph_3)_2Cl_2$) were purchased from Sigma Aldrich and used without further purification. The donor polymers PTB7-Th and monomer 5,5'-bis (trimethylstannyl)-2,2'-bithiophene 97 % used in all-polymer solar cell study were purchased from Lumtech and used without further purification.

3.2.2 Measurements

^{1}H NMR spectra were recorded using 400 MHz Brucker NMR spectrophotometer in $CDCl_3$ or 1,1,2,2-tetrachloroethane -d_2 containing small amounts of TMS as an internal standard. The molecular weights of polymers were determined using gel permeation chromatography (GPC). GPC measurements were carried on a Thermo Quest (TQ) GPC at 25^{o}C using chloroform as the mobile phase. The analysis was carried out at a flow rate of 1 mL/min using a set of five μ-Styragel HT columns (HT-2 to HT-6) and a refractive index (RI) detector. Columns were calibrated with polystyrene standards and the molecular weights are reported with respect to polystyrene. UV–Vis spectra were recorded using Perkin Elmer Lambda 950 UV-Vis spectrometer. Thermogravimetric analysis (TGA) was performed using a Perkin Elmer thermogravimetric analyzer. Samples were run from 30 to 800 °C with a heating rate of 10 °C/min under nitrogen. WAXRD were recorded using Rigaku, MicroMax-007HF with high-intensity Microfocus rotating anode X-ray generator. All the spectra were recorded in the range of 2θ = 2-50 degrees and data were collected with the help of Control Win software. Electrochemical behavior of copolymers was studied by using BAS-Epsilon potentiostat. The device fabrication was carried out by self at SEM-TEL, IIT- Kanpur.

3.2.3 Fabrication and Characterization of the Photovoltaic Cells

PTB7-Thas donor and P(NDI2OD-T2) and PNDI-Th-PCBMx (x = 5, 7.5, 15 mole % of PCBM) acceptors were used**.** PTB7-Th was blended with each of the four acceptors separately in chloroform and stirred at 25 °C for more than 24 h in a glove box. The optimized donor: acceptor (D:A) ratio was 1.3:1 (w/w) and total concentrations of (D+A) in chloroform solution was ~12 mg/ml. Preparation of ZnO sol-gel was done as follows. Zinc acetate dihydrate [$Zn(CH_3COO).2H_2O$] (Aldrich, 99.9 %) with 0.1 M concentration was first dissolved in anhydrous 2-methoxyethanol [$CH_3CH_2OCH_3$] (99.5 + % Aldrich) and subsequently, ethanolamine was added to the solution as sol stabilizer followed by thorough mixing with a magnetic stirrer for 12-15 h at room temperature. Inverted type all polymer solar cells were fabricated using an indium tin oxide (ITO)/ZnO/active layer/MoO_3/Ag structure. ITO-coated glass substrates were subjected to ultrasonication in soap, deionized water, acetone and in isopropyl alcohol. The ITO substrates were treated with UV-plasma before ZnO sol-gel was spin-coated on the ITO-coated glass substrate with 2000 rpm for 60 sec. The ZnO films were annealed at 250 °C for 20 minutes in the air. Then, each active blending solution was spin-casted onto an ITO/ZnO/ substrate at 2000 rpm for 120 s. The final thickness of each film was ~100-110 nm. Then, MoO_3 (~ 10 nm) was thermally deposited in high vacuum (~1 x 10^{-6} torr). Finally, Ag (~100 nm) was deposited under high vacuum (~1 x 10^{-6} torr), through a shadow mask. The active area of the devices was 16 mm^2 in all the cases. The photovoltaic performance of the devices was characterized using a solar simulator using Keithley 2400 source-meter under 1 sun AM 1.5 G illumination from (Class AAA, Newport-Oriel, USA). The illumination intensity was adjusted using a calibrated reference silicon solar cell. To ensure well defined active areas, the J-V measurements were performed using laser-cut stainless steel square masks.

3.2.4 Synthesis of Monomers

The synthesis NDI-2OD-Br_2 was detailed in **Chapter 2** in **section 2.2.6.**[23]

1) [6,6]-Phenyl-C61-butyric Acid (PCBA) (1)

25 mL of glacial acetic acid and 15 ml of HCl were added in the solution of [6,6]-phenyl-C61-butyric acid methyl ester (PCBM) (250 mg, 0.274 mmol) in 50 mL of o-dichlorobenzene solution. This solution was further refluxed for 18 h. After the completion of reaction solvent was removed and the crude product was washed with methanol and dried over sodium sulfate

(Na_2SO_4). Yield = 230 mg (93 %, brown powder). ^{1}H-NMR ($CDCl_3$, 200 MHz) δ ppm: 7.76 (d, 2H), 7.39-7.29 (m, 3H), 2.78-2.73 (m, 2H), 2.30 (t, 2H), 2.05-1.98 (m, 2H).

2) (2,5-dibromo thiophene-3-yl)methanol (2)

Thiophene-3-ylmethanol (5 g, 43.79 mmol) in dry THF (150 mL) and NBS (19.48 g, 109.49 mmol) was added dropwise and stirred for 72 hours at room temperature under nitrogen atmosphere. The solvent was evaporated by rotary evaporator. Then the crude material was washed with KOH (1.0 M, 25 mL), extracted with diethyl ether and dried over sodium sulfate (Na_2SO_4). It was further purified by column chromatography (pet ether: ethyl acetate = 4:1, as eluent). Yield = 10 g, (84 %, crystalline white solid). ^{1}HNMR ($CDCl_3$, 200 MHz) δ ppm: 7.01 (s, 1H), 4.57-4.54 (s, 2H), 1.91 (broad, 1H).

3) PCBTM (3)

A 25 mL two neck-round bottom flask was charged with [6,6]-phenyl-C61-butyric acid (PCBA) (1) (100 mg, 0.11 mmol), (2,5-dibromo thiophene-3-yl)methanol (2) (30.2 mg, 0.11 mmol), DMAP (1.8 mg, 0.27 mmol), and 0.7 mL of anhydrous o-dichlorobenzene. The solution was cooled to 0 ^{o}C and EDC (56.6 mg, 0.277 mmol) was added. After removing the ice bath, the reaction mixture was stirred at room temperature for 16 h. The resulting crude product was washed with methanol and purified by column chromatography (toluene as eluent). Yield = 75 mg (58 %). ^{1}HNMR ($CDCl_3$, 200 MHz) δ ppm: 7.90 (d, 2H), 7.52-7.47 (m, 4H), 6.93 (s, 1H), 4.98 (s, 2H), 2.89 (d, 2H), 2.59 (d, 2H), 2.17 (d, 2H).

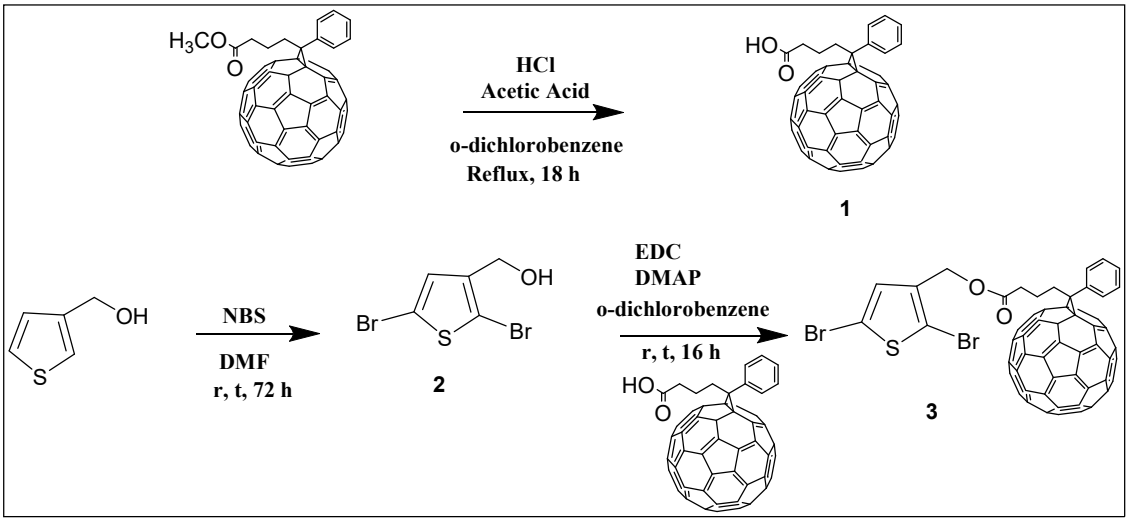

Scheme 3.1. Synthesis of monomer.

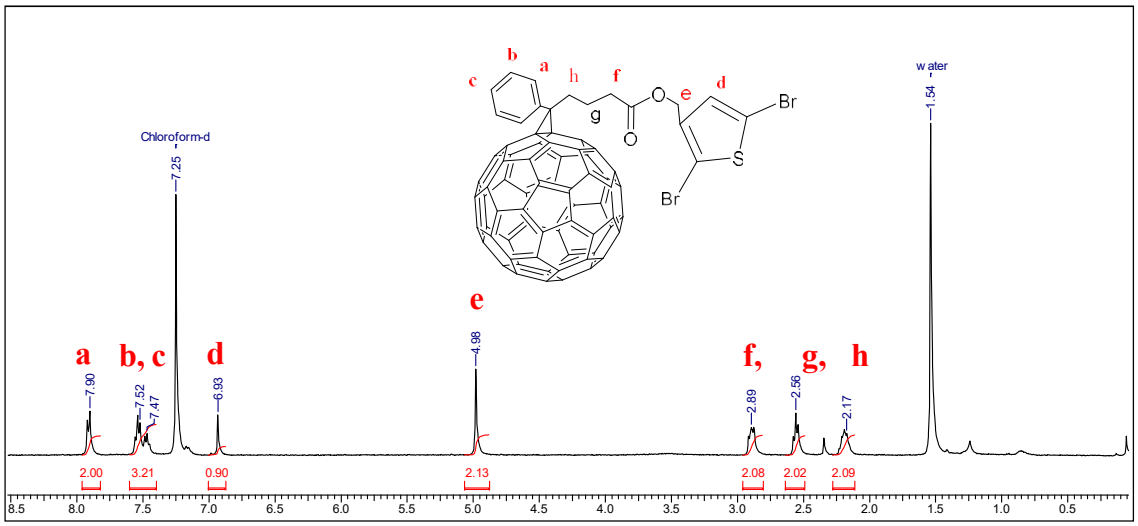

Figure 3.3. ^{1}H NMR spectrum of PCBMT recorded in $CDCl_3$.

3.2.5 Synthesis of Homo and Random Copolymers

1) Poly{[N,N′-bis(2-octyl-dodecyl)-1,4,5,8-naphthalenedicarboximide-2,6-diyl]-alt-5,5′-(2,2′-bithiophene)}, P(NDI2OD-T2)

NDI-2OD-Br_2 (0.4 g, 0.406 mmole) and 5,5'-bis (trimethylstannyl)-2,2'-bithiophene (0.199 g, 0.406 mmol) were taken in Schlenk tube under N_2 atmosphere. Dry toluene (18 mL) was added to the tube followed by purging with nitrogen for half-hour. Bis(triphenylphosphine) palladium (II) dichloride ($Pd(Ph_3)_2Cl_2$) (15 mg, 0.0211 mmol) was added to the tube, and the whole mixture was degassed by nitrogen. The reaction mixture was stirred at 90-95 °C for 72 hours. Bromothiophene (0.2 mL) was then added as end capper, and the reaction mixture was further stirred at 90-95 °C for 12 hours. Upon cooling to room temperature, a solution of potassium fluoride (1 g) in 2 mL water was added and stirred for 2 hours. The reaction mixture was extracted with chloroform (250 mL x 3). The organic layer was washed with water, dried over anhydrous sodium sulfate and concentrated on a rotary evaporator. The obtained residue was dried in vacuum oven and subjected to Soxhlet extraction with methanol (24 hours), acetone (48 hours) and chloroform (12 hours). Half of the chloroform was evaporated and concentrated polymer solution was precipitated in 500 mL methanol, stirred for 2 hours, filtered on Buchner funnel, washed with methanol and dried in vacuum. The polymer was obtained as a deep blue solid, Yield = 0.385 g (97 %). ^{1}H NMR (400 MHz, 1,1,2,2-tetrachloroethane-d_2) δ ppm: 8.82-8.5 (br, 2H), 7.33 (br, 4H), 4.12 (br, 4H), 2.00 (br, 2H), 1.26 (br, 64H), 0.85 (br, 12 H). GPC: M*n*, 21.8 kDa; M*w*, 86.7 kDa; *Đ*, 3.97.

All the random copolymers i,e PNDI-Th-PCBM5, PNDI-Th-PCBM7.5 and PNDI-Th-PCBM15 were prepared using the same procedure as that given for P(NDI2OD-T2), but with different mole ratios of NDI-2OD-Br_2 to PCBMT monomers.

2) PNDI-Th-PCBM5

PNDI-Th-PCBM5 was synthesized using 5,5'-bis (trimethylstannyl)-2,2'-bithiophene (0.200 g, 0.406 mmol), NDI-2OD-Br_2 (380 mg, 0.386 mmol), PCBMT (23.3 mg, 0.0020 mmol) and $Pd(Ph_3)_2Cl_2$ (18 mg, 0.0211 mmol). Yield = 0.38 g (94 %) ^{1}H NMR (400 MHz, 1,1,2,2-tetrachloroethane-d_2) δ ppm: 8.82-8.5 (br, 2H), 7.37 (br, 4H), 4.12 (br, 4H), 2.01 (br, 4H), 1.26 (br, 80H), 0.86 (br, 24H). GPC: M*n*, 33.4 kDa; M*w*, 190 kDa; *Đ*, 5.7.

3) PNDI-Th-PCBM7.5

PNDI-Th-PCBM7.5 was synthesized using 5,5'-bis (trimethylstannyl)-2,2'-bithiophene (0.200 g, 0.406 mmol), NDI-2OD-Br_2 (370.4 mg, 0.370 mmol), PCBMT (35.1 mg, 0.0031 mmol) and $Pd(Ph_3)_2Cl_2$ (18 mg, 0.0211 mmol). Yield = 0.38 g (93 %). ^{1}H NMR (400 MHz, 1,1,2,2-tetrachloroethane-d_2) δ ppm: 8.82-8.5 (br, 6H), 7.37(br, 8H), 4.12 (br, 4H), 3.45-2.55 (m, 1H), 2.00 (br, 4H), 1.26 (br, 80H), 0.86 (br, 24 H). GPC: M*n*, 28.8 kDa; M*w*, 153 kDa; *Đ*, 5.28.

4) PNDI-Th-PCBM15

PNDI-Th-PCBM15 was synthesized using 5,5'-bis (trimethylstannyl)-2,2'-bithiophene (0.150 g, 0.30 mmol), NDI-2OD-Br_2 (255.3 mg, 0.25 mmol), PCBMT (52 mg, 0.0045 mmol) and $Pd(Ph_3)_2Cl_2$ (18 mg, 0.0211 mmol). Yield = 0.253 g (82 %). ^{1}H NMR (400 MHz, 1,1,2,2-tetrachloroethane-d_2) δ ppm: 8.82, 8.5 (br, 2H), 7.94 (br, 0.28H), 7.38 (br, 8H), 4.98 (br, 0.34 H), 4.12 (br, 4H), 2.92-2.54 (m, 1H), 2.00 (br, 2H), 1.26 (br, 80H), 0.86 (br, 16 H). GPC: M*n*, 18.2 kDa; M*w*, 77.2 kDa; *Đ*, 4.25.

3.3 Results and Discussion

3.3.1 Synthesis and Characterization

The poly{[N,N′-bis(2-octyl-dodecyl)-1,4,5,8-naphthalenedicarboximide-2,6-diyl]-alt-5,5′-(2,2′ bithiophene)} P(NDI2OD-T2) and its random copolymers NDI bithiophene / PCBMT bithiophene incorporating various mole percentage of PCBMT were prepared by Stille coupling polymerization. The molecular structure of P(NDI2OD-T2) is shown in **Scheme 3.2,** and the synthesis of their random copolymers are shown in **Scheme 3.3.** The synthesis of monomer *N,N*'-bis(2-octyldodecyl)-2,6-dibromonaphthalene-1,4:5,8 tetracarboxylicdiimide

(NDI-2OD-Br_2) were provided in **Chapter 2** in **section 2.2.6.**[24-26] Synthesis of monomer PCBMT is shown in **Scheme 3.1**. Random copolymers i.e. PNDI-Th-PCBM5, PNDI-Th-PCBM7.5 and PNDI-Th-PCBM15 were synthesized by varying the feed ratio of the two monomers NDI-2OD-Br_2 and PCBMT (5, 7.5, 15 mole % of PCBMT) while maintaining the concentration of the donor bithiophene comonomer constant (1 mole) in the feed. The higher incorporation of PCBMT monomer having bulky C_{60} unit produced random copolymers which had limited solubility in common organic solvents and higher incorporation of PCBM also has been shown to result in phase separation. A maximum incorporation of 15 mole percentage of P**CBM** in random copolymer (PNDI-Th-PCBM15) was found to result in good solubility in common organic solvents like chloroform, chlorobenzene and dichlorobenzene etc.

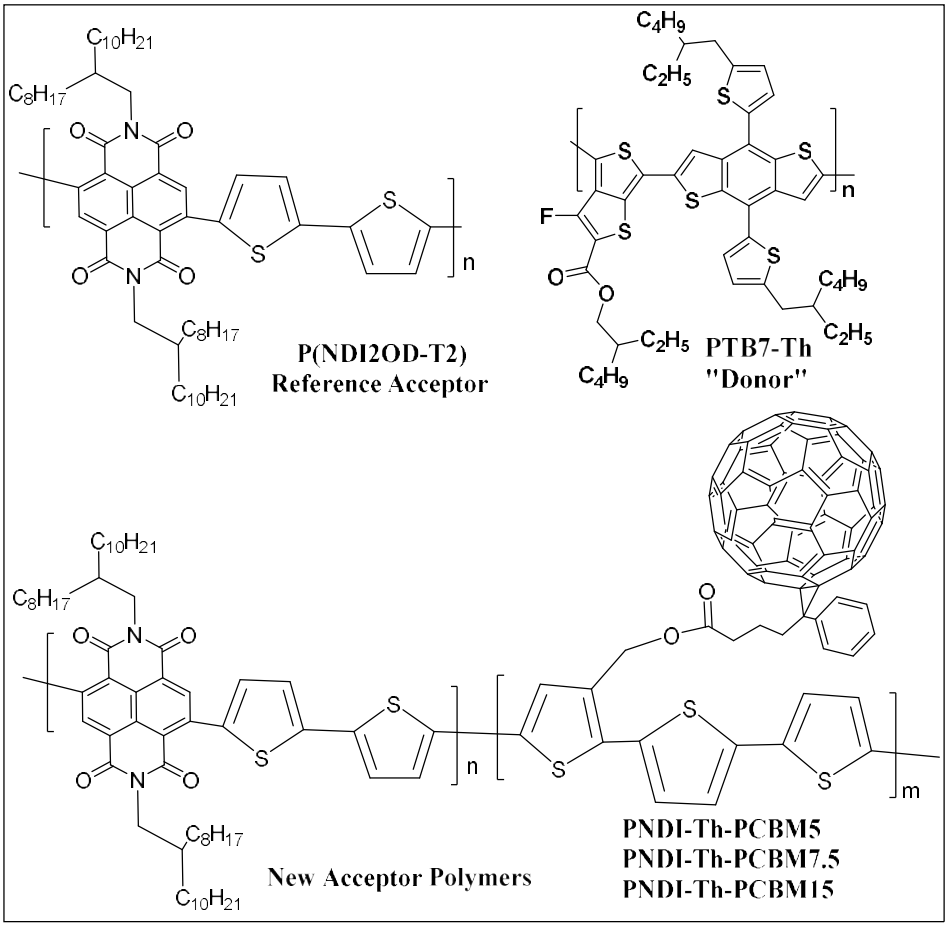

Scheme 3.2. Chemical structure of P(NDI2OD-T2) acceptor, PTB7-Th donor polymers and new random copolymers.

The alternate copolymer NDI-bithiophene (P(NDI2OD-T2) **Scheme 3.2** was synthesized as the reference polymer. The monomers were structurally characterized by proton NMR spectra; polymers were characterized by NMR and GPC. The NMR of the molecules confirmed the structure and high purity of the monomers. The labeled ^{1}H NMR spectrum of monomer PCBMT is shown in **Figure 3.3** while the ^{1}H NMR spectra of copolymers recorded in deuterated 1,1,2,2-tetrachloroethane-d_2, are given in **Figures 3.5-3.7.** Deuterated 1,1,2,2-tetrachloroethane-d_2 is used for recording proton MNR spectra of copolymers to avoid the overlap of the aromatic protons with $CDCl_3$ peaks. The actual incorporation of the PCBM in the random copolymers could be determined from the proton NMR spectra for the random copolymers with the highest PCBM incorporation PNDI-Th-PCBM15. Due to the very less incorporation of PCBM in the copolymers PNDI-Th-PCBM5 and PNDI-Th-PCBM7.5 it was not possible to determine their actual incorporation.

Figure 3.6 shows the expanded region (3.5 to 9.5 ppm) in the proton NMR spectra of the monomer PCBMT, random copolymer PNDI-Th-PCBM15 and reference copolymer P(NDI-2OD-T2). The ^{1}H NMR spectra of polymer P(NDI2OD-T2) and random copolymers exhibited one extra broad peak at ~8.5 ppm which has been attributed to strong inter-chain aggregation in 1,1,2,2-tetrachloroethane-d_2. The peaks at 8.5 and 8.82 ppm together accounted for the two aromatic protons of naphthalene core, while the peak at 7.33 ppm corresponded to the four protons of the bithiophene unit. From the figure it could be seen that in the random copolymer PNDI-Th-PCBM15 new peak appeared at ~7.94 ppm from the PCBMT aromatic protons. In the other two copolymers with lower PCBM incorporation, this peak at 7.94 ppm was hardly visible. For the PNDI-Th-PCBM15 copolymer the actual incorporation of PCBM could be determined by comparing the integration of peaks at 7.98 ppm and at 4.12 ppm, which corresponded to the four CH_2 protons next to the imide N on the NDI ring. The PCBM incorporation was calculated as 14 % for the copolymer having 15 mole % of PCBM in the feed. The molecular weights of the polymers were determined using SEC in $CHCl_3$. The reference copolymer P(NDI2OD-T2) showed number average molecular weight (Mn) of 21.8 kDa and weight average molecular weight (Mw) of 86.7 kDa with PDI (Đ) of 3.97 comparable with literature reports.[24-25] Random copolymers showed higher number average molecular weight (Mn) in the range of 18.2-33.4 kDa and weight average molecular weight (Mw) in the range of 77.3-190 kDa and PDI (Đ) in range of 4.3-5.7 (**Table 3.1**). The Mn, Mw and (Đ) were found to decrease as the content of PCBM unit increased in the random copolymer.

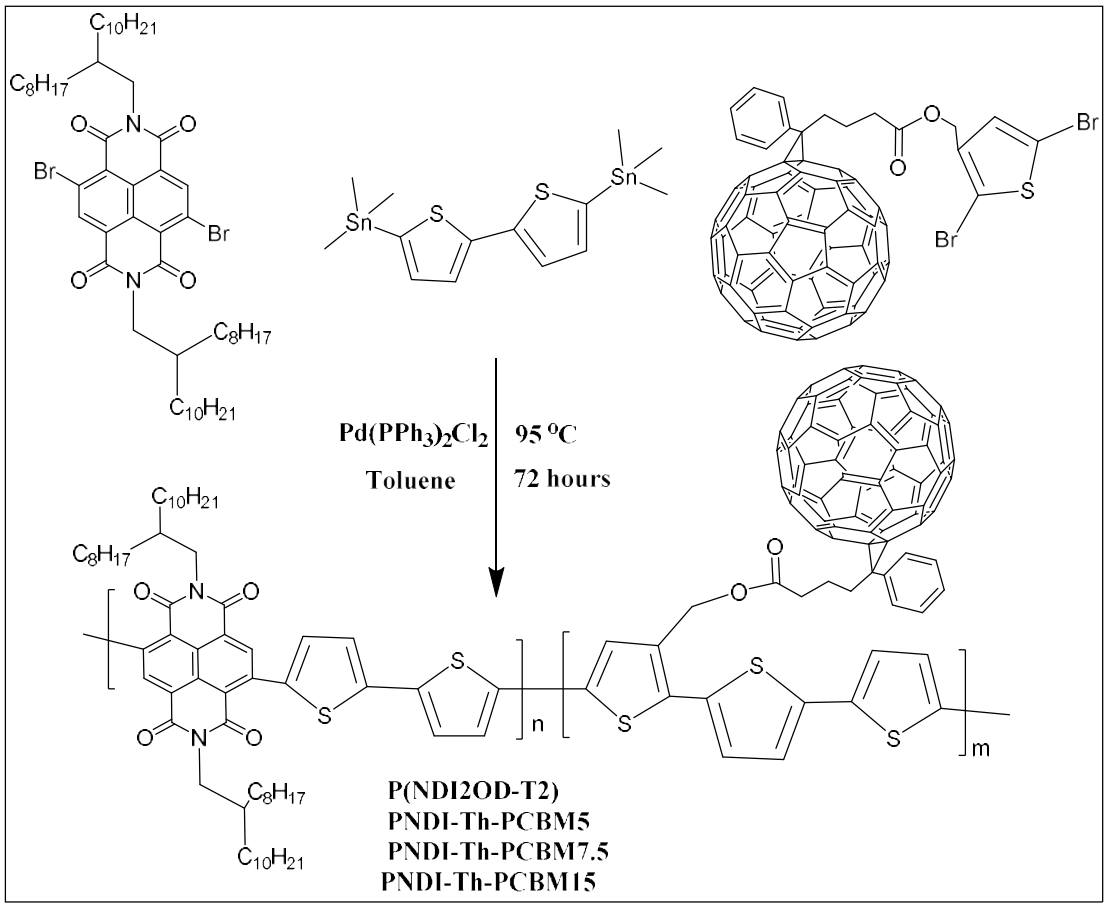

Scheme 3.3. Synthesis of n-type NDI-bithiophene /PCBMT-bithiophene random copolymers

Table 3.1 GPC molecular weight, and thermal characteristics of P(NDI2OD-T2) and PNDI-Th-PCBM*x* random copolymers.

Polymer	Mw[a] (KDa)	Đ[b]	T_d[c] (^oC)	T_m[d](^oC)	ΔH_m[d](J/g)
P(NDI2OD-T2)	86.7	4.0	450	305	7.49
PNDI-Th-PCBM5	190	5.7	451	313	8.34
PNDI-Th-PCBM7.5	153	5.3	450	304	2.39
PNDI-Th-PCBM15	77.3	4.3	445	290	3.55

[a] Weight-average molecular weight (M*w*). [b] Polydispersity index (Đ). [c] The decomposition temperature (10% weight loss) estimated using TGA under N_2. [d] Measured using DSC under N_2.

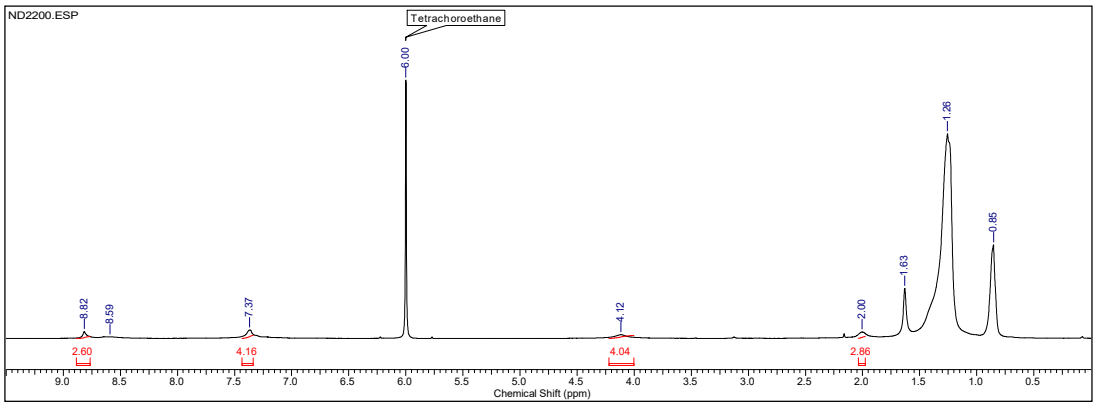

Figure 3.4. ^{1}H NMR spectrum of P(NDI2OD-T2) recorded in deuterated 1,1,2,2-tetrachloroethane-d_2.

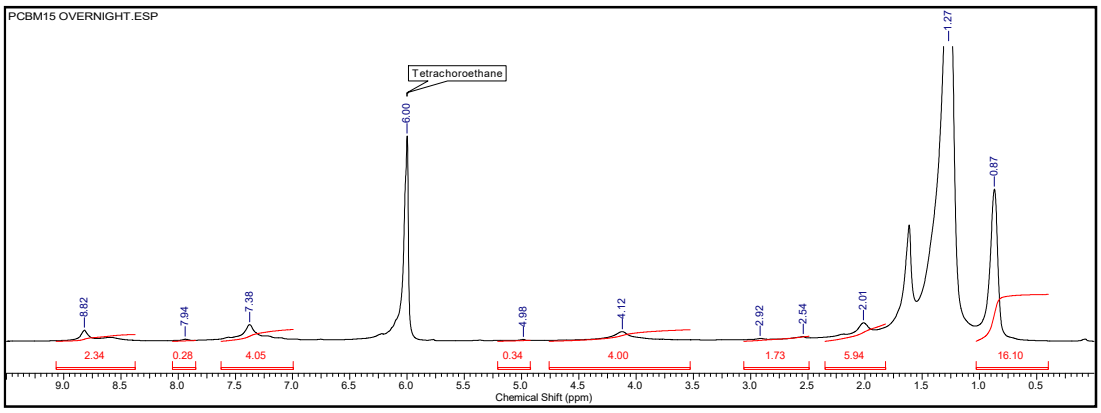

Figure 3.5. ^{1}H NMR spectrum of PNDI-Th-PCBM5 recorded in deuterated 1,1,2,2-tetrachloroethane-d_2.

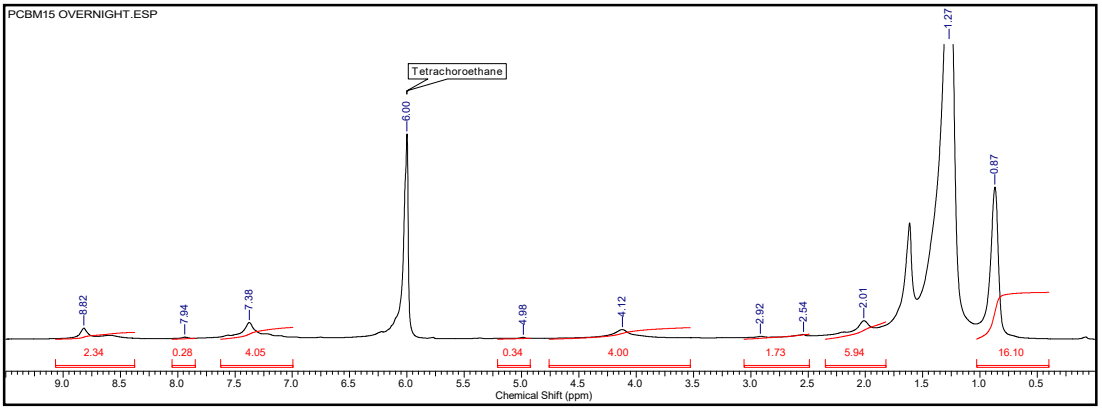

Figure 3.6 ^{1}H NMR spectrum of PNDI-Th-PCBM7.5 recorded in deuterated 1,1,2,2-tetrachloroethane-d_2.

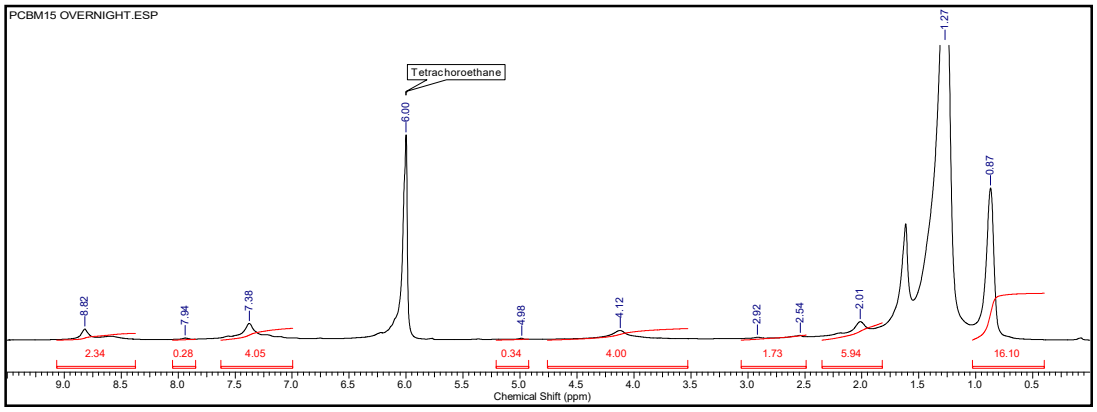

Figure 3.7. ^{1}H NMR spectrum of PNDI-Th-PCBM15 recorded in deuterated 1,1,2,2-tetrachloroethane-d_2.

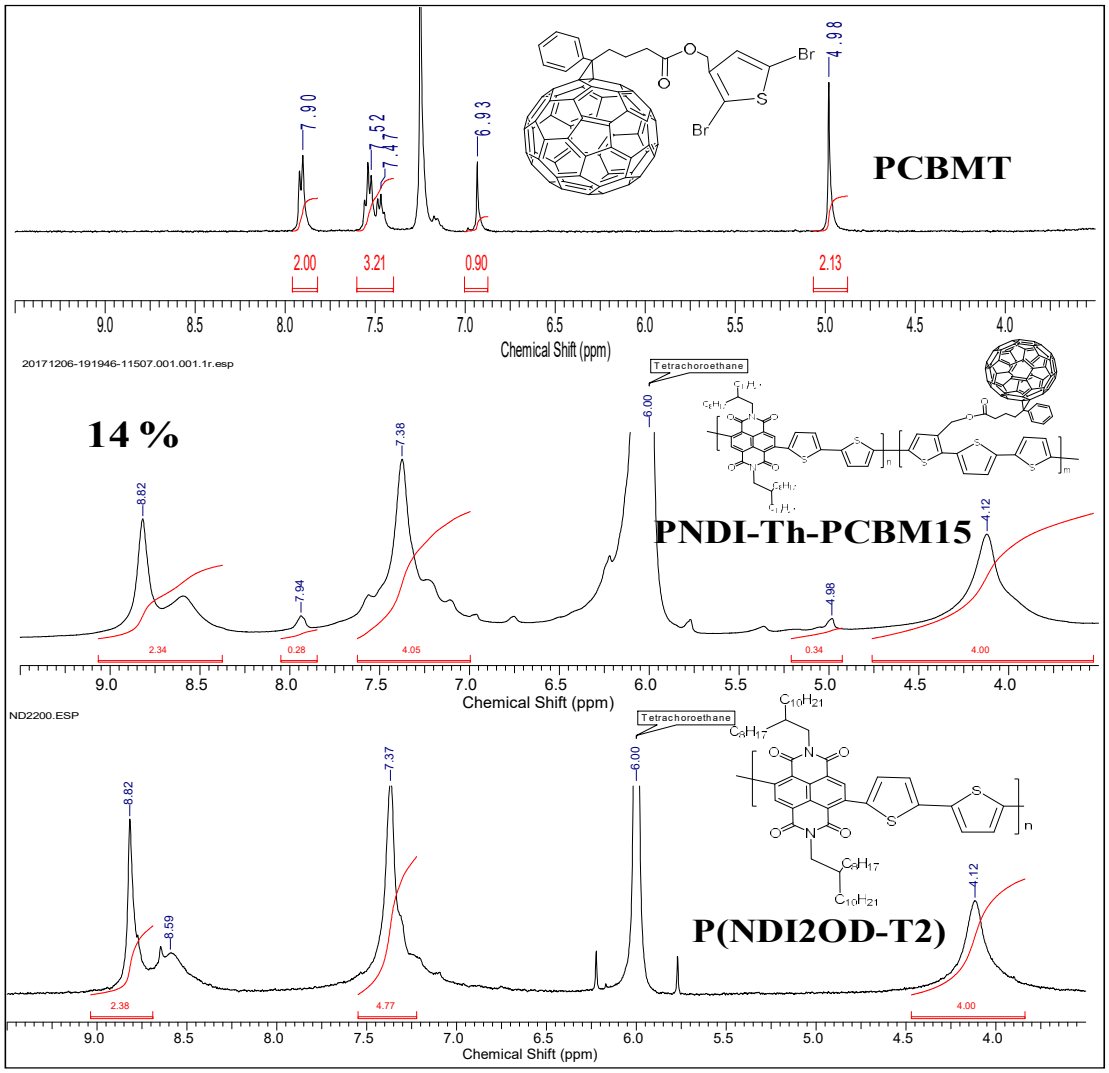

Figure 3.8. ^{1}H NMR spectra of monomers and polymer (expanded region δ ppm 9.0 -3.5) recorded in $CDCl_3$ or 1,1,2,2-tetrachloroethane-d_2.

Thermal properties of the copolymers were determined by thermogravimetric analysis (TGA) as well as differential scanning calorimetry (DSC) measured under a nitrogen atmosphere. TGA curves given in **Figure 3.9** showed good thermal stability for all random copolymers with onset decomposition temperature (T_d) of over > 400 °C. The literature cites melting transition for P(NDI2OD-T2) with onset around 280 °C (heating scan), indicating the crystalline nature of the polymer. DSC curves were recorded for all polymers by heating from 0 °C till 350 °C at 10 ^{o}C /min under N_2 atmosphere. P(NDI2OD-T2) showed a broad thermal transition with an endothermic peak (T_m) at 305 ^{o}C and exothermic peak at (T_c) 277 ^{o}C with melting and cooling enthalpy values (ΔH_m) 7.67 J/g and (ΔH_c) 7.49 J/g respectively (**Figure 3.10)**. All the random copolymers also showed the melting and crystallization transitions in their second heating and cooling cycles.

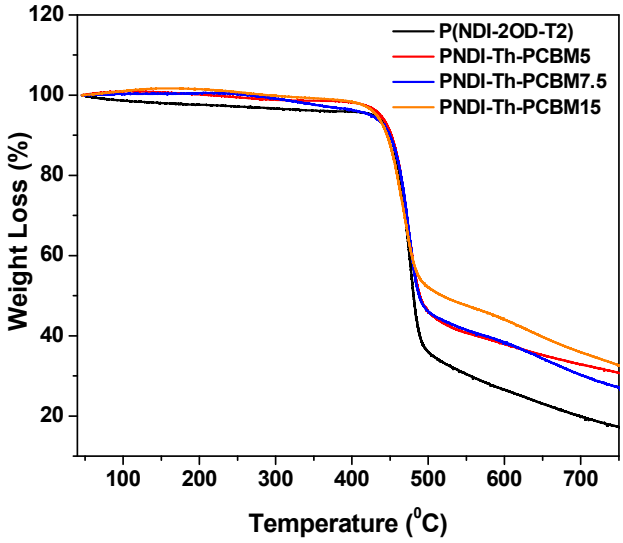

Figure 3.9 TGA thermograms of copolymers at 10 ^{o}C /min under N_2 atmosphere.

Table 3.1 lists the melting temperature (T_m) and corresponding enthalpies (ΔH_m) obtained for the reference polymer as well as random copolymers. PNDI-Th-PCBM5 showed sharper melting and crystallization transitions with nearly double the value for enthalpy compared to P(NDI2OD-T2). Its transition temperatures were also slightly higher compared to the reference polymer. PNDI-Th-PCBM7.5 showed almost similar transition temperature compared to the reference polymer. Reference as well as all random copolymers showed very good reversibility for the endo as well as exothermic transitions. PNDI-Th-PCBM7.5 and PNDI-Th-PCBM15 showed broad endothermic transition at 304 ^{o}C, 290 ^{o}C respectively.

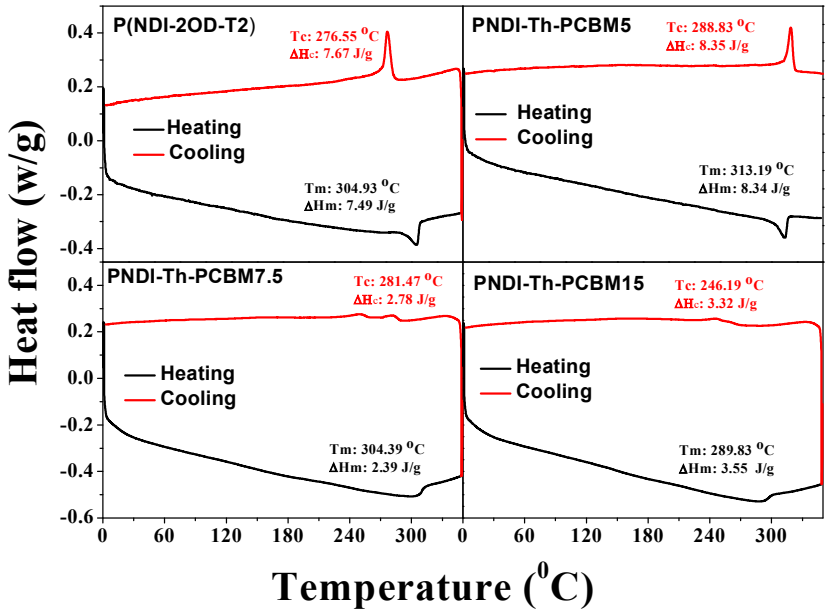

Figure 3.10 Second heating/cooling curves of the copolymers in the DSC scans conducted at 10 °C /min under N_2 atmosphere.

3.3.2. Optical and Electrochemical Properties

UV-Vis absorption spectra of reference polymer P(NDI2OD-T2) and random copolymers (PNDI-Th-PCBM*x*) recorded in thin-film spin-coated on a quartz substrate are shown in **Figure 3.11**. All copolymers showed two distinct absorption bands; the first high energy absorption band at ~300-425 nm was attributed to π-π* transition and another low energy band at ~460- 800 nm was accounted for intra-molecular charge transfer (ICT) from bithiophene unit to NDI.[23, 26-27] The reference polymer P(NDI2OD-T2) showed typical absorption spectrum with π-π* absorption peak at ~400 nm and ICT peak at 645 nm.[28] In the random copolymers, the position of the π-π* absorption peak and the ICT absorption band remained unchanged, since PCBM has very low absorption coefficient.

The optical band gap (E_g^{opt}) of reference and random copolymers were calculated from the lower energy absorption band edge of thin-film and is listed in **Table 3.2**. The optical band gap of reference and random copolymers were very similar The values were 1.44 eV, 1.42eV, 1.45 eV and 1.42 eV for P(NDI-2OD-T2), PNDI-Th-PCBM5, PNDI-Th-PCBM7.5, PNDI-Th-PCBM15 respectively. Cyclic voltammetry was used to analyze electrochemical redox behavior and electronic energy levels of the reference and new n-type random copolymers. Thin-films of polymer were deposited on the platinum working electrode. The measurement was performed in acetonitrile solvent with ferrocene/ferrocenium as an internal standard and

tetrabutylammonium hexafluorophosphate (*n*-Bu4NPF$_6$ 0.1M/ acetonitrile) as supporting electrolyte.[29]

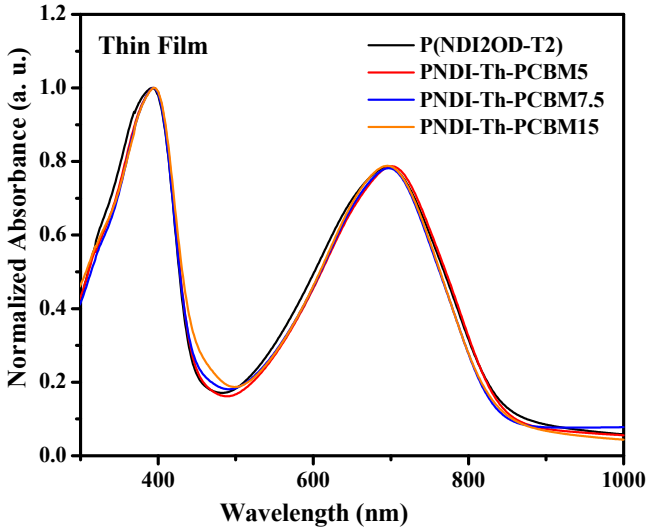

Figure 3.11. UV-Vis absorption spectra of reference P(NDI2OD-T2) and random copolymers in thin film on quartz substrate.

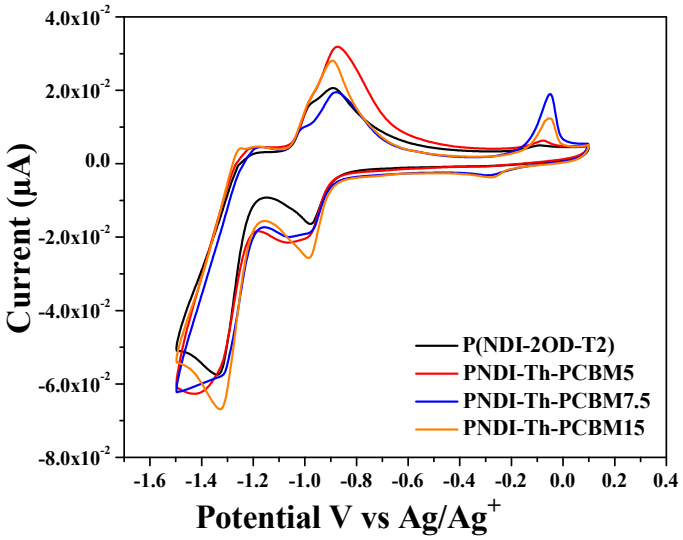

Figure 3.12 Cyclic voltammograms of reference P(NDI2OD-T2) and random copolymers as thin film on platinum working electrode in 0.1 M*n*-Bu$_4$NPF$_6$ acetonitrile at a scan rate of 100 mV/s.

Cyclic voltammograms for all polymers are shown in **Figure 3.12,** and the calculated HOMO and LUMO energy levels are given in **Table 3.2.** Thin-film of reference polymer P(NDI2OD-T2) exhibited two reversible reduction peaks, which accounted for the formation of radical

anion and dianion of NDI in the polymer backbone.[22] All random copolymers showed quasi-reversible reduction peaks with almost similar values of electrochemical reduction like P(NDI2OD-T2). The lowest occupied molecular orbital (LUMO) energy levels were calculated based on the onset value of first reduction peak and reference energy level of ferrocene (4.8 eV below the vacuum level) according to E_{LUMO} (eV) = -e × (E^{red} onset + 4.8) below the vacuum level. The highest occupied molecular orbital (HOMO) levels were estimated based on the optical band gap acquired from the solid-state absorption onset measurements. The HOMO and LUMO energy levels of P(NDI2OD-T2) was found to be -5.31 eV and -3.87 eV respectively which is similar to the previously reported values.[22] Newly prepared novel random copolymers exhibited approximately similar HOMO and LUMO values (**Table 3.2**) as the reference polymer P(NDI2OD-T2). This confirms that there was negligible effect of incorporation of PCBM unit on the energy level of random copolymers.

Table 3.2 Optical band gap, electronic energy levels of P(NDI2OD-T2) and PNDI-Th-PCBM*x* random copolymers.

Polymer	HOMO (eV)	LUMO (eV)	Eg (eV)
P(NDI2OD-T2)	-5.31	-3.87	1.44
PNDI-Th-PCBM5	-5.28	-3.86	1.42
PNDI-Th-PCBM7.5	-5.34	-3.89	1.45
PNDI-Th-PCBM15	-5.29	-3.87	1.42

3.3.3. Thin-film Crystallinity

The bulk crystalline nature and molecular packing of reference P(NDI2OD-T2) and new random copolymers were analyzed using Powder wide-angle X-ray diffraction (PXRD) measurement. **Figure 3.13** shows the X-ray diffraction patterns and the relevant data is summarized in **Table 3.3.** XRD pattern of reference polymer P(NDI2OD-T2) showed lamellar peak (100) at 2θ = 3.63° and π-π stacking peak (010) at 2θ = 19.81° which corresponded to lamellar packing distance of 24.28 Å and π-π stacking distance of 4.47 Å. No change in the position of lamellar peak (100) was observed for all random copolymers compared to reference polymer.

Table 3.3. *2θ* values and d spacing values for the copolymers.

Polymer	2θ°			*d*-spacing (Å)		
	(100)	(010)	Lamellar peaks	d_{100}	d_{010}	$d_{lameller}$
P(NDI2OD-T2)	3.63	19.81	6.61, 12.68	24.28	4.47	13.35, 6.98
PNDI-Th-PCBM5	3.63	19.54	6.61, 12.84	24.28	4.46	13.50, 6.88
PNDI-Th-PCBM7.5	3.63	19.67	6.61, 12.52	24.28	4.50	13.35, 6.89
PNDI-Th-PCBM15	3.63	19.81	6.61, 12.27	24.28	4.47	13.35, 6.35

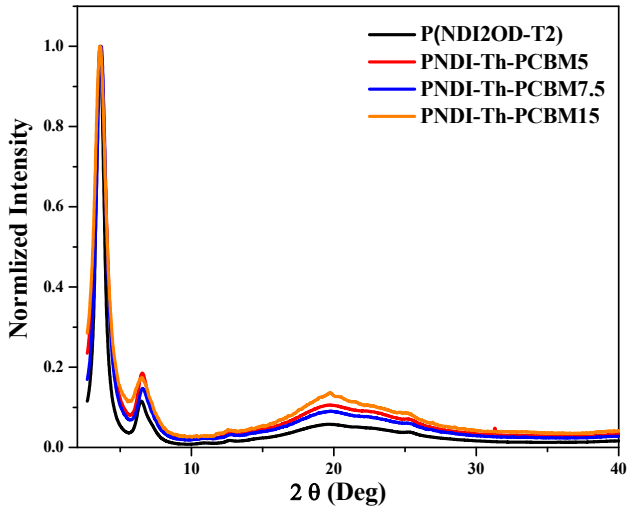

Figure 3.13. Powder XRD diffraction patterns of reference P(NDI2OD-T2) and random copolymers.

3.3.4. All-Polymer BHJ Solar Cells

All random copolymers (PNDI-Th-PCBMx) as acceptor (n-type) materials in all-polymer solar cells was studied by fabricating BHJ all-PSCs using PTB7-Th polymers as donor material. The inverted devices with configuration of ITO/ZnO/polymer blend/Ag were fabricated. The detailed procedure for device fabrication and structure is given in experimental section. The all PSCs device using n-type reference polymer P(NDI2OD-T2) was also fabricated for comparison. The blend active layers of donor: acceptor polymers were deposited by spin coating from chloroform solution (12 mg/ml). The optimum donor: acceptor (D:A) blend ratio and thickness of BHJ active layer films were found to be 1.3:1 (w/w) and 100~ 110 nm, respectively. **Figure 3.14** shows the current density-voltage (*J-V*) curves. The optimized solar cell parameters including short-circuit current density (Jsc), the open-circuit voltage (Voc), fill factor (FF), and PCE, are summarized in **Table 3.4**.

The reference polymer P(NDI2OD-T2) is a well-studied acceptor material used with various low bandgap polymer and small molecule donors in all-polymer solar cells. In our study, using PTB7-Th as the donor material, P(NDI2OD-T2) exhibited maximum PCE of 1.50 % (Jsc of 7.12 mA/cm^2, Voc of 0.58 V, and FF of 36.44 %).

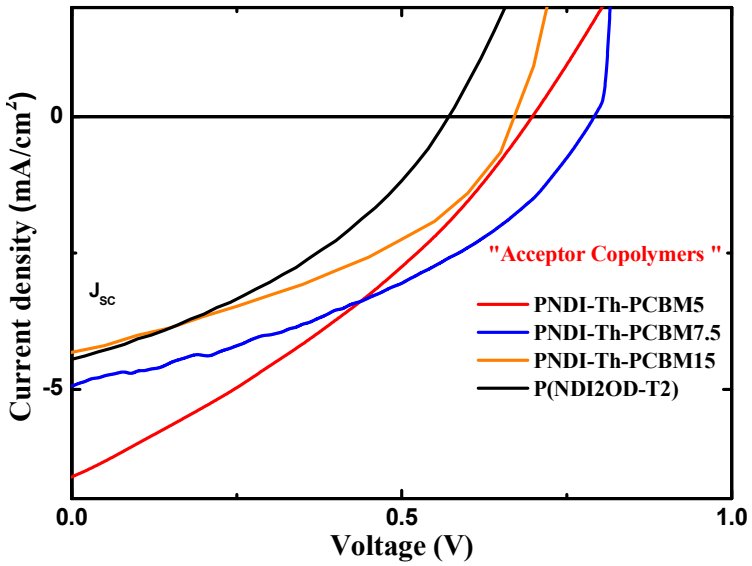

Figure 3.14. Current density- Voltage (*J – V*) characteristics for all polymers using PTB7-Th as the donor.

Table 3.4 Photovoltaic properties of PTB7-Th: PNDI-Th-PCBM*x* and PTB7-Th: P(NDI2OD-T2) blend all-polymer solar cells.

Polymer	Jsc (mA.cm^{-2})	Voc (Volts)	FF (%)	PCE (%)
PTB7-Th: P(NDI2OD-T2)	7.12	0.58	36.44	1.50
PTB7-Th: PNDI-Th-PCBM5	10.59	0.70	32.18	2.39
PTB7-Th: PNDI-Th-PCBM7.5	7.92	0.79	39.16	2.45
PTB7-Th: PNDI-Th-PCBM15	6.91	0.65	41.25	1.85

The device performance of the various PTB7-Th: PNDI-Th-PCBM*x* blend devices showed that all the newly synthesized random copolymers (PNDI-Th-PCBM5, PNDI-Th-PCBM7.5, PNDI-Th-PCBM15) exhibited significant improvement in the PCE as compared to reference polymer P(NDI2OD-T2). For instance, PTB7-Th: PNDI-Th-PCBM5 blend device showed PCE of 2.39 % (Jsc of 10.59 mA/cm^2, Voc of 0.70, and FF of 32.18 %). Further enhancement

in the photovoltaic performance was observed in PTB7: PNDI-Th-PCBM7.5 blend device which exhibited PCE of 2.45 % (Jsc of 7.92 mA/cm^2, Voc of 0.79, and FF of 39.16 %).

However, PTB7-Th: PNDI-Th-PCBM15 blend with highest incorporation of PCBM (15 %) showed lower PCE of 1.85 % (Jsc of 6.92 mA/cm^2, Voc of 0.65, and FF of 41.25 %), which was still higher compared to the reference polymer P(NDI2OD-T2). It could be observed that PNDI-Th-PCBM7.5 showed the best optimized composition with donor polymer and further increase in PCBM incorporation into (PNDI-Th-PCBM*x*) random copolymer did not result in improvement of the photovoltaic performance. The enhancement in the PCE values of random copolymers PNDI-Th-PCBM*x* based all-PSCs devices were mainly due to the increase in the Voc value. Further optimization is needed for improvement in the optoelectronic properties.

3.3.5 BHJ Solar Cell Morphology

Morphology of the active layer (D/A) of BHJ is one of the important factors that influences the solar cell performance. AFM images of donor: acceptor polymer blends were recorded to study the surface morphology of all-PSCs BHJ devices. The donor: acceptor polymer (1.3:1 w/w) blend films were prepared in identical ways as that for all-PSCs devices. **Figure 3.15** shows AFM height images (10 μm x 10μm) of PTB7-Th: P(NDI2OD-T2) and PTB7-Th: PNDI-Th-PCBM*x* blend active layer. The reference PTB7-Th: P(NDI2OD-T2) blend film showed rather coarsened morphology with average root mean square (RMS) surface roughness of 3.44 nm due to the formation of large polymer aggregate domains. The large granular phase-separated morphology observed in PTB7-Th: P(NDI2OD-T2) blend film indicated no proper mixing of donor/acceptor polymers at nanoscale. The incorporation of PCBM unit in the random copolymer resulted in dramatic change in the surface morphology of PTB7-Th: PNDI-Th-PCBM*x* blend films compared to reference PTB7-Th: P(NDI2OD-T2) polymer blend. In addition, the RMS surface roughness reduced to 0.30 nm in PTB7-Th: PNDI-Th-PCBM5 blend and 0.38 nm in PTB7-Th: PNDI-Th-PCBM7.5 blend which suggested the formation of less aggregated domain and showed improved donor/acceptor mixing at nanoscale.

Improved nanoscale interpenetrating network in blend films is helpful for exciton dissociation and charge carrier transport. The PTB7-Th: PNDI-Th-PCBM5 and PTB7-Th: PNDI-Th-PCBM7.5 blend films showed uniform micro-phase separation with smaller phase-separated domain size. Compared to the other two random copolymer blend, the PTB7-Th: PNDI-Th-PCBM15 blend film showed higher RMS surface roughness of 0.94 nm with

coarsened morphology, which was still more uniform with smaller phase-separated domain size compared to the reference PTB7-Th: P(NDI2OD-T2) polymer blend. The reduced roughness can play vital role in the charge collection process as it decreases surface recombination.[30]

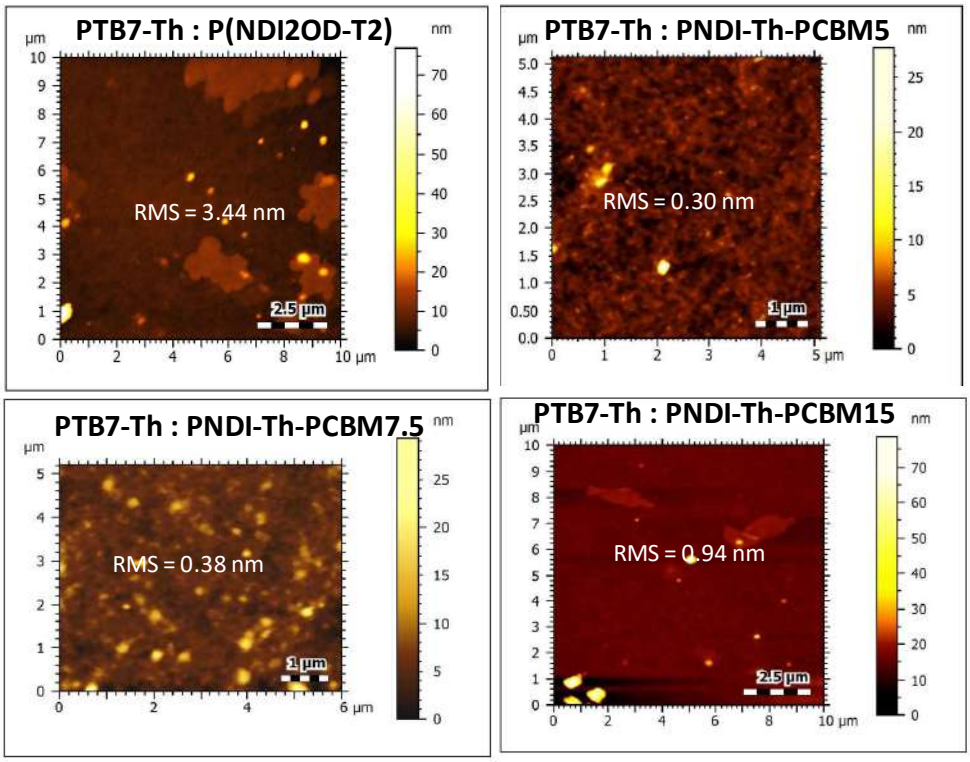

Figure 3.15. AFM height images (10 μm x 10μm) of PTB7-Th: P(NDI2OD-T2) (1.3:1 w/w) and PTB7-Th: PNDI-Th-PCBM*x* (1.3:1 w/w) blend solar cell.

3.4 Conclusions

In this Chapter, we have synthesized a series of new n-type semiconducting random copolymers NDI-bithiophene/PCBM-bithiophene (PNDI-Th-PCBMx) by incorporating various amount of PCBM (xPCBM = 5, 7.5, 15 mole % of PCBM) co-acceptor unit into P(NDI2OD-T2) polymer. The properties of the newly synthesized acceptor copolymers were investigated in the pristine form as well as their donor-acceptor (D:A) blends with donor PTB7-Th in order to understand the structural properties and their influence on the solar cell performance. Overall, the random copolymers showed better compatibility with the donor polymer compared to reference polymer P(NDI2OD-T2). This was observed in their bulk photovoltaic properties as well with the random copolymers exhibiting higher PCE compared to P(NDI2OD-T2). A maximum PCE of ~2.5 % was observed in the case of PTB7-Th: PNDI-Th-PCBM7.5 blend devices. Our studies showed that most likely PNDI-Th-PCBM7.5

showed optimal miscibility with donor polymer which produced the best D/A compatibility, and bulk carrier charge transport in blend. The incorporation of PCBM into P(NDI2OD-T2) polymer is a very effective strategy to tune its photovoltaic properties and improved PCE observed in new n-type random copolymers proved its potential application in future all-PSCs. Further optimization is needed to improve the efficiency and other photovoltaic properties.

3.5. References

(1) Roncali, J. *Chem. Soc. Rev*. **2005**, *34*, 483-495.

(2) Sariciftci, N. C.; Smilowitz, L.; Heeger, A. J.; Wudl, F. *Science* **1992**, *258*, 1474-1476.

(3) Stalmach, U.; Boer, B.; Videlot, C.; van Hutten, P. F.; Hadziioannou, G. *J. Am.Chem. Soc.* **2000**, *122*, 5464-5472.

(4) Frankevich, E.; Maruyama, Y.; Ogata, H. *Chem. Phys. Lett.* **1993**, *214*, 39-44.

(5) Kim, T. D.; Nam, S. Y.; Park, E. Y.; Cho, S.; Park, J. G.; Lee, K. S. *Curr. Appl. Phys* .**2011**, *11*, E44-E48.

(6) Jarrett, C. P.; Pichler, K.; Newbould, R.; Friend, R. H. *Synth. Met.* **1996**, 77, 35-38.

(7) Guldi, D. M.; Neta, P.; Asmus, K. D. *J. Phys. Chem.* **1994**, *98*, 4617-4621.

(8) Imahori, H.; Hagiwara, K.; Akiyama, T.; Aoki, M.; Taniguchi, S.; Okada, T.; Shirakawa, M.; Sakata, Y. *Chem. Phys. Lett.* **1996**, *263*, 545-550.

(9) Imahori, H.; Sakata, Y. *Adv. Mater.* **1997**, *9*, 537-546.

(10) Reed, C. A.; Bolskar, R. D. *Chem. Rev.* **2000**, *100*, 1075-1120.

(11) Ramos, A. M.; Rispens, M. T.; van Duren, J. K. J.; Hummelen, J. C.; Janssen, R. A. J. *J. Am. Chem. Soc.* **2001**, *123*, 6714-6715.

(12) Tan, Z. A.; Hou, J. H.; He, Y. J.; Zhou, E. J.; Yang, C. H.; Li, Y. F. *Macromolecules* **2007**, *40*, 1868-1873.

(13) Miyanishi, S.; Zhang, Y.; Tajima, K.; Hashimoto, K. *Chem. Commun.* **2010**, *46*, 6723-6725.

(14) Lanzi, M.; Salatelli, E.; Benelli, T.; Caretti, D.; Giorgini, L.; Di-Nicola, F. P. J. *Appl. Polym. Sci.* **2015**, *132*, 42121.

(15) de Boer, B.; Stalmach, U.; van Hutten, P. F.; Melzer, C.; Krasnikov, V. V.; Hadziioannou, G. *Polymer* **2001**, *42*, 9097-9109.

(16) Lee, J. U.; Cirpan, A.; Emrick, T.; Russell, T. P.; Jo, W. H. *J. Mater. Chem.* **2009**, *19*, 1483-1489.

(17) Lee, J. U.; Jung, J. W.; Emrick, T.; Russell, T. P.; Jo, W. H. *Nanotechnology* **2010**, *21*, 105201.

(18) Yang, C.; Lee, J. K.; Heeger, A. J.; Wudl, F. *J. Mater. Chem.* **2009**, *19*, 5416-5423.

(19) Chen, M. Q.; Li, M. H.; Wang, H. T.; Qu, S. X.; Zhao, X. M.; Xie, L. X.; Yang, S. F. *Polym. Chem*. **2013**, *4*, 550-557.

(20) Pierini, F.; Lanzi, M.; Nakielski, P.; Pawłowska, S.; Urbanek, O.; Zembrzycki, K.; Kowalewski, T. A. *Macromolecules* **2017**, *50*, 4972-4981,

(21) Yan, H.; Chen, Z.; Zheng, Y.; Newman, C.; Quinn, J. R.; Dötz, F.; Kastler, M.; Facchetti, A. *Nature* **2009**, *457*, 679-686.

(22) Chen, Z.; Zheng, Y.; Yan, H.; Facchetti, A. *J. Am. Chem. Soc.* **2009**, *131*, 8-9.

(23) Sharma, S.; Kolhe, N. B.; Gupta, V.; Bharti, V.; Sharma, A.; Datt, R.; Chand, S.; Asha, S. K. *Macromolecules*, **2016**, *49*, 8113-8125.

(24) Jones, B. A.; Ahrens, M. J.; Yoon, M. H.; Facchetti, A.; Marks, T. J.; Wasielewski, M. R. *Angew. Chem. Int. Ed.* **2004**, *43*, 6363-6366.

(25) Popere, B. C.; Della Pelle, A. M.; Thayumanavan, S. *Macromolecules* **2011**, *44*, 4767-4776.

(26) Kolhe, N. B.; Ashar, A. Z.; Narayan, K. S.; Asha, S. K. *Macromolecules* **2014**, *47*, 2296-2305.

(27) Steyrleuthner, R.; Schubert, M.; Howard, I.; Klaumünzer, B.; Schilling, K.; Chen, Z.; Saalfrank, P.; Laquai, F.; Facchetti, A.; Neher, D. *J. Am. Chem. Soc.* **2012**, *134*, 18303-18317.

(28) Jenekhe, S. A.; Lu, L.; Alam, M. M. *Macromolecules* **2001**, *34*, 7315-7324.

(29) Durban, M. M.; Kazarinoff, P. D.; Luscombe, C. K. *Macromolecules* **2010**, *43*, 6348-6352.

(30) Huang, Y.; Kramer, E. J.; Heeger, A. J.; Bazan, G. C. *Chem. Rev.* **2014**, *114*, 7006-7043.

Chapter 4

Naphthalene Diimide Copolymers by Direct Arylation Polycondensation as Highly Stable Supercapacitor Electrode Materials

This chapter has been adapted from the following publication

Sandeep Sharma, Roby Soni, Sreekumar Kurungot*, S. K. Asha*. *Macromolecules* **2018***, 51*, 954−965.

4.1. Introduction

In the last two chapters, the discussion was mainly focused on the Naphthalene diimide (NDI) based donor-acceptor (D-A) π-conjugated random copolymers for energy generation using organic solar cell. Equally important to energy generation is the energy storage systems as it plays a major role in the availability of sustainable renewable energy on demand. This chapter describes the synthesis of NDI based conjugated polymers for energy storage devices (Supercapacitors).

Conjugated polymers are generally synthesized by transition metal catalyzed polycondensation reactions like the Stille, Suzuki etc.[1, 2] However, the requirement of prefuntionalization of monomers, toxic nature of the organostannyls used in Stille coupling as well as the difficulties in their purification reduces the scale-up potential of monomers prepared using these routes. In early 1999, there was a report of synthesis of poly(3-octylthiophene) by direct heteroarylation polycondensation method.[3] However, since this gave rather low number average molecular weight (3 kDa) and regioregularity (90 %), the approach did not gain prominence. Interest in direct arylation polymerization resurfaced a decade later in 2010 once a better understanding of the mechanisms was known. Ozawa et. al[4] successfully synthesized P3HT with high molecular weight and regioregularity that was comparable to P3HT obtained using McCullough[5], Rieke or GRIM polymerization methods.[5] Since 2012 there has been a flurry of activity in this area with several articles and a couple of reviews published. The biggest advantage of the direct arylation polycondensation is that it produces cleaner polymers and less amounts of metal impurities.[7] This faster, less toxic and less expensive approach was mostly reported for developing electron rich or p-type conjugated polymers.[8-11] The first report of push-pull copolymer synthesized by direct (hetero) arylation (DHAP) polymerization was in 2011; Kanbara and co-workers reported a push-pull copolymer made of 2,7-dibromofluorene and tetrafluorobenzene.[12] The first report of successful application of DAP to prepare high molecular weight n-type polymers based on dibrominated naphthalene diimide (NDI-OD-Br_2) was from the research group of Michael Sommer et al,[13] although there were earlier reports which were not so successful in producing high molecular weight polymers.[14] Sommer's group developed P(NDI2OD-T2) (N2200) by the direct arylation route which involved reaction between unsubstituted bithiophene and NDI-2OD-Br_2 using tris-(dibenzylideneacetone) dipalladium (Pd_2dba_3) as catalyst, pivalic acid as the cocatalyst along with K_2CO_3 in toluene or chlorobenzene as solvent to obtain defect free P(NDI2OD-T2) with high and controllable molecular weight shown in **Figure 4.1.**

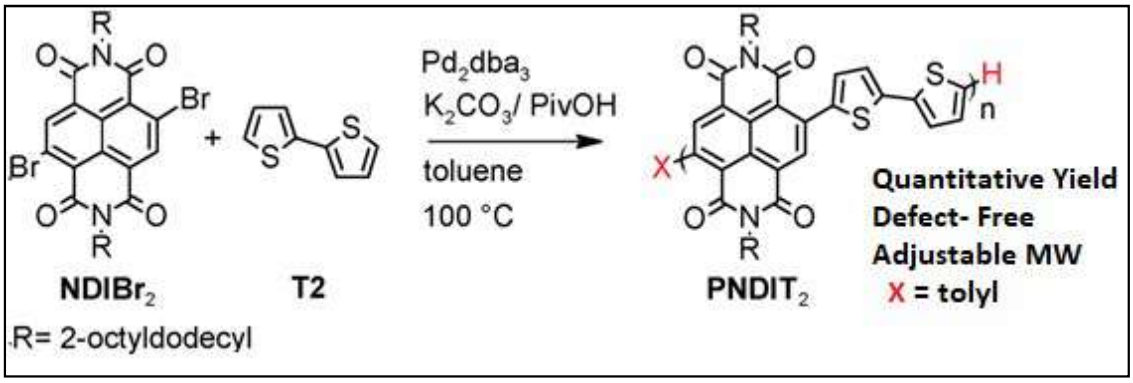

Figure 4.1. Synthesis of P(NDI2OD-T2) via direct arylation polycondensation. (Adapted from ref. 13)

Overall the number of reports on NDI based donor-acceptor (D-A) polymers by the DAP route so far is very less fewer than ten.[13,15-19] All of them except those reported from Sommer's group were made with either thiophene or EDOT flanked naphthalene diimide derivatives. This was because the early attempts using dibrominated NDI as the monomer resulted in low molecular weight oligomers only. We are presenting here novel alternating D-A copolymers involving NDI developed by the direct arylation polycondensation route. The polymer structures are new; thiophene terminated phenylenevinylene as the donor comonomer was polymerized with NDI-OD-Br_2. The phenylenevinylene unit was modified by introduction of electron donating (thiophene) and withdrawing (nitrile) units to achieve panchromatic absorption. The introduction of nitrile groups onto the oligo p-phenylenevinylene backbone has been known to enhance the electrochemical stability of the polymers as well as lower the lowest unoccupied molecular orbital (LUMO) level, which is considered to be desirable for optoelectronic devices.[20]

As discussed in Chapter 1 Conjugated polymers like poly(3,4-ethylenedioxythiophene) (PEDOT), polypyrrole (PPy),[21] polyaniline (PANI),[22] etc., alone or as composites with carbon nanotubes (CNT) or graphene have been extensively utilized as supercapacitor / pseudocapacitive materials, where their high conductivity and easy processability offer them several advantages.[23] According to the nature of the conducting polymers and device configuration, they are classified into type I, type II, type III and type IV supercapacitors. Most of the reported data is focused on type I devices where p-type (electron rich) polymers are used for both electrodes (symmetric). Devices based on polythiophene,[24-27] PPy,[28, 29] PANI[30] abound with specific capacitance values greater than 100 F/g of polymer. Derivatives of polythiophene - specially those based on PEDOT[31-33] have shown great promise due to its

superior chemical and electrochemical stability and fast switching times. Type II[34, 35] devices use different p-type polymers on each electrode (asymmetric); this allows the extension of the working potential window by encompassing the complementary potential windows of both the polymers.[36] The type III supercapacitor utilizes identical n-type (electron poor) or donor-acceptor (D-A) type conducting polymer whereas type IV configuration is an asymmetric type device configuration.[37, 38] Efficient n-type polymers for supercapacitor applications are a major challenge due to inferior stability and cycle life issues. Most of the reported type III supercapacitor π-conjugated polymers are based on derivatives of polythiophene. This dearth of stable, n-type polymer materials is a critical limiting factor in the conjugated polymer based supercapacitor research. Only a handful of reports are available at present utilizing this potential of the n-type or electron transporting π-conjugated polymers or donor-acceptor type polymers.[39, 40] Significant among the n-type conjugated polymers is the Polymer (P(NDI2OD-T2)) (Polyera ActivInk N2200), which was reported by Facchetti *et al* in 2009[41] and which has since then been extensively utilized in all-polymer solar cells and organic field effect transistor (OFET) applications due to its high electron mobility and desirable semiconducting properties. In 2015 Facchetti and Yao et al. evaluated P(NDI2OD-T2) as a charge storage material for rechargeable Li batteries (shown in **Figure 4.1**).[42] Although the specific capacity of ~ 54 mAh/g was lower compared to other inorganic counterparts, they concluded that with the improved molecular design the n-type π-conjugated polymers could see widespread application in the energy storage-related devices such as batteries, supercapacitors, etc. This was one of the early reports of a successful demonstration of the n-type π-conjugated polymer as a promising material for energy storage application. In 2015, Luscombe et al. reported a hyperbranched architecture involving triphenylamine (TPA) core and bay-substituted naphthalene diimide (NDI) terminal units with thiophene rings of varying length between the core and periphery as 'n' type hyperbranched polymer supercapacitor cathode materials (Shown in **Figure 4.2**) .[43]

A moderate capacitance of 22 F /g (for symmetric device 0.50 F/g) and charge storage device stability of > 500 cycles with ~ 10 % loss was reported for a two electrode assembly using organic electrolyte. This work demonstrated the use of synthetic chemistry to precisely control the structure and fine-tune the electrochemical properties of polymeric supercapacitor electrode materials.

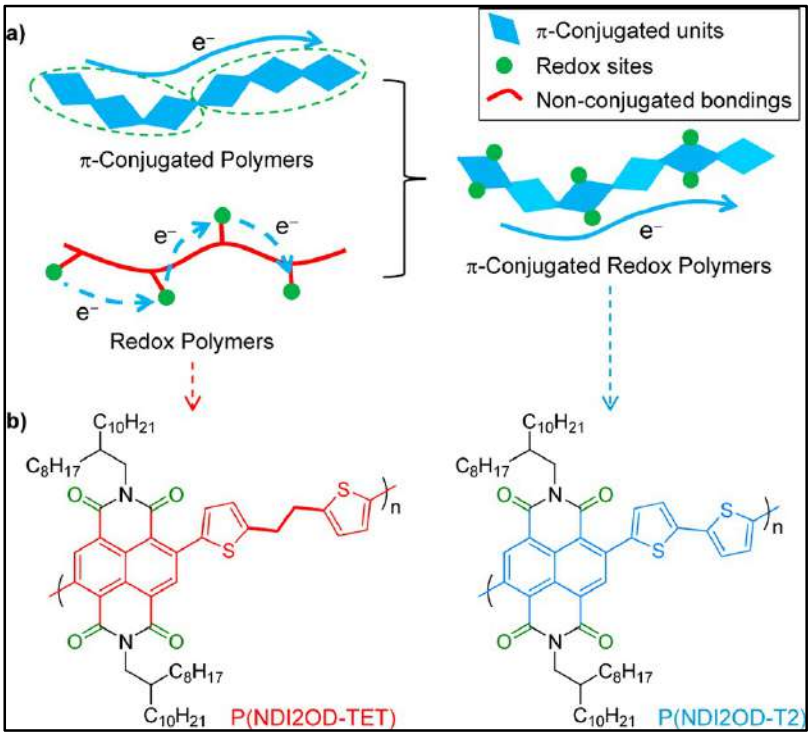

Figure 4.2. (a) Graphical representation of the structural characteristics of π-conjugated polymers, redox polymers, and π-conjugated redox polymers. (b) The molecular structure of the nonconjugated P(NDI2ODTET) and the π-conjugated P(NDI2OD-T2). (Adapted from ref. 42)

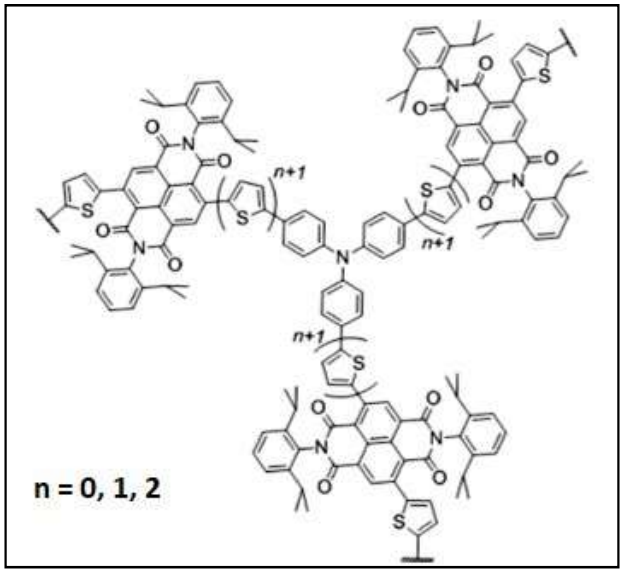

Figure 4.3. Hyperbranched polymer structure (Adapted from ref. 43)

Encouraged by the potential applicability of the n-type conjugated polymers in energy storage devices, in this chapter we report two new NDI-based copolymers that we developed via the

direct (hetero) arylation (DHAP) polymerization route as supercapacitor materials and their performance was compared with that of (P(NDI2OD-T2)) as the reference polymer. The polymers had bay substituted naphthalene diimide as the acceptor moiety in the repeat unit, while the donor strength was varied from bithiophene (P(NDI2OD-T2)) to thiophene end-capped phenylene vinylene (P_1) and thiophene end-capped phenylene vinylene with nitrile group substitution at the vinylene linkage (P_2). The effect of this donor strength variation in the properties of the polymers as symmetric Type III supercapacitor materials was explored.

4.2. Experimental Section

4.2.1. Materials

1,4,5,8-Naphthalenetetracarboxylicdianhydride (NTCDA), 5,5'-bis (trimethylstannyl)-2,2'-bithiophene 97%, 2-octyldodecanol, tris-(dibenzylideneacetone)dipalladium (Pd_2dba_3) were purchased from Sigma Aldrich and used without further purification. P(NDI2OD-T2) Reference polymer was used from Chapter 2.[1]

4.2.2. Measurements

^{1}H NMR spectra were recorded using 200 and 400 MHz Brucker NMR spectrophotometer in $CDCl_3$ containing small amounts of TMS as an internal standard. MALDI TOF spectra of the final monomers were recorded on AB Sciex 5800 TOF / TOF^{TM}. The molecular weights of polymers were determined using gel permeation chromatography (GPC) using Viscotek VE 3580 RI detector at 25 °C and tetrahydrofuran (THF) as the mobile phase. The analyses were carried out at a flow rate of 1 mL/min. Columns were calibrated with polystyrene standards, and the molecular weights are reported with respect to polystyrene. Absorption spectra were recorded using Perkin Elmer Lambda -35 UV-Vis spectrophotometer. Thermogravimetric analysis (TGA) was performed using a TGA Q 5000 thermogravimetric analyzer. Samples were run from 40 to 900 °C with a heating rate of 10 °C/min under nitrogen. DSC (differential scanning calorimetry) measurements were performed on TA Q10 differential scanning calorimeter at a heating rate of 10 °C/min under nitrogen atmosphere. The thin film X-ray diffraction data were recorded using a Rigaku model Dmax-2500 diffractometer using Cu Kα (1.54 Å) emission, and the spectra were recorded in the range of (2θ) 2–50°.

4.2.3. Sample Preparation

For the UV-Vis absorption studies, thin films were prepared by dissolving the polymer in chloroform (10 mg/mL) and spin coating (600 rpm/60 s) on quartz plates.

4.2.4. Electrode Fabrication

For electrochemical tests, a slurry of P(NDI2OD-T2), P_1 or P_2 was prepared by dispersing 5 mg of the polymer and 1 mg of carbon nanotubes (CNTs) in 500 µl N-methyl pyrrolidone by sonication till it formed a uniform dispersion. A 100 µl of the slurry so prepared was drop coated on the carbon paper over an area of 1 cm^2. The electrodes were dried in the oven at 120 °C for 6 hours. The electrochemical tests were carried out in a conventional three electrode cell using 0.5 M H_2SO_4 as the electrolyte. $Hg/HgSO_4$ was used as a reference electrode, and carbon paper served as a counter electrode in the three-electrode setup.

4.2.5. Characterization of Symmetric Supercapacitor Devices

All the electrochemical tests were carried out on BioLogic SP-300 potentiostat. Cyclic voltammograms were recorded at scan rates of 5, 10, 20, 50, 100, 200 and 500 mV s^{-1} in the potential range of -0.7 to 0.5 V in 0.5 M H_2SO_4 electrolyte. Galvanostatic charge-discharge measurements were carried out at different current densities of 0.5, 1, 2, 3, 4, 5 and 10 A g^{-1} for calculation of capacitance. Electrochemical impedance spectroscopy was conducted to analyze the equivalent series resistance in open circuit condition by applying AC amplitude of 10 mV. Similar tests were also carried out in the full cell configuration in which two same electrodes were used in 0.5 M H_2SO_4. The material loading was maintained at 1 mg in all the tests.

4.2.6. Synthesis of Monomers

1)(A) 1, 4-BIS (2-ethylhexyloxy) benzene (1)

p-Hydroquinone (12.0 g, 0.109 mole) and KOH (30.60 g, 0.545 mole) were taken in a two neck round bottom flask. DMSO (240 mL) was added to it under N_2 atmosphere and stirred for 30-45 minutes at room temperature. 2-Ethylhexyl bromide (45.45 ml, 0.272 mole) was added to the reaction mixture at room temperature and stirred further for 48 hours. For workup, the reaction mixture was poured into 1.8 L water, stirred and extracted with chloroform and washed with brine solution. The product was further purified by column chromatography using pet ether and ethyl acetate as eluent to get the pure compound **1** (1, 4-**BIS (**2-ethylhexyloxy) benzene).Yield = 18 g (50 %).^{1}H NMR (200 MHz, $CDCl_3$) δ ppm: 6.81 (s, 4H), 3.78 (d, 4H), 1.72 (t, 2H), 1.45 (m, 16H), 0.88 (m, 12H)

(B) **2,5-Dibromomethyl 1,4bis-(2-ethylhexyloxy) benzene (2)**

1, 4-Bis (2-ethylhexyloxy) benzene (5.0 g, 14.94 mmol) and p-formaldehyde (3.13 g, 104.5 mmol) were taken in a two neck round bottom flask, into which 90 mL glacial acetic acid and

hydrobromic acid (HBr) (4.47 g, 56.04 mmol) was added at room temperature under nitrogen atmosphere. The reaction mixture was refluxed for 24 h, cooled and poured into ice water and filtered to collect the precipitate. The precipitate was recrystallized by dissolving in glacial acetic acid and cooled for crystallization. The crystals were filtered and dried. Yield = 4.28 g (55 %). ^{1}H NMR (200 MHz, $CDCl_3$) δ ppm: 6.85 (s, 2H), 4.50 (s, 4H), 3.86 (d, 4H), 1.74 (t, 2H), 1.57-1.32 (m, 16H), 0.93 (m, 12H).

2) 2,5-bis-2-ethylhexyloxy-1,4 xylenebis(diphosphonate) (3)

2,5 Bisbromomethyl 1,4 di-(2-ethylhexyloxy) benzene (2.0 g, 3.84 mmol) and triethyl phosphite (5 mL) were taken in a round bottom flask and refluxed under N_2 atmosphere for 24 h. The excess triethyl phosphite and ethyl bromide was removed by vacuum distillation. A highly viscous liquid was obtained as the product. Yield = 2.38 g (98 %).^{1}H NMR (200 MHz), $CDCl_3$; δ ppm: 6.92 (s, 2H), 3.96 (m, 8H), 3.76 (d, 4H), 3.25 (d, 4H), 1.68 (m, 2H), 1.50-1.15 (m, 18H), 0.88 (m, 12H).

3) 2,5-bis-2-ethylhexyloxy-1,4 xylenebis(cyanide) (4)

Sodium cyanide (1.17 g, 24.02 mmol) and 2,5 bisbromomethyl 1,4 di-(2-ethylhexyloxy) benzene (5.0 g, 9.6 mmol) were dissolved in 20 ml of dry DMF and solution was heated to 100 °C for 48 hours. For workup the reaction mixture was poured into 0.5 N NaOH solution. The precipitate formed was filtered and dissolved in chloroform and washed with plenty of water and dried over sodium sulfate (Na_2SO_4). The product was further purified by column chromatography using pet ether and ethyl acetate as eluent to get pure compound 4(2,5-bis-2-ethylhexyloxy-1,4 xylenebis (cyanide)).Yield = 2.0 g (50 %).^{1}H NMR (200MHz, $CDCl_3$) δ ppm: 6.91 (s, 2H), 3.87 (d, 4H), 3.69 (s, 4H), 1.67 (m, 2H), 1.50-1.20 (m, 18H), 0.92 (m, 12H).

4) (2,5-bis((2-ethylhexyl)oxy)-1,4-phenylene)bis(ethene-2,1-diyl))dithiophene (5)

2,5-Bis-2-ethylhexyloxy-1,4 xylenebis(diphosphonate) (3) (2.0 g, 3.15 mmol) and 2-thiophene carbaldehyde (0.777 g, 6.93 mmol) were taken in a round bottom flask (R.B) and thereafter 25 mL dry THF was added under N_2 atmosphere. Potassium tert-butoxide (1.76 g, 115.75 mmol) and dry THF were taken in two neck R.B and cooled to 0 °C and the reaction mixture was slowly added into that. After the addition, the reaction mixture was stirred for 30 minutes at 0 °C; subsequently, the ice bath was removed and the reaction mixture was stirred at room temperature overnight. After completion of the reaction, the product was extracted using chloroform and washed with brine and dried over sodium sulfate (Na_2SO_4).Yield = 1.1

g (64 %). ^{1}H NMR (200 MHz, $CDCl_3$) δ ppm: 7.27 (s, 4H), 7.18 (d, 2H), 7.06-6.94 (m, 6H), 3.91-3.94 (d, 4H), 1.80 (m, 2H), 1.38-1.50 (m, 16H), 0.98 (m, 12H). MALDI-TOF Calculated m/z =550.29; Found m/z = 550.32 (M^+), m/z = 551.31 (M^++H^+).

5) 2,2'-(2,5-bis((2-ethylhexyl)oxy)-1,4-phenylene)bis(3-(thiophene-2-yl)acrylonitrile) (6)

2,5-Bis-2-ethylhexyloxy-1,4 xylenebis(cyanide) (4) (1.70 g, 4.10 mmol) and 2-thiophene carbaldehyde (1.38 g, 12.30 mmol) were taken in a two-neck R.B with methanol and stirred at room temperature. Potassium tert-butoxide (2.31 g, 20.06 mmol) in 20 mL methanol was added to this mixture and stirred at room temperature for 48 hours. The precipitate was filtered and washed with brine, extracted in DCM (Dichloromethane) and dried over sodium sulfate (Na_2SO_4) to get the desired product. Yield = 1.20 g (49 %).^{1}H NMR (200 MHz, $CDCl_3$) δ ppm: 8.06 (s, 2H), 7.64 (d, 2H), 7.54 (d, 2H), 7.13(m, 4H), 3.95-3.98 (d, 4H), 1.74 (m, 2H), 1.27-1.56 (m, 16H), 0.98 (m, 12H). MALDI-TOF Calculated m/z =600.28; Found m/z = 600.31 (M^+), m/z = 601.32 (M^++H^+), m/z = 623.29 (M^++Na^+).

4.2.7. Synthesis of Copolymers

1) Polymer P_1

NDI-2OD-Br_2 (7) (0.4 g, 0.406 mmol), (2,5-bis((2-ethylhexyl)oxy)-1,4-phenylene)bis(ethene-2,1-diyl))dithiophene (5) (0.223 g, 0.406 mmol), K_2CO_3 (0.168 g, 1.21 mmol) and pivalic acid (0.041 g, 0.406 mmol) were carefully weighed into a dry Schlenk tube containing a magnetic stir bar. Degassed dry toluene (18 mL) was added to the reaction vessel under N_2 atmosphere and stirred for 5 minutes at room temperature to fully dissolve the monomers. This was followed by the addition of Pd_2dba_3 (4 mg, 0.004 mmol) under N_2 atmosphere and heating the reaction vessel was in a preheated oil bath and at 100 °C with stirring for 14 hours. After cooling to room temperature, the mixture was dissolved in chloroform, precipitated in methanol, filtered and purified via Soxhlet extraction with acetone, ethyl acetate, and hexane and finally collected with chloroform and filtered through a silica plug to get the polymer. Yield = 520 mg, (94 %) ^{1}H NMR (400 MHz, $CDCl_3$) δ ppm: 8.80 (br, 2H), 7.35 (br, 4H), 7.28 (br, 2H), 7.15(br, 2H), 7.05 (br, 2H), 4.10 (br, 4H), 3.96 (br, 4H), 1.98 (br, 2H), 1.84 (br, 2H), 1.56-1.25 (br, 112H), 0.88 (br, 30H). Mn : 31,700, Đ: 4.6.

2) Polymer P_2

Polymer P_2 was synthesized using the same procedure as that given for P_1. NDI-2OD-Br_2 (7) (0.4 g, 0.406 mmol), 2,2'-(2,5-bis((2-ethylhexyl)oxy)-1,4-phenylene)bis(3-(thiophene-2-yl)acrylonitrile) (6) (0.244 g, 0.406 mmol), K_2CO_3 (0.168 g, 1.21 mmol), pivalic acid (0.041

g, 0.406 mmol) and Pd_2dba_3 (4 mg, 0.004 mmol). Yield = 320 mg, (55 %). ^{1}H NMR (400 MHz, $CDCl_3$) δ ppm: 8.80 (br, 2H), 8.17 (br, 2H), 7.71 (br, 2H), 7.32 (br, 2H), 7.20 (br, 2H), 4.03 (br, 8H), 1.96 (br, 2H), 1.83 (br, 2H), 1.56-1.21 (br, 124H), 0.88-0.97 (br, 32H). Mn : 9,750, Đ : 1.5.

4.3. Results and Discussion

4.3.1. Synthesis and Characterization

The synthesis and characterization of NDI-2OD-Br_2 was previously reported[1] in **Chapter 2 section 2.2.6**. The synthesis of the donor moieties started from hydroquinone, which was alkylated and then bis bromomethylated following literature procedure.[2] The bromomethyl derivative was then converted to the diphosphonate by reacting with triethylphosphite. It was then subjected to Wittig-Horner reaction with thiophene-2-carbaldehyde to obtain one of the donor monomers. The second donor monomer with the nitrile substitution was synthesized by refluxing the 1,4-bis(bromomethyl)-2,5-bis-(alkoxy) benzene with sodium cyanide in DMF. The nitrile derivative was then reacted with thiophene-2-carbaldehyde to obtain the thiophene end capped, nitrile substituted phenylenevinylene donor monomer. **Scheme 4.1** shows the synthetic procedure for the two donor monomers. The details of synthesis, structural characterization and confirmation of purity of the monomers are provided in the **Figures 4.4 to 4.7**.

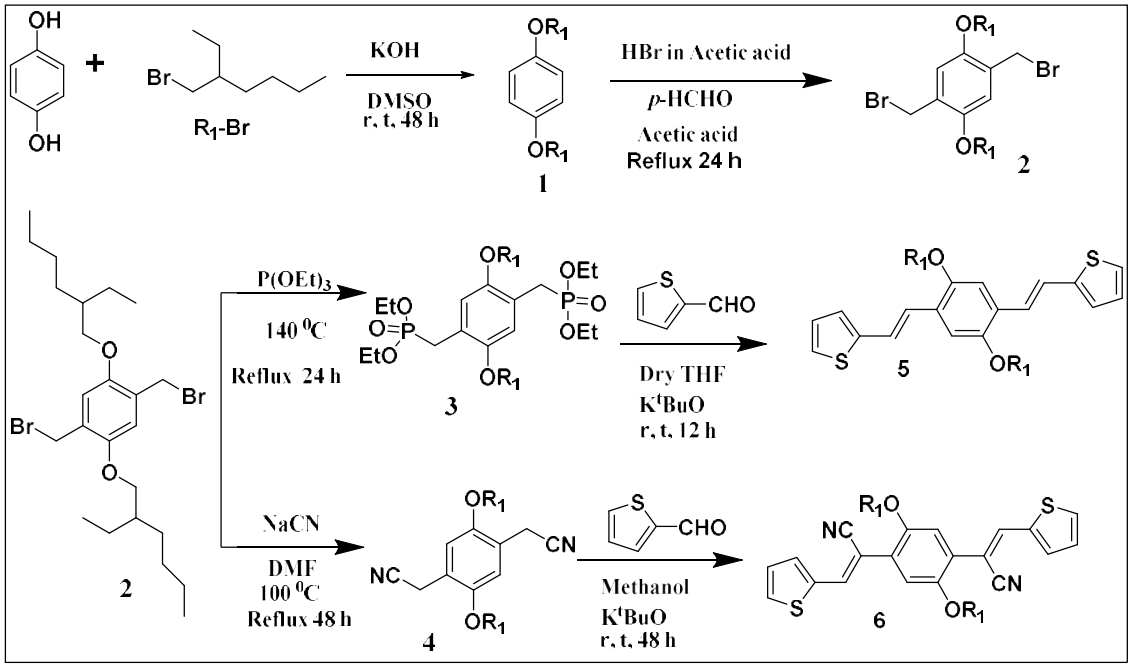

Scheme 4.1. Synthesis of monomers.

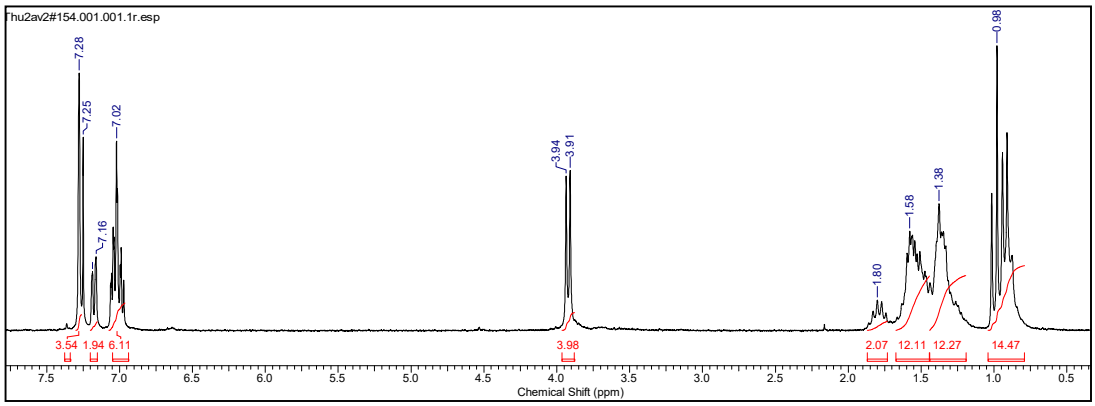

Figure 4.4. ^{1}H NMR spectrum of monomer (2,5-bis((2-ethylhexyl)oxy)-1,4-phenylene)bis(ethene-2,1-diyl))dithiophene (5).

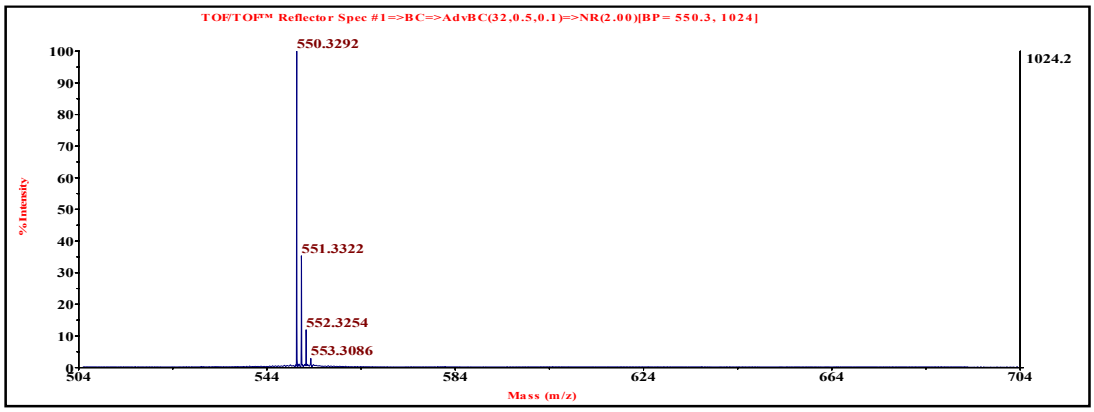

Figure 4.5. MALDI- TOF spectrum of monomer (2,5-bis((2-ethylhexyl)oxy)-1,4-phenylene)bis(ethene-2,1-diyl))dithiophene (5).

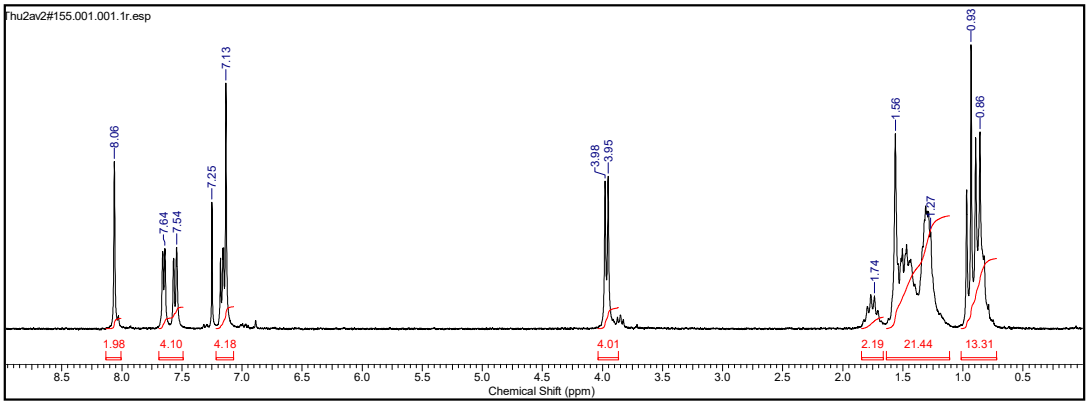

Figure 4.6. ^{1}H NMR spectrum of monomer 2,2'-(2,5-bis((2-ethylhexyl)oxy)-1,4-phenylene)bis(3-(thiophene-2-yl)acrylonitrile) (6).

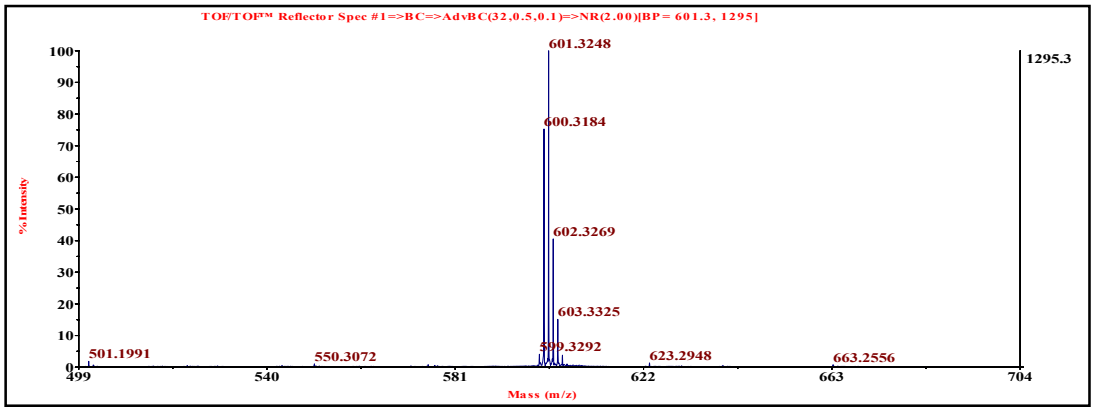

Figure 4.7. MALDI- TOF spectrum of monomer 2,2'-(2,5-bis((2-ethylhexyl)oxy)-1,4-phenylene)bis(3-(thiophene-2-yl)acrylonitrile) (6).

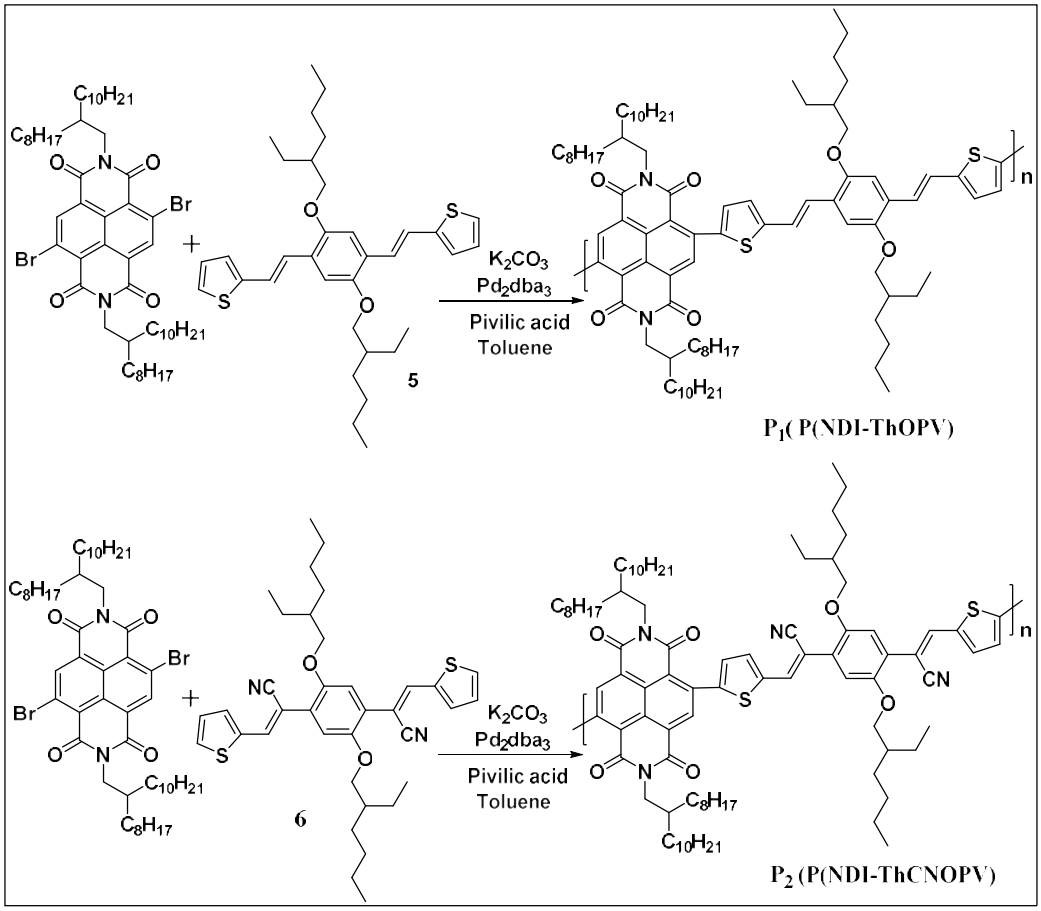

Scheme 4.2. Synthesis of polymers.

The direct heteroarylation polycondensation of NDI-2OD-Br_2 with the donor monomers 5 and 6 was carried out following the procedure outlined by Sommer et.al.[13] **Scheme 4.2** shows the conditions of DHAP for the D-A copolymers. In short, the NDI-2OD-Br_2 was reacted with the donor monomers in the presence of tris (dibenzylideneacetone)dipalladium

(Pd_2dba_3), K_2CO_3, pivalic acid using toluene as solvent at 100 °C. The polymers were named **P(NDI-ThOPV)** or **P_1** for the polymer without nitrile substitution and **(P(NDI-ThCNOPV)** or **P_2** for the polymer with nitrile substitution on the oligophenylene moiety. Throughout the rest of the chapter, the polymers were referred to simply as **P_1** and **P_2**.

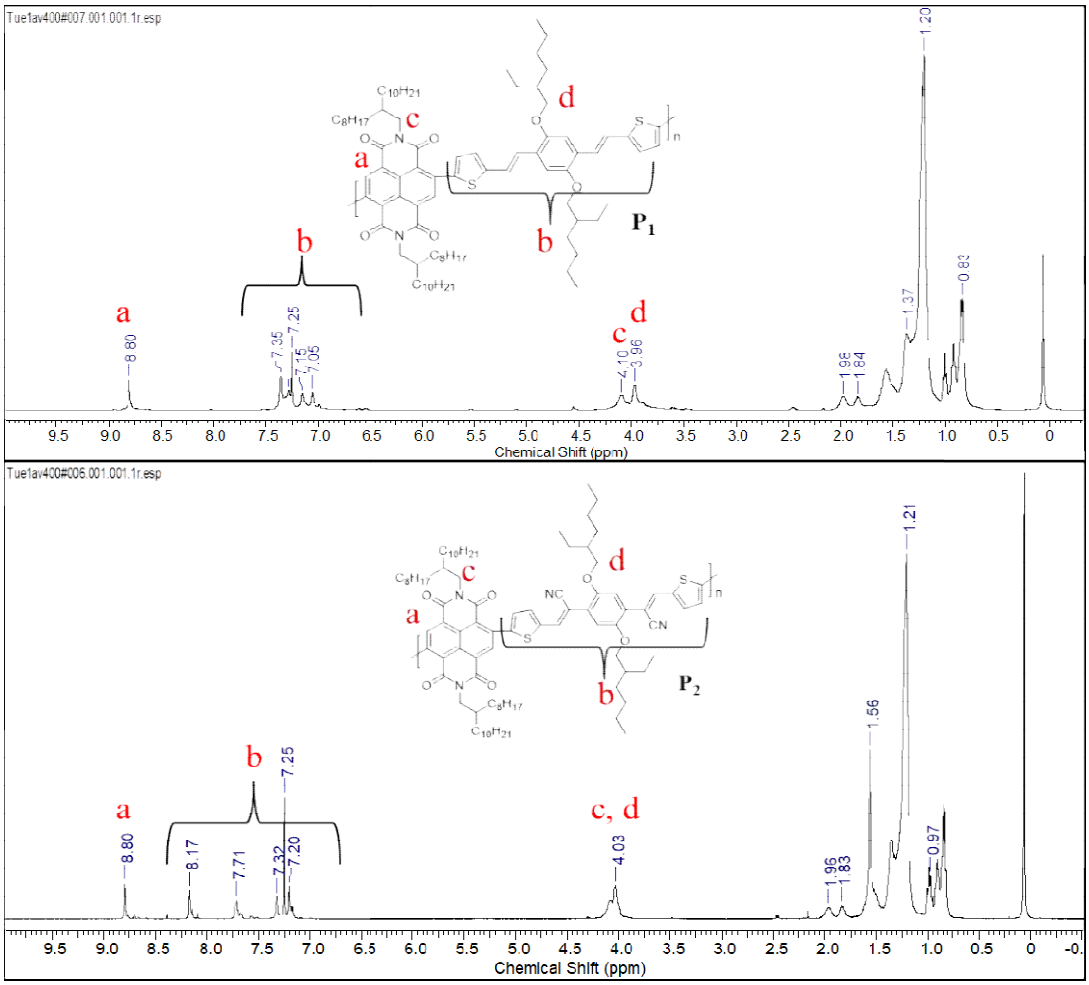

Figure 4.8: ^{1}H NMR spectra of copolymers P_1 and P_2 recorded in $CDCl_3$.

Figure 4.8 shows the labeled stack plot of the proton NMR spectra of the two new D-A copolymers. The spectrum in the top in **Figure 4.8** corresponds to polymer P_1. The two aromatic protons of NDI appeared at 8.80 ppm, while the peaks at 7.35, 7.15 and 7.05 ppm corresponded to the aromatic protons of thiophene coupled phenylenevinylene moiety. The aromatic protons of NDI in polymer P_2 (**Figure 4.8** bottom) also appeared at 8.80 ppm. However, the aromatic protons of the thiophene coupled phenylenevinylene moiety were de-shielded (8.17, 7.71, 7.32 and 7.20 ppm) due to the presence of the electron withdrawing nitrile groups. The two peaks at 4.10 and 3.96 ppm corresponded to the CH_2 protons next to the imide nitrogen on the NDI ring and to the $–OCH_2$- protons of the alkyl substitution on the

central phenyl ring respectively. Some small extra peaks were observed in the aromatic region of P_2 which could be assigned to tolyl end capping with various positional isomers.[13, 44] Aromatic solvents like toluene has been shown to be susceptible to C-H activation under DAP conditions which leads to chain termination with end capping. The lower solubility of the nitrile substituted polymer P_2 compared to P_1 resulted in its lower molecular weight (discussed later on) due to which the tolyl end groups were clearly observed in the proton NMR spectrum. Although P_1 was also equally susceptible to end capping by toluene group, it was not so obvious in its proton NMR spectrum due to its relatively higher molecular weight. The polymers were purified by repeated soxhlet extraction with methanol, acetone, and hexane respectively for 24 hours each. The polymers were sparingly soluble in common organic solvents like DCM, chloroform and, chlorobenzene. However, they had good solubility in tetrahydrofuran (THF) in which the molecular weight was estimated using size exclusion chromatography (SEC) with polystyrene (PS) as the standard and THF as the solvent. **Table 4.1** shows the molecular weight (GPC chromatogram provided in **Figure 4.9**) and other characterization details of the polymers. The details of P(NDI2OD-T2) from Chapter 2 has also been included in the table for comparison.[1] The polymers exhibited high molecular weights with Mn 26.4, 31 and 10 kDa for **P(NDI2OD-T2), P_1** and **P_2**, respectively. The Mw were 152, 146 and 15 kDa, respectively. Thermal characterization of the copolymers was carried out by thermogravimetric analysis (TGA) as well as differential scanning calorimetry (DSC) measurement under a nitrogen atmosphere.

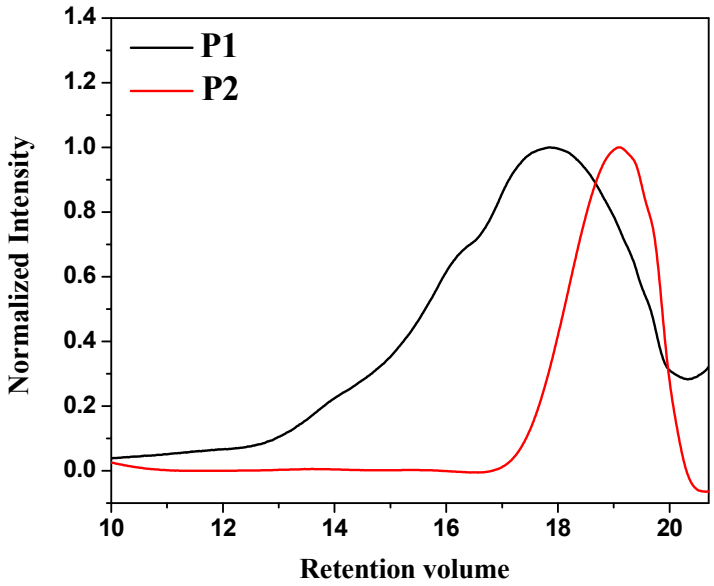

Figure 4.9: GPC chromatograms of the polymers recorded using THF as the eluent.

Table 4.1 Molecular weight and thermal characterization of the polymers.

Polymer	M_n[a] (KDa)	Mw[a] (KDa)	Đ[a]	T_d[b]
P(NDI2OD-T2)	26.4	152	5.7	422
P_1	31	146	4.6	395
P_2	10	15	1.5	420

[a.] Determined by SEC using THF as the eluent and PS as standards. [b.] Determined by thermogravimetric analysis 10 % weight loss Temperature (°C).

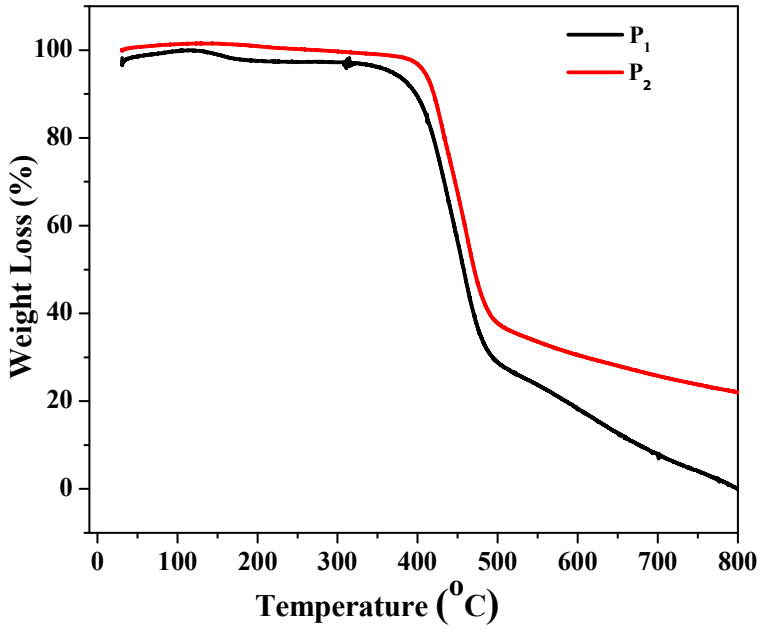

Figure 4.10: TGA of polymers run from 40 to 800 °C with a heating rate of 10 °C/min under nitrogen.

TGA curves (**Figure 4.10**) showed good thermal stability for the polymers with onset decomposition temperature (T_d) more than 400 °C. The DSC thermograms were recorded by heating the polymers from -50 °C to 300 °C at 10 °C /min under N_2 atmosphere (**Figure 4.11**). No transitions were observed in the case of polymer P_1, which indicated its amorphous nature. In the case of polymer P_2, sharp transitions were observed in heating and cooling due to its semi-crystalline nature.

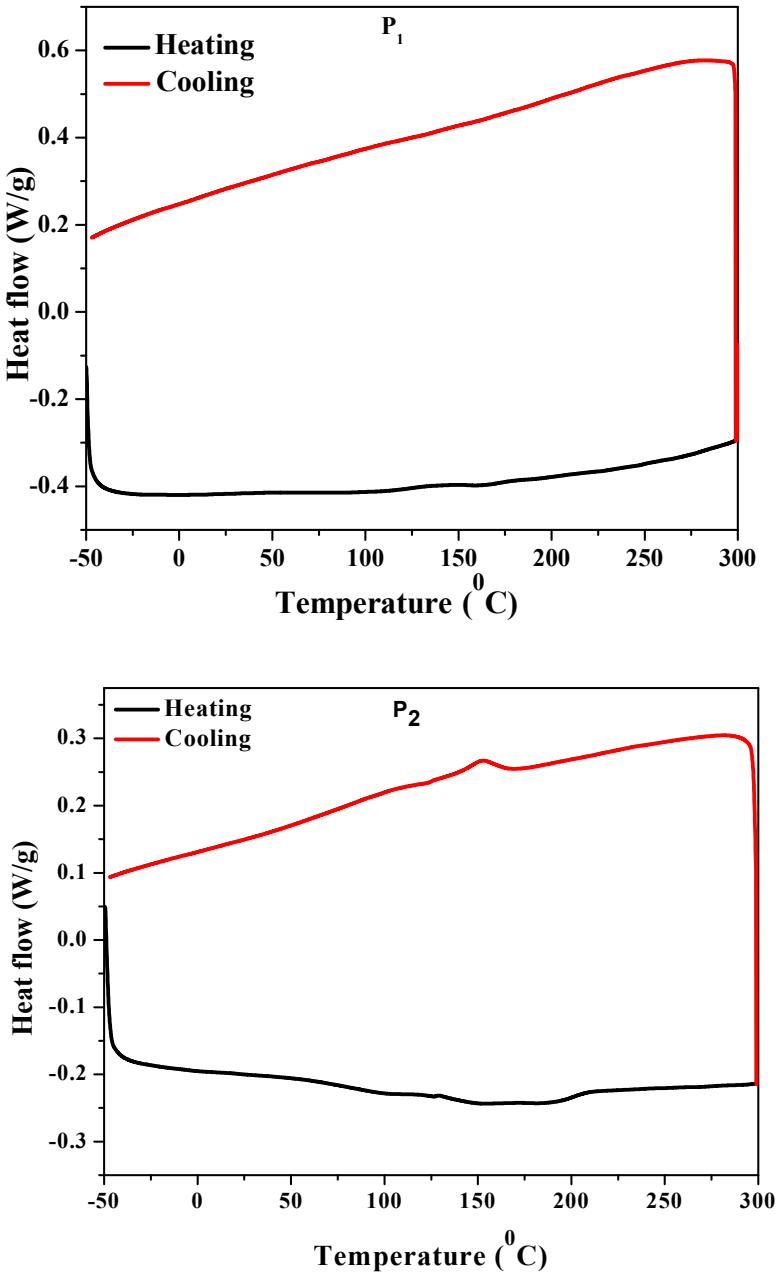

Figure 4.11: DSC thermograms of polymers P_1 and P_2 at a heating rate of 10 °C/min under nitrogen atmosphere.

4.3.2. Optical Characterization and Energy Level

UV-Vis absorption spectra of polymers P_1 and P_2 were recorded in chloroform (dilute solution) as well as in thin-film spin-coated on glass substrate and are shown in **Figure 4.12** along with that of the reference polymer P(NDI2OD-T2). In solution (top) and thin film (bottom) the polymers showed two absorption bands; the high energy absorption band at

~300-480 nm was assigned to the π-π* transition and the low energy band at ~500 - 800 nm was accounted to intramolecular charge transfer (ICT) from thiophene based donor unit to NDI.[1, 2, 45]

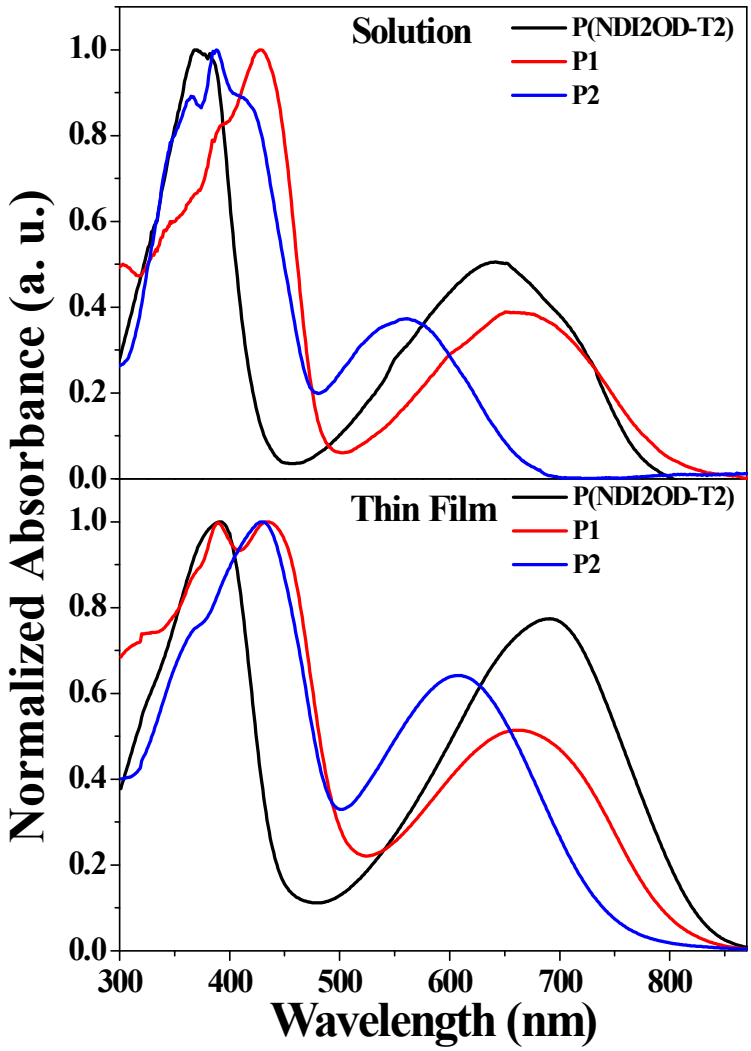

Figure 4.12: UV-Vis absorption spectra of dilute solutions of polymers in chloroform (top) and thin film (bottom) on quartz substrate.

This ICT band is sensitive to the nature of the donor unit i.e the electron donating strength of the donor moiety in the repeat unit.[46] It could be seen from **Figure 4.12** that the ICT band in P_2 was much more blue shifted compared to that of the reference polymer or P_1. It indicated a markedly reduced electron is donating strength of the donor unit in P_2, which could be accounted for by the presence of the two electron withdrawing nitrile groups in P_2 which was absent in P_1. This blue shift is not caused by a lack of planarity in P_2 as the nitrile substitution at the vinylene bridge has been shown to not distort the molecular structure.[47] An

enhancement of the intensity of ICT band with respect to the π-π* band was observed in P_2 in going from solution to film, which demonstrated enhanced donor-acceptor interaction in the film. The optical band gap (E_g^{opt}) of the polymers was calculated from lower energy absorption band edge of thin-film and is listed in **Table 4.2**.

Table 4.2 Electrochemical and optical band gaps.

Polymer	HOMO[a] (eV)	LUMO (eV)	E_g^{opt} (eV)	HOMO[b] (eV)	LUMO[b] (eV)	E_g[b] (eV)
P(NDI2OD-T2)	-5.42	-3.90	1.52	-	-	-
P_1	-5.31	-3.75	1.56	-4.91	-3.28	1.63
P_2	-5.60	-3.95	1.65	-5.34	-3.46	1.88

[a] HOMO values calculated from LUMO and E_g optical, [b] DFT calculation of energy levels and bandgap for the model (dimer).

An optical band gap of 1.52 eV was obtained for the reference polymer P(NDI2OD-T2), which was slightly increased to 1.56 eV and 1.65 eV in P_1 and P_2 polymers, respectively. Electronic energy levels of the new copolymers were measured by cyclic voltammetry. Thin-films of polymer were drop cast on the platinum working electrode.

The measurement was done in acetonitrile solvent with ferrocene/ferrocenium as an internal standard and tetrabutylammonium hexafluorophosphate (*n*-Bu4NPF$_6$ 0.1M/ acetonitrile) as supporting electrolyte.[48] Cyclic voltammograms for polymers are shown in **Figure 4.13,** and the calculated HOMO and LUMO energy levels are given in **Table 4.2**. Copolymer P_1 and P_2 showed two quasi-reversible reduction peaks at -0.806 / -1.11 V and -0.65 / -1.09 V respectively with 0.026 / 0.013 and 0.028 / 0.010 peak current. Decreased reduction potential with increased peak current observed in the case of polymer P_2 confirmed the comparatively higher electron deficiency of P_2 due to the presence of two electron withdrawing nitrile groups along the backbone.[2.] However, oxidation peaks were not observed during anodic scan up to 2V. The lowest unoccupied molecular orbital (LUMO) energy levels were calculated based on the onset value of first reduction peak and reference energy level of ferrocene (4.8 eV below the vacuum level) according to E_{LUMO} (eV) = -e × (E^{red} onset + 4.8) below the vacuum level.[45] The LUMO energy levels of P_1 and P_2 were obtained as -3.75 V and -3.95 V respectively. The highest occupied molecular orbital (HOMO) levels were estimated based on the optical band gap calculated from the absorption onset measurements in a thin film. Thus, HOMO energy levels of P_1 and P_2 were determined as -5.31 V and -5.60 V respectively.

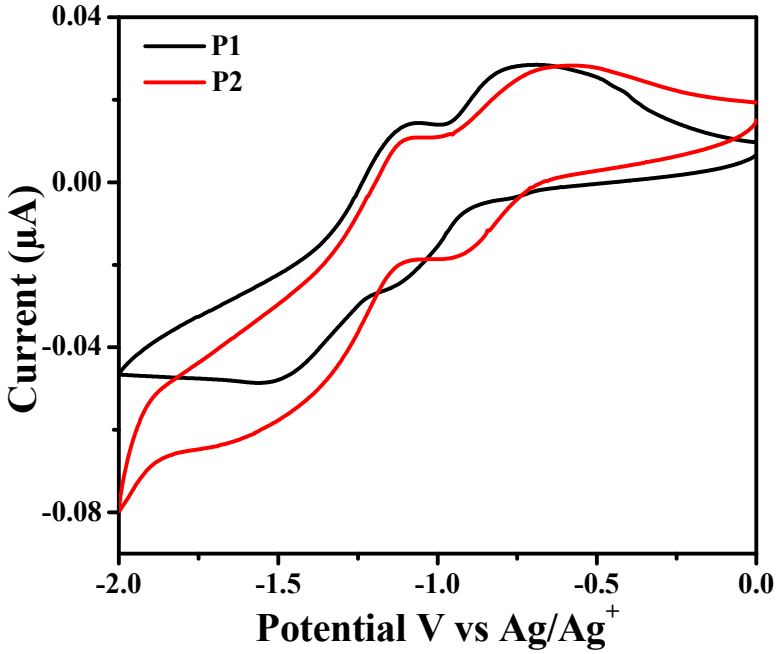

Figure 4.13: Cyclic voltammograms of P_1 and P_2 copolymers as thin film in 0.1 M $(n\text{-}Bu)_4NPF_6$ – acetonitrile solution.

The LUMO and HOMO energy levels of P(NDI2OD-T2) were taken as -3.90 eV and -5.42 eV, respectively from chapter 2.[1] The HOMO and LUMO energy levels of donor-acceptor copolymers can be fine tuned by varying the electron donating or accepting the strength of the donor or acceptor moiety. For instance, in P_1 and P_2, the acceptor part is the same (naphthalene diimide), but the donor strength is reduced in P_2 due to the electron withdrawing nitrile groups. This resulted in lowering of the HOMO level and higher energy band gap in P_2 compared to P_1. These observations could also be confirmed by calculations based on density-functional theory (DFT) performed on oligomeric models (dimer). The energy levels were calculated from Gaussian 09 program using B3LYP functional and polarized 6-31g* basis set. The bulky alkyl substituents in both the donor and acceptor fragments were replaced with a methyl group in order to minimize the computational time. The values of HOMO, LUMO and band gap are listed in **Table 4.2**, while the surface plots of the model dimers are provided in the **Figure 4.14**. In donor-acceptor conjugated systems based on NDI, the LUMO wavefunctions are generally localized on the NDI aromatic unit as we have previously also observed in case of NDI-OPV models.[2] P_1 and P_2 followed this pattern with the LUMO wavefunction localized on NDI and the HOMO wavefunction on the thiophene end-capped OPV unit.

The values of the HOMO /LUMO for the two model units (given in **Table 4.2**) calculated from the DFT, followed the trend of experimental results from cyclic voltammetry and absorption spectra. P_1 and P_2 models (dimeric unit) showed band gap of 1.63 eV and 1.88 eV respectively. The LUMO levels were very similar (-3.28 V and -3.46 V for P_1 and P_2 respectively) since the acceptor part was the same, whereas the HOMO values were lower for P_2 (-4.91 V and -5.34 V for P_1 and P_2 respectively).

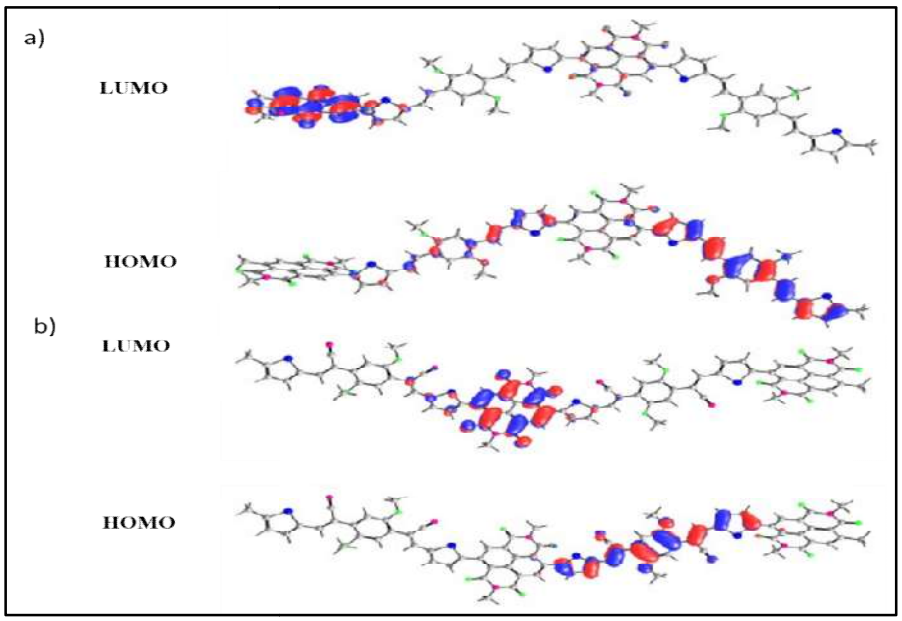

Figure 4.14: HOMO and LUMO surface plots for oligomers (dimer models): (a) P_1; (b) P_2

4.3.3. Thin-film Crystallinity

The molecular packing and bulk crystalline nature of the polymers were analyzed using powder wide-angle X-ray diffraction (XRD) measurement. **Figure 4.15** shows the normalized X-ray diffraction patterns of the two polymers. Both of them showed sharp reflections with multiplicity indicating lamellar nature. A sharp (100) reflection was observed at 2θ = 4.30° and 3.94° corresponding to d spacing of 20.53 Å and 22.56 Å for P_1 and P_2 respectively. This distance corresponded roughly to the length from one end of the naphthyl ring (at para position to the thiophene linkage) to the thiophene ring at the end of the oligothiophene phenylenevinylene unit. The lamellar peaks were obtained at 2θ values of 4.30°, 8.91° and 11.97 ° (1:2:3 ratio) for P_1 (indicated by arrows in **Figure 4.15**). For P_2, the peaks were observed at 2θ values of 3.94°, 7.97° and 11.65°(indicated by arrows in **Figure 4.15**). **Table 4.3** compiles the 2θ values, and corresponding d spacing is observed for both the polymers.

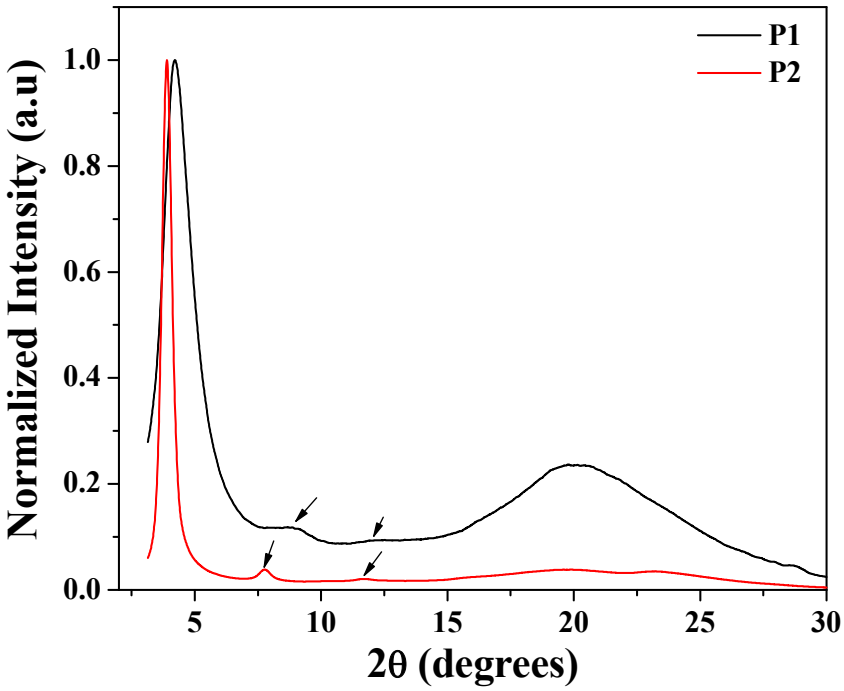

Figure 4.15: Powder WXRD diffraction patterns of P_1 and P_2 copolymers.

Table 4.3. *2θ* values and d spacing values for the polymers.

Polymer	2θ°		*d*-spacing (Å)		% Crystallinity
	(100)	Lamellar peaks	d_{100}	$d_{lameller}$	
P_1	4.30	8.91, 11.97	20.53	9.91, 7.38	16.4 %
P_2	3.94	7.97, 11.65	22.56	11.32, 7.59	31.5 %

The percent crystallinity of the two polymers were estimated from the areas of the peak under the crystalline and amorphous regions with the help of "X'Pert Highscore plus software" as shown in the equation.

$$\% \text{ Crystallinity} = \text{Area}_{\text{Cryst}} / \text{Area}_{\text{Amp+Cryst}}$$

Using the above formula, the percent crystallinity was estimated to be 16.4% for P_1 and 31.5% for P_2. Better crystallinity implied improved polymer chain alignment and reduced chain defects, which are beneficial as far as charge transport and device performance are concerned.

4.3.4. Electrochemical Characterization of the Symmetric Polymer Composite Supercapacitor

The electrochemical properties of the polymer composite electrodes (< 16 wt % carbon) were evaluated using cyclic voltammetry (CV) with $Hg/HgSO_4$ as the reference electrode and carbon paper as the counter electrode in 0.5 M H_2SO_4 as the electrolyte. This analysis served as a guide for setting the parameters for the device fabrication. The details of the CV experiments depicting the enhancement in the capacitive performance and current are provided in the **Figure 4.16.**

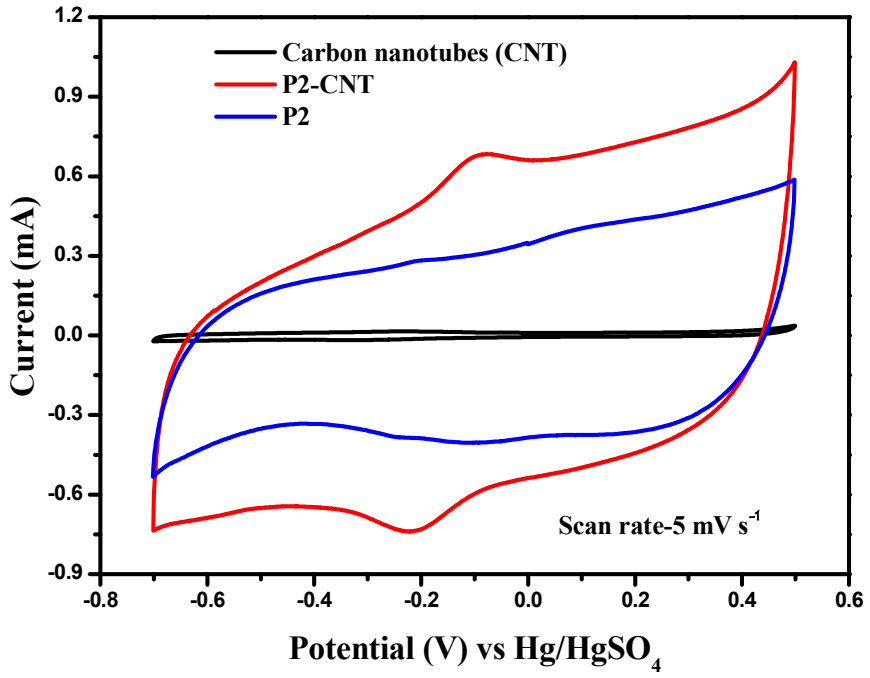

Figure 4.16: Cyclic voltammogram of the composite material, neat polymer and bare carbon electrodes.

The carbon nanotubes have been shown to improve the structural ordering of the conducting polymer chains thereby facilitating delocalization of charge carriers leading to enhanced conductivity.[49] The properties of the two polymers were compared with that of (PNDI2OD-T2) synthesized in the lab (see our previous report) as a reference polymer.[1] **Figure 4.17a** shows the cyclic voltammograms for the polymers inspected under a potential range of -0.7 – 0.5 V at a scan rate of 10 mVs^{-1}. The nearly square shape of the CV curve indicated good capacitive behavior. The polymers exhibited a redox peak around -0.3 V. From the CV, the oxidation peak for P(NDI2OD-T2) was observed at -0.10 V and the reduction peak at -0.26 V. For $P_{1,}$ these peaks were observed at -0.07 V and -0.25 V, respectively, while the

oxidation and reduction peaks for P_2 were observed at -0.06 and -0.25 V, respectively. The area under the CV curve is a measure of the capacitance of the material. As seen in **Figure 4.17a**, P_2 exhibited the highest area under the CV indicating the highest capacitance among the three polymers tested.

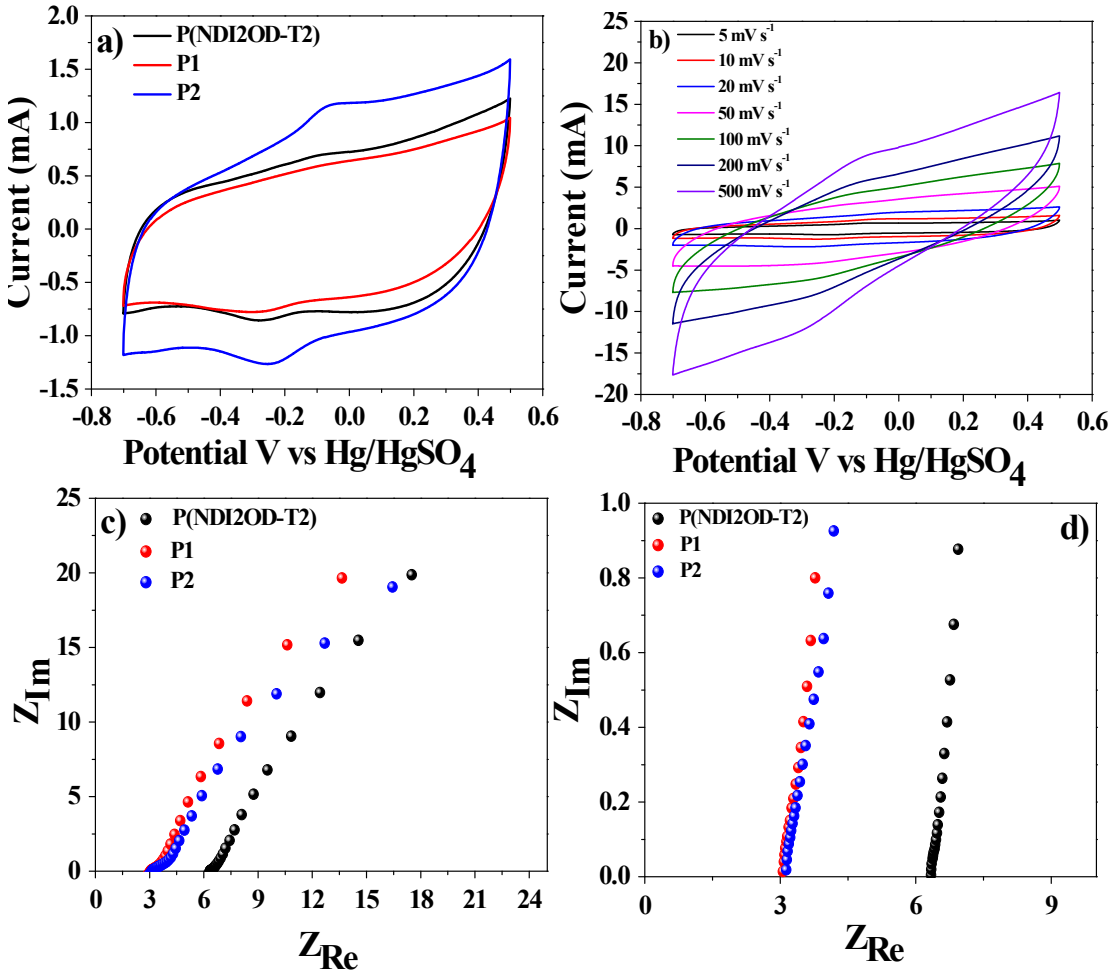

Figure 4.17: a) CV Spectra of different polymers recorded at a scan rate of 10 mVs^{-1}. b) CVs recorded at different scan rates for the P_2 polymer. c) Nyquist plots for different polymers. d) Represent the zoomed part of the Nyquist plot given in Figure c.

The capacitance values of P(NDI2OD-T2) and P_1 were more or less similar. The high capacitance of the P_2 could be ascribed to the increased electron delocalization along the polymer backbone brought about by the presence of two nitrile groups which allowed for more negative charge to be accepted compared to the other two polymers.[40] Cyclic voltammograms recorded at different scan rates for (P_2) are shown in the **Figure 4.17b**. The polymer showed a behavior which is typical of a capacitive material with the peak current

increases with the increase in the scan rate. However, the CV recorded at high scan rates became relatively more resistive as the electrolyte ions could not get ample time for the adsorption on the polymer surface. For gathering more insightful information on the charge transfer nature of the polymer, the redox activity of the polymers was probed with the help of the electrochemical impedance spectroscopy (EIS) in the frequency range of 1 MHz to 1 MHz under open circuit voltage (OCV) conditions at an AC amplitude of 10 mV. **Figure 4.17c** shows the Nyquist plots of the imaginary component of the impedance (Z'') versus the real component (Z') for the three polymers. In the Nyquist plot, the high-frequency intercept on the abscissa gives the equivalent series resistance (ESR) which is the combination of solution resistance and other resistive contributions arising from the electrode materials, current collector, and electrical contacts.

The ESR measured for P_1 and P_2 were 3 Ω while that observed for P(NDI2OD-T2) was more than double at 6.31 Ω. This indicated high conductivity for P_1 and P_2 polymers in comparison to P(NDI2OD-T2). For high power density, it is necessary to have low ESR value as the maximum power output is inversely proportional to ESR, *i.e.*, $P_{max}= V^2/ 4R$. The enlarged region in the high-frequency range of the Nyquist plot given in **Figure 4.17d** confirmed the absence of any appreciable semi-circle signature for the charge transfer resistance (CTR) or plateau in the mid-frequency region that gives Warburg diffusion. Overall, the Nyquist analysis showed higher conductivity and faster kinetics for the P_2 polymer. The slightly higher ESR value for the polymer P_2 could be ascribed to the high band gap of P_2 (1.65 eV) compared to P_1 (1.56 eV).

The Galvanostatic charge/discharge (GCD) characteristics was investigated for the polymers P_1 and P_2 along with P(NDI2OD-T2). **Figure 4.18a** shows the GCD profiles for the n-doped polymer films. The GCD curves showed deviation from the triangular geometry, which is normally considered as the case of ideal electrochemical double layer behavior. The slightly distorted GCD profiles appearing in the case of the polymers suggested the existence of pseudocapacitive contribution by the systems.[50] P_2 showed a gravimetric capacitance of 124 F g^{-1} at a current density of 0.5 A g^{-1}. This is one of the highest values reported for D-A conjugate polymers reported so far.[42] The corresponding values for P_1 and P(NDI2OD-T2) were 61 and 84 F g^{-1}, respectively. **Figure 4.18b** shows the charge-discharge profiles recorded at increasing current density values. **Figure 4.18c** illustrates how the specific capacitance of the system changes with respect to the current density, where a decrease in the capacitance was clearly observed with increase in the current density. This is expected behavior in the case of the organic materials. When the current density is increased to 5 A g^{-1},

P_2 could retain 40 % of the capacitance as measured at 0.5 A g^{-1}. Such modest rate capability displayed by the system is ascribed to the restricted ion movement incurred by the system.

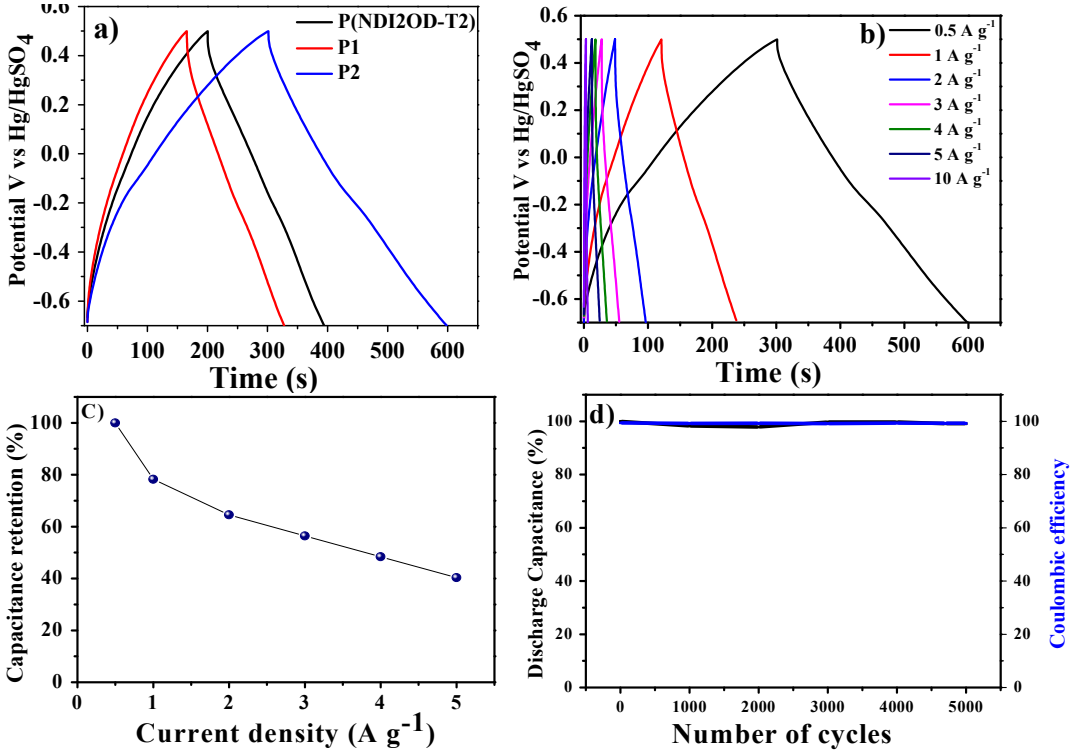

Figure 4.18: a) Charge-discharge profile of different polymers recorded at a current density of 0.5 A g^{-1} b) Charge-discharge profile of P_2 polymer measured at different current densities c) represents the rate capability and capacitance retention of P_2 polymer d) Durability test conducted at a current density of 5 A g^{-1} for the P_2 polymer.

The cycling stability of the system was tested using cycling experiments by recording 5000 CV cycles at a current density of 5 A g^{-1}, which is shown in **Figure 4.18d**. Even after 5000 cycles, P_2 could retain almost 100 % of the initial capacitance. Moreover, the complete retention of the coulombic efficiency was observed throughout the cycling tests (**Figure 4.18d**). The energy density and power density of 2 Wh kg^{-1} and 22 kW kg^{-1}, respectively, was observed for P_2, which are comparable to values reported for p-type of conducting polymers in the literature.[51, 52]

4.3.5. Full Cell Characterization

Performance of P_2 was analyzed in full cell device configuration in 0.5 M H_2SO_4 as an electrolyte. Cyclic voltammogram recorded at a scan rate of 5 mV s^{-1} is given in the **Figure 4.19a**; it shows typical rectangular CV behavior of the capacitive material expected for

complete two-electrode cell. Furthermore, **Figure 4.19b** shows the CVs recorded at increasing voltage scan rates, the peak current increases proportionally with scan rate (a characteristic of capacitive behavior).

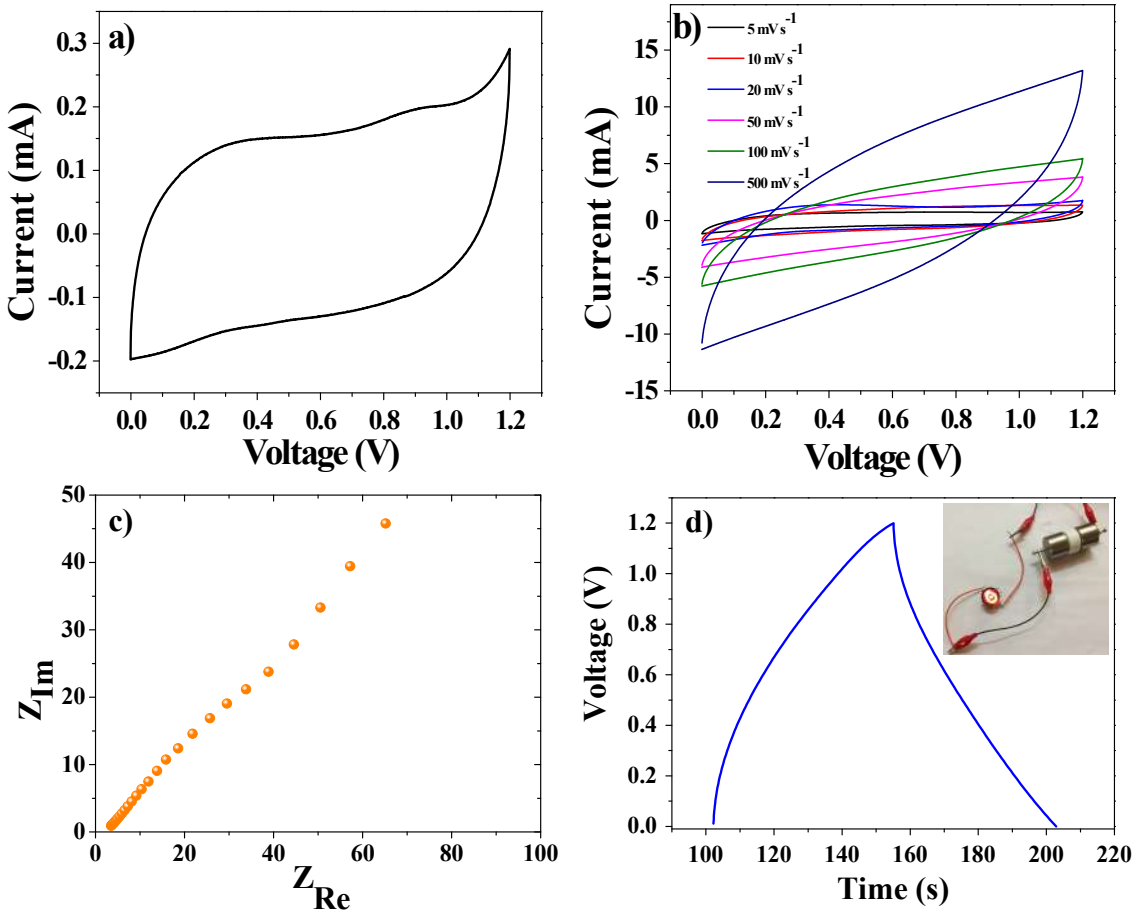

Figure 4.19: Electrochemical characterization of symmetric supercapacitor fabricated for P_2 polymer; the electrolyte used for the test was 0.5 M H_2SO_4 a) cyclic voltammogram recorded at a scan rate of 5 mV s^{-1} b) represents the CVs recorded at increasing voltage scan rates c) represents the Nyquist plot depicting the ESR and frequency behavior of the device d) galvanostatic charge-discharge recorded at a current density of 0.5 A g^{-1}. The inset shows the glowing of a red LED using P_2 based full cell configuration.

However, CVs at higher scan rate show more resistive behavior which is caused by the fast movement of electrolyte ions in and out of the polymer, thereby, electrolyte ions does not get enough time to participate in charge storage. The equivalent series resistance measured from EIS for the device is 8 **Ω** which is depicted in the Nyquist plot given in the **Figure 4.19c**; also any semi-circle representative of the charge transfer resistance is not evident in the Nyquist

plot. Finally, capacitance was measured by recording galvanostatic charge-discharge curves at a current density of 0.5 A g-1, capacitance of 40 F g-1 could be obtained in the full cell configuration (**Figure 4.19d**). Theoretically, the capacitance obtained in the two electrode cell is half of the capacitance obtained for the single electrode in the three electrode set up. However, the capacitance measured here is less than half of the capacitance obtained for single electrode. This loss in capacitance can be attributed to the ESR obtained for the full cell. The inset in **Figure 4.19d** demonstrates the full cell configuration of polymer P_2 as a power source used to glow a red light emitting diode (LED) The results shown in this report are superior compared to the results reported for similar polymer systems in the literature, and it embarks a significant contribution to the development of n-type polymers in the field of charge storage.

4.4. Conclusion

In summary, π-conjugated polymers based on naphthalene diimide as the acceptor and thiophene terminated phenylenevinylene as the donor were synthesized following the Direct (hetero) arylation polycondensation (DHAP) route. The polymer was successfully evaluated as composite electrode in supercapacitors in a type III device configuration. A specific capacitance of 124 F/g with excellent stability up to 5000 cycles with almost 100% retention of the initial capacitance was observed for the polymer with nitrile substituents along the OPV backbone (P_2). We are not aware of any other reports of application of donor-acceptor conjugated polymer as supercapacitor electrode materials with such exceptional long-term cycle life (5000 cycles) with 100 % retention of capacitance value. The energy and power density was obtained as 2 Wh kg^{-1} and 22 kW kg^{-1} respectively. Development of materials for type III supercapacitor device application is very crucial since not many materials can meet the challenge of stability under reduced conditions. Although donor-acceptor polymers have earned their place as efficient materials for photovoltaic applications, they are yet to be explored for their applicability in type III and type IV supercapacitor devices. The observations presented here highlight the importance of donor-acceptor π conjugated polymers in energy storage applications.

4.5. References

(1) Sharma, S.; Kolhe, N. B.; Gupta, V.; Bharti, V.; Sharma, A.; Datt, R.; Chand, S.; Asha, S. K. *Macromolecules*, **2016**, *49*, 8113-8125.

(2) Kolhe, N. B.; Ashar, A. Z.; Narayan, K. S.; Asha, S. K. *Macromolecules* **2014**, *47,* 2296-2305.

(3) Sévignon, M.; Papillon, J.; Schulz, E.; Lemaire, M. *Tetrahedron Lett*. **1999**, *40*, 5873-5876.

(4) Wang, Q.; Takita, R.; Kikuzaki, Y.; Ozawa, F. *J. Am. Chem. Soc.* **2010**, *132*, 11420-11421.

(5) McCullough, R. D.; Lowe, R. D. *J. Chem. Soc., Chem. Commun*. **1992**, *0*, 70-72.

(6) Chen, T. A.; Rieke, R. D. *J. Am. Chem. Soc.* **1992**, *114*, 10087-10088.

(7) Nohara, Y.; Kuwabara, J.; Yasuda, T.; Han, L; Kanbara, T. *J. Polym. Sci. Part A: Polym. Chem.*, **2014**, *52:* 1401-1407.

(8) Shao, J.; Wang, G.; Wang, K.; Yang, C.; Wang, M. *Polym. Chem*. **2015**, *6*, 6836-6844.

(9) Wang, Q.; Wakioka, M.; Ozawa, F. *Macromol*. *Rapid Commun*. **2012** *33*, 1203-1207.

(10) Facchetti, A.; Vaccaro, L.; Marrocchi, A. *Angew. Chem. Int. Ed*. **2012,** *51*, 3520-3523.

(11) Berrouard, P.; Najari, A.; Pron, A.; Gendron, D.; Morin, P. O.; Pouliot, J. R.; Veilleux, J.; Leclerc, M. *Angew. Chem. Int. Ed.* **2012**, *51*, 2068-2071.

(12) Lu, W.; Kuwabara, J.; Kanbara, T. *Macromolecules* **2011**, *44*, 1252-1255.

(13) Matsidik, R.; Komber, H.; Luzio, A.; Caironi, M.; Sommer, M. *J. Am. Chem. Soc.* **2015**, *137*, 6705-6711.

(14) Chang, S. W.; Waters, H.; Kettle, J.; Kuo, Z. R.; Li, C. H.; Yu, C. Y.; Horie, M. *Macromol. Rapid Commun*., **2012,** *33,* 1927-1932.

(15) Yasuda, T.; Kuwabara, J.; Han, L.; Kanbara, T. *Org. Electron*. **2015**, *25*, 99-104.

(16) Nohara, Y.; Kuwabara, J.; Yasuda, T.; Han, L.; Kanbara, T. *J. Polym. Sci., Part A: Polym. Chem.* **2014**, *52*, 1401-1407.

(17) Bohra, H.; Shao, J.; Huang, S.; Wang, M. *Tetrahedron Lett*. **2016**, *57,* 1497-1501.

(18) Luzio, A.; Fazzi, D.; Nübling, F.; Matsidik, R.; Straub, A.; Komber, H.; Giussani, E.; Watkins, S. E.; Barbatti, M.; Thiel, W.; Gann, E.; Thomsen, L.; McNeill, C. R.; Caironi, M.; Sommer, M. *Chem. Mater*. **2014**, *26*, 6233-6240.

(19) Nakabayashi, K.; Mori, H. *Chem. Lett*. **2013**, *42*, 717-718.

(20) Mikroyannidis, J. A.; Stylianakis, M. M.; Balraju, P.; Suresh, P.; Sharma, G. D. *ACS Appl. Mater. Interfaces* **2009***, 1*, 1711-1718.

(21) Liu, T.; Finn, L.; Yu, M.; Wang, H.; Zhai, T.; Lu, X.; Tong, Y.; Li, Y. *Nano Lett*. **2014**, *14,* 2522-2527.

(22) Talbi, H.; Just, P.-E.; Dao, L. H. *J. Appl. Electrochem*. **2003**, *33*, 465-473.

(23) Snook, G. A.; Kao, P.; Best, A. S. *J. Power Sources* **2011**, *196*, 1-12.

(24) Balducci, A.; Henderson, W. A.; Mastragostino, M.; Passerini, S.; Simon, P.; Soavi, F. *Electrochim. Acta* **2005**, *50*, 2233-2237.

(25) Di Fabio, A.; Giorgi, A.; Mastragostino, M.; Soavi, F. *J. Electrochem. Soc.* **2001**, *148,* A845-A850.

(26) Fusalba, F.; El Mehdi, N.; Breau, L.; Bélanger, D. *Chem. Mater*. **1999,** *11*, 2743-2753.

(27) Skompska, M.; Mieczkowski, J.; Holze, R.; Heinze, J. *J. Electroanal. Chem.* **2005**, *577*, 9-17.

(28) Hashmi, S. A.; Latham, R. J.; Linford, R. G.; Schlindwein, W. S. *Polym. Int.* **1998**, *47*, 28–33.

(29) Garcia-Belmonte, G.; Bisquert, J. *Electrochimica Acta* **2002**, *47*, 4263-4272.

(30) Bélanger, D.; Ren, X.; Davey, J.; Uribe, F.; Gottesfeld, S. *J. Electrochem. Soc.* **2000**, *147*, 2923-2929.

(31) Carlberg, J. C.; Inganäs, O. *J. Electrochem. Soc.* **1997**, *144*, L61-L64.

(32) Anothumakkool, B.; Soni, R.; Bhange, S. N.; Kurungot, S. *Energy Environ. Sci.* **2015**, *8*, 1339-1347.

(33) Soni, R.; Anothumakkool, B.; Kurungot, S. *ChemElectroChem* **2016**, *3*, 1329-1336.

(34) Sonmez, G.; Meng, H.; Wudl, F. *Chem. Mater*. **2003**, *15*, 4923-4929.

(35) Arbizzani, C.; Mastragostino, M.; Meneghello, L.; Paraventi, R. *Adv. Mater.* **1996**, *8*, 331-334.

(36) Kurra, N.; Wang, R.; Alshareef, H. N. *J. Mater. Chem. A* **2015**, *3*, 7368-7374.

(37) Stenger-Smith, J. D.; Lai, W. W.; Irvin, D. J.; Yandek, G. R.; Irvin, J. A. *J. Power Sources* **2012**, 220, 236-242.

(38) Schon, T. B.; DiCarmine, P. M.; Seferos, D. S *Adv. Energy Mater*. **2014**, *4*, 1301509 (1 of 6).

(39) Estrada, L. A.; Liu, D. Y.; Salazar, D. H.; Dyer, A. L.; Reynolds, J. R. *Macromolecules* **2012**, *45*, 8211-8220.

(40) DiCarmine, P. M.; Schon, T. B.; McCormick, T. M.; Klein, P. P.; Seferos, D. S. *J. Phys. Chem. C* **2014**, *118*, 8295-8307.

(41) Yan, H.; Chen, Z.; Zheng, Y.; Newman, C.; Quinn, J. R.; Dötz, F.; Kastler, M.; Facchetti, A. *Nature* **2009**, *457*, 679-686.

(42) Liang, Y.; Chen, Z.; Jing, Y.; Rong, Y.; Facchetti, A.; Yao, Y. *J. Am. Chem. Soc*. **2015**, *137*, 4956-4959.

(43) Zeigler, D. F.; Candelaria, S. L.; Mazzio, K. A.; Martin, T. R.; Uchaker, E.; Suraru, S. L.; Kang, L. J.; Cao, G.; Luscombe, C. K. *Macromolecules* **2015**, *48*, 5196-5203.

(44) Matsidik, R.; Komber, H.; Sommer, M. *ACS Macro Lett*. **2015**, *4*, 1346-1350.

(45) Steyrleuthner, R.; Schubert, M.; Howard, I.; Klaumünzer, B.; Schilling, K.; Chen, Z.; Saalfrank, P.; Laquai, F.; Facchetti, A.; Neher, D. *J. Am. Chem. Soc.* **2012**, *134*, 18303-18317.

(46) Jenekhe, S. A.; Lu, L.; Alam, M. M. *Macromolecules* **2001**, *34*, 7315-7324.

(47) Chen, Z.; Gao, D.; Huang, J.; Mao, Z.; Zhang, W.; Yu, G. *ACS Appl. Mater. Interfaces* **2016**, *8*, 34725-34734.

(48) Durban, M. M.; Kazarinoff, P. D.; Luscombe, C. K. *Macromolecules* **2010**, *43*, 6348-6352.

(49) Zhang, L.; Ding, Q.; Huang, Y.; Gu, H.; Miao, Y. -E.; Liu, T. *ACS Appl. Mater. Interfaces* **2015**, *7*, 22669-22677.

(50) Le, T. -H.; Kim, Y.; Yoon, H. *Polymers* **2017**, *9*, 150 (1-32).

(51) Wang, D. W.; Li, F.; Zhao, J.; Ren, W.; Chen, Z. G.; Tan, J.; Wu, Z. S.; Gentle, I.; Lu, G. Q.; Cheng, H. M. *ACS Nano* **2009**, *3*, 1745-1752.

(52) Hsu, Y. K.; Chen, Y. C.; Lin, Y. G.; Chen, L. C.; Chen, K. H. *J. Power Sources* **2013**, *242*, 718-727.

Chapter 5

Naphthalene Diimide and Perylene Diimide Based Alternate and Random Copolymers for Supercapacitor Electrode Materials

5.1. Introduction

Electrolytes play a very important role in supercapacitor device fabrication.[1] Electrolytes can be either ionic solute (salt) dissolved in solvent or it can be pure salt (ionic liquid). The electrolyte provide ionic conductivity and thereby allows charge collection on electrodes in the supercapacitors, it also contributes to the redox reactions for charge storage (pseudocapacitors). It also participates in the formation of an electrical double-layer in electrical double-layer capacitors (EDLC). Depending on their application, aqueous and organic electrolytes are used for supercapacitors. An aqueous electrolyte shows high capacitance and high ionic conductivity.[2] The most common aqueous electrolyte is H_2SO_4 due to its very high ionic conductivity (0.8 S cm^{-1} for 1 M H_2SO_4 at 25 ^oC).[3-5] In the previous chapter donor-acceptor polymers based on naphthalene diimide as the acceptor and thiophene terminated phenylenevinylene as the donor was investigated in aqueous electrolyte.[6] Some of the limitations of aqueous electrolyte is the small potential window. This issue can be overcome by using organic electrolytes.

The organic electrolyte is alternative of aqueous electrolytes, they have higher potential operating voltage and it shows very high energy density.[7-23] Supercapacitor using liquid electrolytes has the problem of electrolyte leakage and packaging of device with metal casing makes the device quite expensive. To address this problem, gel electrolytes have been introduced recently and researchers are trying to replace liquid electrolytes with gel electrolytes.[24-25] Gou et al. fabricated flexible asymmetric supercapacitor from poly[4,7-bis(3,6-dihexyloxy-thieno[3,2-*b*]thiophen-2-yl)] benzo[*c*][1,2,5]thiadiazole (PBOTT-BTD) as a positive electrode and PEDOT as negative, the device showed electrochromic properties which changed color with the amount of charge stored.[26] The donor-acceptor polymers demonstrated till now suffer from high equivalent series resistance, low capacitance and low energy density. A great deal of improvement in the performance of donor-acceptor polymers is needed to use them in commercial devices. In 2014, Seferos et al. had studied different types of donor-acceptor polymers for charge storage; they also studied the effect of position of acceptor molecules on the polymer chain on the polymer conjugation and charge storage in organic electrolyte 0.1 M tetrabutylammonium hexafluorophosphate ($TBAPF_6$).[27] They observed an improvement in the charge storage for the alternate arrangement of donor and acceptor moieties caused by the enhanced delocalization in the polymer backbone.

A very few reports are available at present for the n-type or electron transporting π-conjugated polymers or donor-acceptor type polymers for supercapacitor application. Zeigler

et al. has demonstrated capacitive properties of n-type TPA-3Th-NDI polymer; in this work, they fabricated an asymmetric supercapacitor with n-type polymer as a negative electrode.[28] However, high charge-transfer resistance severely impacted its performance, delivering a capacitance of only 22 F g^{-1}.

Considering all above mentioned factors in this chapter, reported the synthesis of four different polymers with NDI and PDI as acceptor moiety and bidithiazole (BDT) as donor units. Polymers with alternate and random arrangement of donor and acceptor units were tested for charge storage in Propylene carbonate-lithium perchlorate (PC-$LiClO_4$) electrolyte and their flexible supercapacitor device were fabricated. All copolymers structural and electrochemical properties were investigated.

5.2. Experimental Section

5.2.1 Materials

1,4,5,8-Naphthalenetetracarboxylicdianhydride (NTCDA), 3,4,9,10- perylene tetracarboxylicdianhydride (PTCDA), 2-octyldodecanol, 3-thiophene carboxylic acid 97 %, 2-ethylhexylamine, bis(triphenylphosphine) palladium (II) dichloride ($Pd(Ph_3)_2Cl_2$) were purchased from Sigma Aldrich and used without further purification. 2-(tributylstannyl) thiophene-98 % was purchased from Lumtech and used without further purification.

5.2.2 Measurements

^1H NMR spectra were recorded using 200 and 400 MHz Brucker NMR spectrophotometer in $CDCl_3$ containing a small quantity of TMS as an internal standard. The molecular weights of polymers were determined using gel permeation chromatography (GPC). GPC measurements were carried on a Thermo Quest (TQ) GPC at 25 ^oC using chloroform as the mobile phase. The analysis was carried out at a flow rate of 1 mL/min using a set of five μ-Styragel HT columns (HT-2 to HT-6) and a refractive index (RI) detector. Columns were calibrated with polystyrene standards, and the molecular weights are reported with respect to polystyrene. Absorption spectra were recorded using Perkin Elmer Lambda -35 UV-Vis spectrophotometer. Thermogravimetric analysis (TGA) was performed using a PerkinElmer thermal analyzer STA 6000 model at a heating rate of 10 °C/min in a nitrogen atmosphere.

5.2.3 Sample Preparation

For the UV-Vis absorption studies, thin films were prepared by dissolving the polymer in chloroform (10 mg/mL) and spin coating (600 rpm/60 s) on quartz plates. Solution studies carried out in chloroform and solution was made 0.1 OD (optical density) at peak maximum.

5.2.4. Electrode Fabrication

To fabricate electrode, slurry of polymers with carbon nanotubes in 16.6 wt % was prepared in N-methyl pyrrolidone (NMP) in a concentration of 1 mg cm^{-1}. Carbon nanotubes were added as a conductive additive to improve charge collection and transfer in the polymers. The polymer slurry was then drop coated on the carbon current collector over an area of 1 cm^{-2}. The electrodes were then dried under IR lamp.

5.2.5 Characterization of Supercapacitor Devices

Charge-storage characteristics of the polymers were analyzed through cyclic voltammetry, electrochemical impedance spectroscopy, and galvanostatic charge-discharge. All the electrochemical test were conducted on BioLogic VMP-3 potentiostat-galvanostat.

5.2.6 Synthesis

I) Synthesis of Monomers

1) The synthesis NDI-2OD-Br_2 (1) was detailed in **Chapter 2** in **section 2.2.6.**

2) 2,6-Bis(2-thienyl)naphthalene-1,4,5,8-tetracarboxylic-*N*,*N*'-bis(2-octyldodecyl) diimide TNDIT (2)

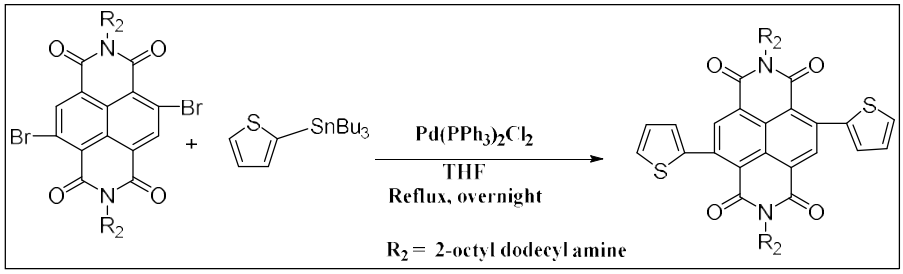

TNDIT was prepared by Stille coupling reaction according to a standard reported protocol. NDI-2OD-Br_2 (1 g, 1.015 mmol), $Pd(PPh_3)_2Cl_2$ (16 mg, 0.022 mmol) and 2-(tributylstannyl)thiophene (0.886 g, 2.37 mmol) was added into a two-neck R.B. flask, equipped with a magnetic stirring bar and a reflux condenser. Anhydrous THF (25 ml) was added by syringe under argon atmosphere. The mixture was refluxed overnight, evaporated to dryness and dissolved in boiling isopropanol. An orange solid, precipitated upon cooling, which was separated by filtration, washed with cold isopropanol, methanol and dried in vacuum at 40 °C. Yield = 0.905 g (90 %). ^{1}H NMR (200 MHz, $CDCl_3$) δ ppm: 8.75 (s, 2H), 7.57-8.54 (dd, 2H), 7.28 (dd, 2H), 7.21-7.19 (dd, 2H), 4.07-4.04 (d, 4H), 1.94 (m, 2H), 1.4-1.15 (m, 64H), 0.87 and 0.86 ppm (m, 12H).

3) 2,6-Bis(2-bromothien-5-yl)naphthalene-1,4,5,8-tetracarboxylic-*N*,*N*'-bis(2-octyldodecyl) diimide Br-TNDIT-Br (3)

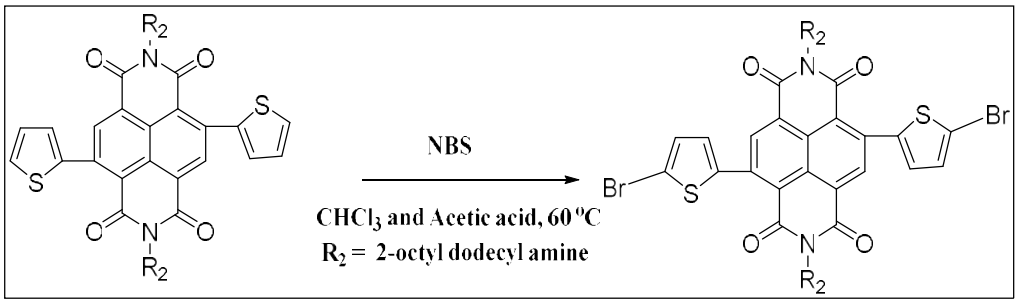

TNDIT (0.80 g, 0.8 mmol) was dissolved in 60 ml of 1:1 mixture of chloroform and acetic acid (v/v). *N*-Bromosuccinimide (0.413 g, 2.41 mmol) was added to the solution and the mixture was stirred at 60 °C and the reaction was monitored with TLC. The chloroform was evaporated under reduced pressure, the precipitated dark red solid was collected by filtration, washed with MeOH and recrystallized from boiling EtOH (~100 ml/g). Yield = 650 mg (81 %). ^{1}H NMR (200 MHz, $CDCl_3$) δ ppm: 8.70 (s, 2H), 7.12 (dd, 2H), 7.08 (dd, 2H), 4.08 (d, 4H), 1.93 (m, 2H), 1.22 (m, 64H), 0.87 and 0.84 ppm (m, 12H).

4) N, N′-Bis(2-octyldodecyl)-2,8-dibromo-3,4,9,10-perylene tetracarboxylicdiimide (PDI-2OD-Br2) (4)

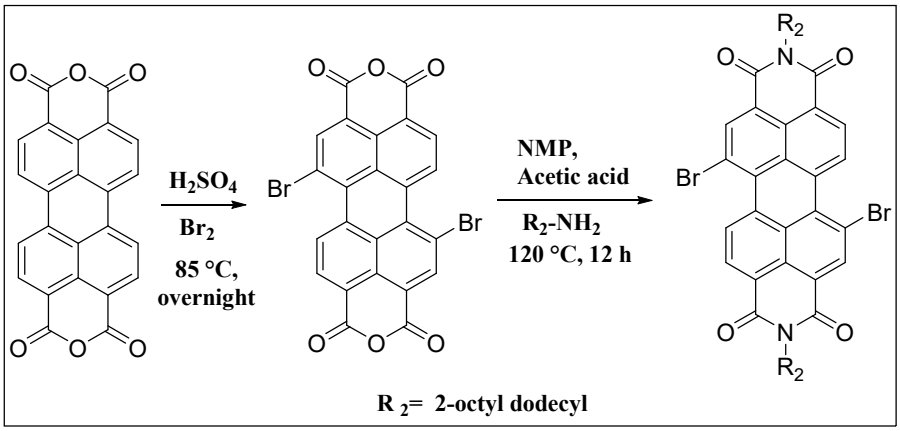

A mixture of PTCDA (31.3 g, 80 mmol) and 270 mL 96 % sulfuric acid was stirred for 12 h at room temperature and subsequently iodine (0.77 g, 3.0 mmol) was added. The reaction mixture was heated up to 85 °C, and bromine (28.2 g, 9.0 mL, 176 mmol) was added dropwise over a period of 1 h. The mixture was heated overnight at 85 °C and then cooled down to room temperature. A stream of air was used to remove the excess bromine. Water (65 mL) was added carefully, and the resulting precipitate was separated by Buchner

filtration, washed with 86 % sulfuric acid (300 g) and a large amounts of water, some acetone (about 50 mL), and dried in vacuum to get the product. Yield = 40 gm (92 %)

Step (ii) a mixture of PTCDA-Br_2 (3.00 g, 5.4 mmol, 1 equiv.) was suspended in the mixture of 60 mL N-methyl pyrrolidine (NMP) and 20 mL glacial acetic acid and purged with argon. The mixture was stirred at 60 °C for 20 minutes to get a homogeneous dispersion which was followed by addition of 2-octyldodecylamine (4.86 g, 16.3 mmol, 3 equiv.). The reaction temperature was raised to 120 °C. After 12 hours, the reaction mixture was cooled down to room temperature and poured into 500 mL of water. The suspension of water was stirred for 2 hours and filtered on Buchner funnel under vacuum. The residue was washed with a large amount of water and dried under vacuum. The crude product was column purified by using pet ether/ethyl acetate (1:6) to get the pure red product. Yield = 3.0 g (40 %). ^{1}H NMR (200 MHz, $CDCl_3$) δ ppm: 9.48-9.44 (d, 2H,), 8.90 (s, 2H), 8.69-8.65 (d, 2H), 4.11(d, 4H), 1.97 (m, 2H), 1.21, (m, 64 H), 0.84 (m, 12H).

5) 2,6-Bis(2-thienyl)perylene-3,4,9,10- tetracarboxylicdiimide-*N*,*N*'-bis(2-octyldodecyl) diimideTPDIT (5)

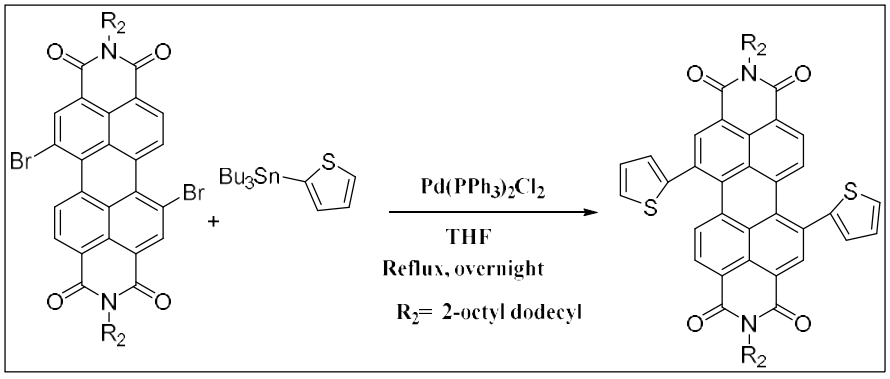

Under argon, a mixture of PDI-2OD-Br2 (1.00 g, 0.89 mmol, 1 equiv.), 2-tributylstannyl-thiophene (1. g, 2.69 mmol, 3 equiv.), and Pd $(PPh_3)_2Cl_2$ (0.031 g, 0.05 equiv.) in anhydrous toluene (25 mL) was refluxed overnight. After cooling down to room temperature, the solvent was removed by rotary evaporator and the reaction residue was purified by column chromatography with a mixture of pet ether:ethyl acetate (40:1 v/v) as eluent, affording a purple solid. The solid was then recrystallized in ethanol to get pure **TPDIT.** Yield = 0.93 g (78 %) . ^{1}H NMR (200 MHz, $CDCl_3$) δ ppm: 8.64 (s, 2H,), 8.25-8.21 (dd, 2H), 8.06 (dd, 2H), 7.48 (dd, 2H), 7.32 (dd, 2H), 7.18 (dd, 2H), 4.11(d, 4H), 1.97 (m, 2H), 1.21, (m, 64 H), 0.84 (m, 12H).

6) 2,6-Bis(2-bromothien-5-yl)perylene-3,4,9,10-tetracarboxylicdiimide -*N*,*N*'-bis(2-octyldodecyl) diimide Br-TPDIT-Br (6)

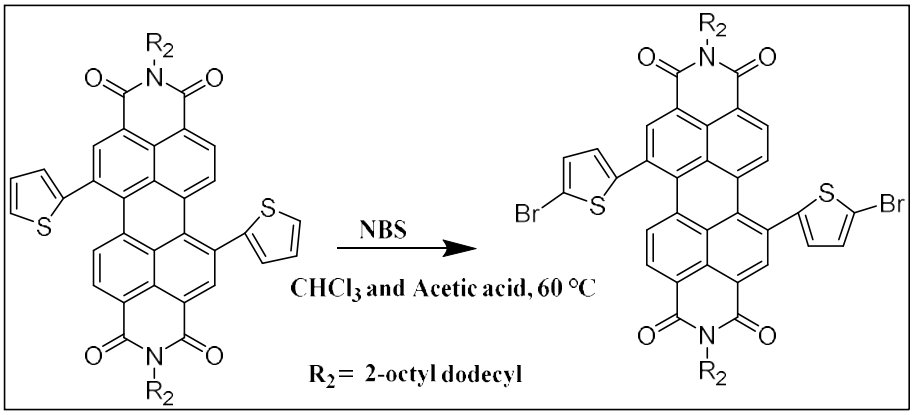

TPDIT (1.4g, 1.2 mmol, 1 equiv.) was dissolved in $CHCl_3$ (30 mL) and acetic acid (30 mL) then NBS (0.67 g, 3.76 g, 3 equiv.) was added. Then the mixture was heated to 60 °C and stirred overnight. Solvent was removed by rotary evaporator; the residue was washed with methanol and purified by column chromatography on silica gel using a mixture of pet Ether: ethyl acetate (40:1 v/v) as eluent, affording pure **Br-TPDIT-Br** as a purple solid as the pure 1,7-isomer. The solid was then recrystallized in ethanol. Yield = 1.2 g (88 %). ^{1}H NMR (200 MHz, $CDCl_3$) δ ppm: 8.59 (s, 2H,), 8.30 (d, 2H), 8.19 (dd, 2H), 7.48 (d, 2H), 7.14 (d, 2H), 7.11 (d, 2H), 4.12(d, 4H), 1.99 (m, 2H), 1.56-1.21, (m, 64 H), 0.83 (m, 12H).

7) N,N-Diethylthiophene-3-carboxamide

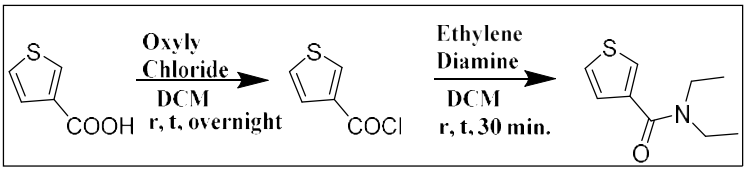

Thiophene-3-carboxylic acid (3.0 g, 23.41 mmol) and 10 mL of DCM were taken in a 50 mL flask. The mixture was cooled ice-water bath, and then oxalyl chloride (5.94 g, 46.8 mmol) was added in one portion. The reactant was stirred overnight at ambient temperature and a clear solution was obtained. After evaporation of the solvent, the product (thiophene-3-carbonyl chloride) was obtained as colorless solid. Yield = 3.42 g (90 %). It was dissolved in DCM and used as such for the next step.

In a 100 mL round bottom flask, cooled using ice bath, diethylamine (3.42 g) and 10 mL of DCM was mixed, and dropwise addition of thiophene-3-carbonyl chloride was done. After all of the solution was added, the ice bath was removed, and the reactant was stirred at ambient temperature for 30 minutes. Then, the reactant was washed with water several times, and the

organic layer was dried over anhydrous sodium sulfate (Na_2SO_4). After removing the solvent, the crude product was purified by distillation under vacuum, and the compound was obtained as pale yellow oil. Yield = 3.5 (91 %). ^{1}H NMR (200 MHz, $CDCl_3$) δ ppm: 7.44 (dd, 2H), 7.30 (dd, 2H), 7.18 (dd, 2H), 3.43 (s, 4H), 1.96 (m, 2H), 1.18 (m, 6H).

8) 4,8-Dihydrobenzo[1,2-b:4,5-b′]dithiophen-4,8-dione

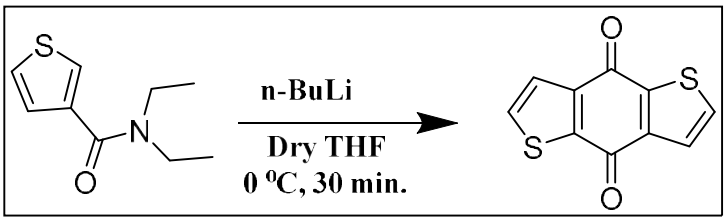

N,N-Diethylthiophene-3-carboxamide (19.1 mmol, 3.5 g) was put into a well dried flask with 20 mL of THF under an inert atmosphere. The solution was cooled by an ice-water bath, and 9.5 mL of n-butyllithium (19.1 mmol, 2.5 mol/L) was added to the flask dropwise within 30 minutes. Then, 100 g of ice water was added and stirred for 5 to 6 hours. The mixture was filtrated through Buchner funnel, and the yellow precipitate was washed with 200 mL of water, 50 mL of methanol, and 50 mL of hexane successively. Yield = 1.5 g (71 %). ^{1}H NMR (200 MHz, $CDCl_3$) δ ppm: 7.66 (dd, 2H), 7.44 (dd, 2H).

10) 2-(2-Ethyl-hexyl)thiophene

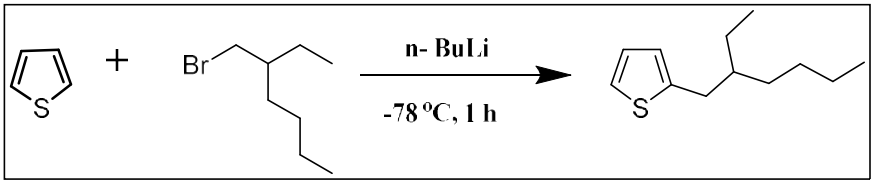

Thiophene (5.00 g, 59.43 mmol) was dissolved in 100 mL of THF under nitrogen atmosphere. The solution was cooled down to -78 °C and 26.0 mL of n-butyllithium (62.4 mmol, 2.4 M) was added dropwise. After stirring at -78 °C for 1 h, 12.05 ml of 2-ethylhexyl bromide (62.4 mmol) was added. The mixture was stirred at -78 °C for another 1 h and warmed up to room temperature overnight. 20 mL of cold water was added to quench the mixture, which was then extracted by diethyl ether three times. The organic layer was dried over anhydrous sodium sulfate (Na_2SO_4). After removing solvent, the residue was purified by vacuum distillation to yield the 2-(2-ethyl-hexyl)thiophene as a colorless oil. Yield = 10.0 g (86%). ^{1}H NMR (200 MHz, $CDCl_3$) δ ppm: 7.77 (dd, 2H), 7.51 (dd, 2H), 7.08 (dd, 2H), 4.21 (s, 4H), 1. 69 (m, 2H), 1.33 (m, 8H), 0.89 (m, 6H).

11) 4,8-Bis(5-(2-ethylhexyl)thiophene-2-yl)benzo[1,2-*b*:4,5-*b'*]dithiophene (7)

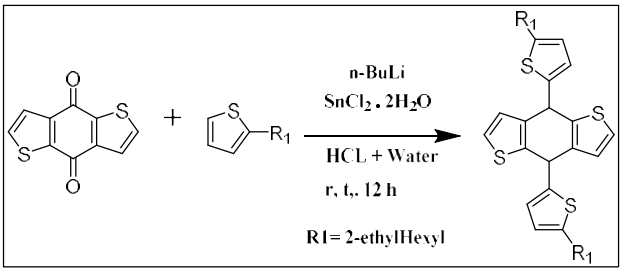

7.3 mL of n-butyllithium (18.16 mmol, 2.5 M) was added dropwise to the solution of 2-(2-ethyl-hexyl)thiophene (3.57 g, 18.16 mmol) in 50 mL of anhydrous THF at -30°C under nitrogen atmosphere. The mixture was heated up to 50 °C for 2 h. Then the mixture was cooled in an ice-water bath. Subsequently, 4,8-dihydrobenzo[1,2-b:4,5-b′]dithiophen-4,8-dione (1.00 g, 4.54 mmol) was added, and the mixture was heated at 50 °C for another 2 h. After cooling the mixture down to room temperature, a mixture of $SnCl_2 \cdot 2H_2O$ (8.20 g, 36.32 mmol) in 20 mL of dilute HCl (10 %) was added, and the mixture was stirred for 12 h. The reaction mixture was washed with water followed by brine solution, dried with sodium sulfate (Na_2SO_4), filtered and concentrated via rotary evaporation. Further purification was carried out by silica gel column chromatography eluting with pet ether to obtain pure compound 4,8-bis(5-(2-ethylhexyl)thiophene-2-yl)benzo[1,2-b:4,5-b']dithiophene as a yellow oil. Yield = 2.0 g (76 %) ^{1}H NMR (200 MHz, $CDCl_3$) δ ppm: 7.66-762 (dd, 2H), 7.46-7.43 (dd, 2H), 7.29-7.28 (dd, 2H), 6.88-6.87 (dd, 2H), 2.87-2.84 (d, 4H), 1.68 (m, 2H), 1.33 (m, 16H), 0.94 (m, 12H).

12) 2,6-Bis(trimethyltin)-4,8-bis(5-(2-ethylhexyl)thiophene-2-yl)benzo[1,2-*b*:4,5-*b'*]dithiophene (8)

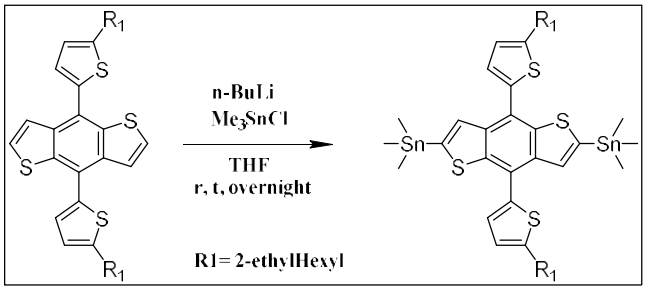

4,8-Bis(5-(2-ethylhexyl)thiophene-2-yl)benzo[1,2-b:4,5-b']dithiophene (1.00 g, 1.73 mmol) and 50 mL of THF were added into a two neck round bottom flask under nitrogen atmosphere. The solution was cooled to 0 °C, and 1.72 mL of n-butyllithium (4.31 mmol, 2.5 M) was added dropwise. The reaction mixture was stirred for 2 h at room temperature,

followed by cooling to 0 °C and addition of trimethyltin chloride (4.31 mmol, 4.31 ml, 1.0 M in hexane) in one portion. The mixture was stirred at room temperature overnight. The mixture was quenched by addition of 20 mL of water and extracted with diethyl ether. The combined organic phase was dried with sodium sulfate Na_2SO4, filtered, concentrated via evaporation. The residue was recrystallized by isopropanol to obtain pure compound as pale yellow solid. Yield = 0.80 g (51 %). ^{1}H NMR (200 MHz, $CDCl_3$) δ ppm: 7.68 (d, 2H), 7.32 (d, 2H), 6.89 (s, 2H), 2.86 (s, 4H), 1. 72 (m, 2H), 1.36 (m, 16H), 0.95 (m, 12H), 0.39 (18H).

13) Synthesis of 2,6-dibromo4,8-bis(5-(2-ethylhexyl)thiophene-2-yl)benzo[1,2-*b*:4,5-*b'*]dithiophene (BDT-Br) (9)

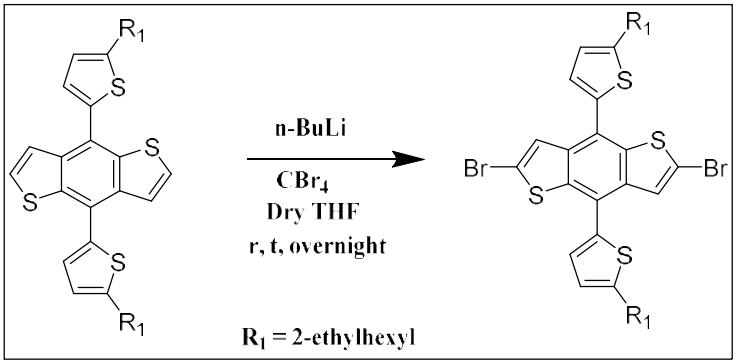

4,8-Bis(5-(2-ethylhexyl)thiophene-2-yl)benzo[1,2-b:4, 5-b']dithiophene (0.6 g, 1.03 mmol) was dissolved in dry THF and cooled down to -78 ^{o}C followed by the dropwise addition of n-BuLi (0.116 g, 2.58 mmol). The reaction mixture was stirred at -78 ^{o}C for 1 hour and warmed to 25 ^{o}C, then the solution was again cooled to -78 ^{o}C and tetra bromomethane (0.806 g, 2.59 mmol) in THF was added. The mixture was slowly brought to 25 ^{o}C and stirred for 12 hours. After completion of reaction the crude product was washed with water and extracted in ethyl acetate. Purification was done by recrystallization from isopropanol to get pure BDT-Br. Yield = 0.50 g (66 %). ^{1}H NMR (200 MHz, $CDCl_3$) δ ppm: 7.57 (s, 2H), 7.21-7.19 (d, 2H), 6.87-6.85 (d, 2H), 2.82 (d, 4H), 1.72 (m, 2H), 1.36 (m, 16H), 0.90 (m, 12H).

II) Synthesis of Polymer

a) Poly{[2,6-Bis(2-thienyl)naphthalene-1,4,5,8-tetracarboxylic-N,N'-bis(2-octyldodecyl) diimide(TNDIT]-alt-4,8-Bis(5-(2-ethylhexyl)thiophene-2-yl)benzo[1,2-b:4,5-b']dithiophene)}, P(NDI-alt-BDT)

Br-TNDIT-Br (0.381 g, 0.33 mmol) and 2,6-bis(trimethyltin)-4,8-bis(5-(2-ethylhexyl)thiophene-2-yl)benzo[1,2-b:4,5-b']dithiophene (0.300 g, 0.33 mmol) were taken

in Schlenk tube under nitrogen atmosphere. Dry toluene (15 mL) was added to the tube and purged with nitrogen for half an hour. Bis(triphenylphosphine) palladium (II) dichloride ($Pd(Ph_3)_2Cl_2$) (31 mg, 0.0211 mmol) was added to the tube quickly by opening rubber septa, and the whole mixture was degassed by nitrogen. The reaction mixture was stirred at 110 ^oC for 48 hours. Bromobenzene (0.2 mL) was then added, and the reaction mixture was further stirred at 110 ^oC for 12 hours. Upon cooling to room temperature, a solution of potassium fluoride (1g) in 2 mL water was added and stirred for 2 hours. The reaction mixture was extracted with chloroform (150 mL x 3). The organic layer was washed with water, dried over anhydrous sodium sulfate and concentrated on a rotary evaporator. The obtained residue was dried in a vacuum oven and subjected to Soxhlet extraction with methanol (24 hours) then acetone (48 hours) followed by hexane (24hours) and chloroform (12 hours). Half of the chloroform solution was evaporated on rotary evaporator, and the concentrated polymer solution was precipitated in 500 mL methanol, stirred for 2 hours, filtered on Buchner funnel, washed with methanol and dried in vacuum. The polymer was obtained as a solid, Yield = 465 mg (80 %). ^1H NMR (400 MHz, $CDCl_3$) δ ppm: 8.80 (br, 2H), 7.76 (br, 2H), 7.32 (br, 4H), 6.94 (br, 4H), 4.09 (br, 4H), 2.90 (br, 4H), 1.96 (br, 2H), 1.31-1.21 (br, 124H), 0.82 (br, 24H).

All the alternate and random copolymers were synthesized using the same procedure as that given for P(NDI-alt-BDT) but with different molar ratio of monomers.

b) Poly{[2,6-Bis(2-thienyl)perylene-3,4,9,10- tetracarboxylicdiimide-*N*,*N*'-bis(2-octyldodecyl) diimide(TPDIT]-alt-4,8-Bis(5-(2-ethylhexyl)thiophen-2-yl)benzo[1,2-b:4,5-b']dithiophene)}, P(PDI-alt-BDT)

P(PDI-alt-BDT) was prepared using 2,6-bis(2-bromothien-5-yl)perylene-3,4,9,10-tetracarboxylicdiimide -N,N'-bis(2-octyldodecyl) diimide Br-TPDIT-Br (422 mg, 0.33 mmol), 2,6-bis(trimethyltin)-4,8-bis(5-(2-ethylhexyl)thiophen-2-yl)benzo[1,2-b:4,5-b']dithiophene (0.300 g, 0.33 mmol) and bis(triphenylphosphine) palladium (II) dichloride ($Pd(Ph_3)_2Cl_2$) (31 mg, 0.0211 mmol). Yield = 410 mg (73 %). ^1H NMR (400 MHz, $CDCl_3$) δ ppm: 8.88 (br, 2H), 8.34 (br, 4H), 7.70-6.93 (br, 10H), 4.10 (br, 4H), 2.86 (br, 4H), 1.98 (br, 4H), 1.55-1.20 (br, 124H), 0.82 (br, 24 H).

c) Poly{([N N' -bis(2-octyldodecyl)-naphthalene-1,4,5,8- bis-(dicarboximide)-2,6-diyl]]-ran-2,5-thiophene-ran-4,8-Bis(5-(2-ethylhexyl)thiophen-2-yl)benzo[1,2-b:4,5-b']dithiophene) P(NDI-r-BDT)

P(NDI-r-BDT) was prepared using NDI-2OD-Br_2 (201 mg, 0.2 mmol), 2,5-bis (trimethylstannyl) thiophene (168.1 mg, 0.40 mmol), BDT-Br_2 (150 mg, 0.2 mmol) and bis(triphenylphosphine) palladium (II) dichloride ($Pd(Ph_3)_2Cl_2$) (31 mg, 0.0211 mmol). Yield = 310 mg (82 %). ^{1}H NMR (400 MHz, $CDCl_3$) δ ppm: 8.93-8.81 (br , 2H), 7.75 (br, 2H), 7.43-7.32 (br, 4H), 6.94 (br, 4H), 4.12 (br, 4H), 2.90 (br, 4H), 1.98 (br, 2H), 1.78(br, 2H), 1.31-1.21 (br, 124H), 0.82 (br, 24 H).

d) Poly{(N,N′-Bis(2-octyldodecyl)-3,4,9,10-perylene tetracarboxylicdiimide-ran-2,5-thiophene-ran-4,8-Bis(5-(2-ethylhexyl)thiophen-2-yl)benzo[1,2-b:4,5-b']dithiophene) P(PDI-r-BDT)

P(PDI-r-BDT) was prepared using PDI-2OD-Br_2 (226 mg, 0.2 mmol), 2,5-bis(trimethylstannyl) thiophene (168.1 mg, 0.40 mmol) , BDT-Br_2 (150 mg, 0.2 mmol) and bis(triphenylphosphine) palladium (II) dichloride ($Pd(Ph_3)_2Cl_2$) (31 mg, 0.0211 mmol). Yield = 280 mg (58 %). ^{1}H NMR (400 MHz, $CDCl_3$) δ ppm: 8.89 (br, 2H), 8.32 (br, 4H), 7.68-6.93 (br, 10H), 4.10 (br, 4H), 2.86-2.58 (br, 4H), 1.98 (br, 4H), 1.68 (br, 2H) 1.55-1.20 (br, 124H), 0.82 (br ,24 H).

5.3 Results and Discussion

5.3.1 Synthesis and Characterization

Novel random and alternate copolymers were designed and synthesized where naphthalene and perylene diimide based moieties were used as acceptor and BDT and Thiophene units were used as donor unit. Naphthalene and perylene diimide are well-known acceptor units because of their electron defficient nature, while BDT exhibited a large planar conjugated structure and small steric hindrance between the adjacent repeating units. All the monomers were synthesized following by previously reported literature procedures detailed synthetic procedure and characterization, is given in the experimental section.[29-32] All the alternate and random copolymers were polymerized via stille polycondensation in the presence of catalyst $Pd(PPh_3)_2Cl_2$ and toluene as solvent 2-bromothiophene and 2-trimethyl stannane thiophene were used as end-capping agents. **Scheme 5.1** and **Scheme 5.2** show the synthetic steps of polymerization. **Scheme 5.1** shows the synthesis of alternate copolymers where thiophene terminated naphthalene (**3**) or perylene diimide (**6**), and BDTT (**8**) monomers were used. In

Scheme 5.2 three different monomers were used for random copolymerization where 1 equivalent of thiophene monomer was used and 0.5 equivalent of naphthalene (1) or perylene diimide (4) were taken and 0.5 equivalents of BDT (9) monomers were used to maintain the same stoichiometry as an alternate copolymer.

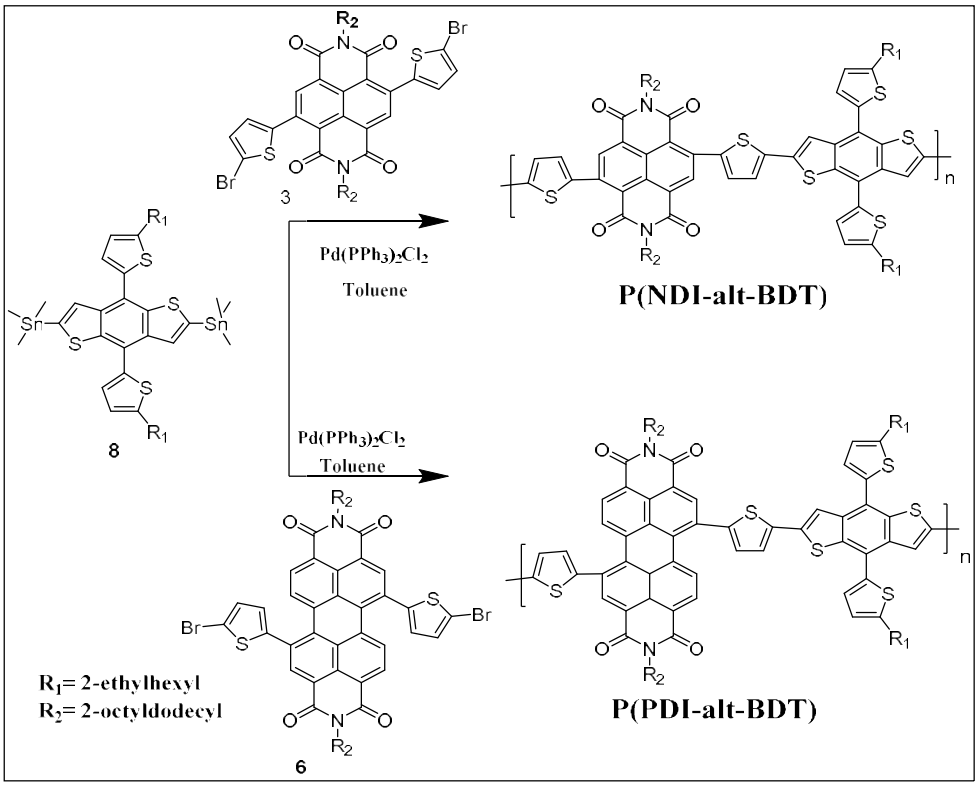

Scheme 5.1: Synthesis of alternate copolymers P(NDI-alt-BDT) and P(PDI-alt-BDT).

Table 5.1. Molecular weight, Electrochemical and Optical band gaps and thermal characterization of the copolymers.

Polymer	Mw[a] (KDa)	Đ[b]	E_g^{opt}(eV)	LUMO(eV)	HOMO(eV)	T_d[c] (^oC)
P(NDI-alt-BDT)	31.9	2.6	1.45	-4.15	-5.60	445
P(NDI-r-BDT)	41.6	2.7	1.41	-4.05	-5.46	435
P(PDI-alt-BDT)	31.2	3.2	1.51	-4.13	-5.64	447
P(PDI-r-BDT)	21.1	2.3	1.53	-4.17	-5.70	450

[a] Weight-average molecular weight (M*w*). [b] Polydispersity index (Đ). [c] The decomposition temperature (5% weight loss) estimated using TGA under N_2.

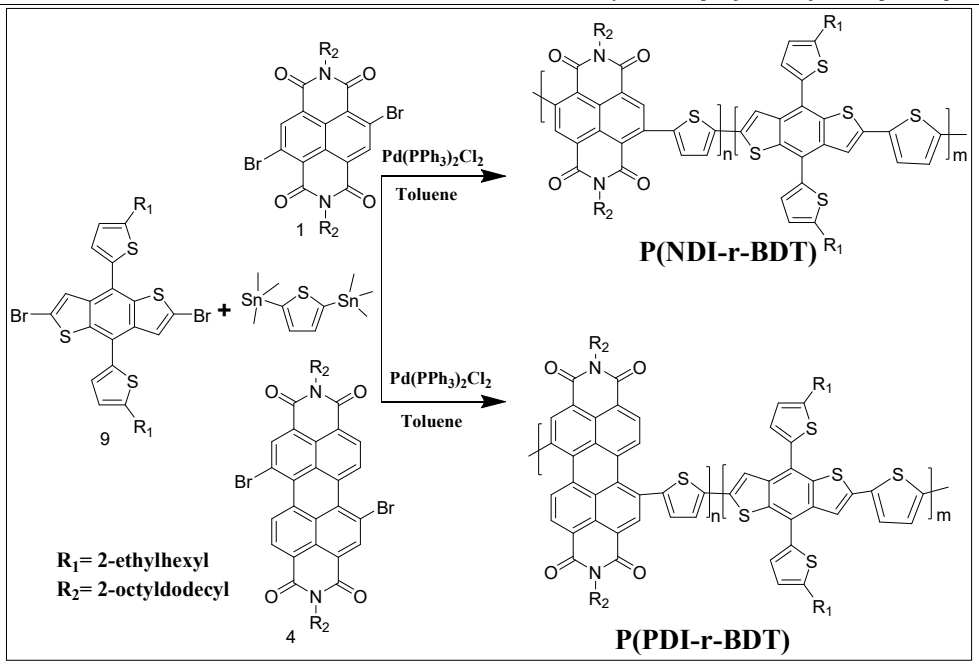

Scheme 5.2: Synthesis of random copolymers P(NDI-r-BDT) and P(PDI-r-BDT).

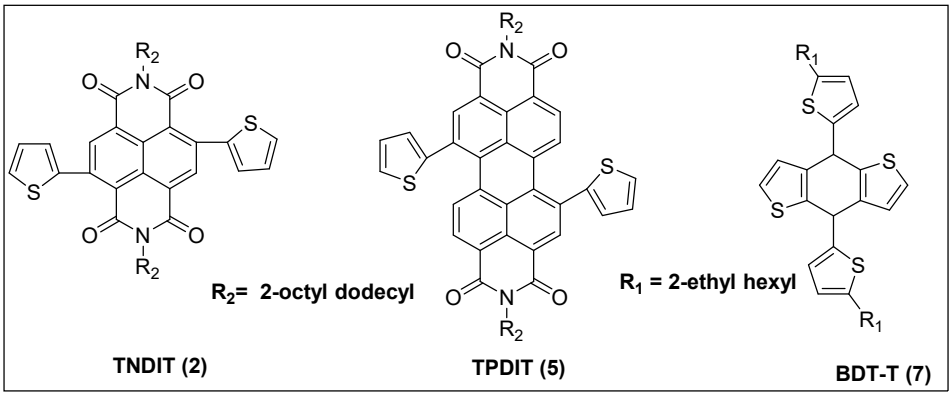

Scheme 5.3: Structure of model compounds.

For a better understanding of the polymer properties model compounds representing the donor and acceptor fragments TNDIT (2), TPDIT (5) and BDT-T (7) were also prepared. The structure of the model compounds are shown in **Scheme 5.3**.

All polymers were purified via Soxhlet extraction with methanol and acetone and precipitated. The structure of monomers and polymers were characterized by proton NMR spectroscopy. NMR spectra of the polymers are shown in **Figure 5.1-5.4.** The polymers were sparingly soluble in common organic solvents like DCM, chloroform and chlorobenzene. The molecular weight and polydispersity (Đ) was measured by gel permeation chromatography (GPC) at 25 ^{0}C with chloroform as solvent and polystyrene as standard. Characteristics of

polymers are shown in **Table 5.1**. All polymers exhibited M_w (Weight-average molecular weight) in the range of 21.1 to 41.6 KDa, and polydispersity (Đ) in the range of 2.3 to 3.2.

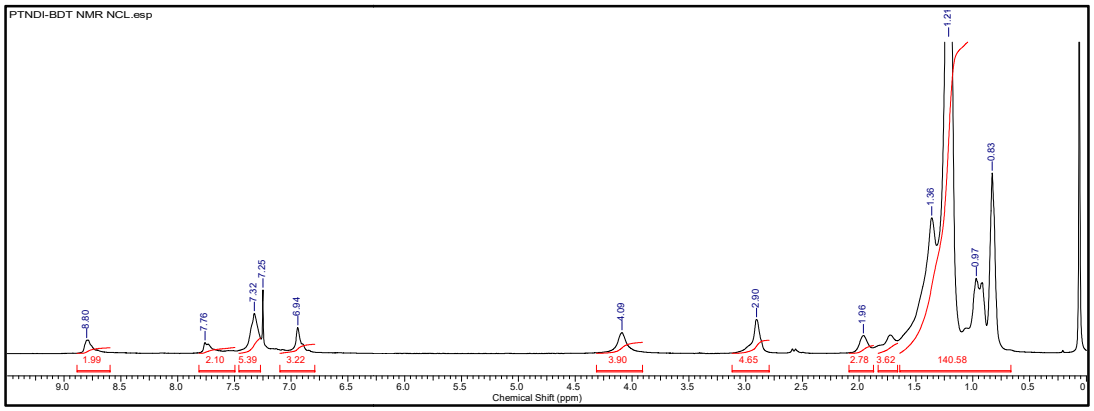

Figure 5.1. ^{1}H NMR spectrum of polymer P(NDI-alt-BDT) recorded in $CDCl_3$.

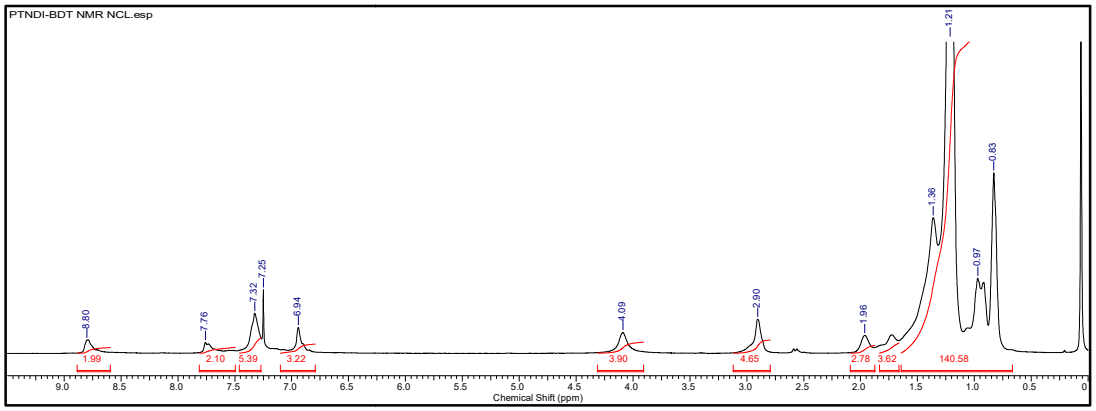

Figure 5.2. ^{1}H NMR spectrum of polymer P(PDI-alt-BDT) recorded in $CDCl_3$.

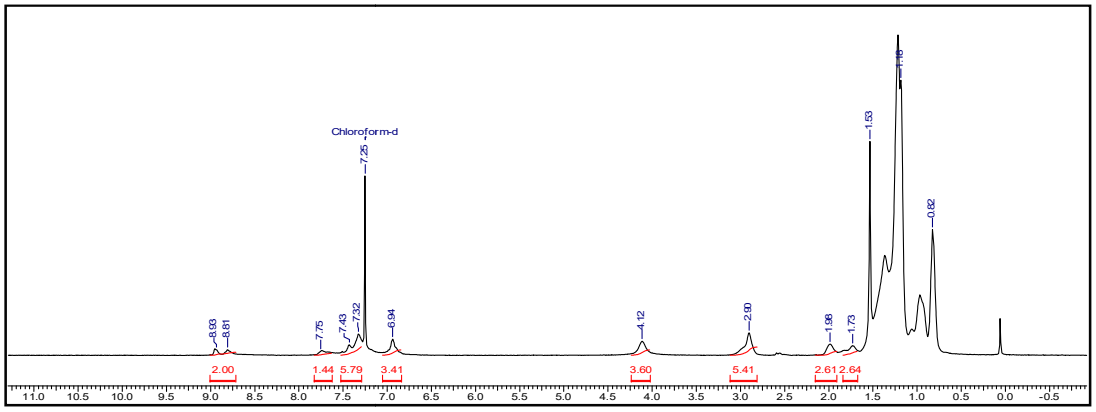

Figure 5.3. ^{1}H NMR spectrum of polymer P(NDI-r-BDT) recorded in $CDCl_3$.

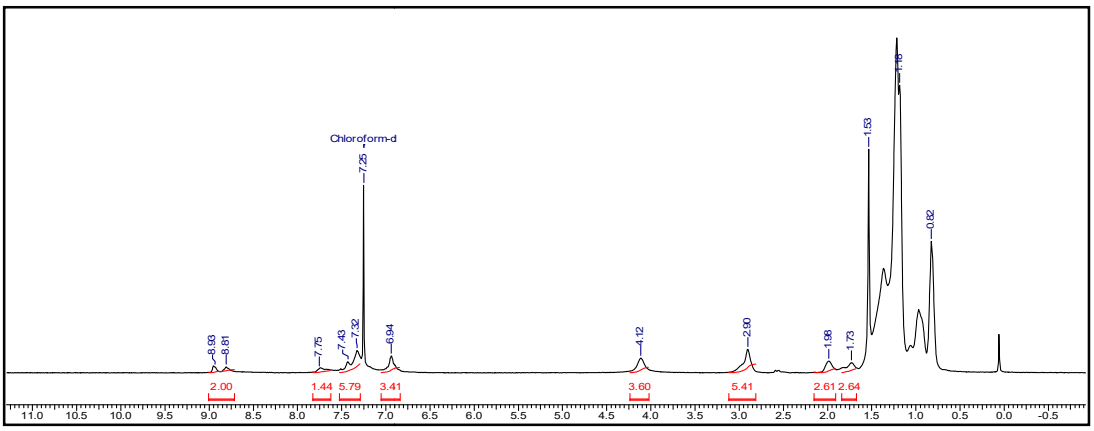

Figure 5.4. ^{1}H NMR spectrum of polymer P(PDI-r-BDT) recorded in $CDCl_3$.

Thermal characterization of the copolymers was carried out by thermogravimetric analysis (TGA) as well as differential scanning calorimetry (DSC) measurement under nitrogen atmosphere. TGA curves (**Figure 5.5**) showed good thermal stability for the polymers with onset decomposition temperature (T_d) more than 400 °C (values enlisted in **Table 5.1**). The DSC thermograms were recorded by heating the polymers from 0 °C to 350 °C at 10 ^oC /min under N_2 atmosphere. **Figure 5.6** shows the DSC thermograms of all the copolymers. No transitions were observed for most of the polymers, which indicated their amorphous nature.

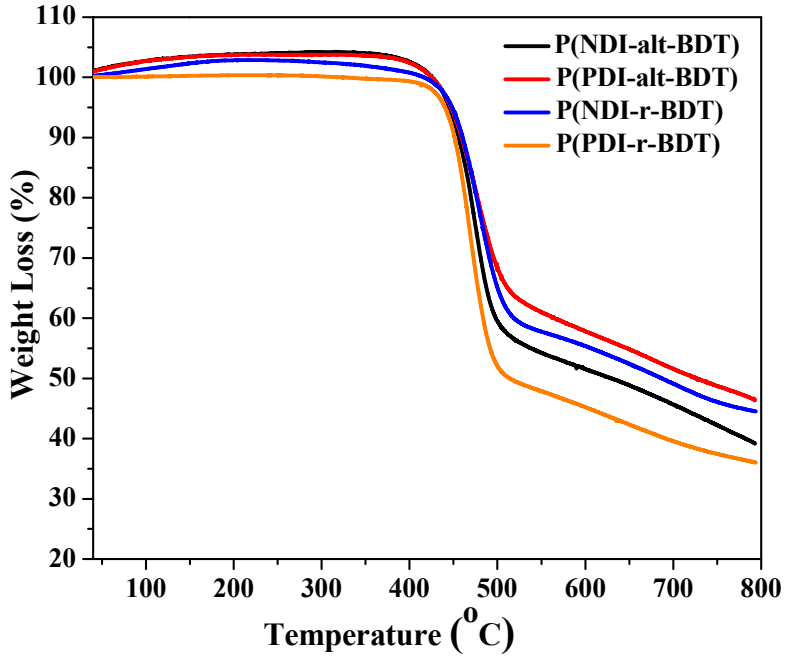

Figure 5.5: TGA of polymers run from 40 to 800 °C with a heating rate of 10 °C/min under nitrogen.

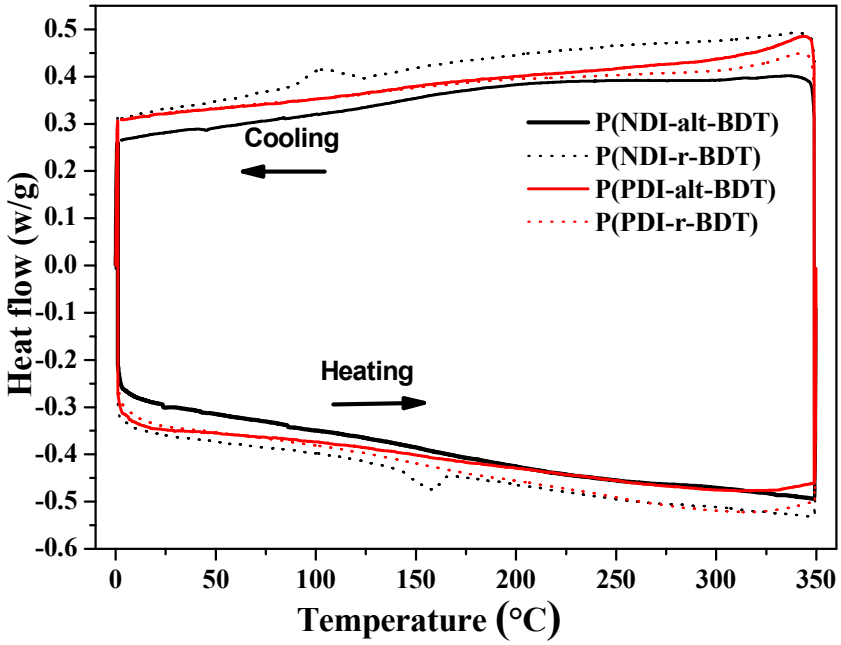

Figure 5.6: DSC thermograms of copolymers at a heating rate of 10 °C/min under nitrogen atmosphere.

5.3.2 Optical Properties and Energy Level of Polymers

Absorption spectra of the donor-acceptor alternate copolymers of both NDI and PDI were compared with that of a 1:1 physical mixture of the respective donor and acceptor fragments in order to understand the nature of the different absorption bands. **Figure 5.7** compares the absorption spectra of the donor and acceptor model compounds (structure shown in **Scheme 5.3**) and their 1:1 mixtures recorded in chloroform. NDI model compound TNDIT (2) showed two absorption bands. The first band observed between 350 nm to 400 nm corresponded to the π-π* transition of NDI core and thiophene, while the second band observed between 415 and 565 nm was attributed to intra molecular charge transfer (ICT) band.[33] BDT-T (7) (donor) model compound showed a single absorption band between 315 to 415 nm which crousponded to π-π* transition of the BDT core. The 1:1 mixture of the two model compounds (TNDIT and BDT-T) exhibited absorption bands, which was the sum of their individual absorption bands. The perylene based model compound TPDIT (5) showed absorption band in the high energy region (370 nm) corresponding to the π-π* transition of PDI core and thiophene.[34] TPDIT exhibited several peaks in the region from 400 to 650 nm of which those in the range 400 to 540 nm corresponded to typical perylene core transitions and broad shoulder beyond 550 nm was assigned to the ICT band. Compared to the TNDIT

model compound the peaks of TPDIT were red-shifted due to extended conjugation in the latter. The **Figure 5.7b** also compares the absorption spectra of 1:1 mixture of BDT-T and TPDIT, which like its lower analogue represented a sum of the corresponding absorption bands. The **Figure 5.7** also compares the absorption spectra of alternate copolymers of donor and acceptor fragments namely P(NDI-alt-BDT) and P(PDI-alt-BDT). A clear difference could be seen in the absorption spectra of the alternate copolymers compared to the respective 1:1 donor-acceptor model compound mixture. A clear redshift of the ICT band and overall broadening of all bands were observed as shown in **Figure 5.7**, signifying increased conjugation in the polymer.

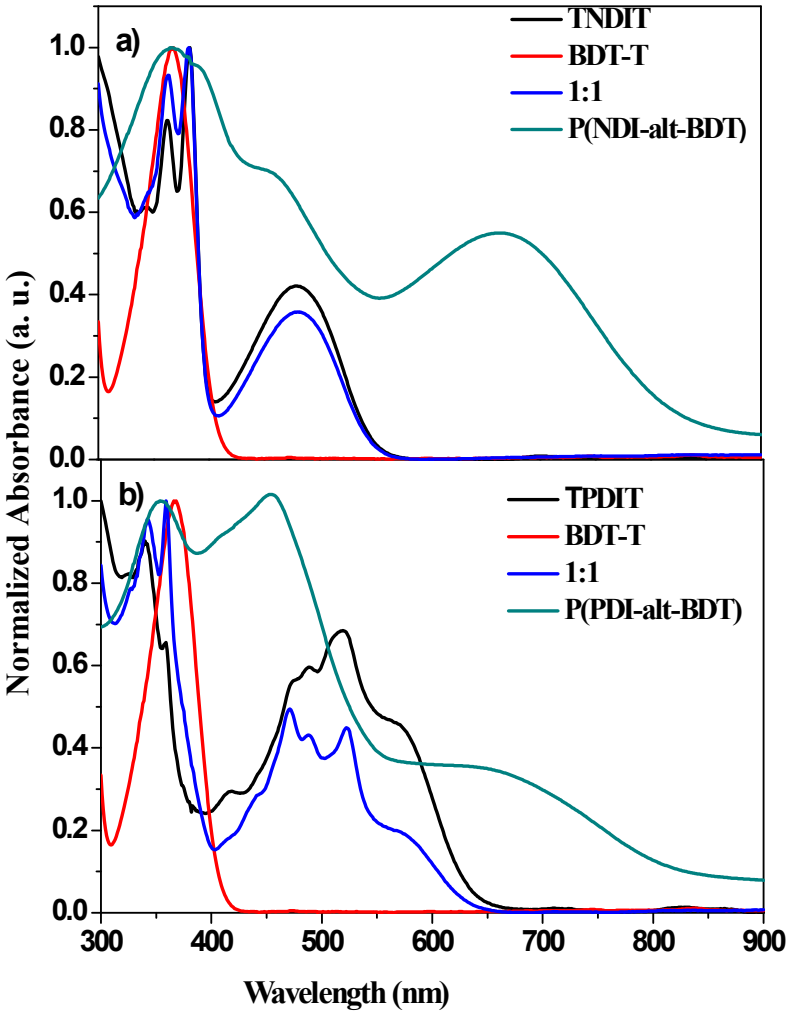

Figure 5.7. Normalized absorption spectra of model compound and 1:1 mixtures and alternate copolymers.

Alternate copolymers P(NDI-alt-BDT) and P(PDI-alt-BDT) both in chloroform solution and thin film showed similar characteristic absorption bands as shown in **Figure 5.8**. Absorption spectra of the film showed more red shift compared to the solution which is a very common phenomenon arising from the more ordered molecular organization in the film relative to the solution.

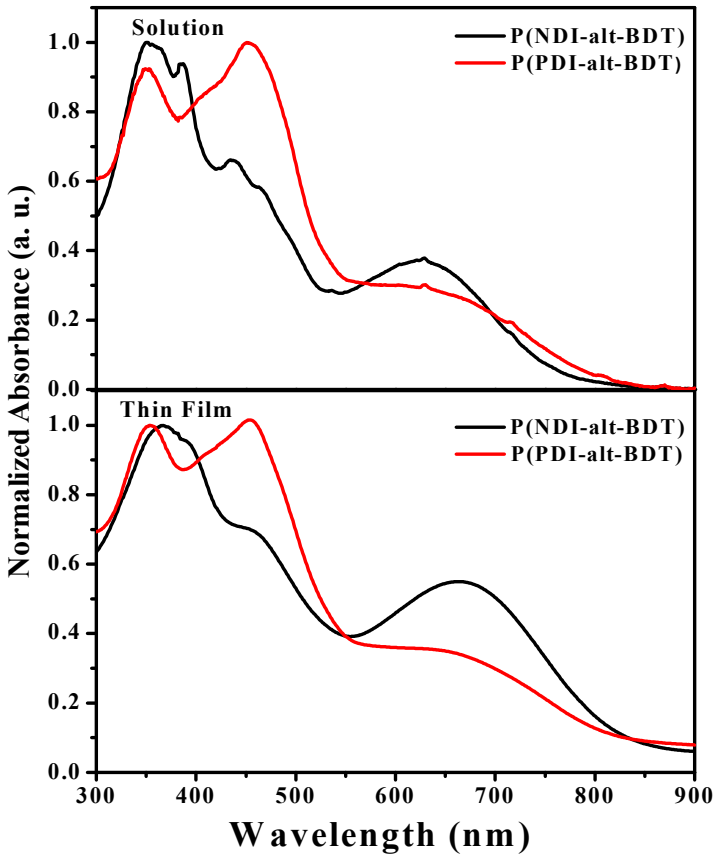

Figure 5.8. Normalized absorption spectra of alternate copolymers in solution and thin films.

Figure 5.9 shows the thin absorption spectra of the alternate as well as random copolymers. It could be seen from the figure that in P(NDI-r-BDT) copolymer the second absorption band was more red-shifted compared to its alternate analogue P(NDI-alt-BDT). The band was shifted from 460 nm in the alternate copolymer to 500 nm in the random copolymer. This red shift in the second absorption band could reflect inhomogeniety in the incorporation of donor and acceptor units. Infact an indication of this was reflected in the proton NMR spectra (See **Figure 5.3**) of the P(NDI-r-BDT) copolymer. It showed two distinct peaks for the NDI aromatic core protons. In the alternate copolymer P(NDI-alt-BDT) there was regular alteration of NDI and BDT units and the two aromatic protons of NDI appeared at 8.81 ppm.

On the other hand, in the random copolymer an additional peak was observed at 8.93 ppm which could correspond to NDI units bridged with thiophene moieties.[36] Only the random copolymer design had the probability of continued arrangement of NDI and thiophene units along segments of the polymer chain without incorporation of BDT units. The chemical shifts of the NDI aromatic protons in such segment along the chain backbone would be slightly different from that of an NDI unit which had thiophene bridged BDT as neighbors.

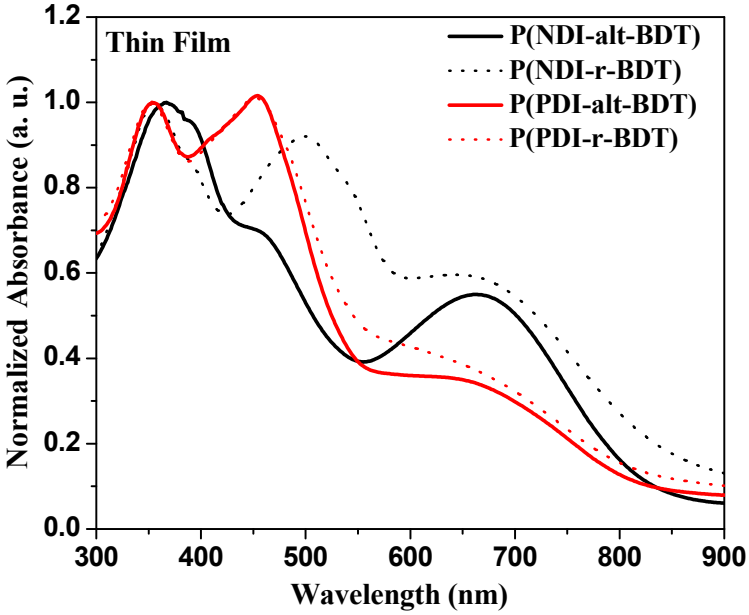

Figure 5.9. Normalized absorption spectra of thin films of all copolymers.

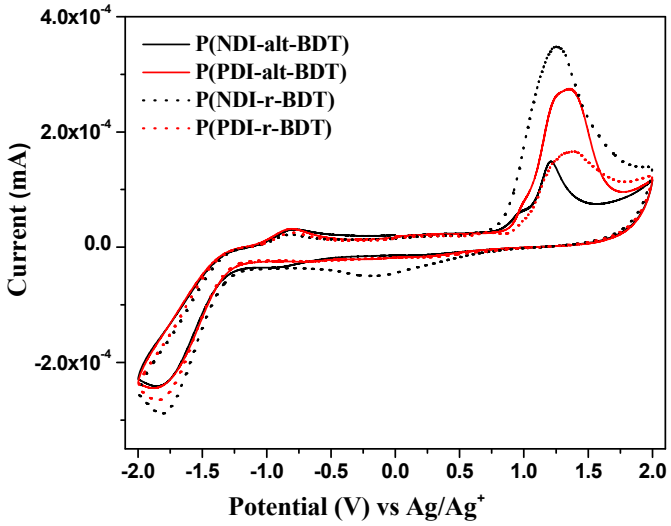

Figure 5.10: Cyclic voltammograms of Copolymers as thin film in 0.1 M $(n\text{-}Bu)_4NPF_6$ – acetonitrile solution

The optical band gap (E_g^{opt}) of the copolymers was calculated from lower energy absorption band edge of thin-film and is listed in **Table 5.1**. Generally NDI based polymer used to show a low optical band gap compared to PDI based copolymers.[37-38] The optical band gap of NDI based copolymers were 1.45 eV and 1.41 eV for P(NDI-alt-BDT) and P(NDI-r-BDT) respectively, while for PDI based polymer, the band gap was higher at 1.51 eV and 1.53 eV for P(PDI-alt-BDT) and P(PDI-r-BDT) respectively. Electronic energy levels of the new copolymers were measured by cyclic voltammetry. Thin-films of polymer were drop casted on platinum working electrode for recording the CV.

The measurement was done in acetonitrile solvent with ferrocene/ferrocenium as an internal standard and tetrabutylammonium hexafluorophosphate (*n*-Bu4NPF_6 0.1M/ acetonitrile) as supporting electrolyte. Cyclic voltammograms for copolymers are shown in **Figure 5.10.** All polymers were showing the oxidation as well as reduction peaks. The oxidation peaks were irreversible indicating n-type behavior of polymers.[35] Generally, most of the NDI and PDI based copolymers show two reduction peaks.[37-40] Two quasi reversible reduction peaks were observed for all copolymers. The lowest occupied molecular orbital (LUMO) energy levels were calculated based on the onset value of first reduction peak and reference energy level of ferrocene (4.8 eV below the vacuum level) according to E_{LUMO} (eV) = $-e \times (E^{red}$ onset + 4.8) below the vacuum level.[41-42] The highest occupied molecular orbital (HOMO) levels were estimated based on LUMO values and the optical band gap obtained from the absorption onset measurements.[42] All copolymers showed a LUMO level in the range from -4.05 eV to -4.17 eV where as HOMO energy level in the range from 5.46 eV to 5.70 eV. The values of HOMO and LUMO are listed in **Table 1**.

5.3.3 Electron Microscopy Analysis of Polymers

Morphology of the polymers was observed by scanning electron microscopy; the corresponding images are given in **Figure 5.11**. The polymers showed similar morphology consisting of thick agglomerated fiber-like porous structures. Presence of porosity is beneficial for the electrochemical application since it allows for the penetration of electrolyte.

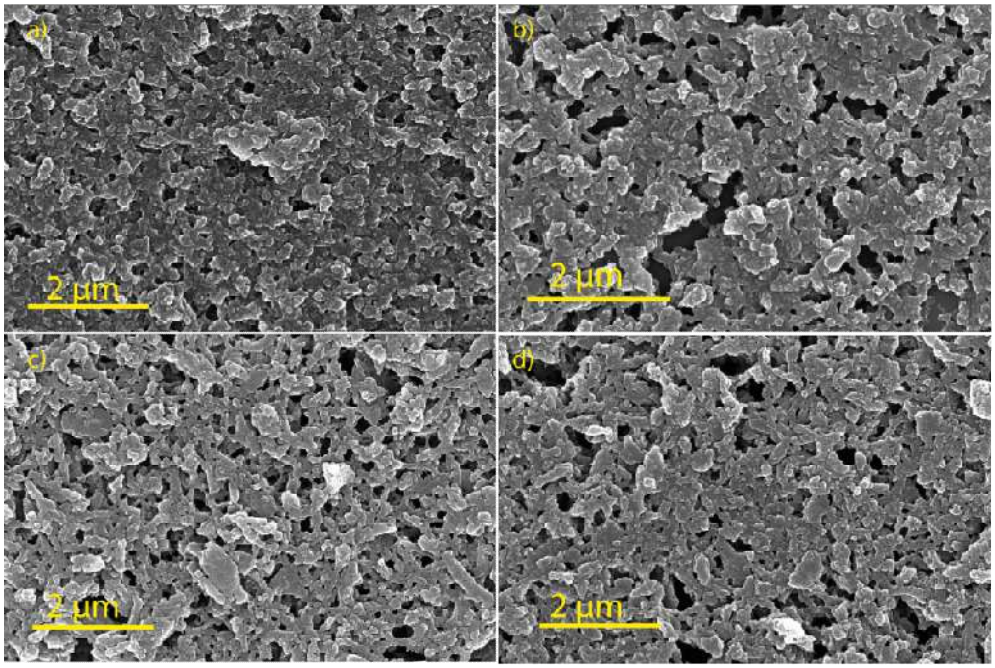

Figure 5.11 SEM images of a) P(NDI-alt-BDT) b) P(PDI-alt-BDT), c) P(NDI-r-BDT) and d) P(PDDI-r-BDT).

5.3.4 Electrochemical Characterization of the Electrodes

All liquid state electrochemical test of the polymer were performed in 1 M (PC-$LiClO_4$) electrolyte with Ag/Ag^+ as a reference electrode and graphite sheet as a counter electrode. Working electrodes of the respective polymers consisted of 1 mg cm^{-2} of active material (16.6 wt. % carbon nanotubes and 83.4 wt. % polymer) and area of the electrode was kept 1 cm^2. The effect of alteration of the acceptor molecule in the polymer chain on electrochemical behavior was investigated by cyclic voltammetry; **Figure 5.12a** shows the cyclic voltammograms, recorded at a scan rate of 5 mV s^{-1}, for the two polymers with alternate arrangement of D-A molecules. High charging current was observed for both the polymers in the negative region of the potential scanning; this region signifies reduction of polymers. Reduction charge measured in the potential region -1.5 to - 0.85 for P(PDI-alt-BDT) was 118 mC where as reduction charge measured for P(NDI-alt-BDT) was 105 mC. A higher reduction charge for P(PDI-alt-BDT) suggested greater degree of reduction of the polymer chain. The CV features observed here are similar to the features obtained for perylene dianhydride based alkali-ion batteries.[43] Interesting thing to note here is the inception of reduction in the two polymers. In P(NDI-alt-BDT), reduction of the polymer chain began at -0.41 V, however, reduction in the P(PDI-alt-BDT) started at a more negative

potential (-0.45 V). NDI molecule has low electron density compared to PDI due more delocalization in the PDI chain making PDI comparatively electron rich. Thus reduction of P(NDI-alt-BDT) started at low negative potential than P(PDI-alt-BDT). A huge difference in the area of CV was observed for P(NDI-alt-BDT) and P(NDI-r-BDT) polymers in **Figure 5.12b**.

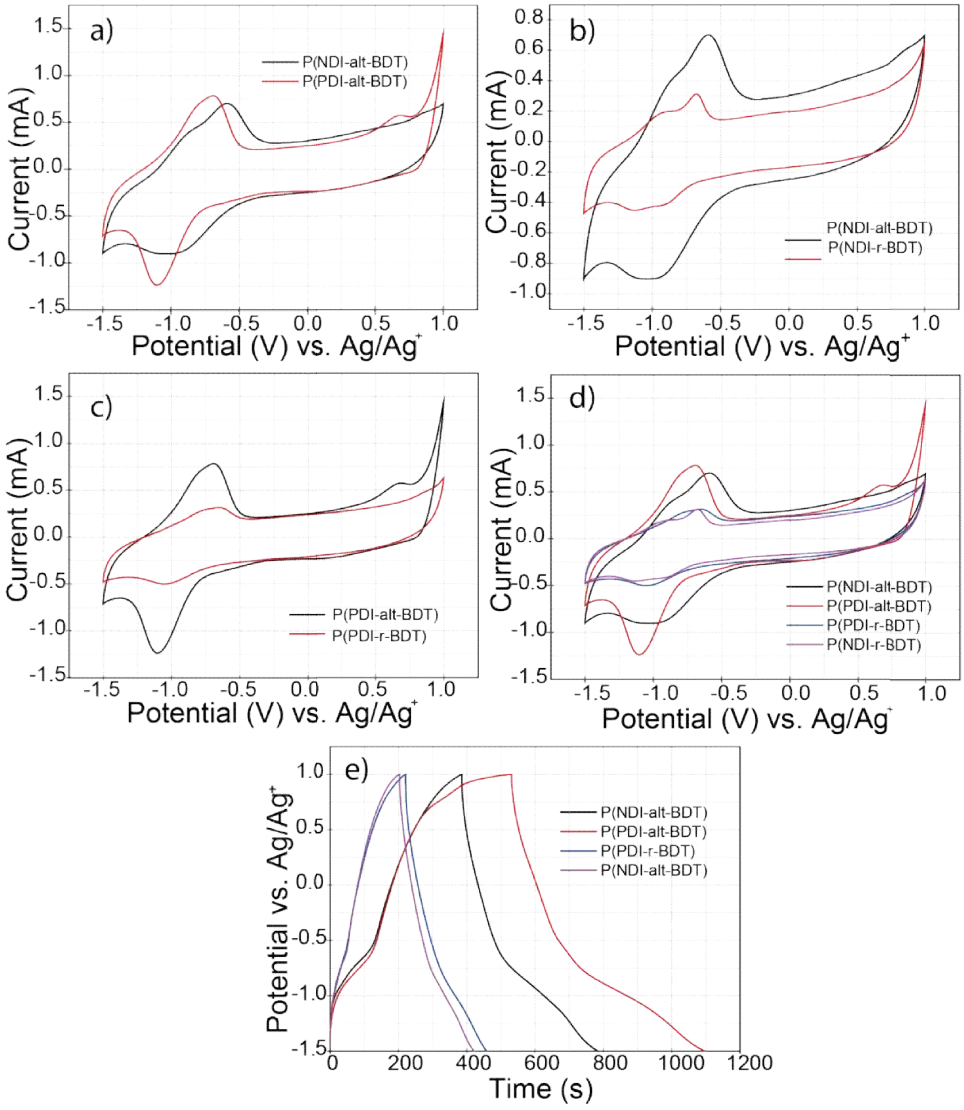

Figure 5.12. Cyclic voltammetry of different polymers recorded at a scan rate of 5 mV s^{-1}. a) CV depicting the electrochemical behavior of polymer with NDI and PDI as a acceptor molecules; b) and c) shows the change in the CV features for the alternate and random arrangement of NDI and PDI based polymers respectively; d) CV depicting the electrochemical behavior of all four polymer with different configurations, e) the GCD plots for all copolymers.

P(NDI-r-BDT) stored 58 mC of charge in the reduction region which was 55 % of the charge stored by its alternate counterpart. Similarly, **Figure 5.12c** compares the CVs of P(PDI-alt-BDT) and P(PDI-r-BDT), the charge stored by the random polymer was 55 mC which was 47 % of the charge obtained for its alternate counterpart in the reduction region. The above results indicated that alternate arrangement of D-A molecules was better for improved charge storage. DiCarrmine et al. in their work on donor-acceptor molecules found improvement in the charge storage properties of acceptor polymer by installing an acceptor molecule next to it.[27] They observed that delocalization of negative charges in the polymer chain was poor; however, incorporation of an acceptor molecule improved the negative charging stability and also its ambipolar nature. The alternate arrangements of donor-acceptor molecule permits better charge storage with significant reduction in leakage current. In our work also the alternate arrangement of donor-acceptor molecules showed superior charge storage. Random counterparts showed nearly half charge-storage; this may be accounted for by the reduced conjugation in the polymer chain caused by the irregular arrangement of donor and acceptor moieties. To get a picture of difference in the electrochemical behavior of all the four polymers, **Figure 5.12d** compares combined CV profiles of all polymers. It can be seen from the figure that the polymers with alternate arrangement of donor-acceptor units outperformed their random counterpart for charge storage.

Capacitance of the respective polymers in a three electrode cell was measured by galvanostatic charge-discharge (GCD); the GCD plots for P(PDI-alt-BDT), P(NDI-alt-BDI), P(NDI-r-BDI) and P(PDI-r-BDT) recorded at a current density of 0.5 A g^{-1} are given in **Figure 5.12 e**. A large discharge time was observed for polymer with alternate arrangement of acceptor and donor molecules whereas small discharge time was observed for the random counterparts. The CD results complemented the CV results indicating high charge storage for P(PDI-alt-BDT) and P(NDI-alt-BDI) and low charge-storage for P(NDI-r-BDI) and P(PDI-r-BDT). The capacitance measured for P(PDI-alt-BDT) was the highest with a value of 113 F g^{-1} followed by P(NDI-alt-BDT) with capacitance of 80 F g^{-1}; the capacitance obtained for random polymers P(PDI-r-BDT) and P(NDI-alt-BDT) were 48 and 44 F g^{-1}, respectively.

Full cell studies by fabricating type III device was carried out for P(PDI-alt-BDT) as it was the best performing polymer in terms of capacitance. Electrodes were prepared in a similar manner to the single cell study. The loading of active material was kept 1 mg cm^{-2} and 1 M PC-$LiClO_4$ was used as the electrolyte. Cyclic voltammograms recorded at increasing scan for type III device is shown in **Figure 5.13a**; CV behavior was typical of the symmetric

devices fabricated using two similar electrodes. The behavior became more resistive at higher scan rates. When the potential is scanned at high rate, the electrolyte ions are forced to move with greater speeds to and from the interphase. Thus for better rate behavior the ions should be highly mobile and more conducting, also, the electrode must be easily accessible to the electrolyte ions. In this study, PC-$LiClO_4$ electrolyte has low conductivity compared to aqueous electrolytes and solvated Li^+ is large which experience large viscous drag. Therefore, at high scan rates, the behavior becomes resistive.

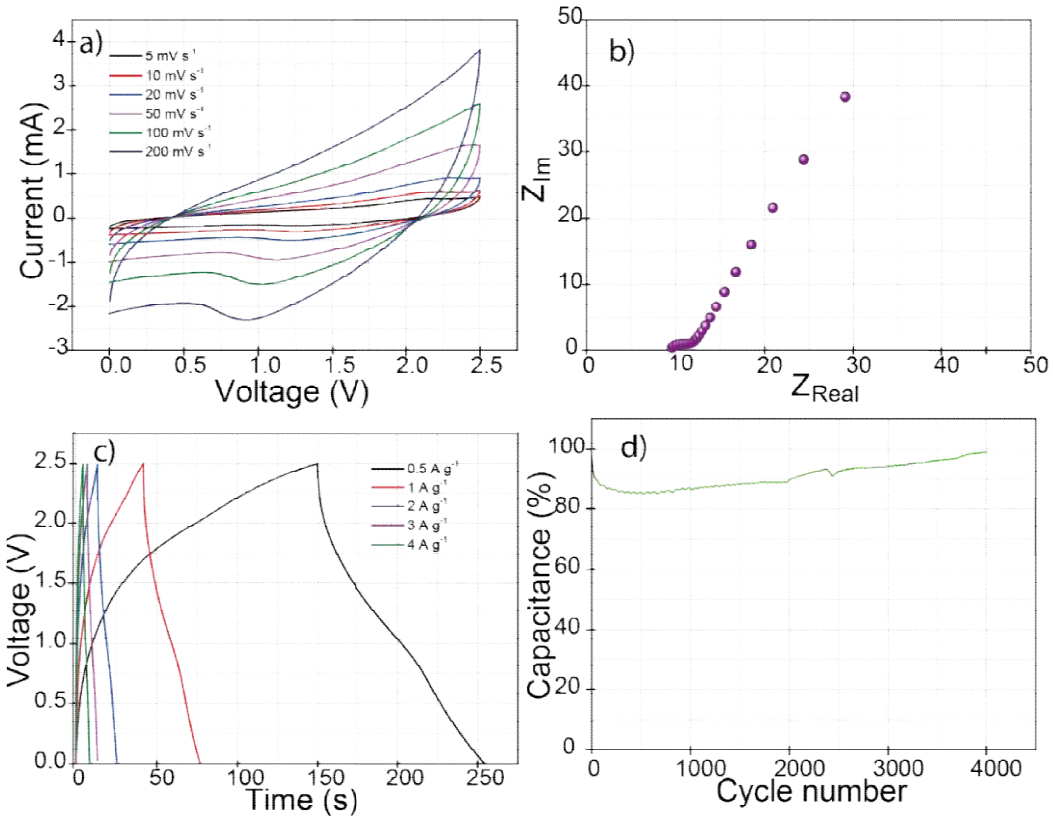

Figure 5.13 Full cell characterization of P(PDI-alt-BDT) a) cyclic voltammograms recorded at different scan rates; b) Nyquist plot; c) galvanostatic charge-discharge measured at different current densities, d) durability test performed at a current density of 4 A g^{-1}.

EIS spectroscopy can assess the internal resistance, ion diffusion, charge-transfer resistance and frequency behavior of the supercapacitor device. EIS analysis of the device was performed in the frequency range of 1 MHz-100 MHz in the open circuit voltage (OCV) condition with ac amplitude of 10 mV; the Nyquist plot obtained for the device is given in Figure **5.13b**. equivalent series resistance (ESR) measured for the device was 9.5 **Ω**, the major contribution comes from low conductivity of organic electrolyte. The device fabricated

with P(PDI-alt-BDT) showed low ESR than PBOTT-BDT based devices where resistance as high as 272 Ω was measured.[26] The intercept at x-axis was followed by a semi-circle; it represented charge transfer resistance at the electrode-electrolyte interface. A small semi-circle means low charge-transfer resistance (Rct) and vice-versa. The Rct shown by P(PDI-alt-BDT) was lower than that exhibited by other donor-acceptor polymers; the low Rct value indicates faster kinetics. Semi-circle in the Nyquist plot was followed by a small horizontal line which is called as Warburg diffusion line; this region represents the resistance towards the diffusion of ions in the electrode. The diffusion line was observed in the region of 10.5 to 11.2 Ω, this diffusion resistance could be attributed to the bulkier solvated ions in the electrolyte. The Warburg diffusion line then changes to a straight almost vertical line, representative of the capacitive behavior. For ideal capacitive behavior this line is parallel to the imaginary axis, however, the deviation observed for the device is caused by the diffusion resistance of the electrolyte.

Capacitance measurement and its retention at increasing current densities were analyzed by galvanostatic charge-discharge; the corresponding plot is given in **Figure 5.13c**. Capacitance measured at a current density of 0.5 A g^{-1} for the type III device was 42 F g^{-1}, the capacitance obtained here was twice the capacitance obtained for TPA-1Th-NDI based donor-acceptor polymers in Type IV device reported by Zeigler et al.[28]. At a current density of 2 A g^{-1} which was 4 times the initial capacitance, the device retained 19.2 F g^{-1} i.e. 42.66 % of the capacitance at 0.5 A g^{-1}. This modest retention at a high current density is caused by the low mobility of the electrolyte ions and also due to inferior inter-chain charge-transfer in the polymer structure. Improving the inter-chain charge transfer in the polymer along with creation of porosity can ameliorate the rate capability. The energy density obtained for the device was 9.1 Wh Kg^{-1} which was higher than energy densities obtained for 6,6-BEDOT-iI-But_2, PBOTT-BDT[27] and PDDDBT[24] based donor-acceptor polymers, The maximum power deliverable by the P(PDI-alt-BDT) device calculated by V2/4R, where V is the initial voltage R is the equivalent series resistance, is 164 kW kg^{-1}. These results suggest its superior charge storage capabilities compared to other similar systems reported in literature.

Figure 5.13d shows the durability test conducted at a current density of 2 A g^{-1} for 4000 cycles. The device could retain almost 100 % of the initial capacitance. The cycling stability of P(PDI-alt-NDI) donor-acceptor polymer in organic electrolyte is superior than many of the durability results reported for donor-acceptor polymers. Pulverization of the polymer due to expulsion-insertion of counter-ion during oxidation-reduction dissolution in electrolyte or

detachment of the material from the current collector are some of the reasons for the capacitance decay of conducting polymers during cycling. The stable performance P(PDI-alt-BDT) showed that it did not suffer from aforementioned issues.

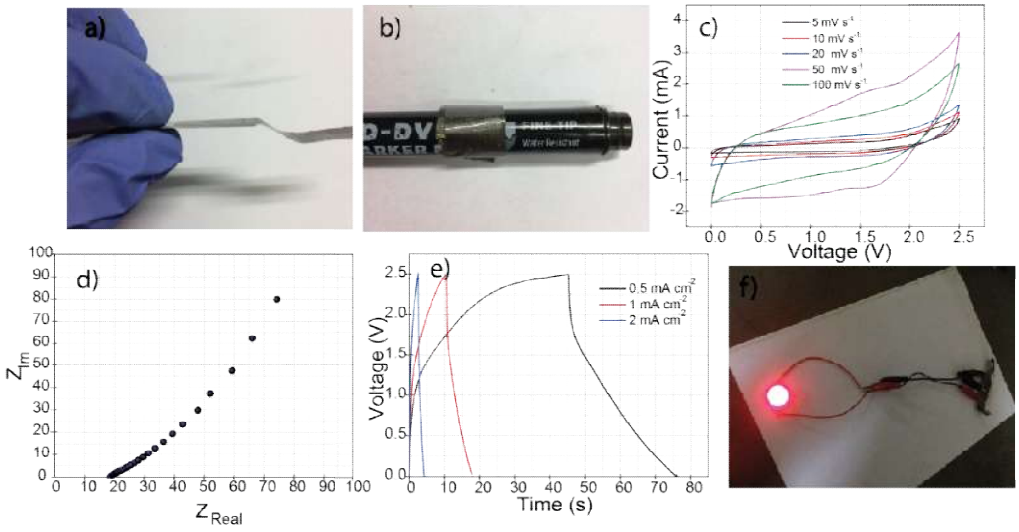

Figure 5.14. Solid flexible supercapacitor study, a) Photograph demonstrating the thin and flat nature of the flexible device; b) show the flexibility aspect of device where it can easily rolled on a pen; c) cyclic voltammogram recorded at different scan rates; d) Nyquist plot; e) galvanostatic charge-discharge curves and f) demonstration of device where it is to light a 2.5 V light emitting diode with a single device.

Supercapacitor using liquid electrolytes has the problem of electrolyte leakage and packaging of device with metal casing makes the device quite expensive. To address this problem, gel electrolytes have been introduced recently and researchers are trying to replace liquid electrolytes with gel electrolytes. Also, flexibility of charge storage devices will be an added advantage as it will allow their application in flexible electronics, and they are expected to be more cost-effective when produced on a commercial scale. Considering all above mentioned factors, we also fabricated a solid flexible supercapacitor with P(PDI-alt-NDI) polymer. A PMMA-based PC-LiClO4 gel electrolyte replaced the liquid electrolyte in solid supercapacitor. To fabricate solid device, active material was drop coated on a grafoil-scotch tape derived flexible conducting substrate with a loading of 3 mg cm^{-2} and the area of the device was 2 cm^2. Digital photographs of the device demonstrating the flexible attributes are given in **Figure 5.14a & 5.14b.** The device is very thin with the thickness of 0.418 mm; it could be bent, rolled and twisted also. Cyclic voltammogram of the flexible device given in **Figure 5.14c** show features similar to the characteristics observed for liquid counterpart. ESR

measured for solid device was 18.4 Ω, the resistance measured here was higher than the resistance measured for liquid counterpart. The electrolyte ion in gel electrolytes are less mobile due to high viscosity thus have low conductivity. The areal capacitance measured for the flexible device from GCD curve (**Figure 5.14e**) at a current density of 0.5 mA cm^{-2} is 35 mF cm^{-2}, the capacitance at high current density of 2 mA cm^{-2} decreased to 3.2 mF cm^{-2}. The reduction in capacitance at high current density is caused by the slow diffusion of ions in the gel electrolyte. However, the areal capacitance obtained in this work is higher than the capacitance obtained for other donor-acceptor polymers.[27] Finally, we have demonstrated practical utility of capacitor by lighting a 2.5 V light emitting diode, the demonstration is given **Figure 5.14f**. The high output voltage allows the device to power electronics that require high power and energy.

5.4 Conclusions

In summary, π-conjugated alternate and random copolymers based on NDI and PDI as the acceptor and BDT as the donor were synthesized following stille polymerization method. The polymer was successfully evaluated as composite electrode in supercapacitors in a type IV device configuration. A specific capacitance of 113 F g^{-1} with excellent stability up to 4000 cycles with almost 100% retention of the initial capacitance was observed for the P(PDI-alt-BDT) polymer in single electrode setup in PC-LiClO4 organic electrolyte. Flexible supercapacitor device was also fabricated to show the commercial application of the polymers. The areal capacitance of 35 mF cm^{-2} observed for the flexible device at a current density of 0.5 mA cm^{-2}.

5.5. Reference

(1) Zhong, C.; Deng, Y.; Hu, W.; Qiao, J.; Zhang, L.; Zhang, J. *Chem. Soc. Rev.* **2015**, *44*, 7484-7539.

(2) Galinski, M.; Lewandowski, A.; Stepniak, I. *Electrochim. Acta* **2006**, *51*, 5567-5580.

(3) Torchala, K.; Kierzek, K.; Machnikowski, J. *Electrochim. Acta* **2012**, *86*, 260-267.

(4) Wu, H.; Wang, X.; Jiang, L.; Wu, C.; Zhao, Q.; Liu, X.; Hu, B.; Yi, L. *J. Power Sources* **2013**, *226*, 202-209.

(5) Zhang, X.; Wang, X.; Jiang, L.; Wu, H.; Wu, C.; Su, J. *J. Power Sources* **2012**, *216*, 290-296.

(6) Sharma**,** S.; Soni, R.; Kurungot, S.; Asha, S. K. *Macromolecules* **2018**, *51*, 954-965.

(7) Brandt, A.; Isken, P.; Lex-Balducci, A.; Balducci, A. *J. Power Sources* **2012**, *204*, 213-219.

(8) Jung, N.; Kwon, S.; Lee, D.; Yoon, D. M.; Park, Y. M.; Benayad, A.; Choi, J. Y.; Park, J. S. *Adv. Mater.* **2013**, *25*, 6854-6858.

(9) Francke, R.; Cericola, D.; Kotz, R.; Weingarth, D.; Waldvogel, S. R. *Electrochim. Acta* **2012**, *62*, 372-380.

(10) Lai, Y. Q.; Chen, X. J.; Zhang, Z. A.; Li, J.; Liu, Y. X. *Electrochim. Acta* **2011**, *56*, 6426-6430.

(11) Perricone, E.; Chamas, M.; Cointeaux, L.; Lepretre, J. C.; Judeinstein, P.; Azais, P.; Beguin, F.; Alloin, F. *Electrochim. Acta* **2013**, *93*, 1-7.

(12) Vali, R.; Laheaar, A.; Janes, A.; Lust, E. *Electrochim. Acta* **2014**, *121*, 294-300.

(13) Janes, A.; Eskusson, J.; Thomberg, T.; Lust, E. *J. Electrochem. Soc.* **2014**, *161*, A1284-A1290.

(14) Yu, X. W.; Ruan, D. B.; Wu, C. C.; Wang, J.; Z. Shi, Q. *J. Power Sources* **2014**, *265*, 309-316.

(15) Qian, W. J.; Sun, F. X.; Xu, Y. H.; Qiu, L. H.; Liu, C. H.; Wang, S. D.; Yan, F. *Energy Environ. Sci.* **2014**, *7*, 379-386.

(16) Hanlon, D.; Backes, C.; Higgins, T. M.; Hughes, M.; O'Neill, A.; King, P.; McEvoy, N.; Duesberg, G. S.; Sanchez, B. M.; Pettersson, H.; Nicolosi, V.; Coleman, J. N. *Chem. Mater.* **2014**, *26*, 1751-1763.

(17) Huang, X. D.; Sun, B.; Chen, S. Q.; Wang, G. X. *Chem. Asian J.* **2014**, *9*, 206-211.

(18) Cho, M. Y.; Kim, M. H.; Kim, H. K.; Kim, K. B.; Yoon, J. R.; Roh, K. C. *Electrochem. Commun.* **2014**, *47*, 5-8.

(19) Wang, D. W.; Fang, H. T.; Li, F.; Chen, Z. G.; Zhong, Q. S.; Lu, G. Q.; Cheng, H. M. *Adv. Funct. Mater.* **2008**, *18*, 3787-3793.

(20) Zhang, H.; Wang, J.; Chen, Y.; Wang, Z.; Wang, S. *Electrochim. Acta* **2013**, *105*, 69-74.

(21) Zheng, C.; Gao, J. C.; Yoshio, M.; Qi, L.; Wang, H. Y.; *J. Power Sources* **2013**, *231*, 29-33.

(22) Zheng, C.; Yoshio, M.; Qi, L.; Wang, H. Y. *J. Power Sources* **2014**, *260*, 19-26.

(23) Lim, E.; Kim, H.; Jo, C.; Chun, J.; Ku, K.; Kim, S.; Lee, H. I.; Nam, I. S.; Yoon, S.; Kang, K.; Lee, J. *ACS Nano* **2014**, *8*, 8968-8978.

(24) Łatoszynska, A. A.; Zukowska, G. Z.; Rutkowska, I. A.; Taberna, P. L.; Simon, P.; Kulesza, P. J.; Wieczorek, W. *J. Power Sources* **2014**, *274*, 1147-1154.

(25) Fan, L. Q.; Zhong, J.; Wu, J. H.; Lin, J. M.; Huang, Y. F. *J. Mater. Chem. A* **2014**, *2*, 9011-9014.

(26) Guo, Y.; Li, W.; Yu, H.; Perepichka, D. F.; Meng, H. *Adv. Energy Mater.* **2017**, *7*, 1601623.

(27) DiCarmine, P. M.; Schon, T. B.; McCormick, T. M.; Klein, P. P.; Seferos, D. S. *J. Phys. Chem. C* **2014**, *118*, 8295-8307.

(28) Zeigler, D. F.; Candelaria, S. L.; Mazzio, K. A.; Martin, T. R.; Uchaker, E.; Suraru, S. L.; Kang, L. J.; Cao, G.; Luscombe, C. K. *Macromolecules* **2015**, *48*, 5196-5203.

(29) Liu, W.; Tkachov, R.; Komber, H.; Senovskyy, V.; Schubert, M.; Wei, Z.; Facchetti, A.; Neher, D.; Kiriy, A. *Polym. Chem.* **2014**, *5*, 3404-3411.

(30) Senkovskyy, V.; Tkachov, R.; Komber, H.; Sommer, M.; Heuken, M.; Voit, B.; Huck, W. T. S.; Kataev, V. Petr, A.; Kiriy, A. *J. Am. Chem. Soc.* **2011**, *133*, 19966-19970

(31) Ye, L.; Zhang, S.; Zhao, W.; Yao, H.; Hou, J. *Chem. Mater.* **2014**, *26*, 3603-3605.

(32) Homyak, P. D.; Tinkham, J.; Lahti, P. M.; Coughlin, E. B. *Macromolecules* **2013**, *46*, 8873-8881.

(33) Sefera, E.; Koyuncu, F. B. *Electrochim. Acta* **2014**, *143*, 106-113.

(34) Ganesamoorthy, R.; Vijayaraghavan, R.; Ramki, K.; Sakthivel, P. *J. Sci.: Adv. Mater. Dev.* **2018***, 3*, 99-106.

(35) Gu, C.; Hu, W.; Yao, J.; Fu, H. *Chem. Mater.* **2013**, *25*, 2178-2183.

(36) Kim, Y.; Hong, J.; Oh, J. H.; Yang, C. *Chem. Mater.* **2013**, *25*, 3251-3259.

(37) Dai, S.; Huang, S.; Yu, H.; Ling, Q.; Zhan, X. *J. Polym. Sci., Part A: Polym. Chem.* **2017**, *55*, 682-689.

(38) Xiao, B.; Ding, G.; Tan, Z.; Zhou, E. *Polym. Chem,* **2015**, *6*, 7594-7602.

(39) Ye, L.; Jiao, X.; Zhang, H.; Li, S.; Yao, H.; Ade, H.; Hou, J. *Macromolecules* **2015**, *48*, 7156-7163

(40) Zhang, Y.; Wan, Q.; Guo, X.; Li, W.; Guo, B.; Zhang, M.; Li, Y. *J. Mater. Chem. A* **2015**, *3*, 18442-18449.

(41) Durban, M. M.; Kazarinoff, P. D.; Luscombe, C. K. *Macromolecules* **2010**, *43*, 6348-6352.

(42) Sharma, S.; Kolhe, N. B.; Gupta, V.; Bharti, V.; Sharma, A.; Datt, R.; Chand, S.; Asha, S. K. *Macromolecules*, **2016**, *49*, 8113-8125.

(43) Luo, W.; Allen, M.; Raju, V. Ji, X. *Adv. Energy Mater.* **2014**, *4*, 1400554.

Chapter 6

Summary and Outlook

There is a dearth of good performing n-type polymers compared to p-type polymers. However, among the reported n-type polymers, rylenebisimide based π conjugated polymers are very promising candidates which exhibited high device performance under ambient condition. The most important rylenebisimide based materials are naphthalene and perylene diimides (NDI and PDI). Despite the rapid development in NDI and PDI based polymeric materials, there is still ample scope for newer polymer designs with improved performance. Hence, this area is still very important and active, demanding new design strategies to synthesize novel materials with desirable physical and semiconducting properties for energy applications. In this context, the present thesis entitled **"Alternate and Random Copolymers of Bay substituted Rylenebisimides for Energy Applications"** describes the design and synthesis of NDI/PDI based novel polymers that find application in energy generation as well as energy storage.

In the initial part of the thesis, a series of NDI based random copolymers were investigated and their photovoltaic properties were compared with the reference copolymer naphthalene diimide bithiophene P(NDI2OD-T2) or PolyeraActivInk N2200. P(NDI2OD-T2) polymer is a commercially available donor-acceptor polymer, which is extensively investigated for its high power conversion efficiency (PCE) ~5% in all-polymer solar cells (PSC)s, good solution processability, high crystallinity and light absorption capability near-visible and infrared region. However, the inherent π-stacking tendency of the naphthalene diimide unit hampers good intermixing with donor copolymers when used in solar cell devices. Random copolymerization is a very promising strategy to tune the photovoltaic properties of the copolymers.

In the initial part of the work, a series of NDI based copolymers with varying extents of PDI incorporation were studied. The presence of randomly incorporated PDI in the P(NDI2OD-T2) polymer backbone reduced the self-aggregation of the polymer and enhanced the intermixing of the donor and acceptor polymers. All the synthesized copolymers showed better photovoltaic properties compared to reference copolymer. The properties of these acceptor copolymers were investigated in depth in the pristine form as well as their donor-acceptor (D:A) blends with PTB7-Th as a donor to understand the structural features that influence the all-PSCs performance. Polymer with 30 % incorporation of the PDI (PNDI-Th-PDI30) showed optimum photophysical properties and showed a maximum PCE of ~**5 %** with the PTB7-Th donor. It exhibited optimal crystallinity and miscibility with donor polymer which lead to the best D/A compatibility, nano-scale phase separation and improved

balanced bulk carrier charge transport in the blend. Thus, the structure-property analysis established that the incorporation of n-type PDI building block into P(NDI2OD-T2) polymer was a very effective strategy to tune the photovoltaic parameters and improve PCE in new n-type random copolymers, thereby proving its potential application in future all-PSCs.

NDI based copolymers are very promising materials, but it still has not surpassed the excellent charge transport properties of PCBM. PCBM exhibits outstanding characteristics such as high charge carrier mobility, small reorganization, very high electron affinity and comparable energy levels. So to improve the charge carrier mobility and efficiency of the polymers a series of n-type random copolymers with PCBM incorporation were synthesized and their properties were investigated. The random copolymers showed better compatibility with the PTB7-Th donor polymer compared to reference copolymer P(NDI2OD-T2). A polymer having 7.5 % incorporation of the PCBM (PNDI-Th-PCBM7.5) showed optimum photophysical properties and showed a maximum PCE of ~**2.5 %** with the PTB7-Th donor. It showed optimal miscibility with donor polymer which produced better donor-acceptor compatibility. Further optimization is needed to improve the photovoltaic performance of the copolymers.

Equally important to energy generation is the energy storage systems as it plays a major role in the availability of sustainable renewable energy on demand. Two new NDI-based copolymers were developed via the direct (hetero) arylation (DHAP) polymerization route as supercapacitor materials and their performance was compared with that of (P(NDI2OD-T2)) as the reference polymer. The polymers had bay substituted naphthalene diimide as the acceptor moiety in the repeat unit, while the donor strength was varied from bithiophene (P(NDI2OD-T2)) to thiophene end-capped phenylene vinylene (P_1) and thiophene end-capped phenylene vinylene with nitrile group substitution at the vinylene linkage (P_2). The effect of this donor strength variation in the properties of the polymers as symmetric Type III supercapacitor composite materials with carbon nanotubes was explored employing 0.5 M H_2SO_4 as the electrolyte. A specific capacitance of 124 F/g with excellent stability up to 5000 cycles with almost 100% retention of the initial capacitance was observed for the polymer with nitrile substituents along the OPV backbone (P_2). The energy and power density was obtained as 2 Wh kg^{-1} and 22 kW kg^{-1} respectively. Development of materials for type III supercapacitor device application is very crucial since not many materials can meet the challenge of stability under reduced conditions. The newly designed

NDI based D-A copolymers exhibited excellent stability, thereby establishing themselves as promising polymers for energy storage applications.

The last chapter of the thesis describes the copolymerization strategy to compare the electrochemical properties of random and alternate copolymers. NDI/PDI and BDT based alternate and random copolymers were synthesized and their electrochemical properties were investigated. Polymers with the alternate and random arrangement of donor and acceptor units were tested for charge storage in the PC-$LiClO_4$ electrolyte. Devices were fabricated with P(PDI-alt-BDT) polymer as composite electrode materials both with liquid electrolyte and solid-state flexible device. The alternate copolymer of both NDI and PDI outperformed their random copolymers. These results suggested that alternate copolymer resulted in better conjugation and charge balance which is essential for better charge storage. A specific capacitance of 113 F/g with excellent stability up to 4000 cycles with almost 100% retention of the initial capacitance was observed for the polymer P(PDI-alt-BDT). The energy and power density was obtained as 9.1 Wh kg^{-1} and 164 kW kg^{-1} respectively. These polymers showed very high energy and power density compared to previous work.

To conclude, this dissertation is focused on the synthesis and structure-property studies of NDI/PDI based donor-acceptor conjugated polymers for energy application. In the first part, an important question of the effect of random incorporation of the higher analogue PDI in NDI based copolymers on the photovoltaic properties was addressed. Furthermore, the NDI/PDI containing n-type polymers with fine-tuned optical, electrochemical and semiconducting properties were synthesized by utilizing alternating and random strategy. In short, the structure-property relationships reported in this thesis would help to design future generation NDI based materials for energy application.

A major challenge in the field of the organic solar cell is the scale-up of the polymers. Every batch the molecular weight of the polymer can vary and their photovoltaic properties also can vary. Also, the stille polymerization process is time-consuming. Flow synthesis is a technique that allows preparing a polymer in large scale with reproducible molecular weight distribution in short reaction times. Up scaling of such polymers using flow synthesis could be an attractive option in future.

In chapter 4 and 5 NDI and PDI based polymers were synthesized and their electrodes were fabricated by mixing with carbon nanotubes. The physical mixing of the polymer with carbon nanotubes is often done to get comparable conductivity. To improve the interaction between

polymer and carbon nanotube in-situ polymerization can be performed. In this strategy, carbon nanotubes will be mixed with the monomers and in this way polymer chains can grow on the carbon nanotubes, resulting in increased interaction. Increased interaction will ultimately lead to enhanced electrochemical properties of the polymer.

Publications in International Journals

1. Sandeep Sharma, Nagesh B. Kolhe, Vinay Gupta,* Vishal Bharti, Abhishek Sharma, Ram Datt, Suresh Chand, S. K. Asha.* Improved All-Polymer Solar Cell Performance of n-Type Naphthalene Diimide−Bithiophene P(NDI2OD-T2) Copolymer by Incorporation of Perylene Diimide as Coacceptor" *Macromolecules* **2016**, *49*, 8113-8125.

2. **Sandeep Sharma,** Roby Soni, Sreekumar Kurungot*, S. K. Asha.* Naphthalene Diimide Copolymers by Direct Arylation Polycondensation as Highly Stable Supercapacitor Electrode Materials. *Macromolecules* **2018**, *51*, 954-965.

3. Sandeep Sharma, S. K. Asha*. All-Polymer Solar Cell Performance of *n*-type Naphthalenediimide-bithiophene P(NDI2OD-T2) Copolymer with PCBM as Co-acceptor (*Manuscript under preparation*).

4.Sandeep Sharma, S. K. Asha*.Naphthalenediimide and perylene diimide Based Alternate and Random Copolymers for flexible Supercapacitor Electrode Materials (*Manuscript under preparation*).

Patents

1. Asha Syamakumari, Nagesh B. Kolhe, **Sandeep Sharma**. "Novel Copolymer Compositions for Improved Performance In All-polymer Solar Cells". Patent IN201611023584, 2016 (**Published Fab 2018**).

2. Asha Syamakumari, **Sandeep Sharma.** "Synthesis of Donor and Acceptor Random and Alternate Copolymers for Photovoltaic Application." Provisional Patent filed. Application number – IN201711018191, 2017.

3. Asha Syamakumari, **Sandeep Sharma,** Roby Soni, Sreekumar Kurungot. "Naphthalenediimide Copolymers by Direct ArylationPolycondensation as Highly Stable Supercapacitor Electrode Materials. Provisional Patent filed. Application number – IN201711041441, 2017.

Symposia Attended/Poster Presentation

1. Sandeep Sharma and S. K. Asha "Naphthalenediimide Copolymers by Direct Arylation Polycondensation as Highly Stable Supercapacitor Electrode Materials**"** **Macro Meet ,** CSIR-NCL, Pune, 2018. *(Oral Presentation)*

2. Sandeep Kumar Sharma and S. K. Asha "All-polymer Solar Cell Performance of n-type Napthalenediimide/ Perylenediimide - Bithiophene Copolymer" MACRO 2017 - **International Conference on Polymers**, Trivandrum 2017. (*Poster presentation*)

3. Sandeep Sharma and S. K. Asha "All-Polymer Solar Cell Performance of *n*-type Napthalenediimide/ Perylenediimide - bithiophene Copolymer" **National Science Day**, CSIR-NCL, Pune, 2016. (*Poster presentation*)

4. Sandeep Sharma and S. K. Asha "All-polymer Solar Cell Performance of n-type Napthalenediimide/ Perylenediimide - Bithiophene Copolymer" **Semiconductor Meet**, IISER, Pune 2016. *(Oral Presentation)*